Development of a probabilistic population model for the prediction of

subacromial geometric variability

by

Jaclyn N. Chopp-Hurley

A thesis
presented to the University of Waterloo
in fulfillment of the
thesis requirement for the degree of
Doctor of Philosophy
in
Kinesiology

Waterloo, Ontario, Canada, 2015

Author's Declaration

I hereby declare that I am the sole author of this thesis. This is a true copy of the thesis, including any final revisions, as accepted by my examiners.

I understand that my thesis may be made electronically available to the public.

Abstract

Subacromial impingement syndrome (SAIS) is common in the shoulder and precedes several additional pathologies. SAIS occurs when the tissues interposed between the acromion process of the scapula and superior surface of the humeral head become compressed. Though SAIS is well studied, definitive mechanical cause(s) of impingement still remain elusive due to the multitude of parameters contributing to subacromial space reduction. Within this multifactorial etiology, each exhibits considerable interpersonal variability, and because of this, deterministic approaches to estimate the subacromial space size are unable to assess the distribution of risk in the population. This research used a probabilistic modelling approach to quantify the variability in both morphological and fatigue-related kinematic factors in terms of how they modulate the minimum subacromial space width. Through four distinct symbiotic stages, this work employed a combination of experimental and modelling techniques to develop a novel probabilistic model of subacromial space geometry from which SAIS risk was estimated.

The first stage applied probabilistic concepts to an existing deterministic model to evaluate the sensitivity of predicted muscle forces to model parameter variation. This model demonstrated that modest variation of muscle attachment locations and a glenohumeral stability constraint resulted in considerable variability in predicted rotator cuff muscle forces, with differences up to 50% between lower and upper confidence limits. This initial study provided a conceptual framework for the probabilistic subacromial geometry model.

The subsequent interdependent experimental studies (Stages II and III) were designed to acquire the necessary kinematic and morphological input distributions for the large-scale probabilistic subacromial geometry model. The first of these studies evaluated the effects of

muscle fatigue and arm elevation on shoulder kinematic parameters. Specific quantities measured included: superior/inferior humeral head translation and scapular rotation, tilt and protraction/retraction, as well as the minimum subacromial space width (SAS). While significant superior humeral head translation occurred following fatigue (mean = 0.5 to 4.3mm, 0 to 120° elevation), concurrent compensatory scapular movements appeared to maintain the subacromial space size. However, the fatigue responses and elevation responses were highly variable, with half of the population demonstrating a combination of fatigue-induced changes that reduced the subacromial space. The second study quantified intrinsic static morphological characteristics of the scapula, including: acromial anterior slope, lateral acromial angle, acromial tilt, acromion index and glenoid inclination. Additionally, the interposed subacromial tissue thicknesses, specifically the supraspinatus tendon and subacromial bursa, were measured. Similar to the kinematic outcomes, each of the parameters measured in these studies showed considerable interpersonal variability. However, even the average occupation ratio (65.3 [21.6 – 108.9] %) implied a high risk of tissue compression in elevated arm postures.

The distributions of experimentally measured kinematic and morphological characteristics were used as inputs into a three-dimensional probabilistic subacromial geometry model which subsequently generated a distribution of SAS (Stage IV). Additionally, relative importance factors were obtained from the probabilistic modeling approach, which established which parameters (morphological, kinematic) contributed more to the variability in SAIS risk. Overall, the probability of tissue compression (a mechanical indicator of SAIS risk) increased markedly with elevation, from <5% at initial elevation, to ~50% at mid-elevation to 75% at maximal elevation. The considerable variability present in each of the measured characteristics in addition to the modelled output suggested a highly differential risk of fatigue-related SAIS

across the population, with glenoid inclination identified as the most important factor in modulating the size of the subacromial space. At the average population level, the predominant recommendation elucidated from this work is avoidance of overhead exertions, which would contribute to rotator cuff tissue damage, facilitated through repetitive tissue compression at elevation angles $\geq 60°$. Additionally, the presence of fatigue-induced superior humeral head translation, despite the maintenance of the subacromial space size, may increase the likelihood of several other degenerative pathologies (glenoid degeneration, osteophyte formation, glenohumeral instability). Thus, rotator cuff strengthening programs, to maintain a stable glenohumeral relationship, are suggested for those exposed to repetitive elevation or upper extremity fatiguing activities, particularly if diagnosed with scapular dyskinesis. Lastly, the outcomes of this research highlight the utility of probabilistic modelling approaches for characterizing interpersonal variability and subsequently estimating the distribution of musculoskeletal injury risk in a population.

Acknowledgements

Nearly a decade ago, when I was a third year undergraduate student assisting in the lab, I never thought I would come out of that lab with both a doctoral degree and a husband.

I would like to express my utmost appreciation to my supervisor, Dr. Clark Dickerson, for being a fantastic mentor and teacher through two degrees and countless courses. I am extremely grateful for the extensive guidance and assistance provided over the course of these degrees, as well as for the time spent training me to become a successful researcher.

I would like to thank my committee members, Dr. Richard Wells, Dr. Stacey Acker, Dr. Philip Bigelow and Dr. Paula Ludewig, for their helpful insights which undoubtedly strengthened this work.

I also received assistance from members outside of the University of Waterloo community. I would like to thank Dr. Joseph Langenderfer for sharing his probabilistic modelling expertise, and for his continued guidance in this area. Additionally, many thanks to Dr. John O'Neill and the staff at St. Joseph's Healthcare Hamilton for being so helpful and accommodating during the experimental collection of this research.

As a member of the Digital Industrial Ergonomics and Shoulder Evaluation Laboratory for several years, I have had the opportunity to work alongside some remarkable individuals. In particular, I would like to thank both Jackie Maciukiewicz and Alison McDonald for their assistance with data collection. As well, I would like to express a special thank you to Rebecca Brookham for providing fine-wire electromyography training and for her invaluable friendship.

I would like to acknowledge the financial support provided by the Natural Sciences and Engineering Council of Canada and the University of Waterloo.

Dedication

To my husband and best friend, Kevin.

Your perseverance, confidence and untiring drive for success both inspires me and amazes me every day of our lives.

I love you so much xoxo.

Table of Contents

List of Figures

List of Tables

Glossary

The following is a glossary of terms that appear throughout the document. This glossary also provides alternate terms used to describe the same property or characteristic. While footnotes are provided in certain sections to re-iterate terminology, this glossary should serve as an overview or reminder of important terms. While acronyms are defined throughout the text, those that appear frequently are listed below. The glossary is divided into three sections: (1) Clinical Terms, (2) Probabilistic Terms, and (3) Methodological Terms.

A. Clinical Terms

Term	Definition
Subacromial Space	The *Subacromial Space* is a general term describing the area in the internal geometry of the shoulder that is bordered superiorly by the acromion process of the scapula and inferiorly by the superior surface of the humeral head.
Minimum Subacromial Space Width *Acronym:* **SAS**	*Also known as*: acromio-humeral interval (AHI), acromio-humeral distance (AHD), subacromial width, subacromial distance The minimum subacromial space width (SAS) is a measureable characteristic that is used to evaluate injury risk. It is defined as the smallest (superior-inferior) distance between the superior aspect of the humeral head and the dense cortical undersurface of the acromion process. This is a two-dimensional property, measured in millimeters, and can be captured using a variety of imaging techniques, including radiographs, and ultrasound.
Subacromial Tissues	The soft tissues residing within the subacromial space; notably the supraspinatus tendon and subacromial bursa as well as the long head of the biceps tendon and joint capsule.
Subacromial Impingement Syndrome *Acronym:* **SAIS**	In this research, *Subacromial Impingement Syndrome* (SAIS) refers to mechanical impingement or compression of the vulnerable subacromial tissues in the subacromial space. In this document, *subacromial impingement risk* refers to the likelihood or increased likelihood (resulting from morphological or kinematic characteristics) that the subacromial tissue thicknesses will exceed the minimum subacromial space width.
Glenohumeral Kinematics *Acronym:* **GH**	Orthopaedic relationship between the humerus and the glenoid cavity of the scapula; primarily translational in this research.
Humeral Head Translation	*Also known as:* humeral head migration or excursion

	Movement (translation) of the humeral head with respect to the glenoid cavity, primarily in a Superior-Inferior direction (measured in millimeters). Note: no translation indicates that the geometric centre of the humeral head is aligned with the center of the glenoid cavity.
Scapulothoracic Kinematics *Acronym:* **ST**	Orthopaedic relationship between the scapula and the torso; primarily rotational in this research.
Scapular Rotation	Scapular rotation about the anterior-posterior axis of the scapula; upward rotation is lateral movement of the inferior border of the scapula.
Scapular Tilt	Scapular rotation about the medial-lateral axis of the scapula; posterior tilt is anterior movement of the inferior border of the scapula.
Scapular Protraction/Retraction	*Also known as:* Scapular internal/external rotation Scapular rotation about the superior-inferior axis of the scapula; retraction (external rotation) is posterior movement of the lateral border of the scapula
Morphology	Innate bone geometry (shape) characteristics that remain constant across a short-duration exercise period (such as in this research). Changes in morphology primarily result from injury or degeneration accompanying age.
Rotator Cuff Musculature	A group of four muscles (supraspinatus, infraspinatus, subscapularis, teres minor) originating on the scapula and inserting on the humerus thereby influencing the glenohumeral relationship. The supraspinatus functions primarily as an abductor, infraspinatus and teres minor as external rotators and subscapularis as an internal rotator of the humerus. Additionally, the lines of action of each of the muscles are postulated such that they act to compress the humeral head in the glenoid cavity and resist upward translation.
Scapula Stabilizing Musculature	In this document the upper trapezius, lower trapezius and serratus anterior muscles of the upper extremity are collectively referred to as the scapula stabilizer muscles as they are the muscles that primarily guide and control scapular movement during elevation.

B. Probabilistic Terms

Term	Definition
Probabilistic	*Also known as:* Stochastic Probabilistic analysis considers the uncertainty (variability) present in model parameter(s) by treating them as distributions rather than a single value (typically the mean) eliciting a distribution of possible outputs.
Input	In this document, a model *Input* describes a variable(s) that corresponds to a particular experimental condition (i.e. arm elevation angle, fatigue state). The simulation can be run with multiple inputs depending on the experimental condition. Model inputs can directly affect model parameters.

Parameter	In this document, a model *Parameter* describes a variable(s) that is 'hard-wired' into the model's geometric formulation (i.e. acromial shape, muscle origin). Each parameter is modelled as a continuous random variable with a particular distribution.
Random Variable (Continuous)	A variable that can take on any value (either within a particular range, or any real number) which can be used to define each parameter in the model. Therefore, each parameter in this research is described as a random variable with a particular distribution. In this document, all *Random Variables* are *Continuous Random Variables*, as possible values exist on a continuous scale.
Standard Normal Space	A fundamental concept of Probabilistic Reliability Analysis. Describes a transformed coordinate system where the statistical parameters are in their reduced (standard normal) form with a zero mean and unit standard deviation. Therefore, each variable (despite different units) can exist in this non-dimensionalized space, and their relative effect on the output variable(s) can be evaluated.
Limit State Function	Most reliability problems have a particular failure criterion (i.e. breaking point, fracture threshold, etc.). The function that separates the design space into "safe" and "unsafe" regions is the *Limit State Function*.
Beta (β)	*Also known as:* Reliability Index Minimum distance between the coordinate system origin in the transformed coordinate system (standard normal space) and the limit state function. A smaller value of β is associated with a larger probability of failure.
Most Probable Point	The point on the limit state surface corresponding to the minimum distance (β) is termed the *Most Probable Point*. In structural reliability examples, this is the most probable point of failure. This point also coincides with the point of maximal density on the joint probability distribution function.
Alpha (α)	*Also known as:* Importance Factors or Relative Sensitivity Factors Directional cosine of the unit vector at the most probable point. Each parameter will have an associated value for alpha, and as their squared sum is equal to 1, the relative importance of each variable can be assumed from each corresponding value of alpha.
Probability Level (p-level)	The probability of a particular event or output value (z-value) occurring. It is determined by specifying 'performance levels' in probabilistic analysis software from which the corresponding probability level(s) can be calculated.
z-value	The output associated with a particular p-level (probability level). It is determined by specifying 'probability levels' in probabilistic analysis software from which the corresponding z-value(s) can be calculated.

C. Methodological Terms

Term	Definition
Neutral Posture	The arm resting down by the participants' side with 0° of arm elevation and 0° of axial rotation (anatomical position with thumb facing lateral).
Sagittal Plane	The plane dividing the body into medial/lateral components. Arm flexion occurs about this plane (elevating the arm in front).
Coronal/Frontal Plane	The plane dividing the body into anterior/posterior components. Arm abduction occurs about this plane (elevating the arm out to the side).
Transverse Plane	The plane dividing the body into superior/inferior components. Arm horizontal abduction occurs about this plane (moving the arm across the body).
Scapular Plane	The plane located 30° anterior to the coronal plane. Arm movement in this plane is referred to as "scaption" or "scapular plane elevation".
Session	In this document, the term *Session* refers to the fatigue state. There will be two sessions: "Pre-fatigue" session and "Post-fatigue" session.
Exertion	In Chapter 3 of this document, the term *Exertion* refers to a particular combination of the three defined inputs (Abduction x Force Direction x Force Magnitude). i.e. A particular exertion may be 45° of abduction, internal rotation force direction, 40N force magnitude.
Condition	In Chapters 4 to 6, the term *Condition* refers to a particular combination of the two primary experimental modifiers: Session (Pre-fatigue, Post-Fatigue) and Arm Elevation Angle (0°, 30°, 60°, 90°, 120°).
Trial	*Also known as:* iteration (primarily in Monte Carlo methods) Probabilistic term (primarily for Advanced Mean Value methods) that is calculated by: (number of parameters + 1) * (number of outputs)
Simulation	Probabilistic term used to describe running a probabilistic analysis (with a particular set of trials) for a particular condition i.e. A simulation for a particular condition (*ex.* pre-fatigue session, 30° arm elevation angle) with a particular set of trials (*ex.* 10 trials ([9 parameters + 1] * 1 output)).

Chapter 1

Introduction

1.1   Motivation

The shoulder is highly mobile, which permits a spectrum of joint translations and

rotations that may precipitate pain and injury. Subacromial impingement syndrome (SAIS) is the

most frequently diagnosed shoulder disorder, accounting for approximately 44 to 65% of all

injuries of the shoulder (Michener et al. 2003, van der Windt et al. 1995, 1996). This disorder

subsequently leads to additional shoulder pathologies, notably rotator cuff tears (preceding 95%

of cases) (Neer 1983).

Shoulder pain prevalence is positively related to occupational physical shoulder demands.

The Workplace Safety and Insurance Board (WSIB) has identified overexertion to be the leading

cause of lost time claims in the shoulder, with the number of reported claims remaining steady

over the past five years (WSIB 2013). Extensive research has specifically associated overhead

and/or repetitive working tasks with an increased risk of shoulder pain and injury (Bernard 1997,

Herberts et al. 1981, Grieve and Dickerson 2008, Punnett et al. 2000, van Rijn et al. 2010). Jobs

in the construction and manufacturing industries, specifically, have a particularly high

prevalence of shoulder disorders. A comparison of shoulder pain development in welders and

office workers showed that 27% of welders reported shoulder pain, compared to 2% of office

workers (Herberts et al. 1981). Further, the prevalence of shoulder tendinitis in the group of

welders was 18%. A two- to three-fold increase in shoulder injury risk existed for automobile

assembly plant worker whose jobs required flexion/abduction above 90° (Punnett et al. 2000);

this risk was further elevated if this posture was maintained for greater than 10% of the work cycle. Researchers studying the mechanistic link between repetitive overhead working postures and shoulder injury have identified upper extremity muscle fatigue as a possible intermediary, with work-induced muscle fatigue altering healthy shoulder kinematics and subsequently leading to subacromial space reduction (Michener et al. 2003, Grieve and Dickerson 2008, Dickerson et al. 2011).

Despite the increased prevalence of workplace shoulder pain and injury development, workers in jobs requiring shoulder intensive tasks are not the only population at risk. A review of shoulder pain in the general population identified the point prevalence to be 7-27%, and the one month and one year prevalence to be 19-31% and 5-47%, respectively (Pope et al. 1997). Additionally, the pain prevalence in the general population with differing occupations/lifestyles was 30% with a relatively narrow range of 22.6% to 37.8% depending on the occupation (Makela et al. 1999). Specifically, those with sedentary lifestyles had the lowest prevalence (22.6%), agriculture workers the highest prevalence (37.8%) and those working in industry, housewives or miscellaneous were reported to have between 29.1 to 30.6% prevalence. This suggests that while certain workplace exposures exacerbate the risk of shoulder injuries, shoulder pain exists across the entire population.

Much research has identified the increasing risk of shoulder injuries, particularly of the rotator cuff, with age. Both the incidence and severity of tears increases over the age of 60 years, with 28% of the population over 60 years having a full thickness tear and 26% a partial thickness tear (Sher et al. 1995). However, in the middle-aged group between 40 to 60 years, 28% were still diagnosed with a rotator cuff tear, despite 24% being partial thickness tears. In the previously discussed study evaluating welders (unexperienced, experienced and elderly), a

correlation with age was not identified, with the average age of those with supraspinatus tendinitis (39 years) not significantly different from the average age of the entire sample (Herberts et al. 1981). Age has been identified as a factor for increasing the risk of shoulder pathology in research suggesting that the increased pain that exists in workers may be due to age-related degenerative changes that make the rotator cuff more vulnerable to injury after age 40-45 years (Bjelle 1989). Thus, the high prevalence of rotator cuff disease that exists in the aging population may be a function of degenerative changes. However, innate predisposing bone geometry that increases tissue vulnerability, in addition to workplace factors that exacerbate the risk of injury at middle-age, may be contributory to the widespread development of shoulder pathology that accompanies age.

With the increased prevalence of SAIS and subsequent rotator cuff tears accompanying both age and certain occupational exposures, researchers have attempted to identify the mechanistic progression of SAIS development. Several mechanisms have been suggested, including those related to both innate bone geometry and those resulting from upper extremity muscle fatigue. Each of these mechanisms is described in Sections 2.4 and 2.5; from these discussions it is evident that there are several variables that may contribute to subacromial space[1] reduction and subsequent SAIS risk. With the subacromial space existing on a very small measurement scale (less than 2cm across the population), interpersonal variability in each of these mechanisms can pose widely differential risk for SAIS development across the population. In the existing impingement literature, this variability, and especially co-varying variability,

---

[1] The subacromial space is the area between the acromion process of the scapula and the superior surface of the humeral head where impingement of the interposed tissues can occur. It is described in detail in Section 2.3 with the aid of anatomical figures.

while discussed, has not been evaluated with respect to the distribution of risk that exists across the population.

Evaluating the morphological characteristics and kinematic relationships relevant to subacromial space reduction in a young, healthy population not yet confounded with age-related degeneration or many years of high workplace shoulder demands, provides critical information for developing prevention strategies to alleviate the risk of impingement that increases considerably with age. While many studies, including our own (Chopp et al. 2010, 2011, Chopp and Dickerson 2012) have evaluated several partial components in this area, the interrelationship of these factors, particularly in the presence of upper extremity muscle fatigue, remains elusive. Further, though each of these variables has demonstrated significant variability, there have been no attempts to quantify this variability and determine its influence on subacromial space reduction. Determining the influence of predisposing (genetic) and fatigue-related predictive variables and their relative contributions to SAIS risk has substantial rehabilitative, treatment and ergonomic implications, in addition to provoking more targeted research in the area of shoulder mechanics and injury. While morphological measures may suggest recommendations such as task avoidance and the likelihood of eventual surgery necessities, healthy and/or fatigue-related kinematic measures would inform rehabilitative treatment and ergonomic work-design decisions to prevent the risk of SAIS and subsequent injury (i.e. rotator cuff tears) through limiting fatigue likelihood of specific muscles or muscle groups.

1.2   Global Research Aim and Hypothesis

The global aim of this research was: **to evaluate the effects of morphological and fatigue-induced kinematic variability on the prediction of subacromial space geometry as a means of estimating subacromial impingement (SAIS) risk**. A combined experimental and

probabilistic modelling approach was employed to first capture the variability in several

predictive parameters in a young, healthy male population, and then implement that data into a

novel probabilistic model to predict the distribution of the minimum subacromial space width

(SAS) across the population for controlled and fatigued conditions. This distribution was then

compared to healthy and injurious classifications in the literature, as well as to the distribution of

subacromial tissue thicknesses measured from the same participant population. The unique

probabilistic approach additionally quantified the relative importance of each parameter in

reducing the subacromial space to establish whether the risk of SAIS development was more

related to innate morphology, fatigue-induced kinematic alterations, or the inter-relationship of

the two. Overall, it was hypothesized that the SAS, and subsequent risk of SAIS, would be

highly variable in the population, with a subset of participants having innate geometry that

predisposed them to SAIS risk which was further exacerbated by glenohumeral and

scapulothoracic kinematic responses to muscle fatigue.

1.3   Outline

This dissertation was conceptually divided into four symbiotic research projects which

included experimental and modelling approaches. The relationship between these project

components is illustrated in **Figure 1**. The end product was the probabilistic subacromial

geometry model developed in Stage IV (*Chapter 6*). This model was developed using data

collected experimentally in Stages II (*Chapter 4*) and III (*Chapter 5*). Stage I (*Chapter 3*) served

a dual purpose: first, as a training tool to develop a small scale probabilistic model capable of

evaluating the sensitivity of rotator cuff muscle forces to variation in geometric parameters

existing within an upper extremity deterministic model and second, as a development tool for

future research that will in part evaluate the influence of variability in exposure in addition to the variability in the response for a set exposure (which is the focus of the current work).
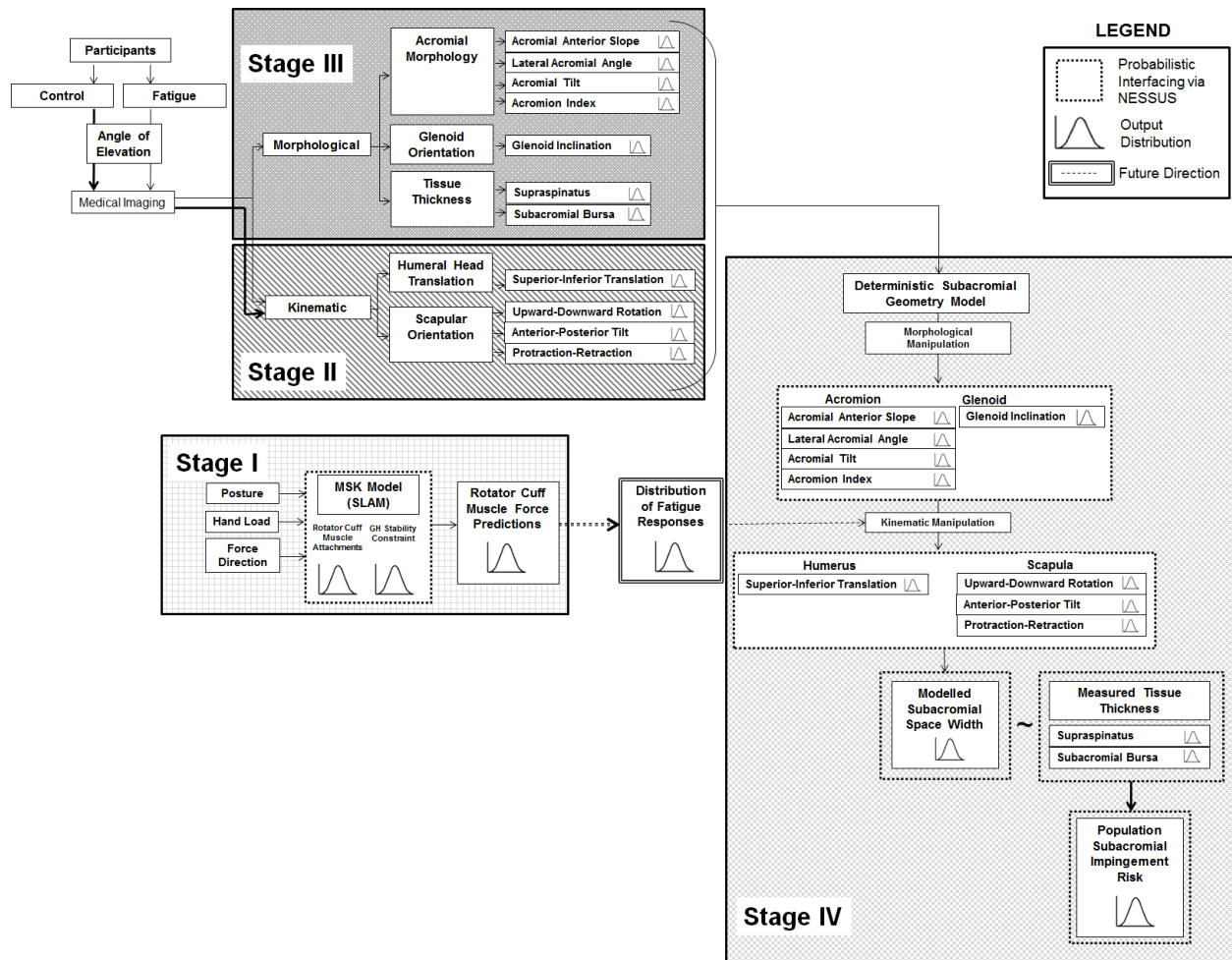
Figure 1. Flowchart outlining the contribution of each of the four projects contained within this research to the overall probabilistic model. Kinematic (Stage II) and Morphological (Stage III) data were used to create population distributions for each of the parameters, which were subsequently used as input into the probabilistic geometry model (Stage IV). Stage I serves as a development tool for future research that will evaluate the influence of exposure variability in addition to the variability in exposure responses (Stages II and III). The legend is displayed in the top, right corner of the figure.

Chapter 2

Literature Review

2.1 Overview of Literature Review

This chapter provides a review of literature relevant to measuring and modelling the subacromial space. Initially, a definition of the anatomy and motion of the shoulder is provided as a context for describing glenohumeral and scapulothoracic kinematics (Section 2.2). Subacromial impingement syndrome is described next, which includes details regarding the subacromial space and its contents (Section 2.3). This section also discusses changes in the size of this space resulting from arm elevation and different workplace factors. The following two sections review the kinematic (Section 2.4) and morphological (Section 2.5) mechanisms of subacromial space modulation, respectively. Each of the documented factors that affect the size of the subacromial space has demonstrated high variability in the population. This variability and contributors to this variability are discussed (Section 2.6). Lastly, in order to capture and describe the variability of subacromial impingement risk, probabilistic modelling methods were applied. Thus, a review of probabilistic theory and simulation methods is included (Section 2.7).

2.2 Anatomy and Motion of the Shoulder

The shoulder is highly flexible kinematically, which allows for greater mobility than any other region in the body. It is comprised of articulations between the humerus, scapula, clavicle and thorax. Motion of the shoulder is made possible by the integration of four joints: (1) acromioclavicular (between the acromion process of the scapula and the clavicle), (2) sternoclavicular (between the sternum and the clavicle), (3) glenohumeral (between the glenoid cavity of the scapula and the humeral head), and (4) scapulothoracic (between the scapula and

7

the thorax). The static and dynamic integrity of these joints is maintained by passive and active tissues, including several morphological constraints (Rockwood et al. 2009). The approximate glenohumeral and scapulothoracic relationships, when the arm is in a resting, neutral posture[2], are well known. Generally, for a healthy individual, the humeral head resides relatively central with respect to the glenoid surface of the scapula. The scapula is approximately positioned 30° anteriorly with respect to the coronal plane (termed the scapular plane), and is rotated upwards approximately 3° with respect to the midline of the sagittal plane (Rockwood et al. 2009). Documented scapulohumeral relationships or "rhythms" have identified that, during scapular plane elevation, the ratio of humeral elevation to scapular upward rotation is approximately 4:1[3] during initial phases of elevation and is then 5:4 for the remainder of elevation (Poppen and Walker 1976). This elicits an average scapulohumeral rhythm of 2:1, indicating that humeral elevation is generally double the amount of scapular upward rotation during elevation. Thus, though these joints can act independently, all work in unison to maintain healthy functional movement of the upper extremity (Inman et al. 1944).

2.2.1 *Anatomical Axes of the Shoulder*

In this section, the anatomical axes of the humerus and scapula are described, as well as humerothoracic and scapulothoracic motion and glenohumeral translations. The joint coordinate systems used to describe upper extremity kinematics are consistent throughout this document and reflect systems recommended by the International Society of Biomechanics (Wu et al. 2005).

---

[2] Neutral posture is defined as the arm resting down by the individual's side with 0° of arm elevation and 0° of axial rotation (anatomical position with thumb facing laterally).
[3] A ratio of 4:1 indicates that for every 4° of humeral elevation there is 1° of scapular upward rotation.

Humerus Joint Coordinate System (Humerothoracic Rotations)

The coordinate system of the humerus is used in conjunction with the coordinate system of the torso to describe the angle of elevation, plane of elevation and axis of rotation of the humerus with respect to the torso. The origin of the humeral coordinate system is the glenohumeral joint center of rotation, which can be estimated by regression or motion recordings (Wu et al. 2005). **Figure 2** displays the humerus coordinate system for a right shoulder;

$+Y_h$ directed approximately superior (along the long axis of the humerus)
$+X_h$ directed approximately anterior
$+Z_h$ directed laterally (approximately to the right)

The rotation sequence for the humerus with respect to the torso is Y-X-Y'. Rotating the humerus about the Y_h axis would determine the plane of elevation. Rotation about the X_h axis, with 0° rotation about the Y_h axis would elicit humeral abduction in the coronal plane (Figure 3). Rotation about the X_h axis with preceding +30° and +90° rotation about the Y_h axis would elicit scapular plane and sagittal plane (forward flexion) elevation, respectively (Figure 3). The third rotation about the Y_h' axis (long axis of the humerus) would determine the axial rotation about the humerus (internal or external rotation). Note: at 0° of humeral elevation (X_h) the plane of elevation and axial rotation are indistinguishable due to gimbal lock.
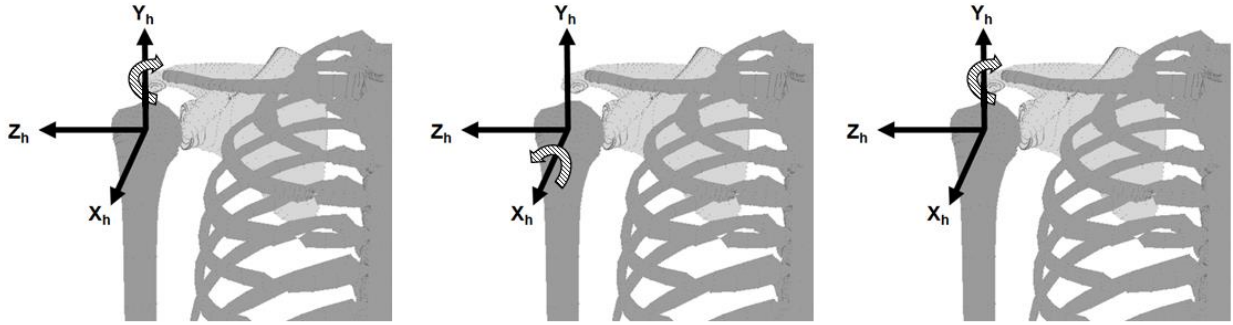
Figure 2. Humerus coordinate system: Axis of rotation: Glenohumeral Joint Center of Rotation; Rotation Sequence Y-X-Y': Y_h = Plane of Elevation, X_h = Elevation, Y_h' = Axial Rotation (Figure adapted from Wu et al. 2005).
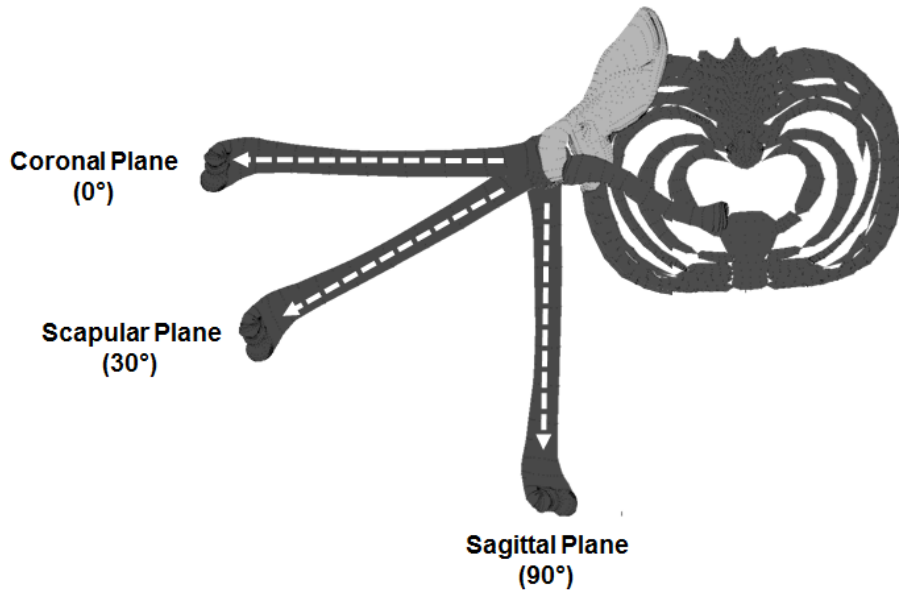
Figure 3. Planes of Humeral Elevation (Superior View): 0° = coronal plane (abduction), 30° = scapular plane, 90° = sagittal plane (flexion).

Scapula Joint Coordinate System (Scapulothoracic Rotations)

The coordinate system of the scapula can be used in conjunction with the coordinate system of the torso to describe the rotation, tilt and protraction/retraction of the scapula with respect to the torso. The origin of the scapular coordinate system is the angulus acromialis, which is the most laterodorsal point on the acromion process of the scapula (Wu et al. 2005). **Figure 4** displays the scapula coordinate system for a right shoulder;

$+Y_s$ directed approximately superior

$+X_s$ directed approximately anterior

$+Z_s$ directed laterally (approximately to the right)

The rotation sequence for the scapula with respect to the torso is Y-X-Z. Rotation about the Y_s axis produces protraction/retraction (internal/external rotation)[4]. Rotation about the X_s axis provides upward/downward rotation. Rotation about the Z_s produces anterior/posterior tilting (Figure 5). Protraction of the scapula is created by anterior movement of the lateral border of the scapula (posterior movement of the medial border of the scapula), therefore creating a "winging" effect. Downward rotation of the scapula coincides with medial movement of the inferior border of the scapula, while anterior tilting coincides with posterior movement of this inferior border.

---

[4] The terms "protraction" and "internal rotation" and the terms "retraction" and "external rotation" of the scapula are used interchangeably in the literature.
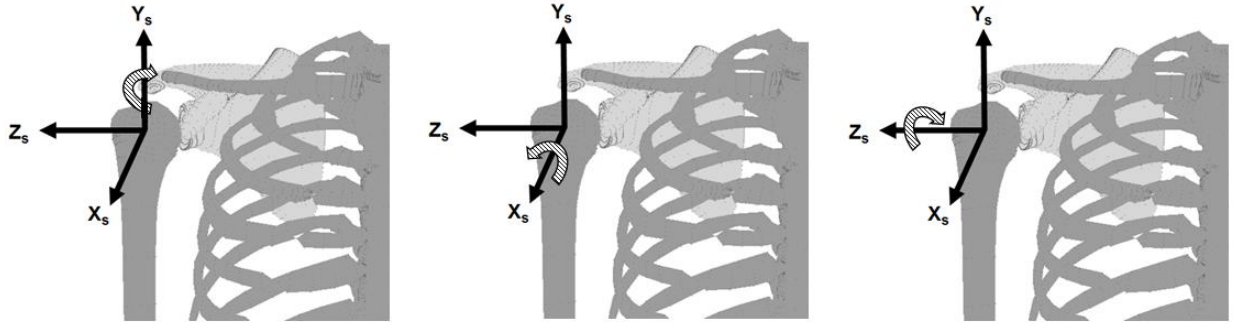
Figure 4. Scapular coordinate system: Axis of rotation: Angulus Acromialis; Rotation Sequence Y-X-Z: Y_s = Protraction/Retraction, X_s = Upward/Downward Rotation, Z_s = Anterior/Posterior Tilt (Figure adapted from Wu et al. 2005).
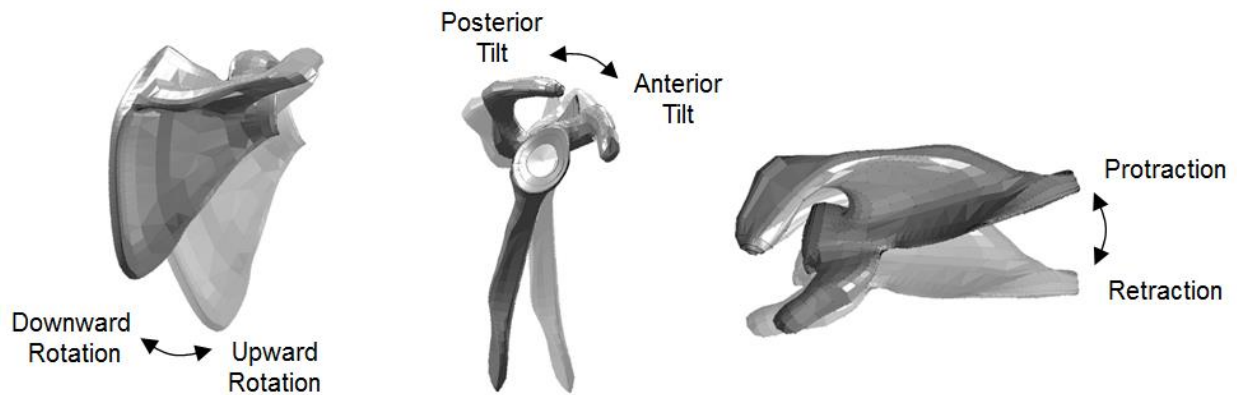
Figure 5. Three-dimensional scapular rotations (Right Shoulder): (A) Posterior view (upward/downward rotation), (B) Lateral view (posterior tilting/anterior tilting), (C) Superior view (retraction/protraction) (Figure adapted from Ludewig and Reynolds 2009).

Glenoid Cavity Joint Coordinate System (Glenohumeral Translations)

Glenohumeral translations are typically described by relating the glenohumeral joint center to the center of the glenoid cavity of the scapula (Bey et al. 2008, Poppen and Walker 1976). Translations describe the three-dimensional movement of the humeral head with respect to the glenoid cavity; these are described using a glenoid coordinate system. The origin of the

glenoid system is the center of the glenoid cavity. **Figure 6** displays the glenoid coordinate

system for a right shoulder;

$+Y_g$ directed approximately superior (from the inferior-most border to the superior-most border of the glenoid cavity, termed the "*glenoid axis*")

$+X_g$ directed approximately anterior (from the posterior-most border to the anterior-most border of the glenoid cavity)

$+Z_g$ directed laterally (approximately to the right)

This coordinate system was developed in accordance with previous definitions of glenohumeral

translation (Poppen and Walker 1976) while maintaining approximate consistency with ISB

recommendations (Wu et al. 2005). Thus, superior translation indicates upward movement of the

humeral head towards the inferior aspect of the acromion process of the scapula $(+Y_g)$, medial

translation indicates compression of the humeral head into the glenoid cavity $(-Z_g)$, and anterior

translation indicates movement of the humeral head along the $+X_g$ axis.
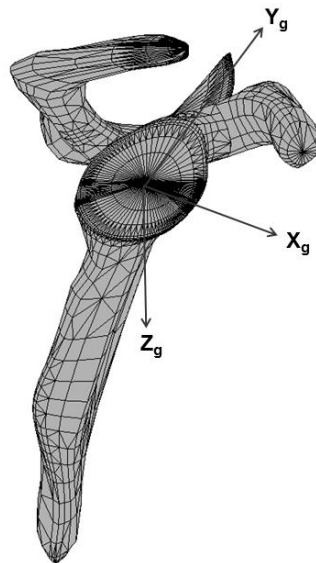
Figure 6. Glenoid coordinate system used to determine glenohumeral translations:

Superior/Inferior translation described along the Y_g axis, Medial/Lateral translation described

along the Z_g axis, Anterior/Posterior translation described along the X_g axis.

2.3   Subacromial Impingement Syndrome

The subacromial space of the shoulder is the site of the largest proportion of shoulder disorders, with subacromial impingement syndrome (SAIS) accounting for approximately half of all shoulder complaints (van der Windt et al. 1995). This space is bordered superiorly by the undersurface of acromion process of the scapula, and inferiorly by the superior portion of the humeral head. Within this space resides the supraspinatus tendon, the long head of the biceps tendon, the subacromial bursa and the shoulder capsule (Michener et al. 2003). The term "SAIS" (or "shoulder impingement syndrome") as a clinical diagnostic label has been the topic of much controversy in recent literature (Braman et al. 2014, de Witte et al. 2014). For this current research, SAIS refers to a process in which morphological or kinematic factors cause the subacromial space to reduce, thereby compressing (mechanically impinging) the interposed tissues.

2.3.1 *Subacromial Space Width in Healthy and Unhealthy Individuals*

Extensive documentation exists for the approximate magnitudes of healthy and progressively unhealthy subacromial space widths. With the arm in a neutral posture, reported healthy widths range from approximately 6 to 14mm. Conversely, in patients with radiological abnormalities, such as rotator cuff tears, the space is markedly reduced (Cotton and Rideout 1964, Golding 1962, Weiner and MacNab 1970). Specifically, the subacromial space width of seven cadaveric specimens with full-thickness rotator cuff and bursa tears was reported to be 1mm in three cases and 2, 3 and 4mm in the other three cases; it was 9mm in the last case (Cotton and Rideout 1964). Similarly, radiographs from 58 living patients who had surgically diagnosed rotator cuff tears showed that 50% had subacromial space widths less than 6mm, with 44% less than 5mm (Weiner and MacNab 1970). Typically spaces with minimum widths below

5mm were characterised as unhealthy, and spaces above 7mm were considered healthy, while spaces in the 5-7mm range remained inconclusive.

2.3.2 *Work-related Impingement Exposures*

Two global theories have been presented regarding the initiation of SAIS. Both intrinsic and extrinsic mechanisms, while precipitated differently, can result in SAIS (Michener et al. 2003, Seitz et al. 2011, de Witte et al. 2011). Intrinsic impingement is a process whereby gradual or acute tissue loading and/or age-related degeneration causes partial or full-thickness tendon tears, which subsequently leads to kinematic changes, and consequently tissue impingement. Alternatively, extrinsic impingement is an exposure-related process, whereby certain factors alter healthy glenohumeral and scapulothoracic kinematics which leads to subacromial space reduction and thus impingement and damage of the interposed tissues.

The differential postulated mechanisms of impingement initiation have resulted in divergent research foci. Intrinsic impingement is not easily preventable. A positive linear relationship exists between partial or full-thickness rotator cuff tears and age, with 50% of the population having tears in their dominant arm by age 60 and 80% having tears by age 80 (Milgrom et al. 1995). Due to these complications, more research has focused on assessing the multitude of extrinsic factors (morphological and/or kinematic) that can mechanically alter the glenohumeral and scapulothoracic relationships in an attempt to predict their effects on subacromial space reduction. This dissertation specifically explores extrinsic impingement.

Many mechanical exposures are capable of modulating the subacromial space. Different agents, such as posture, force and repetitive activity, all interact with the musculoskeletal tissues in this region to create internal exposures (Wells et al. 2004); these exposures can subsequently increase the risk of space reduction and consequently, SAIS.

2.3.2.1 Posture

Arm posture influences the development of shoulder pain and injury. A strong association exists between working with the arms above shoulder height (approximately 90° of elevation) and the development of pain and injury (Bernard 1997, Herberts et al. 1981, Grieve and Dickerson 2008, Punnett et al. 2000, van Rijn et al. 2010). Specifically, SAIS, subsequently leading to damage of the rotator cuff tendons is recognized as the predominant injury resulting from these awkward postures (Miranda et al. 2005, Svendsen et al. 2004, van Rijn et al. 2010). This has resulted in the extensive evaluation of the relationship between upper extremity posture and alterations in subacromial space size.

Both humeral elevation (both passive and active) and axial rotation demonstrably alter the size of the space. The space may decrease by as much as 6mm as the arm is elevated (Bey et al. 2007, Graichen et al. 1999a). This reduction in space with arm elevation is attributed, at least partly, to the greater tuberosity of the humerus, which moves closer toward the acromion process during elevation (Graichen et al. 1999b). However, this finding was only consistent for elevation angles up to approximately 90°, after which conflicting results alternately report increases, decreases or no change in space size (Bey et al. 2007, Graichen et al. 1999b, Hinterwimmer et al. 2003). Humeral elevation and muscular contributions also interact, in that abducting muscle activity further reduces the space compared to passive elevation, and that adducting activity increases the space (Graichen et al. 1999a, 2005, Hinterwimmer et al. 2003). This coincides with findings that strengthening adductor muscles with large depressor moment arms, such as pectoralis major, latissumus dorsi and teres major, increased the subacromial space (Hinterwimmer et al. 2003, Kuechle et al. 1997). Axial rotation of the humerus may also alter the size of the space. In one study, with the arm elevated to 90° in the scapular plane, the space

reduced by 3mm when the humerus was externally rotated, compared to when internally rotated (Graichen et al. 1999a).

2.3.2.2 Repetition

A defined relationship between repetitive working tasks and the development of SAIS exists. However, its influence has rarely been studied independently. Rather, the interaction between overhead arm postures and repetitive activity have been discussed in terms of their relationship to SAIS and rotator cuff pathology (Frost and Andersen 1999, Jobe et al. 2000). However, it was determined that workers whose jobs entailed repetitive tasks were at two to three times greater risk of developing shoulder tendinitis with positive signs of SAIS (Frost et al. 2002). Additionally, the relationship between repetitive tasks and non-specific shoulder pain has been widely reported in the literature (Bernard 1997, Leclerc et al. 2004, Miranda et al. 2005).

2.3.2.3 Force

The relationship between force requirements and SAIS development has received little attention, with only a few existing conflicting studies. In one study, workers having high force requirements ($\geq$10% of their maximal voluntary contraction (MVC)) were more likely to develop shoulder tendinitis (OR = 4.21), compared to those with low force requirements (OR = 2.17) (Frost et al. 2002). Similarly, female participants exposed to heavy lifting greater than 10 times per day, and high hand force requirements for greater than one hour/day for over three years, demonstrated an increased risk of developing shoulder disorders (Miranda et al. 2005). In other research, no significant relationship between low, medium and high hand force requirements and rotator cuff pathologies were identified in machinists, car mechanics and house painters (Svendsen et al. 2004).

2.3.2.4 *Relationship between workplace agents and the development of muscle fatigue*

Upper extremity muscle fatigue is a possible intermediary that relates these work-related task characteristics to SAIS development (Dickerson et al. 2011, Grieve and Dickerson 2008, Michener et al. 2003). The established relationship between repetitive or prolonged work above shoulder height and the development of upper extremity muscle fatigue, in addition to subjective ratings of discomfort (Grieve and Dickerson 2008, Herberts and Kadefors 1976, Herberts et al. 1980, Sakakibara et al. 1995, Wiker et al. 1989), has led to the evaluation of the relationship between differential muscle fatigue and subacromial space modulation, by means of altered glenohumeral and scapulothoracic kinematics. These kinematic alterations and their relevance to SAIS development are discussed in Section 2.4.

2.3.3 *Location of minimal subacromial space width*

Although research evaluating changes in the subacromial space most often solely report absolute magnitudes of the *minimum subacromial space width* (SAS), some have additionally examined the location of the SAS, and associated implications of that location, for tissue impingement risk. During scapular plane elevation, the acromial contact region has been shown to move from the anterolateral edge (neutral posture) to the anteromedial edge (elevated posture) (Flatow et al. 1994). Thus, at all arm positions, the anterior acromion was the primary site for likely impingement; this was previously suggested (Neer 1983). With respect to the humerus, the contact region was initially located at the proximal ends of the biceps and supraspinatus tendons; however, as the arm elevated, the contact region moved more distally along these tendons, and between 60° and 120° the contact was primarily problematic for the supraspinatus tendon. This suggests that mid-range elevation is particularly problematic for SAIS and subsequent tissue damage.

The location of the SAS width respect to the interposed supraspinatus tendon and/or its insertions point on the greater tuberosity has been studied. In one study, at 30° and 60° of abduction, the SAS vector passed through the supraspinatus tendon in all 12 subjects (Figure 7) (Graichen et al. 1999a). At 90° abduction, the vector was located laterally to the supraspinatus tendon in half of the subjects, and with further abduction, it was located laterally in all subjects (Figure 7). Additionally, when the arm was internally rotated, the vector passed through the supraspinatus in all subjects, with the contact point on the anterior-inferior border of the acromion. When the arm was externally rotated, the vector was located at the central part of the acromion and passed through the supraspinatus in just under half of the cases. A subsequent study reported that the SAS vector passed through the supraspinatus tendon at angles of 60° and 90° and passed laterally at 120° (Graichen et al. 1999b). More recently, the SAS vector has been shown to be located within the tendon footprint (insertion point) of the supraspinatus between 34° and 72°, while moving laterally to the humeral shaft with further elevation (Giphart et al. 2012). The discrepancy in this the range deemed to be critical for tissue compression is likely attributed to methodological differences, including the imaging posture and plane of humeral elevation. Specifically, in the earlier research, participants were lying supine with their arm elevated in abduction (Graichen et al. 1999a,b), while in later research participants were seated upright with their arm elevated in both scapular plane elevation and forward flexion (Giphart et al. 2012). The upper end of the range in which the SAS vector was located within the supraspinatus tendon footprint was demonstrated to differ by plane of elevation, with a limit of $72 \pm 12°$ shown for scapular plane elevation and $65 \pm 8°$ for forward flexion (Giphart et al. 2012). It is likely that upper limit of 90° demonstrated in several participants in earlier research was due to the humeral elevation plane, as well as the possible gravitational effects of the supine

posture during the image capture. However, this discrepancy may also be related to the participant population. The sample size in each study was ≤12, with highly variable outcomes demonstrated. Thus, while an upper limit of 90° may be an overestimation, a limit of 72° may not be representative of the entire population.
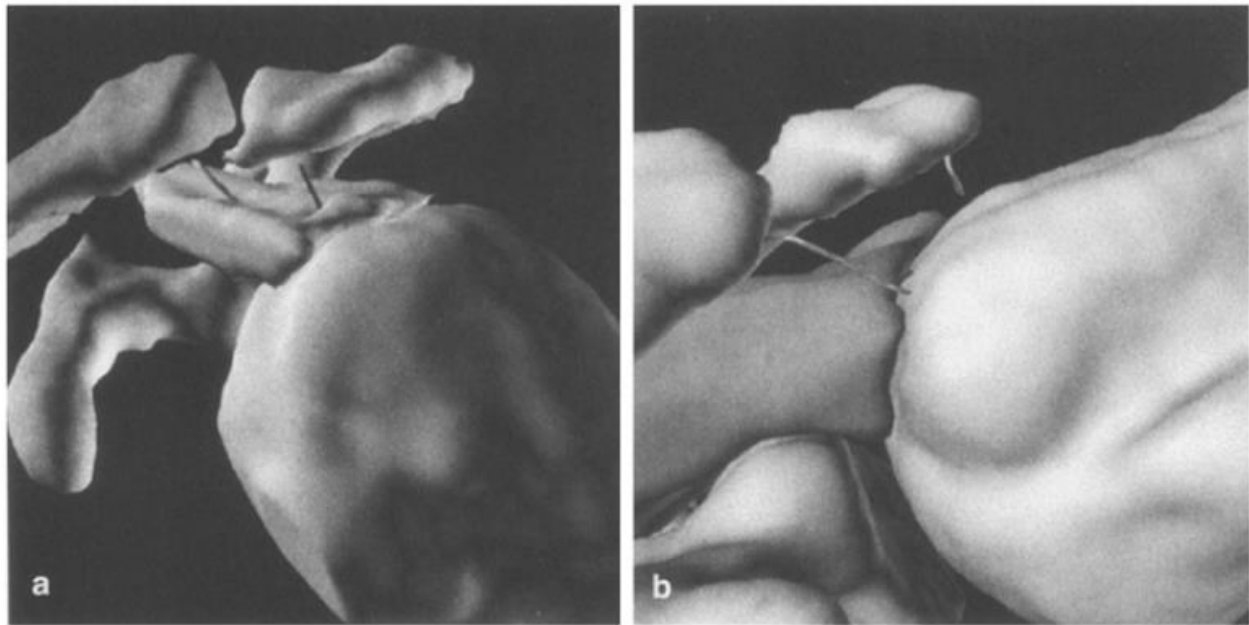
Figure 7. 3D reconstruction of subacromial space: location of minimum subacromial space width (SAS) vector at 60° (a) and 120° (b) of abduction. Note that at 60° (a) the SAS vector is passing through the supraspinatus tendon, whereas at 120° (b) the vector is passing lateral to the tendon (Figure obtained from Graichen et al. (1999a) with kind permission of Springer Science+Business Media).

Arm postures and their related musculoskeletal geometric changes thus critically modify SAIS risk assessment, as, although the SAS may be smaller at higher abduction angles, it may not pose high risk for rotator cuff impingement. Mid-range elevation, in the 60° to 120° range, is consistently implicated as particularly problematic for the development of supraspinatus tendon impingement. Several clinical diagnostic tests for SAIS such as the Hawkins-Kennedy, the Jobe-

Yocum and the internal rotation resistance stress test all involve resisted rotation with the arm first positioned at 90° of elevation (Rockwood et al. 2009). Additionally, the 'painful arc' test is one of the most well-known SAIS diagnostic tests. A positive test occurs when the patient exhibits pain in the 60 to 120° arm elevation range, while pain in a higher range of elevation suggests acromioclavicular joint pain (Kessel and Watson 1977). As recent research suggests that the SAS vector passes laterally to the supraspinatus tendon at elevation angles <90°, this implicates other possible mechanisms of pain development during further elevation to an overhead posture. Internal impingement, which occurs when the articular surface (undersurface) of the supraspinatus tendon becomes entrapped between its attachment site on the humerus and the superior glenoid cavity, is a likely cause for shoulder pain and/or rotator cuff pathologies at higher elevation angles, particularly when coupled with humeral external rotation (Braman et al. 2014). Several additional structures have been implicated as possible contributors to shoulder pain, including the biceps tendon, superior glenoid labrum and the coracoacromial ligament (Braman et al. 2014). Additionally, it is important to consider that while research suggests that the supraspinatus tendon has vacated the subacromial space at elevated postures thereby no longer posing risk for SAIS, thickening of the subacromial bursa may still be cause for SAIS and subsequent pain at higher elevation angles (Kibler et al. 2013, Tsai et al. 2007). Thus, the assessment of SAIS risk requires not only the consideration of the changing SAS, but also the location of this SAS vector in relation to the subacromial tissues.

2.4   Kinematic Mechanisms of Subacromial Impingement

Glenohumeral (GH) and scapulothoracic (ST) relationships modulate the size of the subacromial space posing possible risk for SAIS. Two predominant mechanisms that can reduce the subacromial space are: (1) superior humeral head translation and (2) scapular reorientation.

Humeral head translation reduces the subacromial space from the inferior aspect (bottom-up mechanism) whereby the humeral head position migrates superiorly with respect to the glenoid cavity, consequently impinging tissues interposed within the space. Scapular reorientation involves a series of three-dimensional scapular rotations which orient the acromion more inferiorly, impinging tissues from the superior aspect (top-down mechanism) (Figure 8). The following sections discuss these mechanisms, while also highlighting some key limitations of previous measurement techniques for GH and ST kinematic changes.
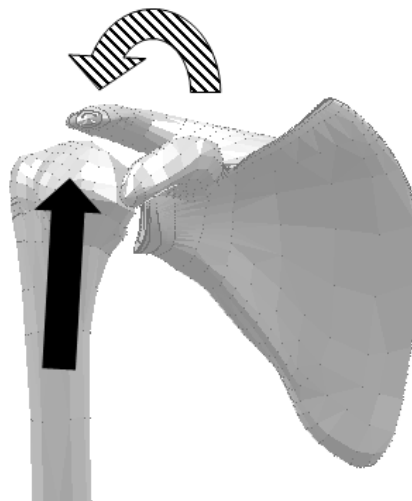
Figure 8. Proposed mechanisms of subacromial impingement: (1) Superior humeral head translation (Solid Arrow), (2) Scapular reorientation (Dashed arrow).

2.4.1 *Superior Humeral Head Translation*

Humeral head translation affects the glenohumeral relationship. Assuming a neutral position, with the geometric center of the humeral head approximately aligned with the center of the glenoid cavity, superior humeral head translation is movement of the center of the head upwards along the vertical glenoid axis (Figure 6), which moves it closer to the acromion process. Mechanically, translation has been attributed to the coupling of the deltoid and rotator cuff musculature. Muscular contributions towards centering or translating the humeral head have

been established through measuring muscle moment arms and their angle relative to the glenoid cavity (Poppen and Walker 1978). The supraspinatus moment arm remained relatively constant in length throughout the range of abduction (22mm) and was angled at approximately 80° to the glenoid face, thereby classifying it primarily as a humeral head compressor, while also an elevator. Concurrently, the moment arms of the anterior and middle deltoid gradually increased over the range of abduction (5 to 44mm and 17 to 32mm, respectively) with angles of 30° at 30° of abduction, 60° at 90° of abduction and 80° at maximal abduction, implying that its upward shearing force, pulling the humeral head superiorly, is primarily present during the initial elevation phase.

GH translation has been evaluated for a variety of conditions. Specifically, the influences of: (1) elevated arm postures, (2) dynamic arm elevation, (3) shoulder instability or rotator cuff tears, and (4) muscle fatigue have all been studied with regards to the magnitude of superior-inferior translation of the humerus with respect to the neutral, centralized position on the glenoid (Table 1). With the rotator cuff positioned such that it compresses the humeral head into the glenoid cavity, mechanical deficiency of the rotator cuff by means of injury would hinder its ability to maintain a centered GH position, thereby creating increased translation throughout the range of elevation. Additionally, aside from the superior humeral translation resulting from shoulder instability or rotator cuff injury, rotator cuff muscle weakness, by means of exhausting the rotator cuff through a fatiguing protocol, produces a similar result, though the magnitude of translation is less than in patients with tears.

Table 1. Trends and approximate magnitudes of superior-inferior humeral head translation with respect to the glenoid cavity for 4 different conditions (static elevated arm postures, dynamic elevation, shoulder injury and muscle fatigue).

Condition	Trend	Magnitudes	Reference
Arm Elevation (Static Arm Positions)	Superior translation during initial elevation, followed by inferior translation to more central position (>45 to 60°)	• 0° to mid-elevation = ~1 to 2.5mm	Chopp et al. 2010, Graichen et al. 2000 Matsuki et al. 2012
	Superior translation during initial elevation, followed by constant position	• 0 to 60° = ~3mm • 60°+ = <1mm superior/inferior	Poppen & Walker 1976
	Constant humeral head position throughout the range of elevation	• Across elevation = <0.7mm	Chen et al. 1999 Deutsch et al. 1996 Yamaguchi et al. 2000
	Continuous superior translation from initial inferior position to central position	• ~2.9mm	Cote et al. 2009
Arm Elevation (Dynamic Arm Elevation)	Greater superior translation during dynamic elevation than at same postures measured statically	• Largest difference = 0.92mm	Bey et al. 2008 Teyhen et al. 2010
Rotator Cuff Tear/ Shoulder instability	Increased superior translation in both neutral and elevated postures	• ~Injured has double superior translation compared to healthy • Tear > Instability > Healthy • Multi-tear > Single tear • Correlation with pain (asymptomatic vs. symptomatic) conflicting	Bey et al. 2008 Bezer et al. 2005 Deutsch et al. 1996 Keener et al. 2009 Paletta et al. 1997 Poppen & Walker 1976 Yamaguchi et al. 2000
Muscle Fatigue	Increased superior translation present generally: Tear ≥ Fatigue ≥ Healthy	• ~1 to 2mm > Healthy • Largest difference at higher elevation angles due to lack of inferior translation present at these angles	Chen et al. 1999 Chopp et al. 2010 Cote et al. 2009 Royer et al. 2009 Teyhen et al. 2008

Though not as well studied as superior-inferior translation of the humeral head, some data exists regarding the anterior-posterior displacement of the humeral head in healthy and injured populations. Though anterior translation has been linked to shoulder instability and/or SAIS

(Ludewig and Cook 2002, Michener et al. 2003, Paletta et al. 1997), the results are inconclusive, and the volume of evidence is limited compared to that for superior translation.

2.4.2 *Scapular Reorientation*

Scapular reorientation affects the ST relationship. While altered scapular positioning as a potential cause of SAIS is less definitive, notable trends exist. In a neutral posture, the scapula has a resting position of 30° anterior with respect to the coronal plane (thus termed the *scapular plane*), and is rotated upwards approximately 3° with respect to the midline of the sagittal plane (Rockwood et al. 2009). The scapula remains stable with respect to the thorax by means of periscapular stabilizing musculature, primarily the upper and lower trapezius and serratus anterior (Michener et al. 2003, Phadke et al. 2009). Similar to humeral head translation, certain normal and abnormal kinematics occur for many scenarios including healthy elevation, unstable or impinged shoulders and with upper extremity muscle fatigue (Table 2).

Table 2. Trends and approximate magnitudes of three-dimensional scapular kinematics for 3 different conditions (arm elevation, shoulder injury and muscle fatigue).

Condition	Trend	Magnitudes	Reference
Arm Elevation	Upward rotation (UR), posterior tilt (PT), retraction (R)	• Inconsistent and highly variable in magnitude • UR ~ 34-50° • PT ~ 15-30° • R ~ 13-24°	Ebaugh et al. 2005 Freedman & Munro 1966 Inman et al. 1944 Ludewig et al. 1996 McClure et al. 2001 Poppen & Walker 1976
Rotator Cuff Tear/ Shoulder instability	Healthy kinematics (UR, PT, R) impaired or reversed = downward rotation, anterior tilt, protraction *One researcher found increased UR and PT trend for injured patients at increased elevation angles*	• Inconsistent and highly variable (~ <10°)	Endo et al. 2001 Lin et al. 2005 Ludewig & Cook 2000 Ludewig & Reynolds 2009 Lukasiewicz et al. 1999 *McClure et al. 2006 Phadke et al. 2009

Muscle Fatigue	Increased or no change (one or all) of: UR, PT, R *Similar to healthy kinematics*	• Inconsistent and highly variable (~ <10°)	Chopp et al. 2011 Ebaugh et al. 2006 McQuade et al. 1998 Suzuki et al. 2006
	Decreased/reversed (one or all) of: UT, PT, R *Similar to injured kinematics*	• Inconsistent and highly variable (~ <10°)	Borstad et al. 2009 Su et al. 2004 Tsai et al. 2003

Though more relative uncertainty exists regarding the directionality of scapular orientation changes that reduce the subacromial space compared humeral head translational changes, certain orientations have been identified in those with SAIS. Specifically, a downwardly rotated, anteriorly tilted and protracted scapula would produce a top-down intrusion of the acromion, thereby reducing the subacromial space (Ludewig and Cook 2000, Ludewig and Reynolds 2009, Michener et al. 2003). Further, kinematic and electromyographic results have prompted discussion regarding the most critical movement impacting SAIS risk. As discussed, most early research solely examined scapular upward/downward rotation (Freedman and Munro 1966, Inman et al. 1944, Poppen and Walker 1976). Upward rotation of the scapula rotates its inferior border laterally and the acromion process upwards, thereby increasing the acromio-humeral interval and allowing more space for the subacromial tissues. This upward motion is controlled by the combined activity of the serratus anterior and the upper and lower portions of the trapezius muscle. Posterior tilting of the scapula rotates the inferior border anteriorly and the acromion process posteriorly, similarly increasing the subacromial space. Some authors argue that this tilting is the most critical scapular movement for SAIS prevention as the anterior portion of the acromion is the most common site of tissue impingement (Flatow et al. 1994, Ludewig and Cook 2000). This in turn would implicate serratus anterior as the most critical muscle for reducing SAIS risk via a scapular orientation mechanism, as it generally has the most advantageous moment arm for tilting the scapula (Borstad et al. 2009). Additionally, Solem-Bertoft et al. (1993) documented that scapular retraction, a motion controlled primarily by the

serratus anterior and lower trapezius muscles, also re-locates the anterior acromion into a more elevated position, thereby increasing the subacromial space (Borstad et al. 2009). Thus, impairment of scapular upward rotation, posterior tilting and retraction during arm elevation may increase the risk of SAIS development. This leads to a further assertion that inhibition of serratus anterior and upper and lower portions of the trapezius muscle by means of injury or fatigue may provoke these potentially harmful orientation changes.

Impingement Mechanisms Summary:

The totality of existing evidence leads to the following conclusions:

I. A superiorly (and possibly anteriorly) translated humerus, mediated by rotator cuff dysfunction, poses risk for SAIS through reduction of the subacromial space from a bottom-up intrusion, primarily when the humerus is in mid-range elevation.

II. A reduction in scapular upward rotation, posterior tilt and retraction, mediated by serratus anterior and trapezius dysfunction, likely poses risk for SAIS through a reduction of the space from a top-down intrusion of the acromion process.

Together, these mechanisms cause the greater tuberosity of the humerus to come into close contract with the anterior portion of the acromion, leaving considerably less space for the interposed tissues (Ludewig and Cook 2000). However, reported statistically significant changes in the above research were on a small measurement scale (<5mm and 5°), making it necessary to evaluate the clinical relevance of these changes.

2.5   Morphological Mechanisms of Subacromial Impingement
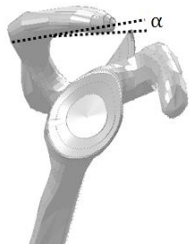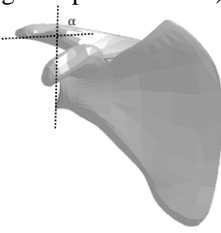
Besides the influence of muscle damage and/or fatigue on GH and ST kinematics, specific innate factors may predispose an individual to SAIS based on their musculoskeletal
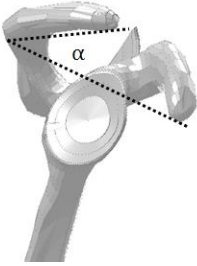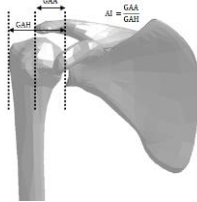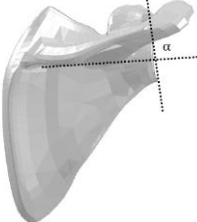
geometry. Acromial morphology, glenoid angulation and subacromial tissue thickness all influence the overall size of the subacromial space, and subsequently, the risk of SAIS.

2.5.1 *Acromial and Glenoid Morphology*

Morphological characteristics of both the acromion and glenoid cavity relate to SAIS and/or rotator cuff pathology (Table 3).

Table 3. Description of morphological variables, their classifications (unhealthy = association with rotator cuff pathology) and relation to age and/or pathology.

Variable	Definition	Classifications	Relation to Age/Pathology	Reference
Acromial Anterior Slope (Acromial Type)	Angle formed by the intersection of a line drawn along the undersurface of the acromion and a line extending from the tip to the junction of the hook (angle: anterior) 	• Type I (0-12°*): *Flat* • Type II (13-27°*): *Curved* • Type III (>27°*): *Hooked*	Increased acromial anterior slope angle associated with: • Increased rotator cuff tear prevalence • Increased tear severity • Increased age	Balke et al. 2013 Bigliani 1986 Edelson 1995 Gill et al. 2002 Kitay et al. 1995 MacGillivray et al. 1998 *Toivonen et al. 1995 Tuite et al. 1995
Lateral Acromial Angle	Intersection of the glenoid axis with a line drawn along the undersurface of the acromion process (angle: superior/medial) 	• ≤70° (Unhealthy) • >70° (Healthy)	Decreased lateral acromial-AG angle associated with increased rotator cuff tear prevalence	Banas et al. 1995 Tetreault et al. 2004

Acromial Tilt	Angle formed by a line connecting the most anterior and posterior points on the inferior aspect of the acromion, and a line connecting the posterior point on the acromion with the most inferior point on the coracoid process (angle: anterior)	• <30° (Unhealthy) • >30° (Healthy)	Decreased acromial tilt associated with increased rotator cuff tear prevalence	Aoki et al. 1986 Balke et al. 2013 Kitay et al. 1995 Zuckerman et al. 1992
Acromion Index	Ratio of the glenoid-acromial distance (glenoid axis to lateral acromion) to the glenoid-humeral distance (glenoid axis to lateral humerus)	• >0.65 (Unhealthy) • <0.65 (Healthy)	Increased lateral extension of the acromion (increased ratio) associated with increased rotator cuff tear prevalence	Balke et al. 2013 Nyffeler et al. 2006 Torrens et al. 2007
Glenoid Inclination	Intersection between the glenoid axis and a line drawn along the floor of the supraspinatus fossa (angle: superior/lateral)	• >90°: *Upward Tilt* • <90°: *Downward Tilt*	Increased glenoid inclination angle associated with: • Increased rotator cuff tear prevalence • Increased superior humeral head migration	Flieg et al. 2008 Hughes et al. 2003 Konrad et al. 2006 Maurer et al. 2012 Wong et al. 2003

Acromial type is the most been widely studied morphological parameter and has exhibited extensive interpersonal variability. Historically reported acromial type variation has been described, noting an incidence of type I acromion that ranged from 3 to 43%, type II from

28 to 62.3% and type III from 2.1 to 69.5% (Wang and Shapiro 1997). Though the relationship between these morphological characteristics and rotator cuff pathology is generally agreed upon, the variability could contribute to other conflicting reports, such as the relationship between acromial type and age (Edelson 1995, Gill et al. 2002, Vahakari et al. 2010). Even among a young, healthy population, high variability in acromial morphology has been documented (Nicholson et al. 1996, Vahakari et al. 2010).

Conflicting research describes the prevalence of different acromial types. It has been theorized that acromial types are not genetic variants, but rather develop over time. Projections or 'bone spurs' extending from the coracoacromial arch may develop due to ossification at the acromial insertion of the coracoacromial ligament (which extends from the acromion to the coracoid processes of the scapula) (Nicholson et al. 1996). These ossifications potentially cause the 'hook' in the acromion. This has implicated mechanistic causes, as tension on the coracoacromial ligament resulting from attempting to limit superior humeral head translation (particularly in the absence of healthy rotator cuff function) may lead to traction-type spurs (Nicholson et al. 1996).

2.5.2 *Tissue Thickness and the Available Subacromial Space*

The vulnerable contents of the subacromial space include the supraspinatus tendon, the long head of the biceps tendon as well as the subacromial bursa. The subacromial bursa acts to allow smooth motion between the rotator cuff and the overlying acromion (Rockwood et al. 2009). Inflammation of the tendons or bursa can create a reduction in the overall space thereby contributing to SAIS. Moreover, those with SAIS often have this tissue inflammation. Neer (1983) first described the three universally known stages of SAIS which are classified based on increasing tissue damage severity.

➢ Stage I impingement: edema and hemorrhaging (symptoms reversible)

➢ Stage II impingement: fibrosis and tendinitis, as well as bursal thickening

➢ Stage III impingement: rotator cuff tears, bicep ruptures, bone changes (i.e. spurs)

Thus, this is a cascading problem, with subacromial space reduction causing the interposed tissues to become inflamed and this tissue inflammation further reducing the subacromial space ultimately resulting in tendon tears.

There are limited measurements of the relationship between the size of the subacromial space and the corresponding subacromial tissue thickness. However, even among healthy individuals, the tissues generally occupy approximately 50-75% of the space (Girometti et al. 2006, Michener et al. 2013, Wang et al. 2005). Reported subacromial tissue thickness measurements vary extensively, with magnitudes of approximately 2.5-7mm reported in healthy individuals (Cholewinski et al. 2008, Girometti et al. 2006, Joensen et al. 2009, Leong et al. 2012, Michener et al. 2013, Wang et al. 2005). The relationship between tissue thickness and injury remains inconclusive. Some suggest that increased tissue thickness is a sign of chronic tearing and SAIS onset (Joensen et al. 2009, Leong et al. 2012, Michener et al. 2013, Wang et al. 2005), while others that impingement reduces the tissue thickness (Cholewinski et al. 2008). Recently, subacromial tissue thickness and the minimum subacromial space width have been measured ultrasonically in healthy participants and those with SAIS (Michener et al. 2013). Participants with SAIS had significantly greater supraspinatus tendon thickness (0.6mm) and occupation ratios (7.5%) (ratio of tissue thickness to minimum subacromial space width) compared to the healthy group. However, even among healthy participants, with their arms in a neutral posture, the tissues occupied over 50% of the space.

Therefore, although documenting the subacromial space width as a function of elevation angle and muscle debilitation is important in predicting SAIS risk, it is critical to consider the thickness of tissues residing within the space. The subacromial space reduces with humeral elevation in healthy individuals. Although the tissue volume conceivably remains constant during arm elevation, the tissue thickness interposed within the minimum subacromial space may change, which may either alleviate or exacerbate SAIS risk.

2.6 Variability in Shoulder Mechanics and Musculoskeletal Geometry

Each of the kinematic and morphological parameters discussed exhibit high interpersonal variability. All of these parameters exist on different measurement scales (millimeters and degrees) while influencing a final minimum subacromial space width that is less than 2cm (typically less than 1.5cm). Thus, large variability in any or all of these parameters has significant implications for SAIS risk (Dickerson et al. 2011). Two main types of variability contribute to the total variability present in these parameters: (1) innate variability ('real' variability), and (2) introduced variability ('error-induced' variability). The following sections describe the many factors that may contribute to each type.

2.6.1 Innate Variability

The population variability present in these parameters is partly attributed to the innate or 'real' kinematic and morphological differences that exist between humans in a given population. Internal geometry, independent of health status, varies substantially, even between those of similar age and the same gender. Differences exist due to variability in factors related to musculoskeletal geometry and differing responses to the same exposure. In research evaluating a specific population sub-group (i.e. those with rotator cuff injury or muscle fatigue), individual differences within that sub-group, such as location and severity of tear, or level of fatigue may

32

have a large effect on study variability (Yamaguchi et al. 2000). Further, whether subjects are given the identical hand load, or even if the load given is scaled to their strength, their level of fatigue and output response to that level of fatigue will vary in the population (Dickerson et al. 2011). The importance of variability in injury assessment was highlighted in a study reporting that even subjects performing the same task under strictly controlled conditions demonstrated considerable inter- and intra-subject variability in responses (Mathiassen et al. 2003). In previous work evaluating fatigue-induced humeral head translation, mean humeral head position in pre- and post- fatigue states with the arm at neutral was -0.85mm and 0.01mm, respectively (Chopp et al. 2010). However, individual analysis demonstrated that the range of humeral head position for these two states was -3.10mm to 3.50mm and -3.10 to 2.60mm. Additionally, maximal upward excursion (from pre-fatigue to post-fatigue) was 4.60mm, while the mean only indicated modest upward translation magnitudes of less than 1mm. Many studies evaluating translation, scapular orientation and other measures have also discussed considerable inter-subject variability, stating that many subjects do not represent the mean (Ebaugh et al. 2005, Graichen et al. 1999a, Ludewig and Cook 2000, Ludewig et al. 2009, McClure et al. 2006, , Seitz and Michener 2011).

This variability has implications that indicate that seemingly small mean differences may have large clinical importance. For example, while differences in scapular positions as small as 4-5° have existed between experimental conditions (active and passive elevation) (Ebaugh et al. 2005), this same magnitude of change previously distinguished healthy and impinged patients (Ludewig and Cook 2000). The clinical implications of these variable results have been considered by evaluating humeral head translation in the context of tissue thickness and allowable space (Chopp et al. 2010). Accordingly, less than 1mm of superior humeral head translation may influence SAIS risk. Thus, with certain members of the population experiencing

greater than 4mm of translation, it is critical to consider population distributions when interpreting SAIS risk. This is by extension potentially relevant to all of the contributing factors influencing the subacromial space size due to their similar levels of variance.

2.6.2 *Introduced Variability*

A second contributor to the variability of reported values of these output parameters is error that is introduced by methodological errors or constraints. These sources of variability include: equipment constraints, methodological differences, modifications in measurement and processing techniques, as well as other human errors. Though equipment constraints are typically consistent within a well-controlled study, all others could introduce artificial inter-subject variability within a study, or could be the source of contrasting results across studies. Some common methodological discrepancies include:

1. Scapular Plane Definition

    ➢ *30° anterior to the coronal plane* as per Chen et al. 1999, Chopp et al. 2010, 2011, Cote et al. 2009, Freedman and Munro 1966, Laudner et al. 2006, Ludewig et al. 1996, Teyhen et al. 2008

    ➢ *40° anterior to the coronal plane* as per Borstad et al. 2009, Ludewig and Cook 2000, Ludewig et al. 2009, Lukasiewicz et al. 1999, McClure et al. 2001, McClure et al. 2006

    ➢ Range (*30-45°* or *40±10° anterior to the coronal plane*) as per Ebaugh et al. 2005, Ebaugh et al. 2006, Poppen and Walker 1976

2. Specific anatomical landmarks used for measurement (Langenderfer et al. 2009)

3. Conventions used to calculate joint angles and describe motion

    ➢ Most researchers have adhered to ISB recommendations (Wu et al. 2005)

4. Human/Experimental Error

   ➢ Consistency in posture

   ➢ Consistency in measurement protocol

   ➢ Consistency in measurement technique (Seitz and Michener 2011)

Processing discrepancies have often been addressed by testing the reliability of the measurement with the use of both intra- and inter- observer reliability techniques. The original experimenter performs the measurement multiple times to test their own reliability (intra-) and then compares those results to a secondary (ideally expert) measurer (inter-).

   Therefore, as each of the measures influencing the subacromial space width vary considerably due to both individual geometric differences and potentially introduced methodological errors there is a critical need, when capturing subacromial space geometry, to consider the distribution of output, rather than collapsing all data and concentrating on summary statistics that depend primarily on mean values. This also provides reinforcement for the recommendation to capture all measures simultaneously and assess the contents of the space in the context of the allowable space (occupation ratio); this will provide more confidence in the identification of those in the population that are at particular risk for SAIS development, while also establishing to a degree, the covariance of parameters.

2.7 Probabilistic (Stochastic) Modelling in Biomechanics and its application to Subacromial Impingement Prediction

Two primary forms of analysis can be employed when modelling the behaviour of a system: deterministic and probabilistic[5]. While deterministic analysis calculates the output associated with a particular set of inputs, probabilistic analysis considers the randomness or uncertainty present in the inputs that elicit a distribution of output (Olofsson 2005). Deterministic analysis can be used in situations in which the uncertainty is small; however in biomechanics research, many variables of interest (such as subject geometry, kinematics, material properties, etc.) have documented high levels of variability that deterministic analysis cannot adequately capture (Choi et al. 2007, Laz and Browne 2010, Mavris and Bandte 1997). To incorporate this variability, the model inputs and/or parameters are modelled as random variables with a specified probability distribution; rather than as a single representative value (typically a population mean) that may not adequately represent the population being modelled. These input distributions produce a distribution of possible outputs, from which the probability of a particular event can be estimated (Laz and Browne 2010).

Random variables can be characterized as discrete or continuous. A discrete random variable is one that can only equal a finite set of possible values $(x_1, x_2, ..., x_N)$. Alternatively, a continuous random variable is one that can take on an infinite set of values, either restricted to a particular range ($A \leq x \leq B$), or any real number ($-\infty \leq x \leq +\infty$) (Choi et al. 2007, Devore 2008, Haldar and Mahadevan 2000). For this dissertation, each manipulated variable was represented by a continuous random variable as each measurement existed on a continuous

---

[5] The terms: *Probabilistic* and *Stochastic* can be used interchangeably

measurement scale. Therefore, only functions and probabilistic methods pertaining to continuous random variables are described.

Randomness is incorporated into probabilistic analysis by representing random variables as distributions rather than a particular value (Laz and Browne 2010). A probability density function (PDF) is often used to describe individual distributions. A PDF is a mathematical function that describes the probability that different events will occur; with higher density representing more probable events and lower density (the tail regions) representing less probable events (Choi et al. 2007, Devore 2008, Haldar and Mahadevan 2000, Laz and Browne 2010). For example, the probability that a random variable, X, will take on a value between values a and b is described by [Eq. 2-1]. A cumulative distribution function (CDF) is most often used in probabilistic analysis to calculate the probability that the random variable, X, will take on a value less than or equal to a specified value (x). A CDF is achieved by integrating all of the values in the PDF less than or equal to x [Eq. 2-2] (Figure 9) (Choi et al. 2007). As well, a CDF can similarly be used to calculate the probability that X will take on a value between two limits (i.e. a and b) [Eq. 2-3].

$$P(a \leq X \leq b) = \int_a^b f(x)dx \qquad \text{[Eq. 2-1]}$$
$$F_x(x) = \int_{-\infty}^x f(x)dx \qquad \text{[Eq. 2-2]}$$
$$F_x(b) - F_x(a) = \int_{-\infty}^b f(x)dx - \int_{-\infty}^a f(x)dx \qquad \text{[Eq. 2-3]}$$
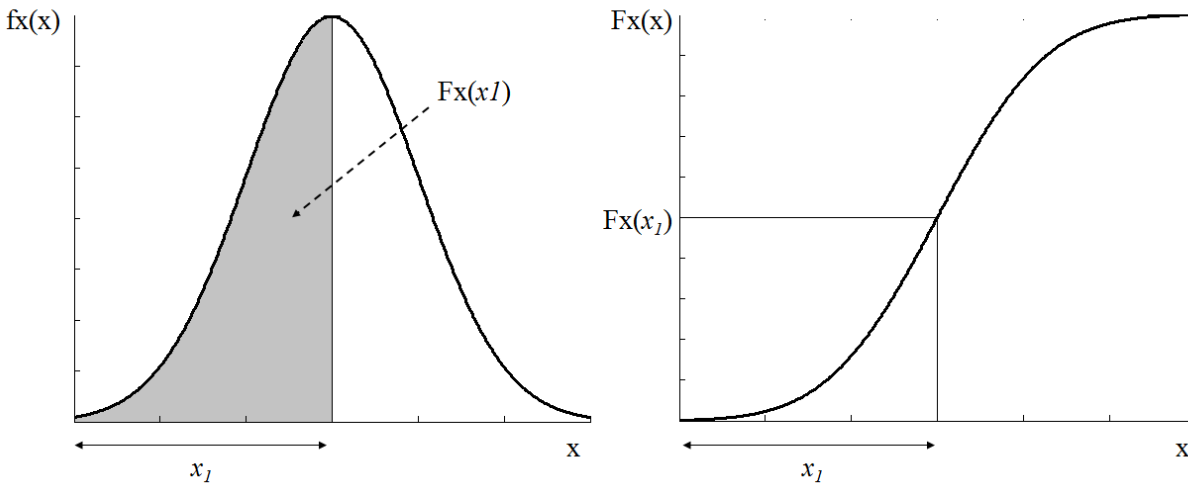
Figure 9. Probability density function (PDF) (left) and cumulative distribution function (CDF) (right) used to determine the probability of random variable x taking on a value of $\leq x_1$ (Figure adapted from Choi et al. 2007).

The following sections provide details regarding the different types of continuous distributions that a random variable can assume, and how they are represented mathematically. Specific probabilistic simulation techniques are also described, including Monte Carlo simulations and Most Probable Point techniques, such as First- and Second-order Reliability Methods and Mean/Advanced Mean Value Methods. Following this, the nature and interpretation of probabilistic output are discussed; this includes a discussion of the theory behind extracting importance factors.

2.7.1 *Types of Continuous Distributions*

Random variables can be represented by distributions with varying characteristics and complexity. Each distribution type requires the definition of specific parameters which are then used in probabilistic simulation methods. Thus, an understanding of common distributions, including their mathematical representation, is essential to applying probabilistic methods. Three

common distributions are described in **Table 4**. The most common type of distribution used in science and engineering is the Normal (Gaussian) distribution. For many probabilistic analysis approaches, random variables (normally or non-normally distributed) are first transformed to standard normal variables, which have a normal distribution with a mean of 0 and a standard deviation of 1, denoted N(0,1). Given the standard normal cumulative distribution function (CDF), widely available tables, can then be used to calculate the probability that a particular event will occur (i.e. the probability that the output will be greater than or less than a specified value, or that it will be between two specified limits).

Table 4. Types of continuous distribution functions: description, necessary parameters, and the probability density function (PDF) (Choi et al. 2007, Haldar and Mahadevan 2000).

Distribution	Description	Parameters	PDF
Normal (Gaussian)	• Bell-shape curve that is symmetric about the mean • Most common distribution in science and engineering	Mean (μ) Standard Deviation (σ)	$f_x(x) = \dfrac{1}{\sqrt{2\pi}\sigma_x} exp\left[-\dfrac{1}{2}\left(\dfrac{x-\mu_x}{\sigma_x}\right)^2\right]$, $-\infty < x < +\infty$
Lognormal	• Non-symmetric bell-shape curve • Natural logarithm will be normally distributed • Used when variables cannot take on negative values	$\lambda_x = ln\,\mu_x - \dfrac{1}{2}\zeta^2{}_x$ $\zeta_x = \sqrt{ln\left[1+\left(\dfrac{\sigma_x}{\mu_x}\right)^2\right]}$	$f_x(x) = \dfrac{1}{\sqrt{2\pi}\zeta_x} exp\left[-\dfrac{1}{2}\left(\dfrac{lnx-\lambda_x}{\zeta_x}\right)^2\right]$, $0 < x < +\infty$
Beta	• Used when the variable is bound between two limits (a and b)	$a = lower\ limit$ $b = upper\ limit$ $\mu = a + \dfrac{q}{q+r}(b-a)$ $\sigma^2 = \dfrac{qr}{(q+r)^2(q+r+1)}(b-a)^2$	$f_x(x) = \dfrac{1}{B(q,r)}\dfrac{(x-a)^{q-1}(b-x)^{r-1}}{(b-a)^{q+r-1}}$, $a \le x \le b$

There are many other less common distributions that can be applied to random variables. These include more simplistic distributions, such as the Uniform, as well as more complicated including those in the Gamma family of distributions, such as Exponential and Chi-Square

distributions, in addition to one of the Extreme Value distributions, such as the Weibull distribution (Choi et al. 2007, Haldar and Mahadevan 2000).

2.7.2 *Probabilistic Simulation*

The following sections describe different probabilistic simulation techniques commonly employed to evaluate the influence of variability in one or a number of model inputs and/or parameters on the corresponding output(s). Specifically, the Monte Carlo technique is described, followed by discussion of Most Probable Point techniques, such as First-order and Second-order Reliability Methods and Mean Value and Advanced Mean Value techniques. The research performed in this dissertation used both Monte Carlo and Advanced Mean Value simulation methods. Other methods are described to provide context for the development of the more advanced techniques.

2.7.2.1 *Monte Carlo Simulation*

A Monte Carlo simulation is an iterative process often considered the 'gold standard' of probabilistic techniques. In concept, given enough iterations, the Monte Carlo simulation will elicit a correct solution, which has been determined by evaluating the solution variation in the final iterations (i.e. final 10% of iterations) (Langenderfer et al. 2008, Reinbolt et al. 2007). However, the accuracy of this method depends on the number of iterations executed (Easley et al. 2007, Laz and Browne 2010). The underlying process of a Monte Carlo simulation involves performing many iterations of a deterministic function using combinations of values obtained through random number generation. The key components of a Monte Carlo simulation are: (1) random number generation for a specific distribution, and (2) repeated iterations, which are used to create the cumulative distribution function for a given random variable and/or determine the reliability of a function (Easley et al. 2007, Laz and Browne 2010, Mavris and Bandte 1997).

Though highly accurate, this method is very computationally extensive, which has led to the development of more computationally efficient techniques with comparable accuracy (Section 2.7.2.2). However, Monte Carlo methods remain the gold standard which most researchers use to validate their simulations. An example describing the specific steps of the simulation is presented in **Appendix 1**.

2.7.2.2 *'Most Probable Point' Reliability Methods*

Depending on the distribution of each of the random variables and the linearity of a given function, a number of reliability methods have been employed, most of which are based on a 'most probable point' (MPP) technique. Compared to the continuous Monte Carlo method, MPP methods can be considered discrete. These methods do not construct an entire cumulative distribution function (CDF), but rather determine the z-values (output values) at particular probability levels (Langenderfer et al. 2008, Mavris and Bandte 1997). The process is then repeated over a number of iterations to construct the CDF, with additional iterations (probability levels) providing more detail to the CDF. These methods can be grouped into: First-Order Reliability Methods (FORM) and Second-Order Reliability Methods (SORM), which can evaluate linear and non-linear (second order) functions, respectively. Additionally, methods such as the Advanced Mean Value (AMV) method have been developed which are capable of evaluating more complex, higher order functions (Wu et al. 1990). The AMV method has been demonstrated to have comparable results to the Monte Carlo technique, while requiring far less computational strength (Laz and Browne 2010). For example, the number of trials performed using AMV is a function of the number of parameters modulated and the number of outputs ([# parameters + 1] * # outputs). However, for the Monte Carlo method, generally many thousands of trials (or iterations) must be performed to obtain an accurate solution (Laz and Browne 2010).

41

Computationally, this could be the difference between minutes/hours versus days/weeks of simulation time per subject and/or condition.

Probabilistic methods have been used most often in risk-based design for structural reliability applications. For this purpose, researchers design a specific performance or "limit state function" that separates the design space into 'safe' and 'unsafe' regions, from which the probability of failure and the corresponding design criteria can be obtained (Haldar and Mahadevan 2000, Wu et al. 1990). A relatively simple technique designed to calculate this failure probability is the *mean value first-order second moment method (MVFOSM);* this is an early, basic FORM method. It is based on a first-order Taylor series approximation in that the function is linearized at the mean values of the random variables [Eq. 2-4] (Haldar and Mahadevan 2000).

For a function, $Y = g(x_1, x_2, \dots, x_N)$, where x_i is a set of uncorrelated random variables, and the mean and standard deviation of each variable are known, the function can be expanded in a Taylor series approximation about the mean values (μ_{x_i}):

$$Y = \underbrace{g(\mu_{x_i}) + \sum_{i=1}^{n}(x_i - \mu_{x_i})\frac{\partial g}{\partial x_i}}_{\text{First-order terms}} + \underbrace{\frac{1}{2}\sum_{i=1}^{n}(x_i - \mu_{x_i})^2 \frac{\partial^2 g}{\partial x_i^2}}_{\text{Second-order terms}} + \cdots \qquad \text{[Eq. 2-4]}$$

$$\cdots + \underbrace{\frac{1}{k}\sum_{i=1}^{n}(x_i - \mu_{x_i})^k \frac{\partial^k g}{\partial x_i^k}}_{\text{Higher-order terms}} (k = 1,2,\dots,n)$$

Given [Eq. 2-4], please note the following:

(1) For two correlated random variables x_i and x_j, the second order (and higher order) terms can be replaced with: $\frac{1}{k}\sum_{i=j}^{n}\sum_{i=1}^{n}(x_i - \mu_{x_i})(x_j - \mu_{x_j})\frac{\partial^k g}{\partial x_i x_j}$

(2) For most probable point methods, the Taylor series approximation occurs about the most probable point $(x_i{}^*)$ rather than the mean value (μ_{x_i}).

(3) Including higher order terms will provide a better representation of a higher order function. However, for a relatively linear function, a first-order Taylor series approximation may be adequate.

The MVFOSM is a relatively easy method to evaluate select cases, such as those in which all random variables are independent normal variables and the function is linear (Example 2-1) or when all variables are independent lognormal variables, and the function is a multiplicative-type function. The most common example used to describe and compare probabilistic methods is the following (from Haldar and Mahadevan 2000):

Example 2-1: Given the following limit state function:

$$g = R - S \qquad\qquad \text{[Eq. 2-5]}$$

Where,

R is the resistance of a cable, defined as a normal random variable with mean (μ_R) 120 kip and standard deviation (σ_R) 18 kip.

S is the load effect, defined as a normal random variable with mean (μ_S) 50 kip and standard deviation (σ_S) 12 kip.

Assuming independent normal variables, the probability that the cable will break; that is, when R < S or g < 0, is given by the equation:

$$p_f = \phi(-\beta) = 1 - \phi(\beta) \qquad\qquad \text{[Eq. 2-6]}$$

Where,

β is standard normal variate at the probability level $1 - p_f$, where p_f is the probability of failure. This is otherwise known as the reliability index, as a large magnitude of β will indicate that the probability of failure (p_f) (or risk of the cable breaking) is small. β is calculated by:

$$\beta = \frac{\mu_{R_N} - \mu_{S_N}}{\sqrt{\sigma_{R_N}{}^2 + \sigma_{S_N}{}^2}} \qquad \text{[Eq. 2-7]}$$

μ_{R_N} and μ_{S_N} are the first order approximate means for R and S respectively, given by [Eq. 2-8].

$$\mu_{R_N} \approx \mu_R \qquad \text{and} \qquad \mu_{S_N} \approx \mu_S \qquad \text{[Eq. 2-8]}$$

σ_{R_N} and σ_{S_N} are the first order approximate standard deviations for R and S respectively, given by [Eq. 2-9].

$$\sigma_{RN} \approx \sqrt{\left((\sigma_R)(\frac{\partial Z}{\partial R})\right)^2} \qquad \text{and} \qquad \sigma_{SN} \approx \sqrt{\left((\sigma_S)(\frac{\partial Z}{\partial S})\right)^2} \qquad \text{[Eq. 2-9]}$$

Therefore, the probability that the cable will fail (p_f) can be calculated:

$$p_f = \phi(-\beta) = 1 - \phi\left(\frac{\mu_R - \mu_S}{\sqrt{\sigma_{R_N}{}^2 + \sigma_{S_N}{}^2}}\right) = 1 - \phi\left(\frac{120 - 50}{\sqrt{((18)(1))^2 + ((12)(-1)^2}}\right) = 1 - \phi(3.24) = 0.00060$$

Note: $\phi(x)$ is the cumulative distribution function of a standard normal distribution of x, and can

be determined using widely available tables.

It is not often the case that all variables will be normal and the limit state equation linear.

As well, comparative calculations indicate that the reliability index (β) is sensitive to both the

type of distribution (i.e. normal or lognormal), as well as the formulation of the limit state

equation; that is, though $[R - S < 0]$ and $\left[\frac{R}{S} < 1\right]$ are mathematically equivalent, the calculated

probability of failure from each equation is different (Haldar and Mahadevan 2000). For

example, given the function $[R - S < 0]$, both R and S are treated as normally distributed

random variables and the probability of failure is calculated with [Eq. 2-7] used to calculate β.

However, given the function $\left[\frac{R}{S} < 1\right]$, both R and S are treated as lognormal variables as they

cannot take on negative values and β is subsequently calculated using [Eq. 2-10].

$$\beta = \frac{\lambda_R - \lambda_S}{\sqrt{\zeta_R{}^2 + \zeta_S{}^2}}$$

[Eq. 2-10]

Where,

λ_R and ζ_R are the lognormal parameters related to the mean and standard deviation of the random variable R

λ_S and ζ_S are the lognormal parameters related to the mean and standard deviation of the random variable S

Due to the aforementioned difficulties of the MVFOSM method, the Hasofer-Lind *Advanced First-Order Second Moment* Method (AFOSM) was developed, which is the currently used FORM method in probabilistic analysis. Provided that the limit state function is linear and all of the random variables are normal, the reliability index calculated by the MVFOSM method and AFOSM method will be equal. These methods differ in that the AFOSM linearizes the function at the most probable point rather than at the mean value (as noted in [Eq. 2-4]). Additionally, the AFOSM method is better able to address non-linear state functions, using an iterative process to calculate the reliability. This iterative technique provides the basis for other 'most probable point' methods (such as Advanced Mean Value) and thus, the steps in the technique, as described by Haldar and Mahadevan (2000), will be provided in detail (Table 5) to provide context for terminology used later in the document (primarily Chapters 3 and 6).

The most fundamental concept in this technique is the transformation of the random variables from the original coordinate system g(x) to standard normal space g(u) [Eq. 2-11] (Figure 10). In this transformed coordinate system, the reliability index (β) can be calculated as the minimum distance between the coordinate system origin and the limit state surface. Recall [Eq. 2-6] – it should be noted that a closer distance between the origin of the transformed coordinate system and the point on the limit state surface coincident with the minimum distance, $x_i'^*$, will be associated with a larger the probability of failure (Example 2-2); thus this point has been termed: *the most probable point* (MPP), indicating it is the most probable point of failure.

The MPP also coincides with the point of maximal density on the joint probability distribution function.

$$x_i'^* = \frac{x_i^* - \mu_{X_i}}{\sigma_{X_i}} \quad (i = 1, 2, \dots, n) \qquad \text{[Eq. 2-11]}$$

Where,

x_i corresponds to each normal random variable, i, in the original coordinate system, with corresponding mean (μ_{X_i}) and standard deviation (σ_{X_i})

x_i' is the standard normal variable in the transformed coordinate system with zero mean and unit standard deviation
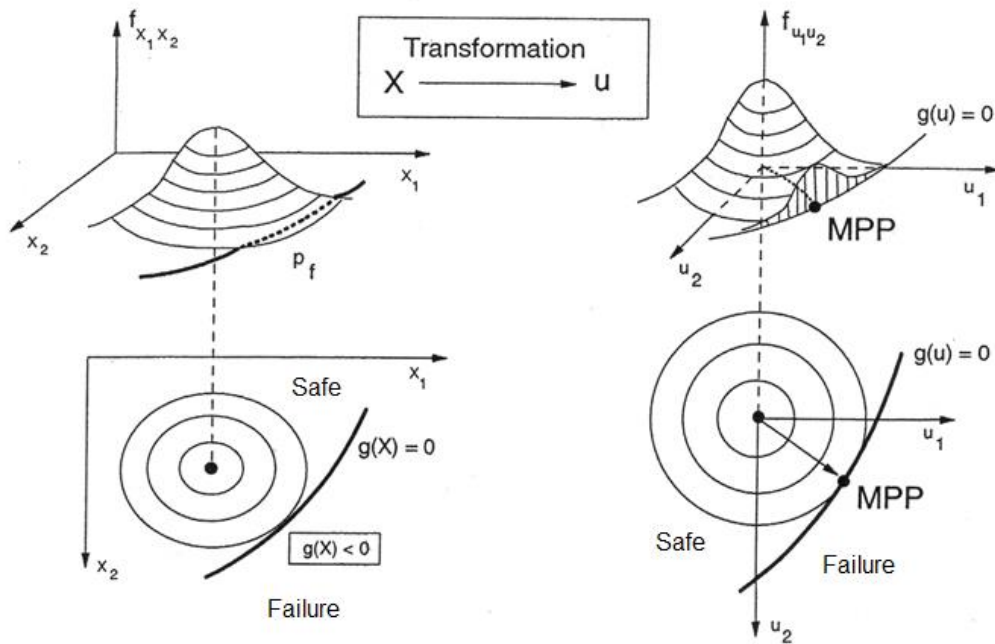
Figure 10. Transformation of random variables into standard normal space in the process of calculating the Most Probable Point (MPP) (Figure obtained from *NESSUS Theoretical Manual* (Version 7.0, 2001) with permission from Southwest Research Institute).

$$p_f = \phi(-\beta) = 1 - \phi(\beta)$$

Case 1: β = 0.5

Case 2: β = 2.0

$$p_f = 1 - \phi(0.5) = 1 - 0.69 = 0.31$$

$$p_f = 1 - \phi(2.0) = 1 - 0.98 = 0.02$$

Therefore, with a smaller minimum distance to the limit state surface, the probability of failure is higher.

This concept of the most probable point (MPP) can also be applied to a non-linear state function, in which the minimum distance must be solved iteratively using an optimization algorithm. The steps provided in **Table 5** outline this iterative process which aims to determine the reliability index (β) and the MPP ($x_i{}^*$). An example of this process using Example 2-1 is presented in **Appendix 2**.

Table 5. Steps in the iterative 'Advanced First-Order Second Moment' probabilistic method used to calculate the reliability index (β) and the Most Probable Point (MPP).

Step	Description	*Associated Equations
1	Define the limit state equation *	$g(x) = 0$
2	Provide an initial assumption for $x_i{}^*$, (i=1,2,...,n) *Note:* In most cases, the mean value (μ) of each random variable is used. Then, calculate the coordinates of each variable in the standard normal space ($x_i'^*$) using [Eq. 2-11] *.	Recall [Eq. 2-11]: $$x_i'^* = \frac{x_i{}^* - \mu_{X_i}}{\sigma_{X_i}} \; (i = 1,2,\dots,n)$$
3	Evaluate the partial derivatives of each reduced variate * and then calculate α_i *	$$\frac{\partial g}{\partial x_i'} = \frac{\partial g}{\partial x_i}\sigma_{x_i}^N \; (i = 1,2,\dots,n)$$ $$\alpha_i = \frac{\left(\frac{\partial g}{\partial X_i'}\right)^*}{\sqrt{\sum_{i=1}^n \left(\frac{\partial g}{\partial X_i'}\right)^{2*}}} \; (i = 1,2,\dots,n)$$ Where, $\left(\frac{\partial g}{\partial X_i'}\right)^*$ is the partial derivative of each reduced random variate (x_i') $\sigma_{x_i}^N$ is the equivalent standard deviation of the reduced random variate (x_i') α_i is the unit normal vector at the MPP at the limit state surface.

4	Obtain the new value for the MPP ($x_i'^*$) in terms of β [*] *Note:* The directional cosines of the unit vector, α_i, satisfy the rule $\alpha_1^2 + \alpha_2^2 + \cdots \alpha_i^2 = 1$; therefore each α_i^2 is a contributor to the probability, where a higher magnitude implies a greater contribution. This will be discussed further in Section 2.7.3.2.	$x_i'^* = -\alpha_i \beta \ (i = 1,2,\dots,n)$ $\beta = -\dfrac{\sum_{i=1}^{n} x_i'^* \left(\frac{\partial g}{\partial x_i'}\right)^*}{\sqrt{\sum_{i=1}^{n} \left(\frac{\partial g}{\partial x_i'}\right)^2}}$
5	Algebraically, substitute the new $x_i'^*$ into the reduced limit state equation $g(x') = 0$ and solve for β [*]	$x_i'^* = -\alpha_i \beta \ (i = 1,2,\dots,n)$
6	Using the new β obtained in Step 5, re-calculate $x_i'^*$ [* *]	$x_i'^* = -\alpha_i \beta \ (i = 1,2,\dots,n)$
7	Repeat STEPS 2-6 until the value of β converges to within a specified tolerance (0.001 is often used as a tolerance level).	
8	Once β converges, each random variable in the original coordinate system (design coordinates) can be calculated [*]	$x_i^* = \mu_{x_i} - \alpha_i \sigma_{x_i} \beta \ (i = 1,2,\dots,n)$

The biggest limitation of this described method is its disregard for the distribution of the random variables; that is, it assumes each variable is normally distributed. If the variables are non-normal (i.e. lognormal), additional steps are required in the above process to transform the non-normal variables into equivalent normal variables. The Rackwitz-Fiessler method is a common transformation used in the literature to transform non-normal variables to normal variables (Haldar and Mahadevan 2000, Wu et al. 1990). An example of this transformation for a lognormal random variable is demonstrated in **Appendix 2**. There are different modifications to the previously described FORM methods to consider different distributions of random variables, but they generally follow the same technique and, therefore, a detailed description of each is not included in this document. The SORM method improves upon the FORM method, considering second order terms, which provides a better estimate of the reliability than FORM for non-linear functions. Additionally, the SORM method can incorporate the covariance between multiple normal or non-normal variables; re-examining [Eq. 2-4], it can be seen that FORM methods are unable to consider the correlated variables, unlike higher order approximations. Specific steps for

additional FORM methods in addition to the SORM method are presented in Haldar and

Mahadevan (2000).

While the SORM method can address non-linear functions, it only considers first and

second order terms and therefore may be inadequate for addressing more complex functions,

particularly at the tail regions. The Advanced Mean Value (AMV) method is a first-order method

which combines the earlier mean value methods with a MPP technique. AMV contains a

correction term that reduces the truncation error caused by the Taylor series approximation, and

is thus better able to evaluate more complex, highly non-linear functions (Wu et al. 1990).

Given the function:
$$Z(x) = Z_1(x) + H(x) \qquad \text{[Eq. 2-12]}$$
Where,

Z_1 represents the Taylor's series first-order approximation at the mean values [Eq. 2-4]

$H(x)$ represents higher order terms

AMV provides an extension of this mean value method, in which the higher order terms, $H(x)$,

are replaced by a function based on the linear approximation $H(Z_1)$ [Eq. 2-13].

$$Z(x) = Z_1(x) + H(Z_1) \qquad \text{[Eq. 2-13]}$$

The correction term of the AMV method, $H(Z_1)$, is the difference between the linear first order

approximation (Z_1 or 'the mean value approximation') and the Z calculated at the most probable

point locus (which connects all of the most probable points for each of the z-values) of Z_1. In

other words, it uses the MPP calculated by the linear approximation to iteratively compute a

more accurate MPP that incorporates higher-order terms (Figure 11).
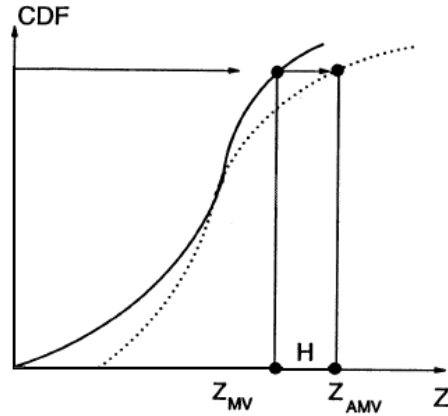
Figure 11. Advanced Mean Value (AMV) method where $Z_{MV} = Z_1$ (first order approximation) and $Z_{AMV} = H(Z_{MV})$ or $H(Z_1)$ (Figure obtained from *NESSUS Theoretical Manual* (Version 7.0, 2001) with permission from Southwest Research Institute).

The AMV method is more computationally efficient compared to other techniques, particularly the Monte Carlo method. Its ability to address highly complex, non-linear functions with this efficiency, while still providing similar results compared to Monte Carlo ('gold standard'), makes it an advantageous probabilistic technique (Laz and Browne 2010, Wu et al. 1990). Small differences of 1.84N and 0.42Nm for lower limb joint forces and moments (Langenderfer et al. 2008), 0.18° for upper limb kinematics and 4mm for anatomical landmark locations (Langenderfer et al. 2009) have been reported to exist between AMV and Monte Carlo methods.

2.7.3 *Probabilistic Output*

2.7.3.1 *Performance vs. Probability Levels*

NESSUS Probabilistic Analysis Software (SwRI, San Antonio, TX) is a tool that enables the user to conduct two forms of probabilistic analysis, depending on the output levels of interest: performance or probability. Performance levels are used most often in reliability problems, where the probability of a particular z-value (such as structural failure, $P(g \leq 0)$), is

50

being evaluated. Alternatively, probability levels can be specified for which the particular z-value associated with that level can be calculated. When specifying probability levels, multiple levels can be applied with more levels corresponding to a more detailed CDF. However, most often the 50% and end limits of a 1-99% confidence interval, are reported (Easley et al. 2007, Langenderfer et al. 2008, Pal et al. 2007).

2.7.3.2 Importance Factors

A unique feature of certain probabilistic methods is the ability to calculate importance factors. Given a function in which the output is influenced by variability of more than one random variable, importance factors can be calculated to determine which variable is more important in modulating the predicted output. Importance factors, otherwise known as relative sensitivity factors, can be calculated when 'Most Probable Point' (MPP) techniques are used; that is, for methods that require the transformation from normal to standard normal space (Figure 10).

The importance (sensitivity) factors, α_i, for each random variable ($i = 1, 2, \ldots, n$) describe their relative contribution to the performance output. Mathematically, the sensitivity factors are represented by [Eq. 2-14], in which α_i describes the change in the reliability index (β) with respect to the standard normal variable in the transformed coordinate system (x_i') (Choi et al. 2007, Easley et al. 2007, Laz and Browne 2010).

$$\alpha_i = \frac{\partial \beta}{\partial x_i'} = \frac{\partial p}{\partial x_i'} \frac{\partial \beta}{\partial p} \hspace{4cm} \text{[Eq. 2-14]}$$

Where,

p is the specified probability level.

Recall [Eq. 2-6],

$$p_f = \phi(-\beta) = 1 - \phi(\beta)$$

And [Eq. 2-15] (Step 4, Table 5) used to calculate the new value for the MPP,

$$x_i'^* = -\alpha_i \beta \ (i = 1,2,\dots,n) \qquad \text{[Eq. 2-15]}$$

As α_i is related to the reliability index (β) [Eq. 2-15] which describes the probability [Eq. 2-6], and since α_i is the direction cosines at the MPP (x_i') such that it follows the rule outlined in [Eq. 2-16], the relative magnitudes of α_i^2 describe the relative contributions of each random variable ($i = 1,2,\dots,n$) to the output (Choi et al. 2007, NESSUS Theoretical Manual 2001).

$$\alpha_1^2 + \alpha_2^2 + \cdots \alpha_i^2 = 1 \qquad \text{[Eq. 2-16]}$$

It is because the probabilistic analysis is being evaluated in standard normal space that variables with different units, distributions, and characteristics can be normalized (or non-dimensionalized) and compared on the same scale to evaluate their relative contributions to the output. Therefore, calculation of these importance factors is a major advantage of using probabilistic methods such as Advanced Mean Value. Monte Carlo simulations can also measure the sensitivity of the output to the corresponding input variables, but do so by calculating correlation coefficients, which exhibit unreliability in highly non-linear functions (Laz and Browne 2010).

This current research used probabilistic methods to evaluate the influence of model parameter variability on the predicted outputs. Specifically, the study discussed in **Chapter 3** used Advanced Mean Value simulations to quantify the sensitivity of predicted rotator cuff muscle forces to variability in muscle attachment locations and glenohumeral stability constraints. Similarly, using the empirical data measured in **Chapters 4 and 5**, the study discussed in **Chapter 6** used both Advanced Mean Value and Monte Carlo simulation methods to examine the variability in subacromial space geometry resulting from kinematic and morphological differences. Using the Advanced Mean Value method, each of these studies

reported which of the several modelled parameters contributed more to modulating the output, which assisted both with output interpretation as well as ergonomic and clinical intervention recommendations. Thus, the concepts discussed in this review (Section 2.7) are briefly reiterated in these chapters in which probabilistic methods are employed to calculate cumulative distribution functions and importance factors (Chapters 3 and 6). Additionally, the definitions/descriptions of several terms related to probabilistic methods are provided *Section B* of the **Glossary**.

Chapter 3

*Probabilistic evaluation of predicted force sensitivity to muscle attachment and glenohumeral stability uncertainty

Overview

A major benefit of computational modelling in biomechanics research is its ability to estimate internal muscular demands given limited input information. However, several assumptions regarding model parameters and constraints may influence model outputs. This research evaluated the influence of model parameter variability, specifically muscle attachment locations and glenohumeral stability thresholds, on predicted rotator cuff muscle force during internal and external axial humeral rotation tasks. Additionally, relative sensitivity factors assessed which parameters were more contributory to output variability. Modest model parameter variation resulted in considerable variability in predicted force, with origin-insertion locations being particularly influential. Specifically, the scapula attachment site of the subscapularis muscle was important for modulating predicted force, with sensitivity factors ranging from $\alpha = 0.2$ to 0.7 in a neutral position. The largest variability in predicted forces was present for the subscapularis muscle, with average differences of $33.0 \pm 9.6\%$ of normalized muscle force (1-99% CI), and a maximal difference of 51% in neutral exertions. Infraspinatus and supraspinatus muscles elicited maximal differences of 15.0% and 20.6%, respectively, between confidence limits. Overall, origin and insertion locations were most influential and thus incorporating geometric variation in the prediction of rotator cuff muscle forces may provide more representative population estimates. This research subsequently demonstrated the

implications of model parameter variation and the advantages of employing probabilistic

modelling methods to estimate variation in biological tissue loads.

3.1   Introduction

Computational modelling has considerable utility for biomechanics research. Modelling

allows the evaluation of tasks and scenarios that are either not feasible, too tedious or time

consuming to evaluate experimentally, for modest financial cost (King et al. 1995). Despite these

advantages, a fundamental criticism of the modelling process is the meticulousness of validation

procedures to ensure model reliability and accurate representation of the modelled system

(Lewandowski 1982). Biological tissues exhibit substantial variability within a human

population, which complicates the validation further, and potentially undermines the adequacy of

deterministic modelling approaches for biomechanics research. To incorporate this variability,

probabilistic approaches can be employed. Model inputs and/or parameters are treated as random

variables, with specified probability distributions, rather than as a single representative value

(typically a population mean) that likely fails to fully characterize the population of interest.

These input distributions subsequently produce a distribution of possible outputs, from which the

probability of a particular event can be estimated (Laz and Browne 2010).

Rotator cuff muscle forces can be predicted as a relative measure of muscular demand

between multiple simulated upper extremity tasks. Frequently, existing deterministic

musculoskeletal upper extremity shoulder models use optimization-based inverse dynamics to

estimate upper extremity muscle forces. These models have considerable utility for shoulder

musculoskeletal disease prevention, allowing assessment of various scenarios (Dickerson et al.

2008, Hogfors et al. 1991). Excessive muscular demands can produce fatigue and exhaustion

which can subsequently lead to numerous pathologies, notably subacromial impingement syndrome (Michener et al. 2003, Phadke et al. 2009).

The sensitivity of predicted force to the modelled location of muscle attachment sites and other geometric model parameters has been evaluated both deterministically and probabilistically, with contrasting results in the literature. Hogfors et al. (1995) determined that small perturbations of model parameters did not elicit a large change in output response, while Raikova and Prilutsky (2001) reported that predicted muscle forces in the leg were highly sensitive to changes in muscle moment arms and physiological cross-sectional area. Further, modest variability can propagate to large errors in predicted force (Delp and Maloney 1993, Dickerson et al. 2008). Hughes and An (1997) used a probabilistic approach to assess the influence of rotator cuff and deltoid moment arms on predicted muscle force in an optimization-based planar model of the glenohumeral joint based on data obtained from cadaveric specimens. This research supported the usefulness of probabilistic techniques to examine variability in muscle force predictions as average muscle forces were in the middle of the 95% confidence interval for predictions obtained using Monte Carlo simulations. Pal et al. (2007) also used a probabilistic approach to evaluate the sensitivity of model predicted moment arms in the lower limb to variability in kinematic parameters as well as muscle attachment locations specifically and determined that small perturbations resulted in substantial variation in predicted magnitudes.

A glenohumeral stability constraint is necessary for biomechanical shoulder models to ensure that the glenohumeral joint contact force does not exceed dislocation tolerances. Lippitt and Matsen (1993) documented glenohumeral stability thresholds based on their cadaveric study in which compressive loads were applied to the humeral head, normal to the glenoid cavity, following which tangential forces were increasingly applied in the superior-inferior, anterior-

56

posterior and intermediate directions until dislocation occurred. These dislocation forces have since been used as constraints in shoulder models, in which a certain percentage of this maximal force is used to constrain the joint (Dickerson et al. 2007). Research has demonstrated that variation in this constraint can substantially influence predicted muscle forces, with a more restrictive dislocation force ratio (i.e. 0.2) increasing the predicted forces.

Evaluating the influence of variability in each of these parameters on rotator cuff muscle force predictions is critical in ensuring the tissues are being modelled appropriately. While there are many parameters that can be considered, muscle attachment sites and glenohumeral dislocation thresholds were selected based on their previously demonstrated importance in both probabilistic and deterministic modelling research, respectively. Determining whether model parameter variability, independent of the variability present in the model inputs (force, posture, etc.), influences muscle force predictions will inform whether both inputs and model parameters related to subject geometry should be treated stochastically.

Primary Research Objectives:

1. To determine the sensitivity of model predicted rotator cuff muscle forces to variability in model parameters, specifically (1) rotator cuff origin and insertion locations and (2) glenohumeral stability thresholds and ratios, using probabilistic methods.

2. To determine whether certain parameters, or sub-parameters (i.e. the origin of a particular muscle) were more important in predicting variation in muscle forces.

3. To evaluate the influence of anthropometrics on the variability of predicted force.

Secondary Research Objectives:

1. Apply probabilistic modelling techniques, specifically Advanced Mean Value (AMV) and Monte Carlo methods, using NESSUS Probabilistic Analysis Software, to a

simplified application as a precursor to developing a large-scale population subacromial geometry model (Chapter 6).

2. To provide a preliminary step towards the larger goal of predicting subacromial impingement risk over a variety of tasks with varying levels of muscular demand.

Research Hypotheses:

It was hypothesized that variation in both muscle attachment sites and glenohumeral stability thresholds, regardless of anthropometrics, would elicit high variation in model predicted muscle forces; indicating the need to consider variation in these musculoskeletal geometric parameters in research using biomechanical shoulder models to predict internal muscular demands.

3.2   Methods

This research consisted of four sequential components: (1) postural data construction, (2) Shoulder Loading Analysis Modules (SLAM) deterministic model, (3) model parameter selection and acquired distributions, (4) probabilistic model development, execution, and assessment (Figure 12).
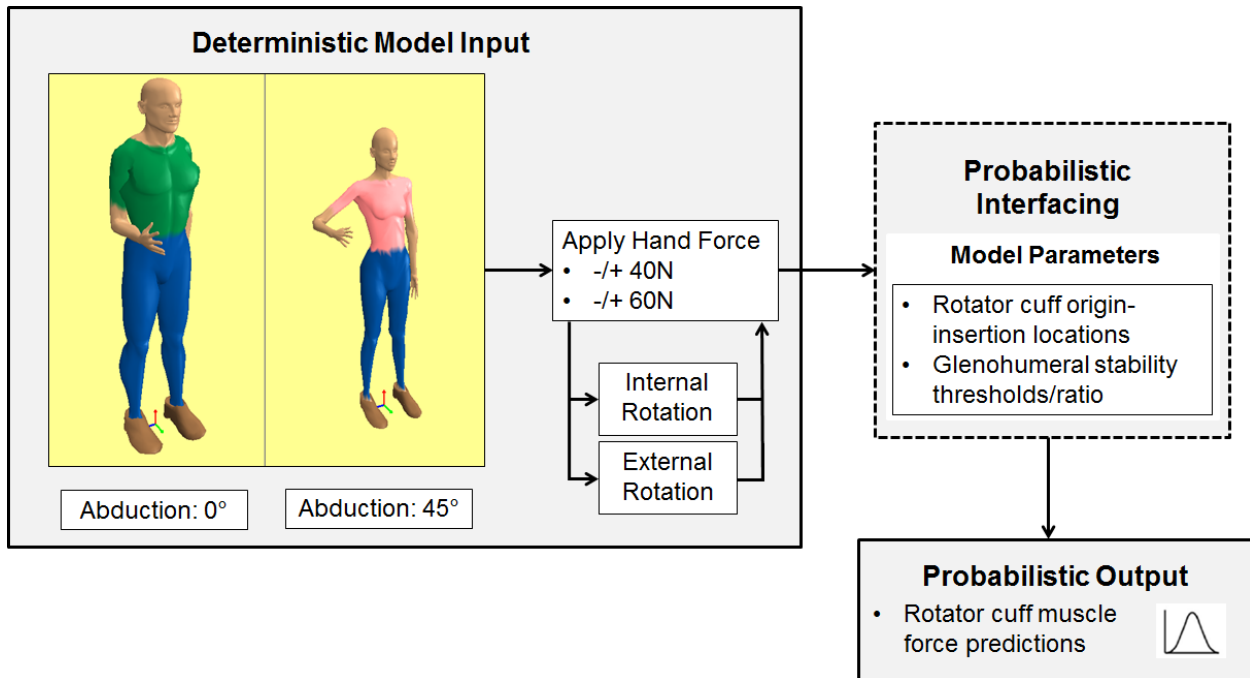
Figure 12. Methodological outline: Postural and anthropometric data [created using 3D SSPP (University of Michigan, Ann Arbor, MI)] and external hand forces [applied within the SLAM upper extremity deterministic model (Dickerson et al. 2007)] were used as input into the SLAM upper extremity model from which a distribution of rotator cuff muscle forces were predicted from probabilistic analysis [using NESSUS Probabilistic Analysis Software (SwRI, San Antonio, TX)], to consider variability in rotator cuff moment arms and glenohumeral stability thresholds/ratio.

3.2.1 *Postural Data Construction*

The three-dimensional static strength prediction program (3D SSPP) (University of Michigan, Ann Arbor, MI) was employed to place two subjects (5th percentile female and 95th percentile male) in two postures (0° and 45° of humeral abduction, both with 90° of elbow flexion) by modifying the body segment angles of the right arm, following which upper

extremity joint center locations were extracted. In these postures, internal and external rotation forces were applied at the hand, which would subsequently target the rotator cuff muscles.

3.2.2 *SLAM Model Description and Manipulation*

The SLAM Model is an inverse upper extremity model that uses joint center locations, anthropometric data, and external hand forces to predict internal muscular demands using optimization to minimize the sum of cubed muscle stresses (Dickerson et al. 2007). The model consists of three modules: a musculoskeletal geometry model of the shoulder bones and muscles, an external dynamic torque model and an internal muscle force model. The geometry model consists of five segments (scapula, clavicle, humerus, torso and combined radial/ulnar forearm link) and 23 muscles modelled as multiple (38) components. Each muscle is modelled as a line connecting the two muscle attachments which are computed as a percentage of segment length (Dickerson et al. 2007, Makhsous 1999). Due to the inadequacy of a straight line-of-action to represent the rotator cuff muscles, a spherical wrapping technique was employed to provide a better physiological representation of the muscles' path from the medial aspect scapula, around the humeral head to their attachment points on the proximal humerus (Dickerson 2005, Makhsous 1999, van der Helm 1994). Additionally, to adequately represent varying arm posture, the relationship between the positions of the scapula, humerus, clavicle and torso were maintained by an established shoulder rhythm which is based on a consistent relationship between the humerus and torso (Dickerson 2005, Hogfors et al. 1991, Karlsson and Peterson 1992, Makhsous 1999). Anthropometric data was varied in the model using the regression equations reported by Zatsiorsky and Seluyanov (1993), while joint center and center of mass locations of each segment were calculated using methods described by Nussbaum and Zhang (2000) and Clauser et al. (1969). The external dynamic torque module of this model used an

60

inverse dynamics approach to calculate the static and dynamic joint forces and moments given a certain external hand force and posture. Lastly, the internal muscle force model used both the geometry and external torque models to predict muscle forces using an optimization approach. SLAM also included a number of constraints to ensure physiological realism. Of particular relevance to the current study was the novel glenohumeral contact force constraint that used the empirical direction-specific joint dislocation force ratio thresholds measured by Lippitt and Matsen (1993).

SLAM was used to predict rotator cuff muscle forces. Two hand force magnitudes (40N, 60N) were applied to the center of the hand with the model positioned according to the 3D SSPP postural data previously obtained to generate internal and external axial rotation moment demands. Muscle force magnitudes were presented as a percentage of the respective maximal producing capability. This normalization allowed comparisons between subjects as well as exertion types (Dickerson et al. 2008). Maximal force bounds for each muscle were calculated based on the individual physiological cross sectional area (PCSA) and a constant specific tension of 87.9 N/cm^2 obtained from cadaveric specimens (Dickerson et al. 2007, Makhsous 1999). This model has demonstrably correlated well with empirical musculoskeletal geometry and muscle activity data (Dickerson et al. 2008, Gatti et al. 2007).

3.2.3 *Model Parameter Selection and Acquired Distributions*

Within SLAM, numerous parameters are defined based on literature datasets. This is similar to other approaches that used living and cadaveric datasets (Dul 1988, Hogfors et al. 1987, 1991, 1995, Karlsson and Peterson 1992, Lippitt and Matsen 1993, Makhsous 1999). In this study, two parameters were evaluated probabilistically: (1) rotator cuff muscle attachment sites and (2) glenohumeral stability thresholds/ratios. The sensitivities of these two parameters

were assessed in terms of their influence on rotator cuff muscle force predictions for each task evaluated.

3.2.3.1 *Rotator Cuff Muscle Attachment Sites*

Three-dimensional coordinates of the humeral and scapular rotator cuff attachment sites were systematically altered. The supraspinatus and teres minor were represented as having a single muscle line of action, while the infraspinatus and subscapularis were divided into two (upper and lower) and three (upper, middle and lower) portions, respectively with different humeral insertion locations. Hogfors et al. (1987) measured origin and insertion locations for three subjects, where coordinates were given as a proportion of segment length from individual segment coordinate systems (Makhsous 1999). The mean and corresponding standard deviation of each coordinate, for each muscle, was used to create the normal distribution (Table 6).

Table 6. Mean and standard deviations used as input for muscle attachment model parameters. Values represent the [x y z] coordinates of the humeral and scapular attachment points of each of the rotator cuff muscles given as percentage of bone length (Hogfors et al. 1987, Makhsous 1999). Coordinates with negative means are highlighted.

Attachment Site	Muscle	Mean			Standard Deviation		
		X	Y	z	x	y	z
Humerus	Infraspinatus (Upper)	-0.018	-0.025	0.094	0.012	0.013	0.013
	Infraspinatus (Lower)	-0.018	-0.025	0.094	0.012	0.013	0.013
	Subscapularis (Upper)	0.012	0.085	0.011	0.003	0.008	0.004
	Subscapularis (Middle)	0.012	0.085	0.011	0.003	0.008	0.004
	Subscapularis (Lower)	0.012	0.085	0.011	0.003	0.008	0.004
	Supraspinatus	-0.042	0.031	0.079	0.004	0.011	0.008
	Teres Minor	0.039	-0.045	0.037	0.006	0.008	0.019
Scapula	Infraspinatus (Upper)	0.607	0.240	-0.106	0.057	0.008	0.024
	Infraspinatus (Lower)	0.760	0.115	-0.069	0.025	0.028	0.031
	Subscapularis (Upper)	0.523	0.307	-0.137	0.049	0.013	0.019
	Subscapularis (Middle)	0.668	0.164	-0.108	0.046	0.036	0.012
	Subscapularis (Lower)	0.763	0.069	-0.064	0.030	0.023	0.030
	Supraspinatus	0.305	0.348	-0.112	0.056	0.023	0.019
	Teres Minor	0.600	-0.049	-0.024	0.042	0.017	0.016

3.2.3.2 *Glenohumeral Stability Constraint*

      The glenohumeral stability ratio and glenohumeral maximal dislocation force thresholds were varied stochastically to evaluate their influence on rotator cuff muscle force predictions. The glenohumeral stability ratio constrains the translational force to a certain percentage of that required to dislocate the joint. Thus, similar to muscle attachment manipulations, a normal distribution was applied to this coefficient assuming a mean of 0.7 and standard deviation of 0.1 (Table 7). As there is limited information regarding physiologic statistics for this coefficient, the multi-directional maximal dislocation thresholds were also treated as normal random variables to determine their influence on the predicted rotator cuff muscle force (Table 7).

Table 7. Mean and standard deviations used as input for glenohumeral stability model parameters. On-axis forces obtained from Lippitt and Matsen (1993), off-axis forces extrapolated from on-axis forces, stability ratio obtained from Dickerson et al. (2007). All maximum translating forces are assuming a 100 Newton glenohumeral compressive load scenario.

Direction	Maximum Translating Force (N)	
	Mean	**Standard Deviation**
Superior (0°)	51.0	9.0
Off-axis (45°)	32.9	6.4
Anterior (90°)	29	5.0
Off-axis (135°)	39.7	7.7
Inferior (180°)	56.0	12.0
Off-axis (225°)	43.9	22.5
Posterior (270°)	30.0	12.0
Off-axis (315°)	35.2	13.1
Stability Ratio	0.7	0.1

3.2.4 *Probabilistic Model Development*

      The probabilistic model was constructed in NESSUS Probabilistic Analysis Software (SwRI, San Antonio, TX). This software acts to interface with other mathematical software, such as Matlab®, to consider random variables as particular distributions and then apply probabilistic analysis methods to determine the output distribution.

This study had 51 random variables that were treated normally using the mean and standard deviations previously described. The muscle attachment parameters constituted 42 of the random variables (7 muscles [rotator cuff portions] x 2 locations [origin and insertion] x 3 coordinates [x y z]) while the stability parameters comprised 9 of the random variables (8 direction-specific thresholds [superior, inferior, anterior, posterior, + 4 intermediate] + 1 stability coefficient) (Table 8). The Advanced Mean Value (AMV) probabilistic simulation method was used due to its computational efficiency and excellent agreement with Monte Carlo methods (Easley et al. 2007, Langenderfer et al. 2009). AMV achieves efficiency by combining reliability techniques with optimization to determine the most probable point (MPP), which is the combination of parameter values predicting performance at the specified probability level (Wu et al. 1990). The AMV method first transforms the original variables, which can have any distribution type, into independent normal variables, then uses optimization to locate the MPP, and lastly computes the performance value at the desired probability level.

Table 8. Example of 2 out of the 51 random variables defined by the muscle, location and coordinate.

Random Variable	Muscle	Location	Coordinate
Infra1_o_x	Infraspinatus – Upper Portion	Origin	x-coordinate
Subscap2_i_z	Subscapularis – Middle Portion	Insertion	z-coordinate

These random variables were defined in two separate sub-programs within the SLAM model, programmed in Matlab® (Mathworks®, Natick, MA). The location of these variables were mapped within NESSUS, ensuring that the input and output format include the maximum plausible ranges of each of the variables. Following correct mapping between programs,

NESSUS enabled the user to select one of many different possible probabilistic analysis methods. The Advanced Mean Value (AMV) probabilistic simulation method was used due to its computational efficiency and excellent agreement with Monte Carlo methods (Easley et al. 2007, Langenderfer et al. 2009).

Each of the 16 exertions (8 exertions x 2 subjects) were evaluated using AMV to determine the distribution of predicted muscle forces for each of the seven rotator cuff muscle portions given the variability in the 51 modified model parameters. Thus, 364 trials were simulated for each of the 16 exertions (total of 5824 simulations).

3.2.4.1 *Validation*

Two different validation techniques were employed to ensure accuracy in the resulting force predictions. First, for a subset of five exertions, a Monte Carlo probabilistic approach with 2500 iterations was performed to compare the accuracy of the AMV method outputs. Secondly, for a different subset of five exertions, the distribution type of all variables with a positive population mean (Table 6) was changed to lognormal to determine the robustness of the simulation results to the assumed distribution.

3.3 Data Analysis

Using the techniques described, a distribution of predicted rotator cuff muscle forces (normalized to their maximal capability) over a 1 to 99% confidence interval was calculated for each exertion. This interval corresponds to ± 3 standard deviations. A total of 56 confidence intervals were thus calculated per subject (8 exertions x 7 muscle force predictions). Additionally, as the AMV method required a transformation of each of the random variables from their original variables to standard normal space, the parameters were non-dimensionalized and their relative influence on the resulting output was obtained. Therefore, relative sensitivity

factors (α) [Eq.3-1] were calculated in order to determine which parameters were more important in predicting the variability in muscle force (Haldar and Mahadevan 2000, NESSUS 2001).

$$\alpha_i = \frac{\mu_i^*}{\beta}$$ [Eq. 3-1]

Where,

α_i is the unit normal vector at the most probable point (MPP) at the limit state surface.

β is the reliability index, calculated as the minimum distance between the coordinate system origin and the limit state surface.

μ_i^* is the MPP or point on the limit state surface corresponding to β. This point also coincides with the point of maximal density on the joint probability distribution function.

Note: The directional cosines of the unit vector, α_i, satisfy the rule $\alpha_1^2 + \alpha_2^2 + \cdots \alpha_i^2 = 1$; therefore each α_i^2 is a relative contributor to the probability, where higher magnitude implies a greater contribution to output variability.

3.4 Results

Probabilistic analysis demonstrated that modest variation in model parameters resulted in a high level of variability in muscle force predictions across exertions, particularly for the subscapularis muscle. This variability in muscle force was mainly attributed to variability in the humeral and scapular rotator cuff muscular attachment sites. For internal rotation exertions, of the rotator cuff musculature, solely subscapularis muscle force was predicted. Alternatively, for external rotation exertions, whereby the hand force was applied by the dorsal surface of the hand, infraspinatus and supraspinatus muscle force was predicted. Teres minor muscle force was not predicted for either type of exertion.

$3.4.1$ *Internal Rotation Exertions: Subscapularis force prediction*

The magnitude of predicted force for the subscapularis muscle components differed considerably depending on arm posture. Generally, results showed that the upper portion of the subscapularis was more active when the humerothoracic angle was neutral (0°), while the lower portion was active when the arm was abducted to the 45° posture (Figure 13). However, compared to the abducted exertions, internal rotation with the arm at neutral showed on average twice the magnitude of predicted force, with predicted force magnitudes reaching their maximal bounds (100%) for the 60N hand force exertion. Further, as expected, the 5th percentile female overall demonstrated higher predicted normalized force for each of the exertions compared to the males for the subscapularis muscle.

Predicted subscapularis muscle force demonstrated high variability as a result of model parameter variation for both simulated subjects. Depending on the particular exertion, muscle component and subject, the subscapularis muscle demonstrated a 10 to 540% increase in predicted force as a result of model parameter variation between end ranges of the population, as calculated by the percent change between lower (1%) and upper (99%) confidence limits. This variability was notably larger for the neutral arm posture, showing 10 to 16 times the variability for middle and upper portions of the subscapularis, compared to the abducted posture. Variability was similar for both anthropometries, with the female demonstrating slightly greater sensitivity to the model parameter variability. The mean difference between upper and lower confidence limits was calculated to be $33.0 \pm 9.6\%$ and $6.7 \pm 5.0\%$ for neutral and abducted arm postures respectively, with the greatest variability exhibited by the 5th percentile female in the 60N hand force internal rotation task with the arm in a neutral posture (Figure 13). For this exertion, the lower extreme (1% confidence limit) demonstrated no muscle force produced for this exertion

67

for the lower portion of the subscapularis, while for the upper extreme (99% confidence limit) for the same 5th percentile female subject, this same muscle component produced 51% of their maximal capability.
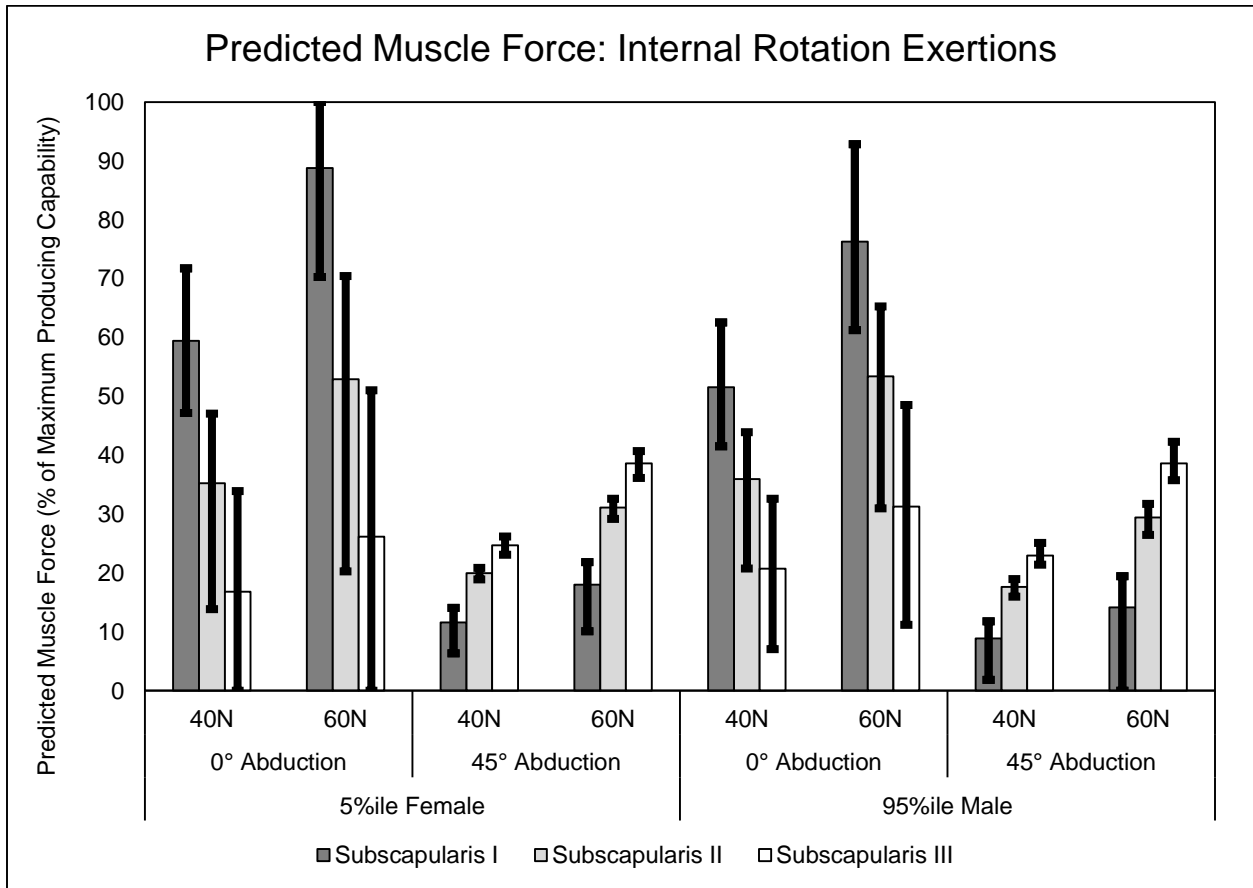
Figure 13. Predicted muscle force (% of Maximum Producing Capability) for the subscapularis muscle through different internal rotation exertions (humeral abduction angle by hand force magnitude) while varying muscle attachment sites and glenohumeral stability properties. Bars represent a 50% probability with the error bars signifying the 1-99% confidence intervals. Results provided for both a 5th percentile female and a 95th percentile male.

3.4.2 *External Rotation Exertions: Infraspinatus and Supraspinatus force prediction*

Despite exhibiting comparable variability (percent change between lower and upper confidence limits) to the subscapularis muscle, the infraspinatus and supraspinatus muscles produced less force during exertions in which they were active (external rotation tasks). Resulting cumulative distribution functions for these muscles demonstrated a 50% confidence level of $24.0 \pm 8.0\%$ and $15.8 \pm 6.5\%$ of their maximal capabilities respectively for the 5th percentile female and $28.1 \pm 9.8\%$ and $16.2 \pm 5.7\%$ respectively for the 95th percentile male, across exertion postures and hand force magnitudes (Figure 14). Unlike the response of the subscapularis muscle during internal rotation tasks, predicted force for the infraspinatus and supraspinatus muscles did not differ markedly with altered arm posture (neutral versus abducted to 45°). Greater hand force requirements (60N versus 40N) demanded an approximate force increase of 30% from both infraspinatus and supraspinatus muscles.

Across all exertions and between subjects, the variability in predicted force for both infraspinatus components remained somewhat uniform. Differences between upper and lower confidence limits demonstrated a mean of $9.9 \pm 3.2\%$ between exertions for the infraspinatus, while showing slightly larger variability with larger hand force demands (Figure 14). Alternatively, for the supraspinatus muscle, the variability was much greater in the elevated posture compared to the neutral posture, with the average difference between upper and lower confidence limits for the abducted exertions demonstrated to be double that of neutral exertions. However, compared to the variability in predicted subscapularis force during internal rotation exertions, variability in the infraspinatus and supraspinatus muscles remained somewhat lower with peak differences between confidence limits shown to be 15.0% and 20.6%, respectively.

69
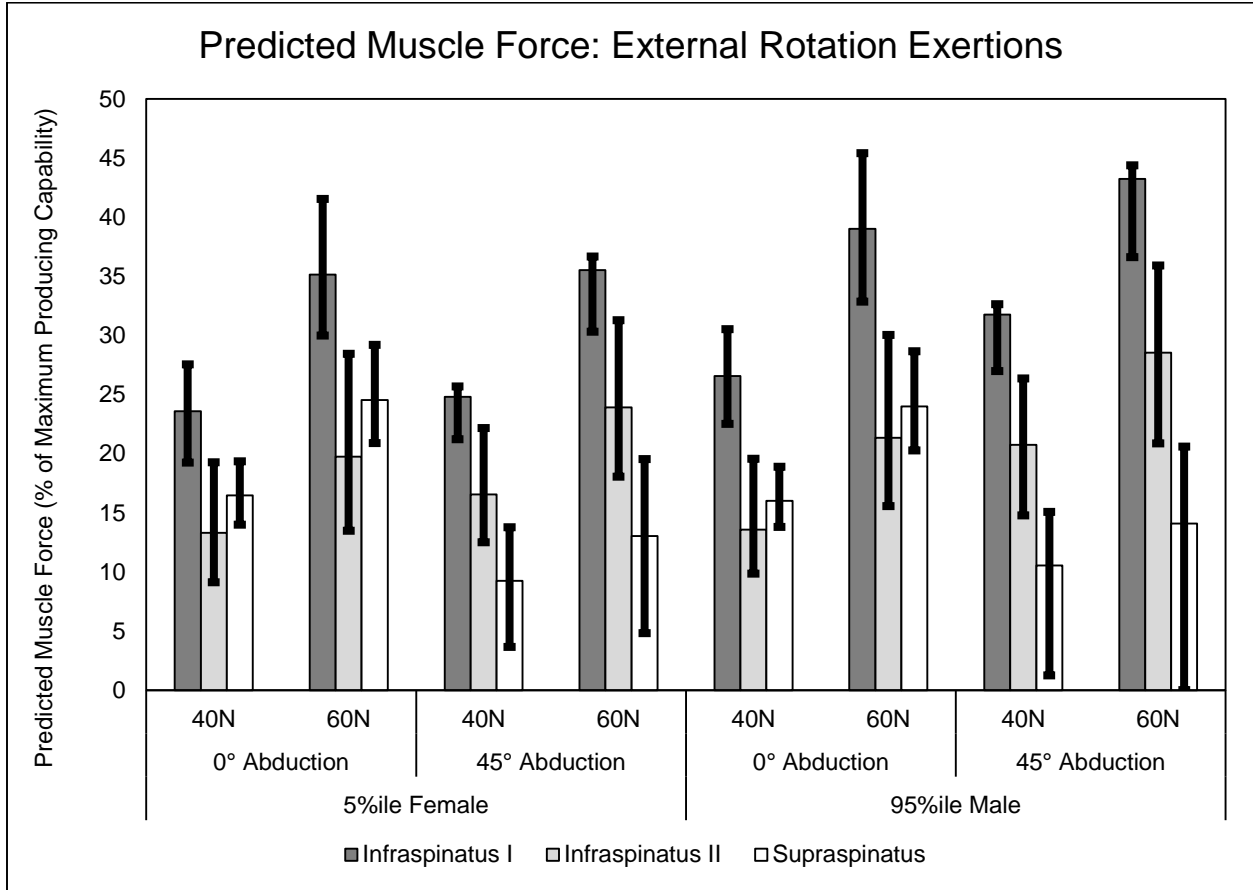
Figure 14. Predicted muscle force (% of Maximum Producing Capability) for the infraspinatus and supraspinatus muscles through different external rotation exertions (humeral abduction angle by hand force magnitude) while varying muscle attachment sites and glenohumeral stability properties. Bars represent a 50% probability with the error bars signifying the 1-99% confidence intervals. Results provided for both a 5th percentile female and a 95th percentile male.

3.4.3 *Importance Factors*

With the AMV probabilistic approach involving a transformation of each random variable into standard normal space, these model parameters with different units and potentially widely varying magnitudes are normalized to evaluate their relative contributions to the

predicted output. Results demonstrated that across exertions, subjects and muscles components, uncertainty in muscle attachment sites was generally far more important in predicting muscle force variability than glenohumeral stability constraints.

For the internal rotation tasks, the sensitivity of subscapularis muscle force predominantly relied on the attachment sites of the middle portion of the subscapularis. While each attachment site showed larger relative importance ($\alpha>0.2$) than those of other muscles and glenohumeral stability constraints, there were particular coordinates that were more influential in contributing to force variability. Specifically, for exertions at a neutral arm posture, the y-coordinate (medial-lateral axis) of scapular insertion (muscle origin) of the subscapularis (middle portion) had a higher relative sensitivity for predicting the force for all three muscular components with sensitivity factors ranging from $\alpha = 0.5$ to 0.7 (Figure 15).
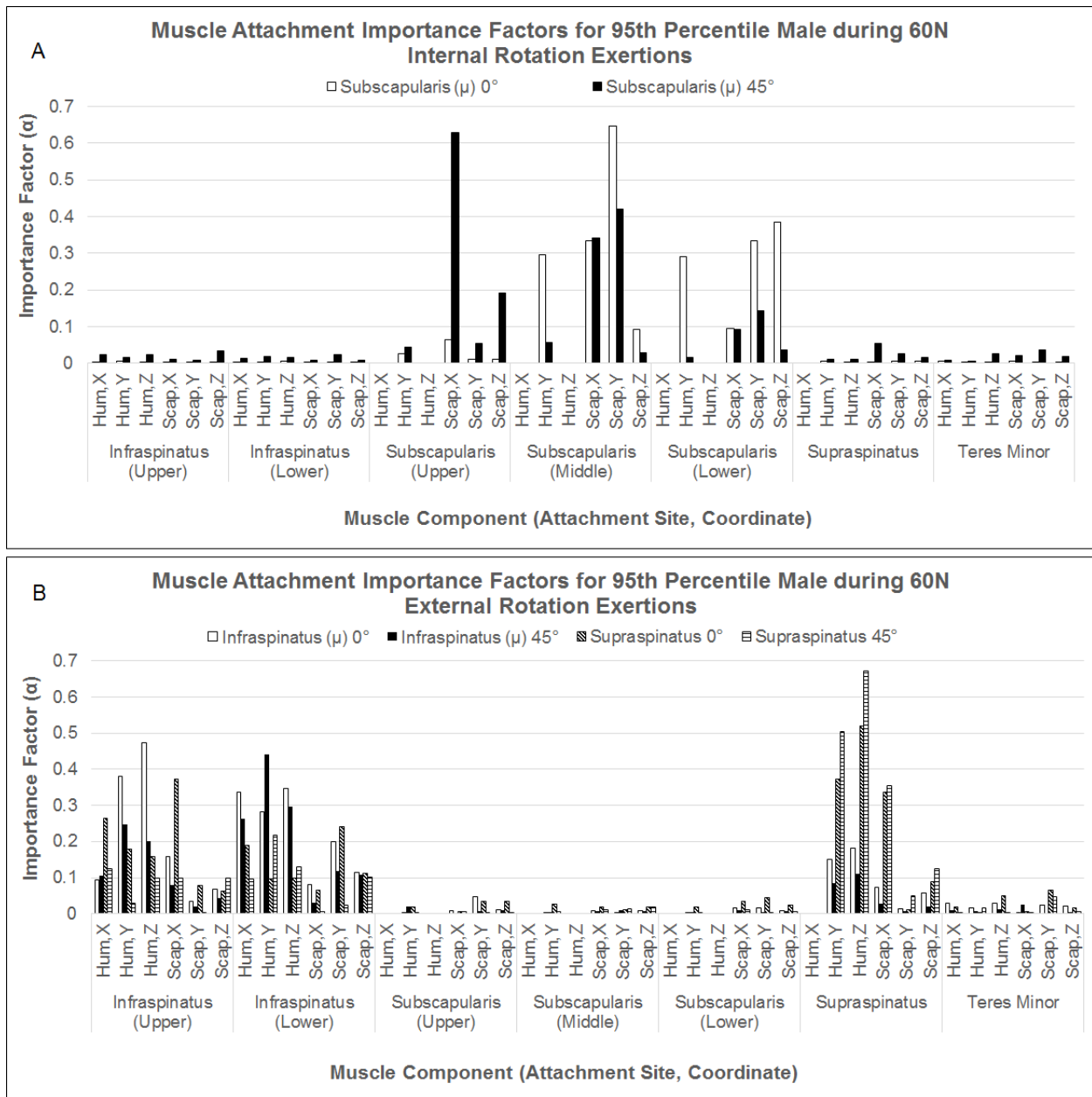
Figure 15. Importance factors (α) of muscle attachment sites for the prediction of (A) average subscapularis muscle force (between muscle components) during internal rotation tasks, and (B) average infraspinatus muscle force and supraspinatus force during external rotation tasks. Results show the 0° and 45° arm posture for a 60N exertion performed by a simulated 95th percentile male. Coordinate description for muscle attachment sites: hum,X = proximal-distal, hum,Y =

anterior-posterior, hum,Z = medial-lateral, scap,X = superior-inferior, scap,Y = medial-lateral, scapZ = anterior-posterior.

For the external rotation tasks, the specificity of importance factors was less pronounced, with many of the muscle attachment parameters related to the infraspinatus and supraspinatus demonstrating sensitivity levels between $\alpha = 0.20$ and 0.50 and limited consistency of those factors exhibiting higher contributions (Figure 15). The trend in importance was generally similar to the internal rotation tasks in that the muscle attachment sites of the infraspinatus influenced infraspinatus force variability and supraspinatus attachments influenced supraspinatus force variability. For both muscles, the trend tended to show higher importance for humeral attachment sites of these muscles, rather than scapular.

While muscle attachment sites were generally more influential for modulating predicted rotator cuff force than glenohumeral stability constraints, the inferior stability threshold was important during both internal and external rotation when the arm was elevated. Notably, for external rotation tasks, forces for the lower portion of the infraspinatus were highly influenced by the inferior constraint, with α-levels greater than 0.45. This infraspinatus component was similarly influenced by the overall stability ratio ($\alpha = 0.3$ to 0.4). For internal rotation tasks, the forces of all three portions of the subscapularis were influenced by the inferior stability constraint (α-levels ~ 0.2 to 0.4).

3.4.4 *Validation: Simulation Techniques and Distribution Effects*

Validation procedures provided confidence in both probabilistic approach and the normality assumption. The AMV probabilistic approach was in good agreement with the Monte Carlo approach with mean differences between techniques for the 1 to 99% confidence interval of $1.5 \pm 1.5\%$ of maximal force capacity (Figure 16). As well, overall, the mean difference

between the two distributions (normal and lognormal) for the 1 to 99% confidence interval was

2.1 ± 2.7%. The largest discrepancies were for the subscapularis predictions at the tail regions,

particularly the middle portion. Alternatively, for the infraspinatus (upper and lower portions)

and the supraspinatus muscles, differences between distribution types was less than 1% of their

total capability for each of the external rotation exertions where force was predicted (Figure 16).
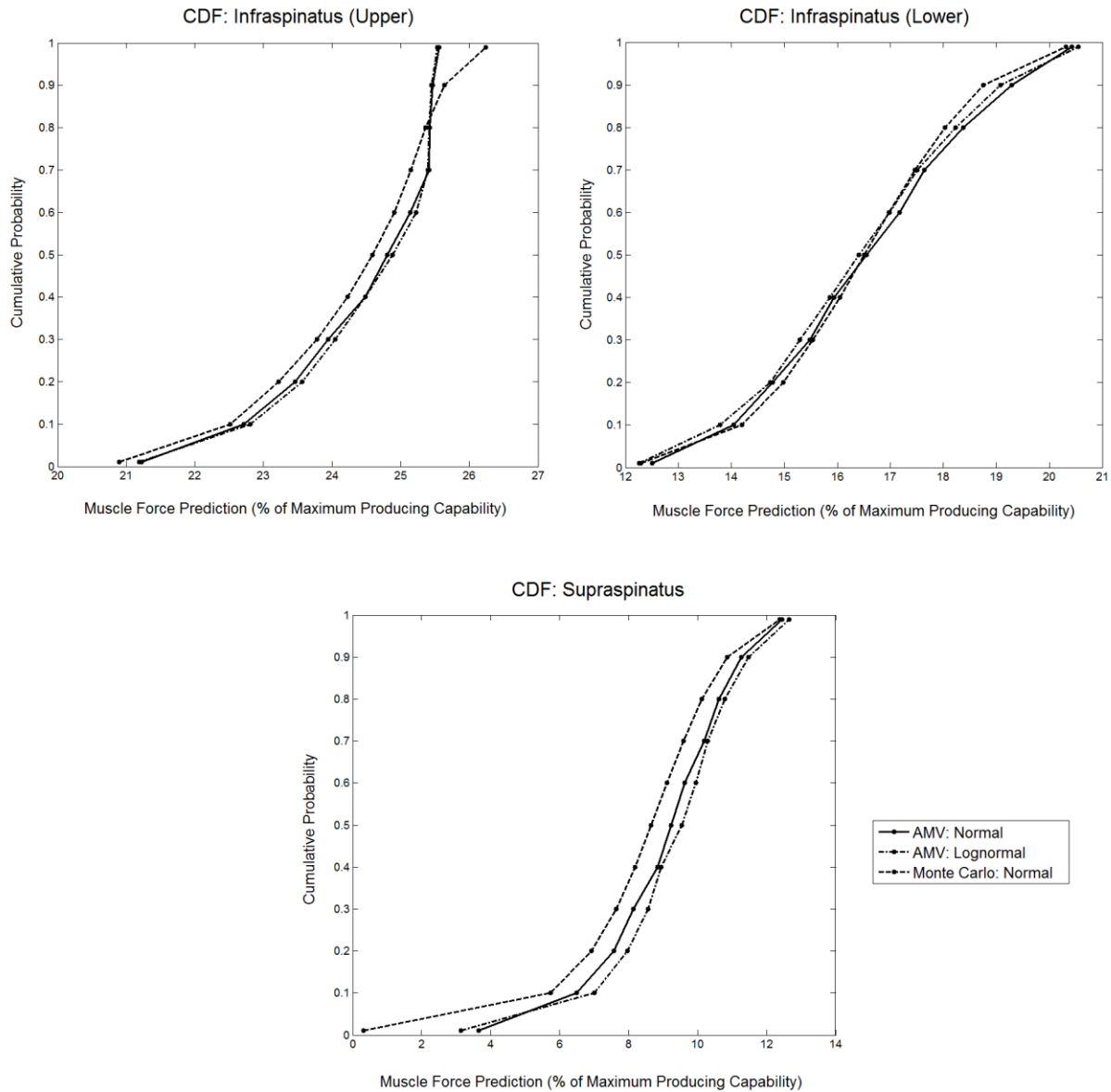
Figure 16. Cumulative distribution function (CDF) representing a 1-99% confidence interval for the Infraspinatus (upper) (top, left), Infraspinatus (lower) (top, right), and Supraspinatus (bottom) muscles for an exertion in which both validation techniques were evaluated: AMV Normal [solid line] versus Monte Carlo Normal [dashed line] versus AMV Lognormal (AMV) [dot-dash line] treated random variables were evaluated. Exertion Description: Abduction (45°), Force direction (external rotation), Force magnitude (40N) for 5th percentile female subject.

3.5   Discussion

This research evaluated the influence of model parameter variability on predicted rotator cuff muscle forces. Modest variation in model parameters resulted in a high level of variability in muscle force predictions illustrating the necessity for incorporating model parameter variability in upper extremity musculoskeletal models.

3.5.1 *Relative contributions of model parameters to muscle force variability*

While both of the modulated parameters related to aspects of musculoskeletal geometry, their influence on force variability differed. The AMV probabilistic method indicated that muscle attachment coordinate variability was more influential in predicting muscle force variability than uncertainty related to glenohumeral stability thresholds (Figure 15). The trend of higher importance for humeral rather than scapular insertions for the supraspinatus and infraspinatus muscles is supported in research by Murray et al. (2002) who concluded that peak moment arms scale to the shortest distance between the axis of rotation and muscle attachment location. Extending this concept to the rotator cuff muscles, with the axis of rotation of the glenohumeral joint being the geometric center of the humeral head, it is intuitive that the shortest distance, and thus more significant parameter, would be the muscle attachment on the humerus. Similarly, in an effort to normalize muscle moment arms between measured cadaveric specimens, a scaling factor considering the radius of the humeral head has been used, further reinforcing the relative importance of the humerus (Kuechle et al. 1997, 2000). While the relative predicted force magnitude and corresponding variability remained somewhat uniform across external exertion types (Figure 14), internal rotation tasks produced notably different trends. Predicted force levels were consistently lower for the 40N exertions compared to the 60N exertions, however, for those exertions with the arm at neutral, greater force was predicted for

76

the subscapularis, with a reverse trend in the magnitude of force predicted for individual muscle components compared to exertions in an abducted posture (Figure 13). That is, for the neutral exertions, larger relative force was predicted for the upper portion of the subscapularis, followed by middle and lower, while for abducted exertions, larger relative force was predicted for the lower portion, followed by middle and upper. Overall, the predicted force for the subscapularis muscle was larger with the arm at neutral with considerably more variability, compared to in an abducted posture. There are several possible hypotheses for this trend. With the arm abducted, it is possible that several surrounding synergistic muscles are better positioned to contribute to the moment, or alternatively, that there are less antagonistic muscles producing competing moments that require much larger subscapularis force to counteract. It is also possible that differences in elicited force for each muscle compartment could be related to changes in their muscle moment arms, however more research is required to substantiate these hypotheses.

Variability in the predicted force across muscles and postures in particular cannot be solely attributed to variability in muscle attachment sites. While the origin and insertion locations overall showed considerably more importance for modulating predicted rotator cuff force than glenohumeral stability constraints, there were exceptions to this trend. Specifically, the inferior glenohumeral stability threshold, demonstrated high importance for both infraspinatus ($\alpha > 0.45$) and subscapularis ($\alpha = 0.2$ to 0.4) muscle force predictions. The selective importance of the inferior stability constraint may be the consequence of the inferiorly directed lines of action of both the subscapularis and infraspinatus muscles. Given that these muscles both compress and resist superior translation of the humerus by applying forces inferiorly, variability in the inferior stability constraint may largely influence the predicted force (Yanagawa et al. 2008). A less restrictive inferior stability threshold may pose risk for inferior dislocation of the glenohumeral

joint, thereby causing lower predicted infraspinatus and subscapularis force to maintain adequate glenohumeral stability. Thus, while previous research suggests that the moment arms of the infraspinatus and subscapularis reduce with abduction, which suggests a corresponding increase in force to achieve the required moment, the similarity in force for the infraspinatus and reduction in force for the subscapularis in these postures may be associated with the glenohumeral stability constraint which may have been more important in modulating force in these abducted postures (Kuechle et al. 2000, Langenderfer et al. 2006).

3.5.2 *Influence of Anthropometrics on Output Variability*

While comparable variability was present across the anthropometric range, these results demonstrate potential implications for task capabilities. Across all exertions, the shoulder capability as calculated by 3D SSPP, was found to be ≥86% for the 95th percentile male and 63% for the 5th percentile female. These capabilities however, do not consider the geometric variation amongst these population, which have been shown to have markedly different predicted force levels. Additionally, for internal rotation exertions, despite demonstrating that 79% of the population had shoulder capability to perform this exertion, the lower portion of the subscapularis muscle demonstrated that for the same 5th percentile female subject, the lower limit predicted the muscle to be inactive, while the upper limit was working at half of their maximal capacity. Similarly, for the same exertion, there were those in the population (upper outliers) that were exerting their maximal producible force for the upper portion of the subscapularis muscle. Thus, failing to incorporate the high variability in muscle demands could significantly underestimate the demands of the task for extremes in the population which in turn would underestimate fatigue development and possible injury.

3.5.3 *Validation Procedures*

A dual model validation was performed. Similar to the findings of previous researchers, the results elicited by the Advanced Mean Value (AMV) probabilistic technique agreed with the Monte Carlo method (Easley et al. 2007, Langenderfer et al. 2008, 2009). The greatest deviance between methods occurred at the tails, with Monte Carlo demonstrating larger variability. Although, differences in the tail region are characteristic of the AMV method, despite improvements from earlier Mean Value techniques, the high variability observed slightly underestimated the variability predicted by Monte Carlo simulations (Easley et al. 2007, Laz and Browne 2010, Wu et al. 1990). The second validation procedure confirmed the normality assumption given for each of the random variables. Normal distributions have been applied in other biomechanics research and were generally identified as adequate for representing the random variables of interest (Flieg et al. 2008, Hughes and An 1997, Langenderfer et al. 2008, Pal et al. 2007). In this research, the 1 to 99% confidence intervals for the lognormal solution of the infraspinatus and supraspinatus muscles agreed to within 1% of the normal solution. The middle portion of the subscapularis muscle demonstrated the highest deviance, with a particular exertion demonstrating a 9% difference between normal and lognormal solutions. Despite showing lower average differences across all other exertions, this deviance highlights the recommendation to, if possible, mathematically determine the particular distribution for each variable using goodness-of-fit tests (Haldar and Mahadevan 2000).

3.5.4 *Model limitations*

Several model limitations should be considered when interpreting this study. Despite using a non-linear objective function, selected based on its previously documented ability to correlate well with empirical data and its ability to better predict synergistic muscle activity

amongst agonists, a fundamental limitation of optimization is the frequent prediction of zero

force for particular muscle(s) (Crowninshield and Brand 1981, Dickerson et al. 2007, 2008, Dul

et al. 1984). The zero predicted muscle force of the teres minor muscle can be explained by its

relatively small physiological cross-sectional area (PCSA). As this objective function acts to

minimize muscle stress among synergistic muscles, it allots larger predicted forces to more

mechanically advantageous muscles, thereby predicting little to no force in smaller muscles that

would otherwise result in high individual stresses (Crowninshield and Brand 1981, Dul et al.

1984). The lack of subscapularis muscle force predicted during the external rotation tasks, and

supraspinatus and infraspinatus during the internal rotation tasks can additionally be attributed to

the optimization approach. Optimization-based models often fail to capture antagonistic activity

as most objective functions are based on mechanical efficiency and muscles that are not directly

contributing to achieving the net joint moment solely increase the physiological cost (Brookham

et al. 2011, Dickerson et al. 2008). Additionally, while muscle origin and insertion locations

were particularly influential in modulating the predicted force, future research is necessary to

evaluate the many other contributors to muscle force variability. Researchers have urged

consideration of model output sensitivity to model parameters including PCSA (Brand et al.

1986, Herzog 1992), muscle line-of-action and/or wrapping (Blajer et al. 2010, Nussbaum et al.

1995), number of modelled muscles (Blajer et al. 2010), muscle moment arms (Hughes and An

1997), body segment parameters (Langenderfer et al. 2008), data collection uncertainties such as

anatomical landmark locations (Langenderfer et al. 2008), in addition to the choice of objective

function as discussed above. Each of these parameters could potentially dramatically influence

predicted individual muscle forces. Thus, the current results highlight the potential importance of

considering the relative influence of each parameter on individual muscle force predictions made by computational musculoskeletal models.

3.6   Conclusions

This research reinforced the importance of considering model parameter variability in musculoskeletal modelling, in particular of the shoulder, highlighting the necessity of incorporating geometric variation, regardless of anthropometry, in the prediction of rotator cuff muscle forces. This study also further emphasized the utility of the AMV probabilistic method in its ability to compute an accurate, computationally inexpensive solution while also identifying the particular variables contributing to output variability. These sensitivity factors may have important surgical, rehabilitative and treatment implications, for applications such as tendon transfers, or the maintenance of adequate active or passive glenohumeral stabilizing structures. Specifically, results showed that for the prediction of rotator cuff muscle forces, failure to incorporate variation in origin and insertion locations can result in output variability up to 50% of maximal capability, between the upper and lower extremes in the population. Thus, solely considering the "average" population in clinical and ergonomic research, may significantly underestimate the risk of injury as these results indicate a likely wide range of tissue-specific task demands within an anthropometrically similar population, consequently leading to possibly different health outcomes.

Chapter 4

Glenohumeral and scapulothoracic kinematic fatigue responses: Implications for subacromial impingement syndrome

Overview

Superior humeral head translation and scapula reorientation can reduce the subacromial space. While these kinematic abnormalities exist in injured populations, the effect of muscle fatigue is unclear. Additionally, these mechanisms were typically studied independently, thereby neglecting potential covariance. This research evaluated the influence of upper extremity muscle fatigue on glenohumeral and scapulothoracic kinematics and defined their relationship. Radiography and motion tracking systems captured these kinematic relationships, during scapula plane elevation, both before and after fatigue. Fatigue-induced changes in humeral head position, scapular orientation and the minimum subacromial space width were measured. High inter-subject variability existed for each measure which precluded identification of mean differences at the population level. However, significant scapula upward rotation occurred following fatigue at $\geq 90°$ elevation, with magnitudes up to 5.5°. Despite similar population mean results, between 35-57% of participants exhibited fatigue-related changes in disadvantageous orientations. Additionally, correlations between measures were generally fair (0.21-0.40) and highly dependent on elevation, likely attributed to the variable fatigue responses. Overall, the data confirms fatigue-induced changes in kinematics that are consistent with elevating the risk of subacromial impingement syndrome are highly variable across individuals. Thus, solely considering the "average" or mean population response likely underestimates potentially injurious fatigue consequences.

4.1   Introduction

Glenohumeral (GH) and scapulothoracic (ST) kinematic variation can influence the healthy geometry of the shoulder by altering the relative relationship between the humerus and scapula. A predominant focus in shoulder biomechanics research has targeted the quantification of these kinematic differences in populations suffering from rotator cuff pathology and/or subacromial impingement syndrome (SAIS) to determine whether a causal relationship can be identified (Deutsch et al. 1996, Endo et al. 2001, Lin et al. 2005, Ludewig and Cook 2000, Ludewig and Reynolds 2009, McClure et al. 2006, Paletta et al. 1997, Poppen and Walker 1976). SAIS results from compression of the tissues, notably the supraspinatus tendon of the rotator cuff, residing between the superior humerus and inferior acromion in an area termed the subacromial space (Michener et al. 2003). This disorder is the most frequently diagnosed injury in the shoulder and has been identified as the primary precursor to the development of rotator cuff pathology, preceding 95% of cases (Michener et al. 2003, Neer 1983, van der Windt et al. 1995, 1996). Debilitating pain, decreased quality of life, lack of independence and compromised function, all accompany rotator cuff pathology (Milgrom et al. 1995). Thus, the prevention of SAIS in society is critical.

While GH and ST kinematic trends have been identified in injured populations, the development of SAIS in healthy individuals is less studied. Different exposures, such as posture, force and repetitive activity historically relate to shoulder pain and injury, with SAIS the predominant diagnosis (Frost and Andersen 1999, Jobe et al. 2000, Svendsen et al. 2004, van Rijn et al. 2010). Upper extremity muscle fatigue is a possible intermediary that relates these work-related task characteristics to SAIS development (Dickerson et al. 2011, Grieve and Dickerson 2008, Michener et al. 2003). Specifically, humeral head position and scapular

83

rotation, tilt and protraction/retraction, demonstrably change as a function of muscular exposure and accompanying fatigue, as the surrounding muscles act to stabilize these bones in a healthy individual (Borstad et al. 2009, Chen et al. 1999, Chopp et al. 2010, 2011, Cote et al. 2009, Ebaugh et al. 2006, McQuade et al. 1998, Teyhen et al. 2008, Tsai et al. 2003).

Primary Research Objectives:

1. Determine the effect of global upper extremity muscle fatigue, from a task that fatigues both the rotator cuff and scapula stabilizer muscles, on GH and ST relationships over the range of scapular plane elevation. Specifically, the effects of fatigue on:

   ➢ Humeral head position (superior-inferior translation)

   ➢ Three-dimensional scapular orientation (rotation, tilt, protraction/retraction)

   ➢ Minimum subacromial space width (SAS)

2. Identify whether a relationship exists, in terms of subacromial space reduction, between fatigue-induced GH and ST changes by assessing the correlation between each kinematic variable and the SAS.

3. Propose an alternate humeral head translation measurement technique that is less dependent on scapular orientation to better quantify the GH relationship.

Secondary Research Objective:

1. Construct population distributions for each of these measures based on the spread of data across subjects to be used as input into a probabilistic subacromial geometry model (Chapter 6).

Research Hypotheses:

It was hypothesized that fatigue would induce changes that reduced the subacromial space, thereby increasing SAIS risk. These changes consist of superior humeral translation (Chopp et al.

2010, Graichen et al. 2000, Matsuki et al. 2012) and downward rotation, anterior tilting and

protraction of the scapula (Ludewig and Reynolds 2009, Phadke et al. 2009). It was also

hypothesized that these subacromial space reducing mechanisms would be correlated with one

another and with the size of the space.

4.2 Methods

This study was collected at St. Joseph's Healthcare Hamilton. The data required to

address the research questions posed in this study were collected simultaneously with that of

Chapter 5.

4.2.1 *Participants*

Thirty healthy, right-hand dominant male participants between the ages of 18 and 35

participated in this research. Healthy was defined as having no self-reported incidences of

shoulder pain or discomfort within the previous year or past shoulder injury or structural

damage, such as fractures or dislocations.

Age was restricted to below 35 years to prevent including participants with degenerative

changes in bone and tissue geometry. Many degenerative changes occur with age, and directly

affect the subacromial space width, thus creating intrinsic impingement (Section 2.3.2). Rotator

cuff tear prevalence and acromial deformities indicative of subacromial space reduction increase

with age, particularly over the age of 50 (Edelson 1995, Milgrom et al. 1995, Sher et al. 1995).

Participants were also selected to represent a younger work force, presumably one that has not

yet been exposed to many years of strenuous and possibly fatiguing-type tasks that may have

already contributed to kinematic changes in the shoulder. In a 2013 statistical report, the

Workplace Safety and Insurance Board (WSIB) identified males between the ages of 50-54 years

in the motor vehicle and transit driver sector as the leading demographic for shoulder-related lost time claims (WSIB, 2013).

Each participant tested negative on Neer and Hawkins-Kennedy clinical impingement tests and had a healthy active range of motion in both sagittal and coronal planes (Boone and Azen 1979, Park et al. 2005). Subjective reports of injury were verified with a full shoulder ultrasound exam (Toshiba Aplio XU, Toshiba Medical Systems Corporation, Japan) using a 7-14MHz linear transducer set to 14MHz. The exam specifically evaluated the rotator cuff, biceps tendon, subacromial bursa, posterior labrum, acromioclavicular joint, and spinoglenoid notch for moderate to severe abnormalities, as well as identified any signs of anterior and/or lateral impingement. Two participants were excluded due to moderate abnormalities in their biceps and supraspinatus tendons. Therefore, twenty-eight participants with a mean age of 24.9 ± 3.6 years and height and weight of 1.8 ± 0.8m and 84.1 ± 14.2kg, respectively, were included.

Sample size was initially selected by conducting an a priori power analysis. A post hoc power analysis was similarly conducted using G*Power3 software (Faul et al. 2007). Statistical power was calculated using a two tailed paired t-test with an alpha level of 0.05. Fatigue-induced differences in scapular rotation with magnitudes previously classified as clinically meaningful (4-5°) (Ebaugh et al. 2005, Ludewig and Cook 2000) and their corresponding standard deviations were used to calculate the power. In addition, power was calculated from the fatigue-induced alternate humeral head translation measurements when differences were of magnitudes which could be considered clinically meaningful (>1mm). Post hoc power of the above measures ranged from 0.92 to >0.99, indicating the sample size was adequate (Cohen 1992).

4.2.2 *Instrumentation*

Digital radiography, optical motion tracking and electromyography systems were used to measure GH, ST and humerothoracic (HT) kinematics and verify muscle fatigue.

4.2.2.1 Digital Radiography

Ten anterior-posterior digital radiographs of the glenohumeral joint were captured for each participant on their right side using the Discovery XR656 Digital Radiography System (GE Healthcare, UK) with technical factors of 70kV and 320mA. Lead shielding protected against radiation.

4.2.2.2 Motion Capture

Six Vicon MX20 motion capture cameras (Vicon, Oxford, UK) were used to track rotations of the scapula and humerus with respect to the torso. Kinematic data was measured at 50Hz. Ten reflective markers were placed on anatomical landmarks of the upper limb (Table 9). Additionally, two marker clusters secured on rigid plates were positioned over the posterior-lateral acromion (van Andel et al. 2009) and on the mid-humerus. These marker clusters tracked the movement of the scapula and humerus during the trials in an effort to reduce skin motion artifact. Cameras were configured around the x-ray system to ensure that each marker was visible on at least two cameras during measurement trials. This allowed for simultaneous measurement of the two systems (radiography and motion capture).

Table 9. Reflective markers required to calculate the local coordinate systems, and subsequently calculate scapulothoracic and humerothoracic joint angles as per ISB recommendations (Wu et al. 2005).

Segment	Markers Required for Calculation of Local Coordinate System
Humerus	Medial Epicondyle (ME), Lateral Epicondyle (LE), Acromioclavicular Joint (AC), Angulus Acromialis (AA)
Scapula	Trigonum Spinae Scapulae (TS), Angulus Inferior (IA), Angulus Acromialis (AA)
Torso	C7 Vertebrae (C7), Incisura Jugularis (IJ), T8 Vertebrae (T8), Xiphoid Process (PX)

4.2.2.3 Electromyography

Electromyography (EMG) was used to measure muscle activity from six muscles. Surface electrodes were used to collect activity from the primary scapula stabilizer muscles: the serratus anterior muscle and the upper and lower portions of the trapezius muscle (Michener et al. 2003). Intramuscular electrodes were used to collect activity from three of the four rotator cuff muscles: supraspinatus, infraspinatus, and subscapularis. Activity collected from the teres minor muscle using intramuscular electrodes often contains significant motion artifacts and was therefore not included (Brookham and Dickerson 2013). Additionally, surface electrodes were placed on the supraspinatus and infraspinatus muscles (surrounding the wire).

Bipolar Ag-AgCl Noraxon dual surface electrodes (Noraxon, Arizona) with a fixed 2cm spacing were placed over the muscle belly of each muscle on the right side of the body using published placements (Cram and Kasman 1998) (Table 10). Prior to placement, the skin overlying the muscle was shaved with a disposable razor and cleaned with isopropyl alcohol to minimize impedance.

Hypodermic needles, each containing two sterilized fine-wires with hooked ends (Motion

Lab Systems, Inc., Louisiana), were inserted into the rotator cuff muscles on the right side of the

body. Electrodes were gamma radiation sterilized and each was contained within its own

sterilized packaging. Prior to insertion, the area overlying the muscle was shaved with a

disposable razor (if required) and cleaned with isopropyl alcohol. The insertions were performed

in accordance with previously published instructions (Geiringer 1999, Nemeth et al. 1990)

(Table 10). After each needle was inserted to the appropriate depth into the muscle (using visual

feedback) it was removed and safely disposed in a sharps biohazardous waste container. The pair

of wires remained inserted into the muscle where they were used to measure muscle activity.

Table 10. EMG electrode placements for collected muscles. Surface EMG electrode placements

from Cram and Kasman (1998), fine-wire EMG electrode placements from Geiringer (1999)

(Supraspinatus, Infraspinatus) and Nemeth et al. (1990) (Subscapularis).

Muscle	EMG Electrode Placement[6]	Figure of Electrode Placement
Supraspinatus (fine-wire/surface)	*Participant lay prone with their arm at their side* Needle was inserted superior to the medial one-third of scapular spine Note: Surface electrodes were placed on either side of the wire once inserted	

---

[6] For all surface electrode placements, participants were in a relaxed seated posture. For fine-wire needle insertions, the participant was positioned as described in Table 10.

Infraspinatus (fine-wire/surface)	*Participant lay prone with their arm at their side* Needle was inserted into the center of the fossa; midway between the scapular spine and the inferior tip of the scapula and between the medial and lateral borders Note: Surface electrodes were placed on either side of the wire once inserted	
Subscapularis (fine-wire)	*Participant seated with their arm elevated in the sagittal plane and elbow flexed to 90° (assistant holding their arm)* Needle was inserted under the edge of the scapula in the posterior axillary line at a point 8cm above the inferior angle of the scapula adjacent to an underlying rib	
Upper Trapezius (surface)	Surface electrodes were placed along the ridge of the shoulder slightly lateral and half the distance between the C7 vertebrae and the acromion	

Lower Trapezius (surface)	Surface electrodes were placed approximately 5cm below the scapular spine at a 55° angle next to the medial edge of the scapula	
Serratus Anterior (surface)	Surface electrodes were placed below the axillary area at the level of the inferior tip of the scapula	

All EMG signals were collected at 3000Hz using the Noraxon Telemyo 2400 T G2 wireless system. Raw signals were band pass filtered from 10-1000Hz and differentially amplified with a common-mode rejection ratio >100dB and an input impedance of 100MΩ. Analog signals were converted to digital using a 16 bit A/D card with a ±3.5V range.

4.2.3 *Protocol*

The experimental protocol was completed in approximately 2.5 hours and involved several stages which have been described as follows.

4.2.3.1 Strength Scaling

Strength scaling procedures were performed to determine the individualized load lifted during the fatiguing protocol (Chopp et al. 2010). With the arm abducted to 90° and the humerus externally rotated (palm facing forward), participants exerted a maximal posterior force and anterior force against an ErgoFet 300™ hand dynamometer (Hoggan Scientific, LLC, Utah). These specific internal (anterior force) and external (posterior force) exertions above shoulder height were selected as they directly relate to rotator cuff muscle demands, while also requiring scapular stabilization; thus they should target each of the six muscles described. Each exertion was performed twice unless directional exertions differ by ±5N, in which case a third exertion was performed. The average of these four exertions (two anterior and two posterior) were defined as participants' "maximal force".

4.2.3.2 Pre-Fatigue Kinematic Measurement

Participants were instrumented with the ten reflective markers and two clusters (Table 9), following which five randomized kinematic trials were collected. For each trial, participants were positioned at 30° (scapular plane) to the plane of the x-ray beam; their arm was elevated to five elevation angles (0, 30, 60, 90 and 120°) in neutral axial rotation. A digital radiograph and five-second motion capture trial were simultaneously collected in each posture. Participants held a 1kg weight during each trial, consistent with previous research (Chen et al. 1999, Chopp et al. 2010, Cote et al. 2009, Teyhen et al. 2008). Foot placement and elevation angles were marked to replicate the kinematic trial posture following fatigue (Section 4.2.3.5).

4.2.3.3 Pre-Fatigue EMG Reference Exertions

Following kinematic trials, participants were instrumented with EMG and completed five-second static reference exertions in two postures. Specifically, lying prone on a clinical

92

bench, participants elevated their arm to 60° and 120° in the coronal plane while holding a load scaled to 10% of their maximal force (Section 4.2.3.1).

4.2.3.4 *Fatiguing Protocol*

Participants performed an upper extremity fatiguing protocol consisting of an overhead, repetitive task designed to exhaust the rotator cuff and scapular stabilizing muscles. Lying prone, participants started with their arm fully extended and abducted to 60° in the coronal plane with their palm facing anteriorly (Figure 17). They repeatedly lifted and lowered their arm from this position to 120° of elevation holding a weight scaled to 10% of their maximal force (Section 4.2.3.1). Participants repeated this motion at a pace set by a metronome (44 beats per minute), while cycling through 15 seconds of exertion, followed by 10 seconds of rest. After each minute of performing the task, participants were asked to indicate their rating on Borg's modified (10-point) rate of perceived exertion (RPE) scale (Borg 1982). This task was performed until participants verbally indicated that they could no longer continue ('10' on the RPE scale), and/or could no longer complete the task properly, such as dropping the arm below 90°, or being unable to maintain the pace set by the metronome.

Figure 17. Experimental Fatiguing Protocol: lying prone, arm was elevated between 60° (left) and 120° (right) in the coronal plane holding a weight scaled to 10% of their maximal force.

4.2.3.5   Post-Fatigue EMG Reference Exertions and Kinematic Measurement

Immediately upon indicating that they could no longer continue the fatiguing protocol, participants completed post-fatigue EMG reference exertions identical to those described in Section 4.2.3.3, the maximal exertions described in Section 4.2.3.1 and post-fatigue kinematic trials, identical to those described in Section 4.2.3.2.

4.3   Data and Statistical Analyses

4.3.1 *Kinematic Measurement*

Six kinematic variables were measured in all trials (Table 11). GH variables (SAS, humeral head position), captured using imaging techniques, were analyzed using GE PACS software (GE Healthcare, United Kingdom). Each variable obtained from radiographic images was measured to the nearest 0.1mm. ST and HT angles, captured using motion capture, were

analyzed using custom Matlab® software. The following sections outline the specific

measurement techniques used to obtain each variable.

Table 11. Glenohumeral and scapulothoracic kinematic variables measured in both pre- and

post-fatigue states, including their units and the measurement system from which they were

captured.

Variable	Units	Measurement System
Minimum Subacromial Space Width	millimeters	Radiography
Superior-Inferior Translation	millimeters	Radiography
Scapular Upward-Downward Rotation	degrees	Motion Capture
Scapular Posterior-Anterior Tilt	degrees	Motion Capture
Scapular Protraction-Retraction	degrees	Motion Capture
Humeral Elevation	degrees	Motion Capture

4.3.1.1   *Minimum Subacromial Space Width (SAS)*

The minimum subacromial space width (SAS) was measured on ten radiographic images

for each participant, corresponding to the two fatigue states (pre-fatigue and post-fatigue) and

five arm elevation angles (0°, 30°, 60°, 90°, 120°). Specifically, the measurement technique has

been described as: the minimum distance between the superior aspect of the humeral head and

the dense cortical undersurface of the acromion process (Gruber et al. 2010, Lehtinen et al. 2000,

Petersson and Redlund-Johnell 1984, Thompson et al. 2011, Weiner and MacNab 1970) (Figure

18).
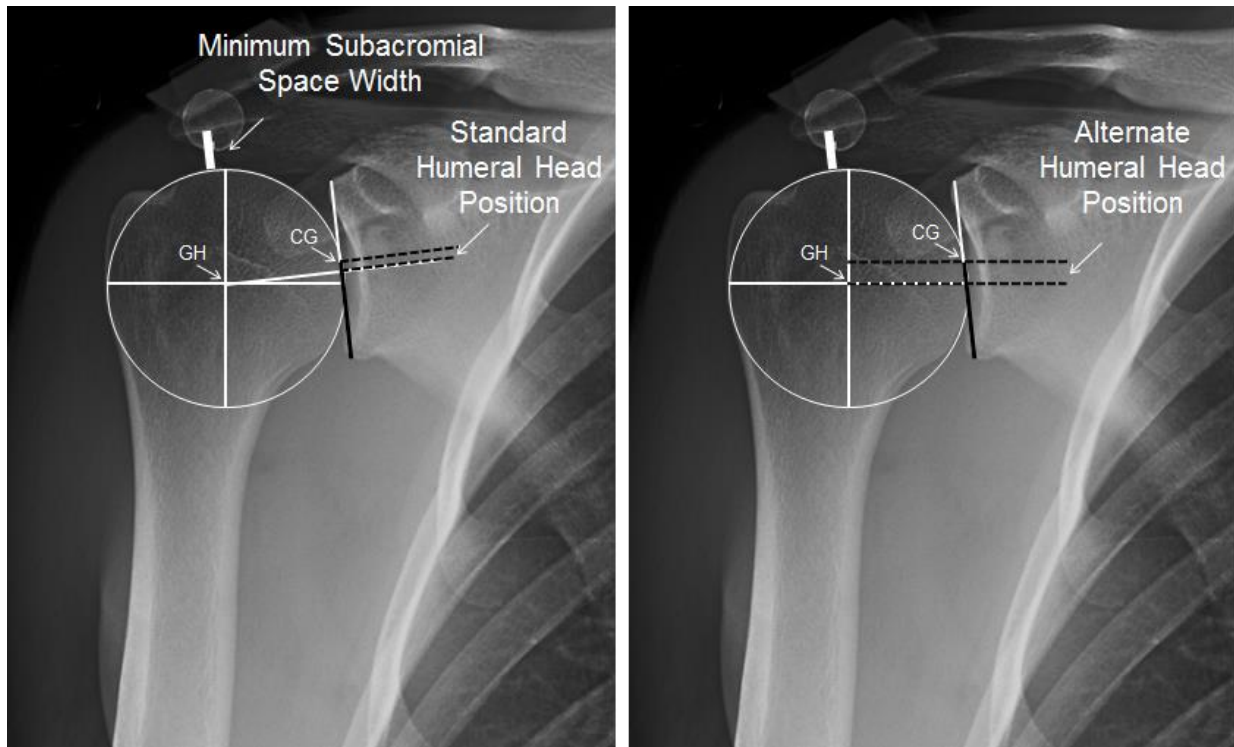
Figure 18. Radiographic measurement of: (1) minimum subacromial space width (left), (2) humeral head position – standard measurement technique (left) and (3) humeral head position – alternate measurement technique (right). GH indicates the center of the humeral head (determined by identifying the center of a true circle fit to the outer contours of the humeral head). CG indicates the center of the glenoid cavity (determined by identifying the midpoint of a line connecting the most superior to the most inferior points of the anterior articular margin of the glenoid cavity [glenoid axis]). Humeral head position is a linear measurement along the glenoid axis. This figure represents an inferior humeral head position as the GH is inferior to the CG.

4.3.1.2 *Superior-Inferior Humeral Head Translation*

The humeral head position was measured on radiographic images for both pre- and post-fatigue states at five elevation angles (0°, 30°, 60°, 90°, 120°). The measurement technique was standardized by Poppen and Walker (1976) and used in many research studies (Chen et al. 1999,

Chopp et al. 2010, Cote et al. 2009, Paletta et al. 1997, Royer et al. 2009, Teyhen et al. 2008, 2010, Yamaguchi et al. 2000). This technique required first identifying the center of a true circle fit to the outer contours of the humeral head and connecting a line (glenoid axis) from the most superior to the most inferior points of the anterior articular margin of the glenoid cavity (Figure 18). A perpendicular line was then drawn from the center of the humeral head to the glenoid axis, from which the distance (along the glenoid axis) between the center of the glenoid axis and this perpendicular line was extracted. This measurement was termed the humeral head position. The difference in this distance (humeral head position) between fatigue states was termed the humeral head translation. A positive translation resulted when the center of the humeral head was positioned more superiorly to the center of the glenoid cavity following fatigue, while negative translation occurred when the humeral head moved to a more inferior position.

The alternate humeral head translation measurement technique developed in the current research involved a modification to the standardized technique to better quantify the glenohumeral superior-inferior shift in conditions where considerable scapular rotation may have confounded measurement outputs. This method first involved determining the centers of the humeral head and the glenoid cavity, using an identical process to the standard method. Two lines horizontal to the image axis were then drawn through these centers. The distance between these two centers, determined from a line drawn parallel to the glenoid axis (to maintain anatomical relevance), was then calculated and the difference in these measurements between fatigue states was considered the humeral head translation (Figure 18). Similar to the previous measurement, a positive magnitude indicated a superior shift, while a negative magnitude indicated an inferior shift.

4.3.1.3 *Scapulothoracic and Humerothoracic Rotations*

ST and HT angles were derived from the Vicon motion capture data using custom

Matlab® software. Kinematic data was low pass filtered using a fourth order Butterworth filter

with 4Hz cut off. Local coordinate systems were then constructed for the humerus, scapula and

torso segments according to International Society of Biomechanics (ISB) recommendations

(Table 12) (Wu et al. 2005) using the landmarks indicated in **Table 9**. Local coordinate systems

for the rigid clusters (acromial cluster, humerus) were constructed, and the relationship between

the clusters and the anatomical landmarks on the corresponding segments were determined from

the static calibration trial. The clusters were then used to track the movements of the scapula and

humerus with respect to the torso during trials. Using the previously defined relationship

between the clusters and the anatomical markers, relative rotation matrices between the

reconstructed scapula and torso and the reconstructed humerus and torso were calculated. Euler

angles were then extracted using a Y-X-Z rotation sequence [Eq. 4-1] for the scapulothoracic

relationship and Y-X-Y′ rotation sequence [Eq. 4-2] for the humerothoracic relationship, as per

ISB recommendations (Wu et al. 2005).

Table 12. Local coordinate systems of the humerus, scapula and torso as per ISB

recommendations (Wu et al. 2005).

Segment	Landmarks Required	Local Coordinate System
Humerus	GH[*], ME, LE, E[**]	$y_h = \frac{(GE-E)}{\|(GE-E)\|}$ $temp_h = \frac{(ME-E)}{\|(ME-E)\|}$ $x_h = \frac{temp_h \times y_h}{\|temp_h \times y_h\|}$ $z_h = x_h \times y_h$

Scapula	TS, IA, AA	$z_s = \frac{(AA-TS)}{\|(AA-TS)\|}$
		$temp_s = \frac{(AA-IA)}{\|(AA-IA)\|}$
		$x_s = \frac{temp_s \times z_h}{\|temp_s \times z_h\|}$
		$y_s = z_s \times x_s$
Torso	C7, IJ, T8, PX	$y_t = \frac{\left(\left(\frac{IJ+C7}{2}\right)-\left(\frac{PX+T8}{2}\right)\right)}{\left\|\left(\left(\frac{IJ+C7}{2}\right)-\left(\frac{PX+T8}{2}\right)\right)\right\|}$
		$temp_t = \frac{(IJ-C7)}{\|(IJ-C7)\|}$
		$z_t = \frac{temp_t \times y_t}{\|temp_t \times y_t\|}$
		$x_t = y_t \times z_t$

[*]GH = Glenohumeral Rotation Center. This landmark is located 60mm caudal from the acromion process (midpoint between AA and AC markers) along the torso long axis (y_t) (Nussbaum and Zhang 2000).

[**]E = Elbow Joint Center. This landmark is obtained by finding the midpoint between the ME and LE markers.

$$R_{T\_S} = R_Z(\alpha)R_X(\beta)R_Y(\gamma) \qquad\qquad \text{[Eq.4-1]}$$

$$R_{T\_S} = \begin{bmatrix} cos\gamma cos\alpha - sin\gamma sin\beta sin\alpha & -cos\beta sin\alpha & sin\gamma cos\alpha + cos\gamma sin\beta sin\alpha \\ cos\gamma sin\alpha + sin\gamma cos\alpha sin\beta & cos\beta cos\alpha & sin\gamma sin\alpha - cos\gamma cos\alpha sin\beta \\ -sin\gamma cos\beta & sin\beta & cos\gamma cos\beta \end{bmatrix}$$

Where,

α is scapula anterior/posterior tilt

β is scapula upward/downward rotation

γ is scapula protraction/retraction

$$R_{T\_H} = R_{Y'}(\gamma_2)R_X(\beta)R_Y(\gamma) \qquad\qquad \text{[Eq.4-2]}$$

$$R_{T\_H} = \begin{bmatrix} cos\gamma cos\gamma_2 - sin\gamma cos\beta sin\gamma_2 & sin\beta sin\gamma_2 & sin\gamma cos\gamma_2 + cos\gamma cos\beta sin\gamma_2 \\ sin\gamma sin\beta & cos\beta & -cos\gamma sin\beta \\ -cos\gamma sin\gamma_2 - sin\gamma cos\beta cos\gamma_2 & sin\beta cos\gamma_2 & cos\gamma cos\beta cos\gamma_2 - sin\gamma sin\gamma_2 \end{bmatrix}$$

Where,

γ is plane of humeral elevation

β is humeral elevation

γ_2 is humeral internal/external rotation

To more accurately quantify the effects of ST kinematics on the radiographic humeral head translation measurements, scapular upward/downward rotation was also measured on radiographs using a simplified technique previously described in the literature (Freedman and Munro 1966, Poppen and Walker 1976). This angle was calculated from a line drawn along the horizontal image axis, approximately perpendicular to the long axis of the torso, and the previously defined glenoid axis (Section 4.3.1.2). The angle in the superior-medial quadrant was the scapula radiographic rotation angle, with 90° indicating neutral rotation, a lower angle (<90°) indicating higher scapula upward rotation and a higher angle (>90°) indicating higher scapula downward rotation.

4.3.2 *Electromyography*

EMG was processed in the frequency domain to assess whether the six measured muscles were fatigued from the protocol, as demonstrated previously in pilot research. Raw signals were first high pass filtered with a 30Hz cut off to remove heart rate contamination (Drake and Callaghan 2006) and a Fourier transform was performed on the resulting signals. The mean power frequency (MPF) of each 0.5 second window for the first two seconds of each trial was then calculated, and an overall mean obtained, which was compared between fatigue states. Changes in EMG amplitude were not used for fatigue verification due to its previously described unreliability (Dimitrova and Dimitrov 2003).

4.3.3 *Statistical Analyses*

4.3.3.1   **Kinematics**

Five two-way repeated measures analysis of variances (ANOVAs) were used to determine the effects of fatigue state (pre-fatigue, post-fatigue) and elevation angle (0°, 30°, 60°, 90°, 120°) on all GH and ST kinematic variables. Paired t-tests were used to evaluate angle-

specific fatigue responses. A p-value of 0.05 was used to determine significance. Statistical analyses was performed using JMP software (SAS Institute, North Carolina).

Variable covariance was determined by calculating correlation coefficients between fatigue-related differences (post-fatigue measurement – pre-fatigue measurement) at each elevation angle. Coefficients were classified as excellent (0.81 – 1.00), good (0.61 – 0.80), moderate (0.41 – 0.60), fair (0.21 – 0.40) or poor (0.00 – 0.20), as described in Balke et al. (2013). As well, the clinical significance of fatigue-induced differences was assessed by considering the proportion of participants exhibiting kinematic changes consistent with SAS narrowing (superior humeral head translation, downward scapula rotation, anterior scapular tilt, scapular protraction and a reduction in SAS).

4.3.3.2 Fatigue

Paired t-tests were used to determine the effect of fatigue state (pre-fatigue, post-fatigue) on: (1) MPF for each of the six muscles during both 60° and 120° exertions, and (2) maximal muscle force for internal and external exertions. Statistically significant decreases in MPF in the post-fatigue state provided evidence of fatigue for the specific muscle, while overall upper extremity fatigue was verified by a statistically significant reduction in maximal force from internal (anterior) and external (posterior) exertions. A p-value of 0.05 was used to determine significance.

4.3.3.3 Verification and Reliability

Measurement reliability was performed on a subset of 15 randomized and blinded images. All measurements were performed by JN Chopp-Hurley who has previous experience extracting humeral head position measurements from anterior-posterior GH radiographs, as confirmed by an experienced musculoskeletal radiologist (Chopp et al. 2010). An intra-rater

101

reliability analysis was conducted to assess the measurement reliability of the SAS and to re-confirm humeral head position measurement reliability. Given this confirmation, an inter-rater reliability analysis was performed for the measured SAS. The second rater was the same experienced musculoskeletal radiologist, who previously confirmed the initial reliability of the primary rater for humeral head position measurements (Chopp et al. 2010). The Bland-Altman approach, conducted using Matlab®, was used to evaluate measurement reliability (Bland and Altman 2010). For each measurement, the differences between initial and repeated measurements (d) were calculated for each participant from which the mean ($\bar{d}$) and standard deviation (s) of these differences were obtained. The average measurement for each participant (*x-axis*) were plotted against the difference between the initial and repeated measurement (*y-axis*) and lines were drawn representing the mean difference ($\bar{d}$) as well as approximate 95% confidence limits ($\bar{d} \pm 2s$) (Bland and Altman 2010). Additionally, paired t-tests ($p<0.05$) were performed and intraclass correlation coefficients calculated using SPSS Statistics 22 (IBM Corporation, USA) to confirm results of the Bland-Altman analysis.

Two verification procedures were performed to evaluate the accuracy of the motion tracking system. The humeral elevation angle, as measured using a hand-held goniometer was compared to that extracted from the motion capture data. As well, the scapula rotation angle, as measured from the motion capture data was compared to the magnitude measured radiographically. As scapulothoracic angles were measured using different procedures, verification was performed by evaluating the pre-post fatigue differences at each elevation angle. Bland-Altman analysis and intraclass correlation coefficients were used to verify the ability of the motion tracking system to adequately measure ST and HT joint angles (Matlab®; SPSS Statistics 22, IBM Corporation, USA).

4.4 Results

4.4.1 *Kinematics*

Considerable inter-subject variability existed across all kinematic variables, which generally resulted in non-significant mean fatigue response differences. However, significant fatigue-induced upward rotation of the scapula was present, as well as angle-dependent responses for each of the GH and ST kinematic variables.

4.4.1.1 *Humeral Head Position*

Humeral head position was not largely influenced by muscle fatigue. Using the standard measurement technique, there was no statistically significant effect of fatigue (p=0.1495) and no angle-fatigue interaction (p=0.9216). Humeral head position was, however, affected by arm angle (p<0.0001). The humeral head, which was located at an inferior position at neutral (0°) elevation, translated approximately 3mm superiorly as the arm was elevated to 120° (Table 13). This trend was consistent between fatigue states. Overall, the mean intra-angle differences between fatigue states (humeral head translation) were ≤ 0.3mm, however considerable variability was present (Table 13, Figure 19).

Humeral head position using the alternate measurement technique demonstrated main effects of both fatigue (p<0.0001) and arm angle (p<0.0001) as well as a significant interaction effect (p=0.0001). Specifically, fatigue-induced superior translation was present at all elevation angles, increasing in magnitude up to 4.3mm as the arm was elevated to 120° (Table 13).

Table 13. Humeral head position for the pre- and post- fatigue states (standard measurement technique), and the fatigue-induced humeral head translation using standard and alternate measurement techniques. Asterisk (*) indicates statistically significant (p<0.05) fatigue-induced translation.

Elevation Angle (°)	Pre-Fatigue (mm) (Mean [1-99% CI])[1]	Post-Fatigue (mm) (Mean [1-99% CI])[1]	Humeral Head Translation: *Standard Measurement* (Mean [1-99% CI])[2]	Humeral Head Translation: *Alternate Measurement* (Mean [1-99% CI])[2]
0	-0.4 [-4.6 – 3.8]	-0.6 [-6.0 – 4.7]	-0.2 [-4.3– 3.8]	0.5 [-10.4 – 11.4]
30	0.7 [-3.1 – 4.4]	0.5 [-4.2 – 5.3]	-0.1 [-2.7 – 2.5]	**1.9 [-5.8 – 9.7]** *
60	1.4 [-2.4 – 5.3]	1.4 [-2.0 – 4.7]	-0.1 [-2.9 – 2.8]	**1.9 [-6.3 – 10.2]** *
90	2.1 [-0.5 – 4.6]	1.8 [-1.2 – 4.8]	**-0.3 [-2.7 – 2.1]** *	**3.6 [-8.2 – 15.3]** *
120	2.5 [-0.6 – 5.5]	2.4 [-0.7 – 5.6]	0.0 [-3.3 – 3.3]	**4.3 [-5.8 – 14.4]** *

[1] Positive values (+) indicate the center of humerus is located superior to center of glenoid cavity
[2] Positive values (+) indicate a superior translation of the humeral head with respect to the glenoid cavity following fatigue.
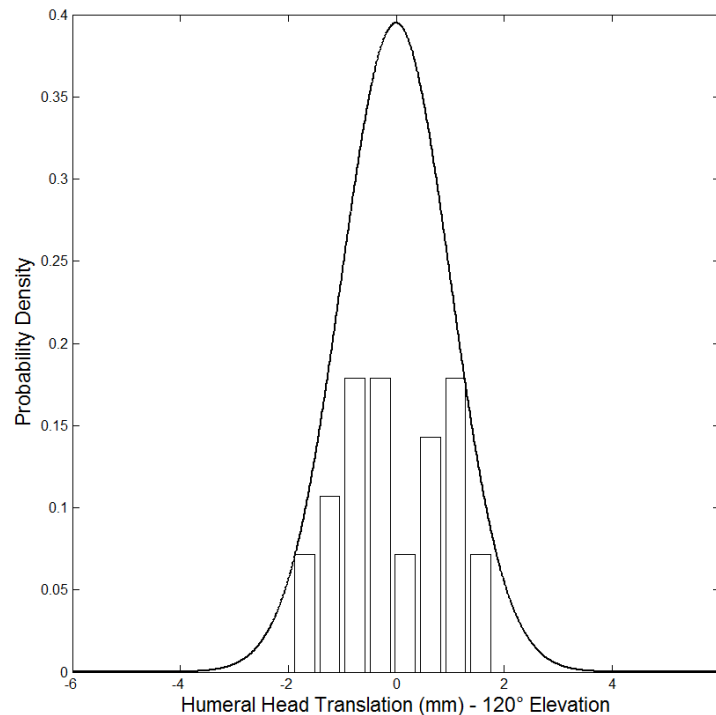
Figure 19. Frequency histogram displaying distribution of humeral head translation at 120° of elevation, fit with a normal curve.

4.4.1.2 Scapular Orientation

Fatigue-related changes only existed for scapula upward rotation (p=0.0002) while both upward/downward rotation and protraction/retraction were significantly influenced by arm angle (p<0.0001). Individual angle-specific evaluation identified fatigue-induced upward rotation magnitudes up to 5.5° at 120° of elevation (Table 14). Scapula tilt and protraction/retraction were not significantly influenced by fatigue. With respect to elevation angle, upward rotation of the scapula existed across the range of elevation with a mean rotation angle of 0.1 ± 5.9° at neutral to 31.3 ± 13.7° at 120° of elevation. Additionally, the scapula demonstrated increased protraction of 5-6°, while the scapular tilt angle remained unchanged.

Table 14. Fatigue-induced scapula rotation, tilt and protraction/retraction across the range of scapular plane elevation. Asterisk (*) indicates statistically significant (p<0.05) fatigue-induced changes.

Elevation Angle (°)	Upward Rotation (°) (Mean [1-99% CI])	Posterior Tilt (°) (Mean [1-99% CI])	Retraction (°) (Mean [1-99% CI])
0	0.7 [-17.1 – 18.5]	-1.0 [-25.6 – 23.7]	-3.0 [-29.5 – 23.5]
30	**2.3 [-14.9 – 19.5]** *	0.4 [-16.5 – 17.3]	-1.6 [-21.8 – 18.6]
60	1.3 [-14.0 – 16.6]	-0.8 [-20.2 – 18.7]	-0.9 [-17.5 – 15.7]
90	**3.6 [-18.2 – 25.5]** *	-0.5 [-18.4 – 17.3]	-1.3 [-19.3 – 16.7]
120	**5.5 [-21.7 – 32.7]** *	-0.9 [-38.8 – 37.1]	2.2 [-25.0 – 29.5]

Negative values (-) indicate downward rotation, anterior tilt, protraction

Scapula rotation quantified from radiographic images was significantly influenced by fatigue (p<0.0001), arm angle (p<0.0001), and demonstrated a fatigue-angle interaction effect (p=0.0046). Fatigue-induced upward rotation of the scapula occurred across all elevation angles with larger differences present at higher elevation angles (Table 15). Additionally, the scapula

upwardly rotated between 35 to 40° (depending on fatigue state) as the arm was elevated from neutral to 120° of elevation.

Table 15. Scapula radiographic rotation angle across the range of scapular plane elevation for the pre- and post-fatigue states. Asterisk (*) indicates statistically significant (p<0.05) difference from pre-fatigue state.

Elevation Angle (°)	Pre-Fatigue (°) (Mean [1-99% CI])	Post-Fatigue (°) (Mean [1-99% CI])
0	96.3 [73.8 – 118.9]	94.8 [71.0 – 118.5]
30	88.1 [64.2 – 112.0]	**83.8 [58.8 – 108.8] ***
60	79.0 [55.5 – 102.5]	**74.9 [51.4 – 98.4] ***
90	72.3 [49.2 – 95.4]	**64.9 [43.5 – 86.2] ***
120	60.9 [38.7 – 83.2]	**54.2 [31.8 – 76.7] ***

90° = Neutral rotation, >90° = Downward rotation, <90° = Upward rotation

4.4.1.3 *Minimum Subacromial Space Width (SAS)*

The SAS was not significantly affected by fatigue (p=0.5896) and there was no angle-fatigue interaction (p=0.7660). However, the SAS was affected by arm angle (p<0.0001), with a significant reduction in space as the arm was elevated (Table 16). Within each fatigue state, the SAS was lowest at the 90° arm angle, and slightly increased as the arm was elevated to 120°. In the post-fatigue state, the SAS was increased at 0° and 60° and reduced at 90° and 120°, compared to the pre-fatigued state (Table 16). However, all of these changes were small and not statistically significant, likely due to high variability.

Table 16. Minimum subacromial space width (SAS) across the range of scapular plane elevation for the pre- and post- fatigue states.

Elevation Angle (°)	Pre-Fatigue (mm) (Mean [1-99% CI])	Post-Fatigue (mm) (Mean [1-99% CI])
0	9.6 [4.1 – 15.2]	10.0 [3.1 – 16.9]
30	7.6 [3.4 – 11.8]	7.6 [2.3 – 12.9]
60	5.4 [1.3 – 9.5]	5.9 [2.6 – 9.2]
90	4.2 [-0.4 – 8.9]	4.1 [-0.3 – 8.6]
120	4.6 [-0.1 – 9.3]	4.4 [0.2 – 8.5]

4.4.1.4 Covariance and Interactions

Correlation coefficients were generally classified as fair and depended largely on elevation angle. The strongest correlation existed between humeral head translation and the SAS (-0.69) (Table 17). Changes in scapular tilt and protraction/retraction were also moderately correlated with the SAS, and posterior tilting was moderately correlated with humeral head translation. All other relationships had a fair correlation (0.21 to 0.40) for at least one elevation angle (Table 17). However, for all variables interactions, both coefficient magnitudes and polarities were markedly different across elevation angles.

Table 17. Correlation matrix between fatigue-induced kinematic changes (strongest (*s*) and weakest (*w*) relationships across elevation angles presented). Relationships classified as moderate to excellent are bolded.

	Δ Humeral Head Position (+=Superior)	Δ Scapular Rotation (+=Upward)	Δ Scapular Tilt (+=Posterior)	Δ Scapular Protraction/ Retraction (+=Retraction)	Δ Subacromial Space Width (+=Increase SAS)
Δ Humeral Head Position (+=Superior)		*s*: 0.29 *w*: -0.23	***s*: 0.41** *w*: -0.13	*s*: 0.27 *w*: -0.25	***s*: -0.69** *w*: 0.20
Δ Scapular Rotation (+=Upward)	*s*: 0.29 *w*: -0.23		*s*: -0.23 *w*: -0.05	*s*: 0.38 *w*: -0.10	*s*: -0.39 *w*: 0.25
Δ Scapular Tilt (+=Posterior)	***s*: 0.41** *w*: -0.13	*s*: -0.23 *w*: -0.05		*s*: -0.33 *w*: -0.12	***s*: 0.49** *w*: -0.42
Δ Scapular Protraction/ Retraction (+=Retraction)	*s*: 0.27 *w*: -0.25	*s*: 0.38 *w*: -0.10	*s*: -0.33 *w*: -0.12		***s*: 0.51** *w*: -0.30
Δ Subacromial Space Width (+=Increase SAS)	***s*: -0.69** *w*: 0.20	*s*: -0.39 *w*: 0.25	***s*: 0.49** *w*: -0.42	***s*: 0.51** *w*: -0.30	

When averaged across elevation angles, a large proportion of participants exhibited fatigue-induced GH and ST orientation changes indicative of subacromial space narrowing. Specifically, between 35-57% of participants, depending on the particular measure, demonstrated changes in disadvantageous orientations (Figure 20). Depending on elevation angle, between 32-46% of participants exhibited superior translation following fatigue, with 80-92% of these participants showing scapular orientation changes indicative of subacromial space reduction and between 31-70% exhibited two or more of these orientation changes. As well, the percentage of

those demonstrating fatigue-related subacromial space reduction ranged from 29% at 0° to 50% at angles ≥ 60° of elevation (Figure 20).
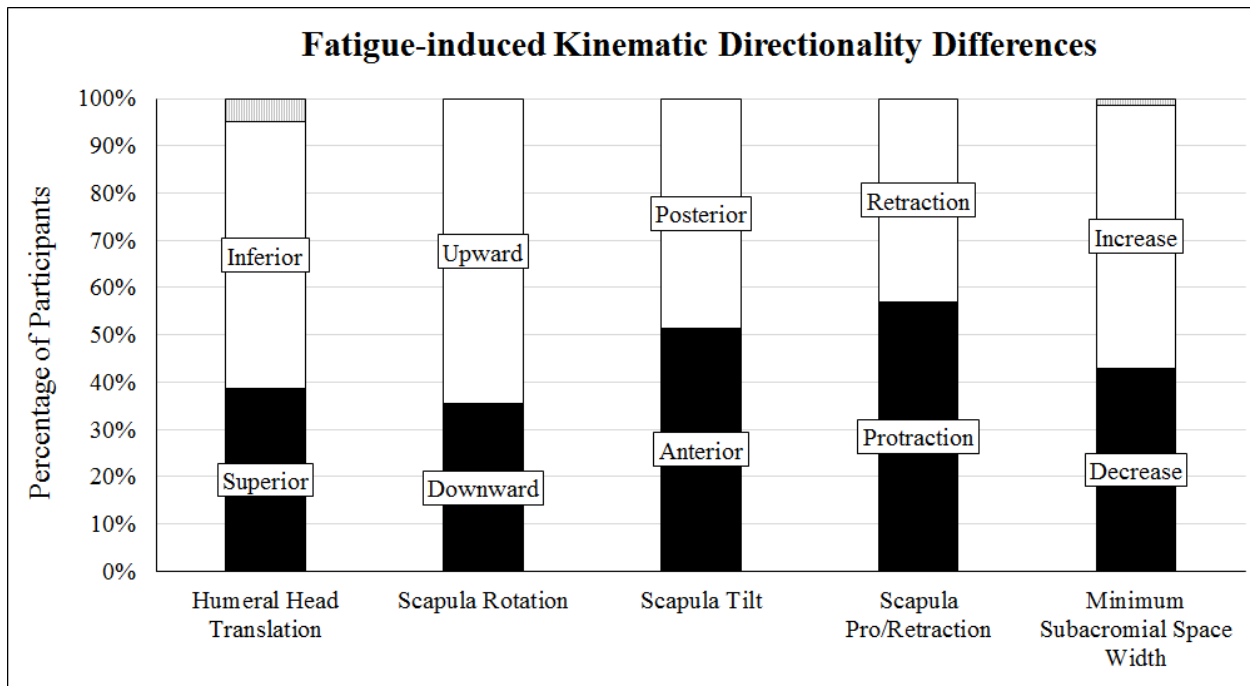
Figure 20. Percentage of participants with fatigue-induced kinematic changes that would increase (white) or decrease (black) the subacromial space, as well the percentage of participants with an increased or decreased SAS. Grey regions indicate no fatigue-related changes.

4.4.2 *Fatigue Verification*

Fatigue analysis confirmed that all muscles were fatigued following the protocol. The average bottle weight lifted during the protocol was 7.8 ± 2.0 N and average time to fatigue was 18.0 ± 10.3 min. Each muscle showed a statistically significant ($p<0.05$) reduction in mean power frequency (MPF) for the 60° exertion with magnitudes ranging from 8.7 to 24.9% (Table 18). For the 120° exertion, each muscle, with the exception of the lower trapezius, also had a significant reduction in MPF ranging from 6.9 to 29.1% (Table 18). A reduction in MPF for the lower trapezius existed, however it was of low magnitude (4.9%) and not statistically significant ($p=0.0569$). Additionally, each muscle with the exception of the lower trapezius and

supraspinatus (surface electrode) for the 120° exertion, demonstrated MPF decreases >8%, which has been used as a criterion for identifying muscle fatigue (Oberg et al. 1990).

Table 18. Mean power frequency reduction (mean ± standard deviation) and corresponding p-value for each of the measured muscles following fatigue. Statistical significance indicated by $p < 0.05$.

	60° exertion			120° exertion		
	Mean (%)	SD (%)	p-value	Mean (%)	SD (%)	p-value
Supraspinatus (Wire)	-24.9	33.8	0.0007	-28.4	16.2	<0.0001
Infraspinatus (Wire)	-23.2	28.0	0.0004	-27.0	19.0	<0.0001
Subscapularis (Wire)	-19.2	22.9	0.0001	-29.1	27.8	0.0010
Upper Trapezius (Surface)	-19.8	12.6	<0.0001	-12.5	12.3	<0.0001
Lower Trapezius (Surface)	-8.7	12.1	0.0015	-4.9	12.8	0.0569
Serratus Anterior (Surface)	-16.2	20.9	0.0003	-18.4	31.2	0.0083
Supraspinatus (Surface)	-13.0	12.7	<0.0001	-6.9	11.3	0.0022
Infraspinatus (Surface)	-22.4	11.7	<0.0001	-15.9	11.3	<0.0001

Beyond EMG, reduction in maximal force was used to confirm global upper extremity fatigue. Statistically significant reductions in both internal (anterior) force ($p = 0.018$) and external (posterior) force ($p < 0.0001$) occurred following the protocol. The reduction was larger for the external force (22.0 ± 14.7 N) than the internal force (8.0 ± 16.8 N).

4.4.3 *Verification and Reliability*

Intra- and inter-rater reliability analysis indicated excellent agreement both within the primary rater and between raters. The Bland-Altman analysis revealed no outliers with the 95%

confidence limits for humeral head position (intra-rater) and one outlier for the minimum subacromial space width for each of the intra- and inter- rater analyses (Bland and Altman 2010). Reliability was confirmed using paired t-tests that revealed there was no statistically significant difference (p>0.05) between the repeated measurements of the primary rater, or measurements between raters. Additionally, intraclass correlation coefficients ranged between 0.90 and 0.98, indicating excellent measurement repeatability. Bland-Altman plots for inter- and intra- rater reliability are presented in **Appendix 3**.

The humeral elevation angles extracted from motion capture data generally overestimated the measured angles at a neutral arm posture (0°) and increasingly underestimated the measured angles as the arm was elevated to 120°. The average difference between measured and extracted angles was -10.0 (±13.9)°. At 0°, the extracted angles overestimated the measured by 9.9 (±6.5)°, while at 30°, 60°, 90° and 120°, the extracted angles underestimated the measured by 4.6 (±7.8)°, 12.9 (±7.1)°, 19.3 (±5.8)° and 24.6 (±7.0)°, respectively. Statistical reliability analysis revealed an intraclass correlation coefficient of 0.95 (95% CI, 0.83 to 0.98) between measured and extracted angles and Bland-Altman analysis revealed between one and three outliers at each angle of elevation. The scapula rotation angles extracted from motion capture data slightly underestimated (mean, 2.2°; SD 5.5°) the angles measured from radiographs. Absolute differences between measured and extracted angles were similar across elevation angles with average magnitudes between 3 to 5.5°. The calculated intraclass correlation coefficient between methods was 0.74 (95% CI, 0.60 to 0.82) and the Bland-Altman analysis revealed five outliers across all elevation angles.

4.5   Discussion

While the population means observed indicate generally low risk for subacromial space

reduction following an upper extremity fatiguing task, this risk is highly variable. Indeed, a

considerable proportion of the population demonstrated kinematic changes associated with SAS

reduction. Analysis using an alternate humeral head translation measurement technique indicated

that the standardized measurement protocol underestimated the humeral head movement with

respect to the glenoid following fatigue which additionally initiated ST movement.

4.5.1 *Fatigue-induced kinematics: glenohumeral interaction*

The minor effect of combined rotator cuff and scapula stabilizer muscle fatigue on

humeral head position was initially unexpected. Superior translation of the humeral head

following upper extremity fatigue is widely reported (Chen et al. 1999, Chopp et al. 2010, Cote

et al. 2009, Royer et al. 2009, Teyhen et al. 2008). While the previously reported translations

have been of modest magnitude, with angle-specific translation magnitudes between 0.1 to

1.3mm, a similar fatigue effect on humeral head translation was expected in this current research.

Assessing the humeral head translation in conjunction with scapular orientation changes,

superior translation occurred but was likely obscured by scapular upward rotation. The standard

method of extracting the GH position from radiographs involves drawing a perpendicular line

from the center of the humeral head to the glenoid axis (Poppen and Walker 1976). Thus, it is

intuitive to suggest that varying the angle of the glenoid axis, corresponding to scapula

upward/downward rotation, would similarly vary the projection of the humeral head center on

the glenoid cavity and could subsequently largely influence the measured humeral head

translation (Table 17). Specifically, a more upwardly rotated glenoid would measure as less

superior translation than a downwardly rotated glenoid (assuming a consistent humeral head

112

position). The scapula rotation angle, as measured on both radiographs and motion capture, showed significant upward rotation of the scapula following muscle fatigue (Table 14 & Table 15), thereby creating the expectation for the resulting negligible superior, or even inferior fatigue-induced humeral head translation. The dependence of this measurement on the scapula position was confirmed using an alternate humeral head translation measurement technique which, following fatigue, demonstrated significant superior translation, up to a magnitude of 4.3mm across the range of arm elevation (Table 13). Thus, it is likely that previous researchers documenting fatigue-induced changes to humeral head position using the standard measurement approach substantially underestimated true superior humeral head translations.

4.5.2 *Fatigue-related kinematic compensation strategies: additional considerations*

The mean effect of fatigue on scapular rotation was protective against subacromial space reduction. It has previously been hypothesized that fatiguing the scapula stabilizing muscles would induce ST kinematic changes analogous to those with SAIS due to the inability of these muscles to maintain healthy scapular kinematics (Michener et al. 2003). Downward rotation, anterior tilting and protraction of the scapula all orient the acromion more inferiorly, such that it reduces the SAS (Chopp and Dickerson 2012). These orientation changes exist in those with SAIS (Ludewig and Reynolds 2009, Phadke et al. 2009). However, significant upward rotation occurred following fatigue. This trend has been documented in previous research and may act as a possible compensatory mechanism to widen the SAS, while assisting with further arm elevation to an overhead posture (Chopp et al. 2011, Ebaugh et al. 2006, McQuade et al. 1998). Despite this apparent protective outcome, excessive scapula upward rotation has been suggested

to potentially lead to glenohumeral instability or alteration of the length-tension relationships of the rotator cuff muscles (McQuade et al. 1998, Michener et al. 2003).

The alternate humeral head translation measurement procedure identified a fatigue-driven superior translation of the humerus. While concurrent scapula upward rotation apparently maintained SAS size, thereby countering this superior translation, several other musculoskeletal health implications bear consideration. Superior humeral head translation may lead to the development of bone spurs and the alteration of the contact area and stresses on the glenoid cavity, which can result in morphologically-induced SAIS, bone degeneration, and instability (Anetzberger et al. 2002, Kelkar et al. 2001, Nicholson et al. 1996, Rockwood et al. 2009, Shah et al. 2001, Terrier et al. 2007, von Eisenhart-Rothe et al. 2008). While acromial morphology has often been attributed to genetic origins (Nicholson et al. 1996, Vahakari et al. 2010), researchers have indicated that a 'hooked' acromion may also be formed by excessive loading of the coracoacromial arch by means of superior humeral head translation (Nicholson et al. 1996, Shah et al. 2001, Wang and Shapiro 1997). This loading can result in the development of an enthesophyte and subsequently increase the risk of SAIS. A superior humeral head position, caused by instability or rotator cuff tears, can also alter the contact area and maximal contact stress imparted on the glenoid cavity (Anetzberger et al. 2002, Kelkar et al. 2001, von Eisenhart-Rothe et al. 2008). This altered loading pattern may promote early cartilage degeneration (Kelkar et al. 2001), wear on the superior glenoid rim and reduced glenoid concavity (Rockwood et al. 2009) as well as possible osteoarthritis (Terrier et al. 2007).

4.5.3 *Kinematic Variability: Implications for SAIS*

While the effect of fatigue on GH and ST kinematics was small, each measure exhibited substantial variability in the participant group. Humeral head position differed by 5.1 to 10.7mm

between 1-99% confidence limits (Table 13) depending on the elevation angle and fatigue state, with the post-fatigue state generally showing higher variation. Further, fatigue-induced ST changes of different polarity and of widely differing magnitudes existed across participants (Table 14). Extensive GH and ST kinematic variability coincided with previous reports (Borstad et al. 2009, Chen et al. 1999, Chopp et al. 2010, Ebaugh et al. 2006, Teyhen et al. 2008) and subsequently produced comparably diffuse magnitudes of changes in SAS size following fatigue, with differences of 5.7 to 9.3mm between confidence limits (Table 16). The thickness of subacromial tissues averages approximately 6mm in healthy individuals (Chapter 5 Results; Michener et al. 2013). Regardless of fatigue status, average subacromial tissue thickness measured in this study exceeded the average SAS as the arm was elevated to and above 60° (Table 16). This suggests that the average individual is at risk for tissue compression during controlled and fatigued arm elevation and further that individuals with tissue thicknesses above the mean and/or a SAS below the mean are at even higher risk for SAIS and eventual rotator cuff pathology. Additionally, the clinical significance of the extensive variability was assessed by considering the proportion of participants exhibiting kinematic changes consistent with SAS narrowing. Across all measures, a large proportion of participants exhibited fatigue-induced changes in disadvantageous orientations (Figure 20). Therefore, despite benign mean kinematic differences, half of the participants were at increased risk for fatigue-induced impingement beyond 60° of arm elevation, and over 2/3 of the population are at risk for alternate musculoskeletal disorders posed by a superior decentering of the humeral head.

4.5.4 *Covariance of Kinematic Fatigue Responses*

Correlation coefficients generally showed weak relationships. The strongest relationship identified was between superior humeral head translation (standard measurement) and SAS

reduction (-0.69) (Table 17). This strong correlation was expected given the significant fatigue-induced upward scapula rotation. Any calculated positive (superior) fatigue-induced translation would indicate either: (1) enough upward movement of the humerus such that it exceeded the confounding effect of scapula upward rotation, or (2) very little to no scapula upward rotation was present following fatigue; either would subsequently result in a reduction of the subacromial space. Each of the three 'injury-related' rotation orientations (downward rotation, anterior tilt, protraction) were expected to strongly correlate with SAS reduction. Anterior tilting (0.49) and protraction (0.51) had moderate correlations, while upward rotation did not. Discrepancies in the directionality and magnitudes of coefficients across the range of elevation angle were likely attributed to the considerable inter-subject variability, and the associated differences in several factors, including the muscle moment arms and lines of action (Poppen and Walker 1978, Yanagawa et al. 2008), as well as individualized muscle fatigue in measured and unmeasured muscles.

4.5.5 *Humerothoracic and Scapulothoracic Joint Angles: Multiple Measurement Verification*

Humeral elevation angles between trials and participants were set using a manual goniometer and verified using angles derived from motion capture data. The derived angles generally overestimated the measured angles at 0° of elevation and increasingly underestimated the angles as the arm was elevated to 120°. Grewal (2011) similarly found that humeral elevation angles derived from recorded motion tracking data differed from the measured arm angles using a goniometer and reported that discrepancies were not uncommon. Overestimation of the extracted angles at a neutral posture may be due to soft tissues surrounding the arm and torso that prohibit the long axis of the humerus (y-axis) at neutral from being aligned with the y-axis of the

116

torso. As well, increasing discrepancies as the arm was elevated could be the result of possible trunk rotation. Similar to research by Grewal (2011), while a back plate was behind participants and upright posture encouraged, trunk posture was not constrained and thus participants may have leaned to assist with achieving higher elevation angles. It was anticipated that participants would have increased trunk lean following fatigue due to the increased difficulty in elevating their arm to the required postures. Thus, participants were verbally reminded not to lean, particularly during the post-fatigue trial. Despite eliciting differences in extracted angles (motion capture) from measured angles (goniometer), the resulting mean difference in elevation angle from pre-fatigue to post-fatigue states was less than 1° with an intraclass correlation coefficient of 0.99 (99% CI 0.98 – 0.99). This verified that participants were able to maintain a nearly identical posture between fatigue states and that differences can be attributed to fatigue effects rather than postural differences.

Scapular upward/downward rotation was both extracted from recorded motion tracking data and measured from anterior-posterior radiographs. While the method of angle calculation differed, reliability was evaluated by comparing the change in rotation angle induced from muscle fatigue. Analysis revealed that there was generally good agreement between the measured and extracted angles, with motion capture slightly underestimating the measured fatigue-induced differences at each elevation angle. However, neither measurement approach could be considered a gold standard, as each had its associated limitations. Deviances may have been due to limitations associated with the acromial tracker which slightly underestimates scapula rotation (~2°) compared to gold standard non-invasive tracking methods (Grewal 2011). For motion capture methods, the scapula local coordinate system was created using markers placed on the skin, overlying anatomical landmarks. While these landmarks can be accurately

palpated, small differences between these landmarks and the radiographic image may persist due to soft tissue artifact (Langenderfer et al. 2008). Deviances may also arise from differences in anatomical axis definitions between measured and extracted angle methods. For angles extracted from motion capture data, three-dimensional anatomical axes were created for the scapula and torso according to ISB recommendations and were used to describe the ST orientation. For radiographic measurement, the long axis (y-axis) of the torso, which was required for scapula rotation measurement, was assumed to be vertically aligned with the image axis. As described earlier, while participants were encouraged to maintain an upright posture, even in neutral, the long axis of the torso may not have been perfectly upright.

4.5.6 *Limitations*

Certain limitations should inform future evaluation of subacromial kinematics. While humeral head position could be accurately extracted from all twenty-eight participants, the landmarks required for SAS measurement were unclear in half of the participants. Thus, presented results for this variable only reflected measurements from 14 participants. The difficulty stems from the three-dimensional positioning of the scapula and frequently sub-optimal density of the inferior acromion. Across participants, those whose SAS was unidentifiable had $6.7 \pm 3.5°$ greater anterior tilting depending on elevation angle, suggesting a more anteriorly tilted scapula as a potential cause for unreliable subacromial space measurements. Additionally, despite the previously confirmed ability of the acromial marker cluster to accurately measure three-dimensional ST changes (Grewal 2011), using a three-dimensional imaging technique would reduce potential errors in extracted angles resulting from minor tracker movements on the skin, soft tissue artifact, or improper placements. Lastly, certain kinematic and electromyographic trials were excluded due to experimental recording error.

Specifically, one pair (pre-fatigue/post-fatigue) of rotation angles (0°), three pairs of protraction/retraction angles (0°, 30°, 60°) and 10 HT angles had to be excluded from analysis. Additionally, occasional channels of EMG from each exertion had to be excluded from analysis due to artifact. Generally, data from ≤ 3 participants were excluded for each muscle/exertion. However, data from four participants had artifact contamination in their infraspinatus wire electrode signal. For these participants, their corresponding infraspinatus surface electrode demonstrated MPF reductions of >25%. In addition, 50% of subscapularis wires for the 120° exertion had to be excluded. Thus, for this muscle, fatigue was primarily verified using the 60° exertion, however both 60° (p=0.0001) and 120° (p=0.0010) exertions indicated a significant reduction in MPF with magnitudes of 19.2 and 29.1%, respectively (Table 9).

4.6   Conclusions

Overall, three central conclusions were generated:

1. Fatigue-induced GH and ST responses were highly variable among the measured population, thus solely considering the population mean may strongly underestimate SAIS risk.

2. While the population mean responses did not implicate fatigue as a probable mechanism for SAIS development, approximately 50% of the measured population demonstrated kinematic responses that were indicative of subacromial space reduction.

3. Fatigue-induced humeral head translation poses risk for the development of several additional pathologies such as bone spurs and/or alteration of contact area and contact stresses that can subsequently lead to glenoid cavity bone degeneration.

Thus, repetitive overhead activity that is likely to exhaust the upper extremity musculature increases the risk for the development of musculoskeletal pathologies, notably

119

rotator cuff disorders. Therefore, exercise programs that strengthen these muscles groups to

enable the maintenance of healthy kinematics should be designed for those frequently exposed to

workplace tasks or activities of daily living that pose risk for their fatigue development.

Chapter 5

Distribution of bone and tissue morphological properties related to subacromial space geometry in a young, healthy male population

Overview

Particular bone and tissue morphological features of the scapula and humerus often exist disproportionately in persons with subacromial impingement syndrome (SAIS) and/or rotator cuff pathology. The reported research evaluated the distribution of and correlation between these characteristics and the minimum subacromial space width (SAS) among a young, healthy, male population. Anterior-posterior and trans-scapular radiographs and musculoskeletal ultrasound were used to measure morphological characteristics related to the subacromial space. Each bone morphological characteristic was classified as healthy or unhealthy based on previous definitions. Further, the distribution of risk was evaluated by calculating the range of subacromial occupation ratios (tissue thickness to SAS) that exists in this population. Each characteristic demonstrated considerable variability, with some participants having 'unhealthy' variants for each bone characteristic examined. The percentage of the population with bone characteristics classified as "unhealthy" ranged from 15 to 55% across those evaluated. The strongest correlation existed between the acromion index and the minimum subacromial space width (-0.59) suggesting that a larger lateral extension of the acromion may predispose an individual to SAIS. The average occupation ratio was 65.3% with a 1-99% confidence interval ranging from 21.6% to 108.9%. Occupation ratios indicated that individuals within this population are at risk for subacromial tissue compression solely based on morphological variation. This suggests that intrinsic predisposing geometry likely contributes to the development of SAIS and eventual rotator cuff pathology.

5.1 Introduction

Variants of different morphological characteristics related to upper extremity bone (acromion, glenoid, and humerus) and tissue (supraspinatus tendon and subacromial bursa thickness) exist in the population. Each characteristic has been studied in terms of its variability across various populations and the differential influences of age and injury. While many of the studies documenting these characteristics have had large samples, included samples primarily consisted of surgical patients (Gill et al. 2002, MacGillivray et al. 1998, Toivonen et al. 1995, Tuite et al. 1995) or cadaveric specimens (Bigliani 1986, Edelson 1995). As well, these large samples were extended over a broad age range, from approximately 14 to 86 years and included both genders (Gill et al. 2002, MacGillivray et al. 1998, Tuite et al. 1995). No existing research defines the distribution of these characteristics amongst a relatively homogeneous group of healthy, young individuals, for which degenerative changes are not expected.

The risk of developing subacromial impingement syndrome (SAIS), while exacerbated by musculoskeletal exposure, has been related to these morphological characteristics of the shoulder region. Bone characteristics such as increased acromial anterior slope (Balke et al. 2013, Bigliani 1986, Edelson 1995, Gill et al. 2002, Kitay et al. 1995, MacGillivray et al. 1998, Toivonen et al. 1995, Tuite et al. 1995), and lateral acromial angulation angles (Banas et al. 1995, Tetreault et al. 2004), reduced acromial tilt angle (Aoki et al. 1986, Balke et al. 2013, Kitay et al. 1995, Zuckerman et al. 1992), and an increased lateral acromion to humerus ratio (acromion index) (Balke et al. 2013, Nyffeler et al. 2006, Torrens et al. 2007) have all been associated with SAIS and/or rotator cuff pathology. Additionally, an increased glenoid inclination angle has been associated with both increased superior migration of the humeral head and rotator cuff tear prevalence (Flieg et al. 2008, Hughes et al. 2003, Konrad et al. 2006, Maurer et al. 2012, Wong et al. 2003). While these abnormal morphological features have been

generally identified in an elderly population, leading researchers to hypothesize mechanistic origins to their development, variability in morphological features also exists in younger populations, suggesting possible genetic origins that would predispose individuals to SAIS (Nicholson et al. 1996, Vahakari et al. 2010). Additionally, while the interdependence of certain variables has been recently evaluated (Balke et al. 2013), the correlation between each of these variables and the minimum subacromial space width (SAS) has not been quantified.

Identifying the bone morphological properties that contribute to reducing the size of the subacromial space amongst a young, healthy population is important in identifying the relationship between predisposing geometry and SAIS risk. However, to adequately assess the risk, a quantification of both the subacromial space and the thickness of the interposed tissues is necessary. Michener et al. (2013) recently calculated the ratio of supraspinatus tendon thickness to SAS, measured with musculoskeletal ultrasound, in participants with SAIS and matched controls and determined that even within a healthy population in a neutral arm posture, the tissues can occupy more than half of the space. This fraction is expected to be greater in elevated arm postures as the space is markedly reduced (Bey et al. 2007, Graichen et al. 1999a).

Evaluating both bone and tissue related morphological features related to SAIS simultaneously on the same young, healthy population provides a comprehensive evaluation of inherent geometric predisposition, independent of age-related degenerative influences. Variability in morphological features within this population sub-group has important implications for the prevention of SAIS and eventual rotator cuff pathology.

Primary Research Objectives:

1. Within a young, healthy male population, determine the distributions of bone and tissue morphological characteristics related to the subacromial space.

2. Classify individual bone morphological characteristics as healthy or unhealthy based on previously defined ranges.

3. Identify the correlation between each of the measured bone morphological characteristics, including the minimum subacromial space width.

4. Calculate the occupation ratio (subacromial tissues to the minimum subacromial space width) as measured using radiographs and ultrasound.

Secondary Research Objective:

1. Construct population distributions for each of these measures based on the spread of data across subjects to be used as input into a probabilistic subacromial geometry model (Chapter 6).

Research Hypotheses:

It was hypothesized that while participants would generally show morphological characteristics that do not predispose them to SAIS risk, these characteristics, and the calculated occupation ratios, would be highly variable in the population. This would result in some individuals demonstrating a high predisposition to SAIS (tissues occupying a larger [>50%] proportion of the space and SAIS-related bone characteristics), and others demonstrating a low predisposition to SAIS (tissues occupying a smaller [<50%] proportion of the space and healthy bone characteristics). It was also hypothesized that the minimum subacromial space width, as measured using radiographs would consistently result in occupation ratios greater than those measured using ultrasound.

5.2 Methods

The data required to address the research questions posed in this study were collected simultaneously with that of Chapter 4. Therefore, this study also took place at St. Joseph's Healthcare Hamilton.

5.2.1 *Participants*

Thirty-three healthy, right-hand dominant male participants between the ages of 18 and 35 participated. A priori power analysis indicated that 30 participants would be sufficient to obtain adequate power (80%) from bone and tissue measurements (Cohen 1992). While the effect size calculated from healthy and rotator cuff tear groups varied across the literature (d = 0.8 − 1.5), a sample size of less than 30 participants was calculated for most characteristics (exception of acromial anterior slope, d = 0.4) using two-tailed independent t-tests (Balke et al. 2013, Faul et al. 2007, Hughes et al. 2003, Tetreault et al. 2004). Participants were initially screened using self-reports of pain and injury. Health status was verified by clinical impingement tests and a full shoulder ultrasound. This exam specifically identified the presence of tears in the supraspinatus, infraspinatus, subscapularis and long head of the biceps tendon, as well as documented any enthesophytes extending from the humerus, osteophytes, joint effusion or capsular distension of the acromioclavicular joint and/or bursal distension greater than 2mm (van Holsbeeck and Strouse 1993). Additionally, any abnormalities to the spinoglenoid notch and the posterior labrum were documented as well as ensuring participants did not exhibit anterior or lateral impingement of the subacromial tissues. As earlier described, two participants were excluded due to moderate abnormalities, including a dislocation of the long head of the biceps tendon superficial to the subscapularis and calcific tendinosis of the supraspinatus tendon. No other abnormalities were identified in any of the included participants, with bursal thicknesses all

≤ 1.4mm. Thus, data from thirty-one participants (25.0 ± 3.5 yrs, 1.8 ± 0.1m, 83.6 ± 13.9kg) were included in these analyses.

5.2.2 *Instrumentation*

Radiography and Ultrasonography systems were used to capture relevant data from the right-side subacromial region of each participant. A Discovery XR656 Digital Radiography System (GE Healthcare, United Kingdom) with technical factors of 70kV and 320mA and a Toshiba Aplio XU (Toshiba Medical Systems Corporation, Japan) with a 7-14MHz linear transducer set at 14MHz were used to capture bone and tissue characteristics.

5.2.3 *Experimental Procedures*

5.2.3.1 **Radiography**

Anterior-posterior (frontal) view and trans-scapular (lateral) view radiographs were captured for each participant's right shoulder. The x-ray beam was positioned perpendicular to the imaging plate with no caudal angulation. For the anterior-posterior radiograph, participants were rotated 30° to the beam (scapular plane) with their arm resting at neutral. For the trans-scapular radiograph, the participants were rotated 90° to the imaging plate and their elbow was bent to 90° resting against their abdomen. Participants held a 1kg weight for each radiograph. Lead shielding was provided to protect against radiation.

5.2.3.2 **Ultrasonography**

Following the full shoulder ultrasound exam (to ensure study inclusion), three tissue measurements were captured: 1) supraspinatus tendon thickness, 2) maximal bursa thickness and 3) minimum subacromial space width (SAS). The supraspinatus tendon was measured with the transducer positioned in a transverse (short axis) orientation, perpendicular to the tendon long axis. Participants placed their arm in the Middleton/Modified Crass position, in which the arm

was extended and elbow flexed such that their hand rested on their ipsilateral hip (Michener et al. 2013, O'Neill 2008). Both the subacromial bursa thickness and the SAS were measured with the participant's arm resting at neutral and the transducer oriented in a longitudinal (long axis) ultrasonic view with its medial margin placed upon the lateral margin of the acromion and spanning over the greater tuberosity.

5.3   Data Analysis

5.3.1 *Morphological Measurement*

Eight measures were extracted from the acquired images. Bone morphological characteristics were extracted from the radiographic images post hoc using GE PACS software (GE Healthcare, United Kingdom), while tissue measurements were obtained from real time freeze-framed ultrasonic images during the experimental collection.

5.3.1.1   *Acromial Anterior Slope (Radiographic)*

Acromial anterior slope, otherwise known as 'acromial type', was measured using the trans-scapular (lateral) radiographic view. First, the most anterior and posterior points on the inferior aspect of the acromion were identified. Two lines were then drawn from the midpoint (junction) of the inferior acromion to each of the identified points. The acromial anterior slope was the angle formed by the intersected lines, which was subsequently used to classify the acromial type (Balke et al. 2013, Bigliani 1986, Kitay et al. 1995).

5.3.1.2   *Lateral Acromial Angle (Radiographic)*

The lateral acromial angle was measured using the anterior-posterior (frontal) radiographic view. The lateral acromial angle, as defined by Banas et al. (1995), was determined by finding the intersection of the glenoid axis and a medial-lateral line drawn along the undersurface of the acromion process. The glenoid axis is a line connecting the superior-most

127

and inferior-most points of the anterior articular glenoid margin. The angle formed in the upper medial quadrant was defined as the lateral acromial angle.

5.3.1.3 Acromial Tilt (Radiographic)

Acromial tilt was measured using the trans-scapular radiographic view. This tilt angle was formed by the intersection of a line connecting the anterior-most and posterior-most points on the inferior aspect of the acromion, with a second line connecting the same posterior point on the acromion with the inferior-most point on the coracoid process (Aoki et al. 1986, Balke et al. 2013, Kitay et al. 1995).

5.3.1.4 Acromion Index (Radiographic)

The acromion index was measured using the anterior-posterior radiographic view. This index was determined by calculating the ratio of the glenoid-acromion distance to the glenoid-humerus distance. Specifically, the distance between the glenoid axis and the most lateral aspect of the acromion was measured and divided by the distance between the glenoid axis and the most lateral aspect of the humerus (Balke et al. 2013, Nyffeler et al. 2006).

5.3.1.5 Glenoid Inclination (Radiographic)

Glenoid inclination was measured using the anterior-posterior radiographic view. The inclination angle was defined as the intersection between the glenoid axis and a line drawn along the floor of the supraspinatus fossa (Maurer et al. 2012). The angle formed in the upper lateral quadrant was defined as the glenoid inclination (Bishop et al. 2009, Hughes et al. 2003). There have been several variations of the glenoid inclination measurement. This definition was selected due to its confirmed reliability (Maurer et al. 2012), however the supplementary angle was recorded to enable comparisons to injury-related research.

5.3.1.6 Supraspinatus Tendon Thickness (Ultrasonic)

The average supraspinatus tendon thickness from three anterior-posterior tendon locations were calculated. Locations were measured at 5, 10 and 15mm lateral to the hyperechogenicity of the biceps tendon (Figure 21). At each location, the thickness of the tendon was defined as a linear measurement perpendicular to the tendon from the hypoechoic thin rim articular cartilage of the humeral head (inferiorly) to the peribursal hyperechoic fat and bursal capsule (superiorly). Specific measurement locations were selected to be more anterior than previously described literature (Cholewinski et al. 2008, Michener et al. 2013, Wallny et al. 1999). The supraspinatus extends approximately 2.3cm (range: 1.8 to 3.3cm) in length (anterior-posterior) and 1.6 cm (range: 1.2 to 2.1cm) in width (medial-lateral) (Curtis et al. 2006) with considerable interdigitation with the infraspinatus occurring at the posterior aspect of the supraspinatus tendon (O'Neill 2008). The contact area and primary site of SAIS is the anterior third of the acromion (Flatow et al. 1994, Neer 1972). Thus, previous techniques that averaged the measured tendon thicknesses at 10, 20 and 30mm (Cholewinski et al. 2008, Wallny et al. 1999) or even 10, 15 and 20mm (Michener et al. 2013) may have underestimated injury risk and included anterior portions of the infraspinatus tendon.

5.3.1.7 Subacromial Bursa Thickness (Ultrasonic)

The subacromial bursa overlays the supraspinatus tendon and thus occupies additional subacromial space. The thickness of the bursa was defined as a linear measurement between the capsular wall/peribursal fat layers on either sides of the bursa at the point of maximum thickness. In a longitudinal orientation, the transducer was moved from the lateral biceps tendon to approximately 15mm posterior, from which the maximal bursa was recorded.

5.3.1.8   *Minimum Subacromial Space Width (Radiographic and Ultrasonic)*

The minimum subacromial space width (SAS) was recorded using both measurement systems. Radiographically, the SAS was measured on the anterior-posterior image. It was defined as the minimum distance between the superior aspect of the humeral head and the dense cortical undersurface of the acromion process (Gruber et al. 2010, Lehtinen et al. 2000, Petersson and Redlund-Johnell, 1984, Thompson et al. 2011, Weiner and MacNab 1970) (Chapter 4). Ultrasonically, the SAS was quantified at two transducer locations, anterior and mid-lateral. The transducer was positioned in a longitudinal orientation with the participant's arm in neutral. For the anterior measurement, the transducer was placed on the anterior-most aspect of the acromion with the long axis of the transducer oriented in the scapular plane, parallel to the flat surface of the acromion (Michener et al. 2013). For the mid-lateral measurement, the transducer was moved to the midpoint of the acromion. The SAS was defined as a linear measurement between the superior aspect of the humeral head and the inferior cortical margin of the acromion.
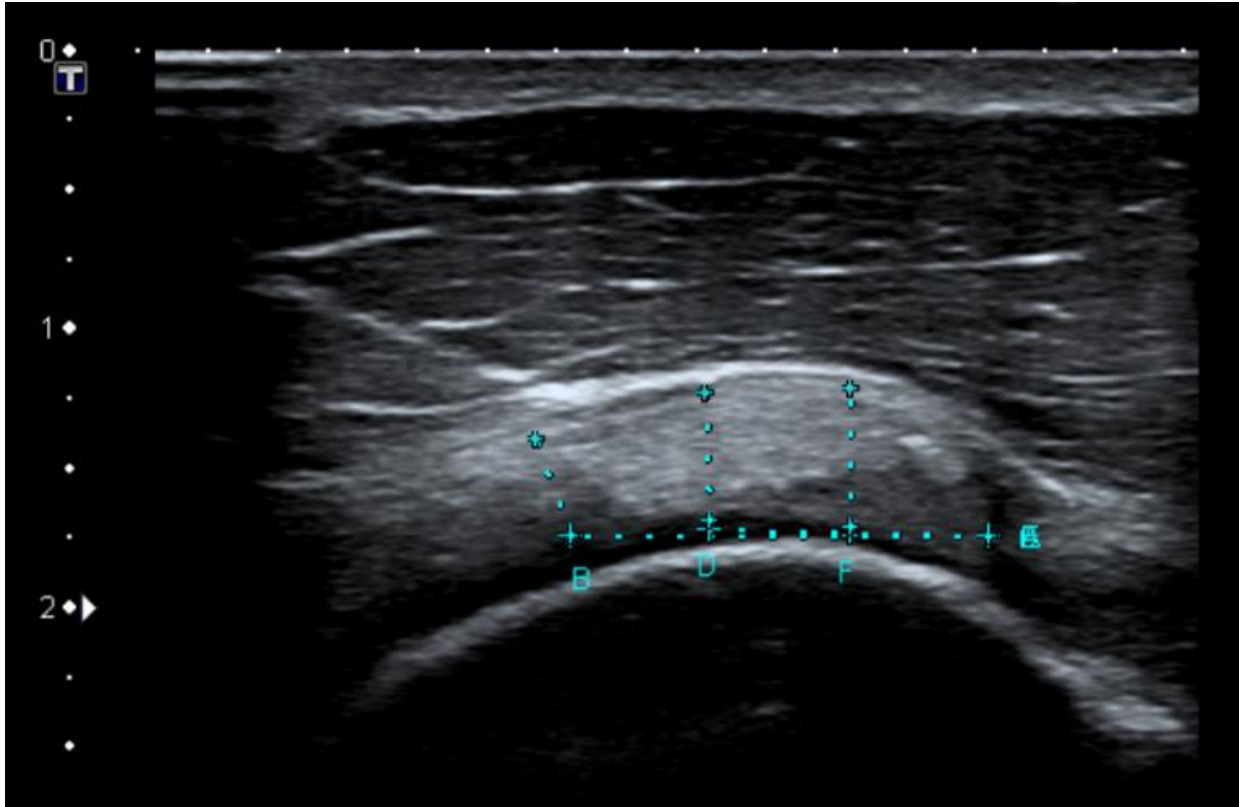
Figure 21. Supraspinatus tendon thickness measurements obtained using a transverse ultrasonic view. Measurements were captured at 5mm (F), 10mm (D) and 15mm (B) lateral to the hyperechogenicity of the biceps tendon. At each location, the thickness of the tendon was measured perpendicular to the tendon from the hypoechoic thin rim articular cartilage of the humeral head (inferiorly) to the peribursal hyperechoic fat and bursal capsule (superiorly).

5.3.2 *Morphological Classifications and Characteristic Comparisons*

Several evaluations of the morphological data contextualized them with respect to SAIS risk. For each characteristic, the mean and 1-99% confidence interval were calculated. Distributions were generated by performing Kolmogorov-Smirnov (K-S) statistical tests using custom Matlab® software to determine the goodness-of-fit between the experimental measures and theoretical distributions (Haldar and Mahadevan 2000, Massey 1951). All characteristics

were first tested for normality using a conservative alpha (α) level of 0.01 and number of participants (*n*) of 35, which elicits a criterion of $d = 0.21$.

Bone morphological characteristics for each participant were classified according to previously defined ranges which assess each participant's relative predisposition to SAIS (Table 19).

Table 19. Classification of bone morphological characteristics (unhealthy = association with rotator cuff pathology).

Morphological Characteristic	Morphological Sub-characteristic	Classification/Health Status		Reference from which classification obtained or healthy/unhealthy trend developed
Acromial Morphology	Acromial anterior slope (acromial type)	$x > 27°$ (Type III)	**[Unhealthy]**	Toivonen et al. (1995)
		$13° \leq x \leq 27°$ (Type II)		
		$0° \leq x \leq 12°$ (Type I)	**[Healthy]**	
	Lateral acromial angle	$x \leq 70°$	**[Unhealthy]**	Banas et al. (1995) Tetreault et al. (2004)
		$x > 70°$	**[Healthy]**	
	Acromial tilt	$x \sim {} < 30°$	**[Unhealthy]**	Zuckerman et al. (1992)
		$x \sim {} > 30°$	**[Healthy]**	
	Acromion index	$x \sim {} > 0.65$	**[Unhealthy]**	Balke et al. (2013) Nyffeler et al. (2006) Torrens et al. (2007)
		$x \sim {} < 0.65$	**[Healthy]**	
Glenoid Orientation	Glenoid inclination	x > 95° Upward Tilt	**[Unhealthy]**	*Extrapolated from* Hughes et al. (2003) who reported 90° using slightly modified measurement technique
		$x < 95°$ Downward Tilt	**[Healthy]**	
Subacromial Space Width	Acromio-humeral distance	$x < 5$mm	**[Unhealthy]**	Cotton & Rideout (1964) Golding (1962) Weiner & MacNab (1970)
		5mm $< x < 7$mm (Grey)		
		$x > 7$mm	**[Healthy]**	

Correlation coefficients between each of the bone morphological measurements, including the minimum subacromial space width obtained from the radiographic image, were calculated to develop a correlation matrix. Correlation coefficients were classified as excellent (0.81 – 1.00), good (0.61 – 0.80), moderate (0.41 – 0.60), fair (0.21 – 0.40), or poor (0.00 –

0.20), similar to previous research (Balke et al. 2013). Additionally, three occupation ratios were calculated for each participant. This ratio was obtained by dividing the combined subacromial tissue thickness by the SAS (Michener et al. 2013). This tissue thickness was divided by each of the three measured SASs obtained from (1) radiographs and (2) ultrasound (both anterior and mid-lateral).

5.3.3 *Measurement Reliability Analysis*

Radiographic measurements were performed by JN Chopp-Hurley who has previous experience extracting kinematic measurements from anterior-posterior shoulder radiographs. An intra-rater reliability analysis was performed by re-measuring a sample of 15 radiographs. All radiographs were blinded with the re-measurement protocol occurring two weeks following the primary measurement. An inter-rater analysis was performed by an experienced musculoskeletal radiologist. A sample of 15 radiographs were randomly selected for which each measurement was performed. Ultrasonic measurements were performed by a senior ultrasound technologist with over 30 years of experience. As measurements were obtained in real-time, solely intra-rater reliability was evaluated. However, the full shoulder ultrasound exam and all measurements were reviewed and confirmed by the musculoskeletal radiologist following completion of the experimental collection. A random sample of nine participants were selected in which all measurements were repeated.

To verify intra- and inter-rater agreement a Bland-Altman analysis was conducted using Matlab® (Chapter 4; Bland and Altman 2010). Additionally, paired t-tests ($p<0.05$) were performed and intraclass correlation coefficients calculated using SPSS Statistics 22 (IBM Corporation, USA) to confirm results of the Bland-Altman analysis.

5.4 Results

Despite the similarity in age and health status of the included participants, there was a wide range of morphological characteristic magnitudes. Each characteristic displayed considerable variance which subsequently produced large confidence intervals (Table 20 – Table 22). The K-S statistical test ($\alpha = 0.01$) indicated that each of the eight characteristics (i) measured were normally distributed with $dmax_i$ values ranging from 0.07 to 0.14 ($dmax_i < d$ [0.21]), thus frequency diagrams plotting real participant-measured data were fit with normal distributions, further highlighting the extensive variability exhibited across all characteristics (Figure 22).

Table 20. Mean (1-99% Confidence Interval) and the percentage of participants in the healthy and unhealthy ranges for each bone morphological characteristic.

Characteristic	Mean [1-99% CI]	% in Healthy Range (n=31)
Acromial anterior slope (°)	18.0 [0 – 53.9] °	84%
		▪ 32% Flat ▪ 52% Curved
Lateral acromial angle (°)	79.9 [49.2 – 110.7] °	84%
Acromial Tilt (°)	31.5 [15.9 – 47.0] °	61%
Acromial Index	0.62 [0.35 – 0.89] °	45%
Glenoid Inclination (°)	95.0 [75.6 – 114.3] °	45%

Table 21. Mean (1-99% Confidence Interval) and the percentage of participants in the healthy and unhealthy ranges for the minimum subacromial space width measured using the anterior-posterior radiograph and ultrasound with the transducer positioned at the anterior (Ant) and mid-lateral (M/L) acromion.

Subacromial Space Measurement Technique	Mean [1-99% CI]	% in Healthy Range (*n)* (>7mm)
Radiograph (*n=28*)	9.7 [4.8 – 14.5] *mm*	97% (*n* = 27)
Ultrasound (Ant) (*n=31*)	11.5 [5.9 – 17.1] *mm*	100% (*n* = 31)
Ultrasound (M/L) (*n=31*)	11.3 [5.1 – 17.6] *mm*	100% (*n* = 31)

Table 22. Mean (1-99% Confidence Interval) of the measured subacromial tissues, their calculated sum and the occupation ratios (Total Tissue Thickness/Minimum Subacromial Space Width – Radiographs and Ultrasound).

Tissue	Mean [1-99% CI]
Supraspinatus Tendon Thickness	5.3 [2.7 – 7.9] *mm*
Subacromial Bursa Thickness	0.9 [0 – 1.8] *mm*
∑Tissue Thickness (Supraspinatus Tendon Thickness + Subacromial Bursa Thickness)	6.1 [3.4 – 8.8] *mm*
Occupation Ratio (∑Tissue Thickness/Minimum Subacromial Space Width [***Radiograph***])	65.3 [21.6 – 108.9] %
Occupation Ratio (∑Tissue Thickness/Minimum Subacromial Space Width [***Ant Ultrasound***])	54.1 [25.2 – 83.0] %
Occupation Ratio (∑Tissue Thickness/Minimum Subacromial Space Width [***M/L Ultrasound***])	54.8 [25.6 – 84.2] %
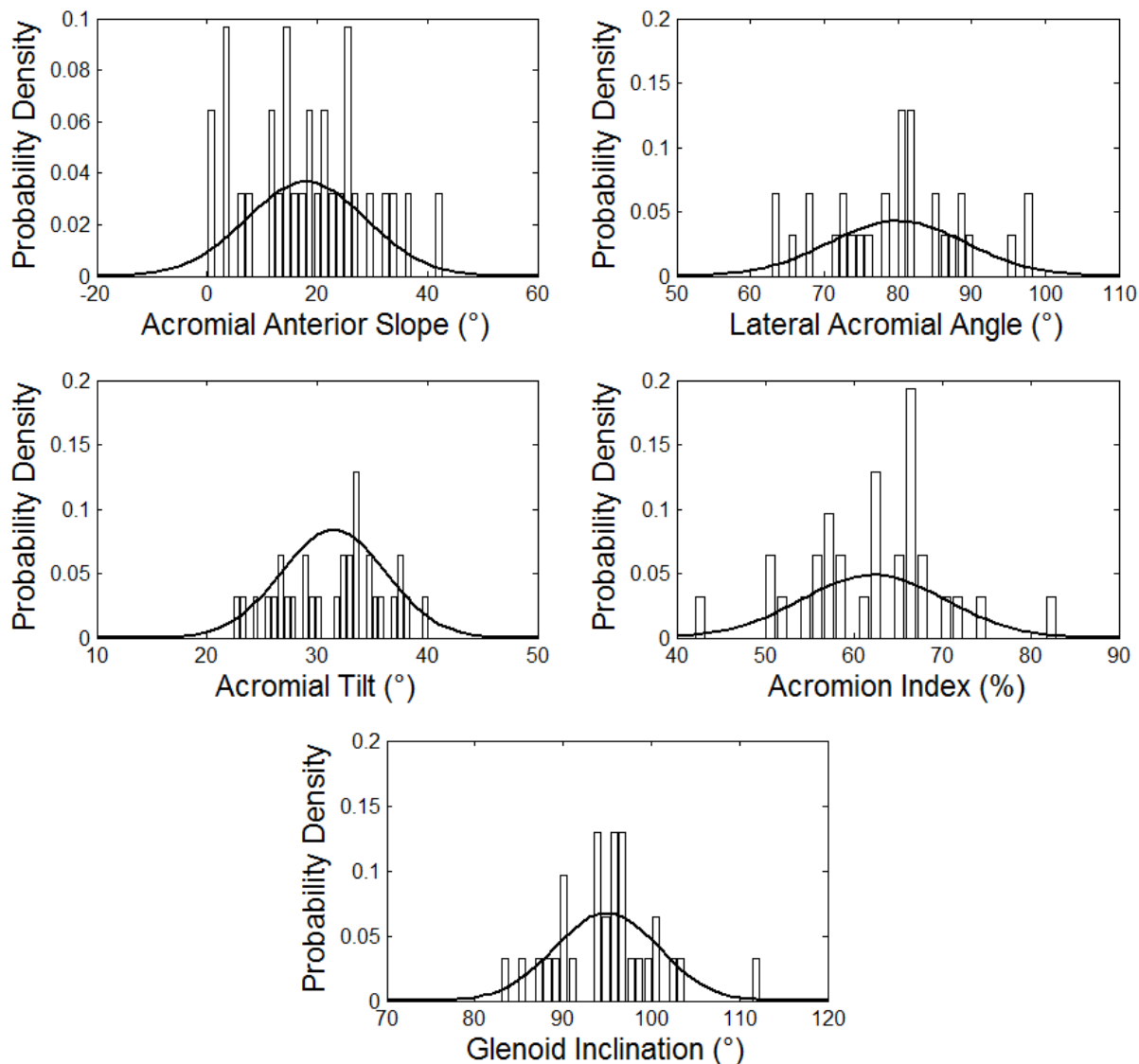
Figure 22. Frequency histograms of each bone morphological characteristic with overlying normal distribution curve.

Bone morphological characteristics were classified for health status based on previously defined ranges for healthy individuals and those with SAIS and/or rotator cuff tears (Table 19). Generally, for each bone morphological characteristic, most participants were classified as healthy (Figure 23). However, over half of participants (58%) presented with two or more unhealthy morphological characteristics. The lateral acromial angle and acromial anterior slope

showed the largest percentage (84%) of healthy measurements across participants (Figure 23, Table 20). For the remaining three characteristics (acromial tilt, acromion index, glenoid inclination), close to half of participants were classified as healthy. However, for the acromion index and glenoid inclination, slightly more than half measured in the unhealthy range (Figure 23, Table 20).

The mean measured SAS was classified as healthy for nearly all participants when captured from both radiographic and ultrasonic images. Only one participant presented with a SAS that was classified in the lower grey region (5.2mm). Further, for three participants, it was not possible to reliably measure the SAS radiographically as they lacked the dense white cortical line of the inferior acromion. While generally identified as healthy, the SAS obtained from radiographs were consistently lower than that obtained from either ultrasound images, with a confidence interval extending into the previously identified injury range (Figure 23). The SAS measured with two different ultrasound views were similar with a maximum intra-participant difference of 2.8mm.
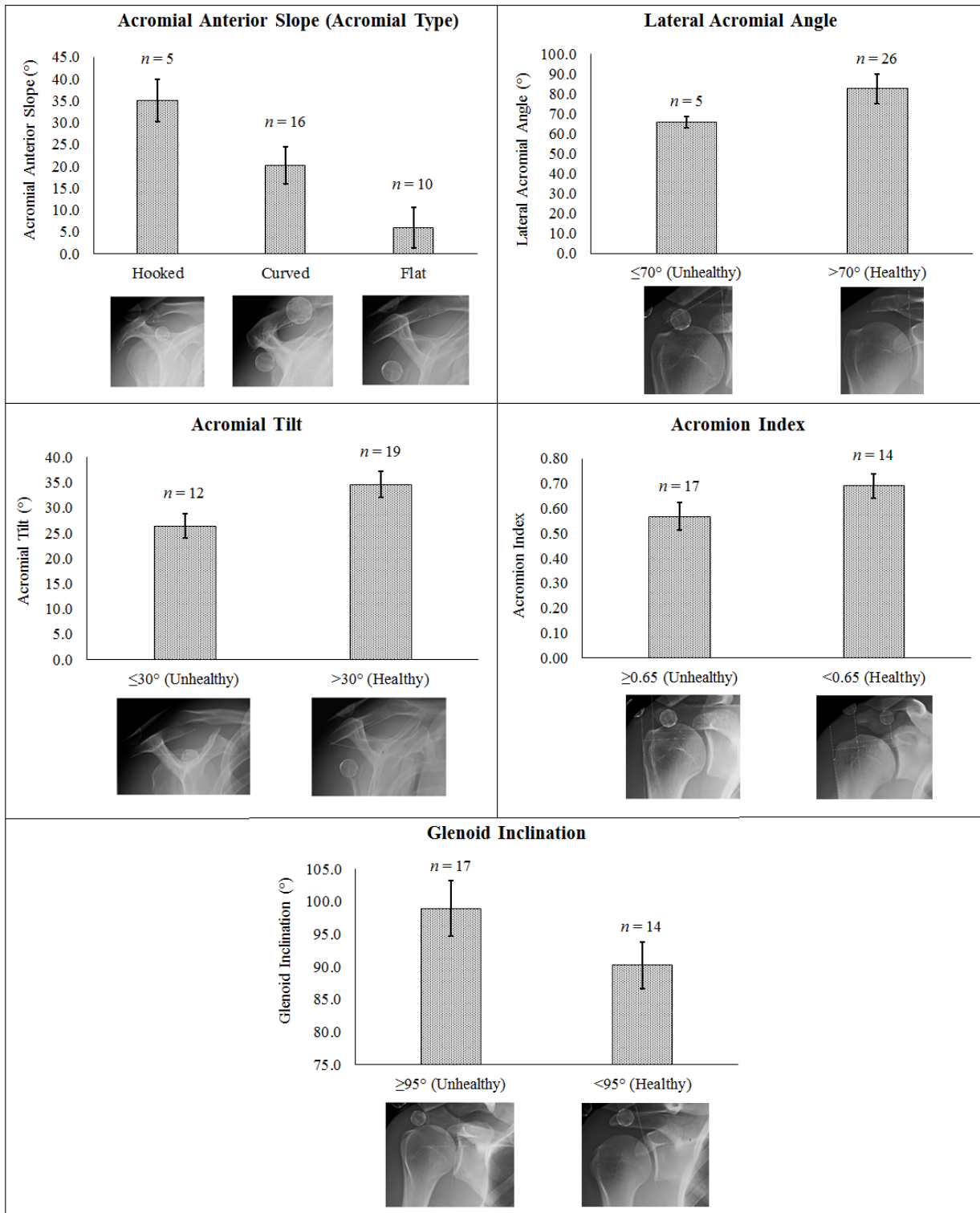
Figure 23. Bone morphological characteristics (mean, standard deviation) classified into healthy and unhealthy ranges; n = the number of participants presenting with each classification (*Note:* n_{total} = 31).

There was a wide distribution of tissue thicknesses and subsequently, occupation ratios, among the population. The radiographic occupation ratio elicited an average of 10.5% and 11.2% greater than mid-lateral and anterior ultrasonic ratios, respectively (Table 22). Due to high variability in both SAS and tissue thickness, substantial overlap exists between their fit normal distributions (Figure 24). This overlap was confirmed by the 99% confidence limit for the radiographic occupation ratio which exceeded 100% (108.9%) (Table 22).
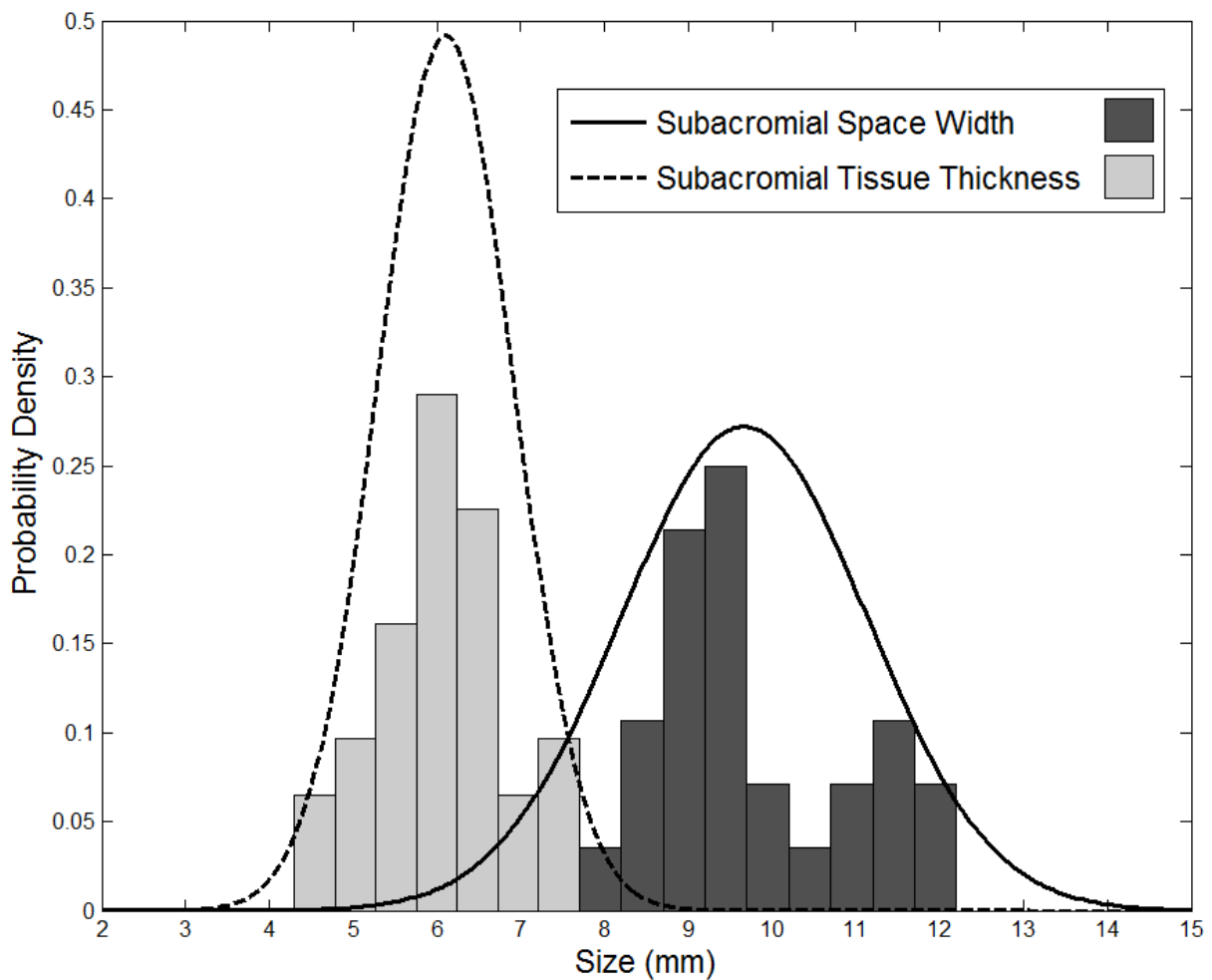
Figure 24. Frequency histograms of the minimum subacromial space width (measured using anterior-posterior radiographs) and the interposed subacromial tissue thickness (sum of

supraspinatus tendon thickness and subacromial bursa) with overlying normal distribution curves.

The covariance between each of the five morphological characteristics and the minimum (radiographic) subacromial space width ranged from poor to moderate (0.01-0.59) (Table 23). The strongest correlations were negative between the acromion index and both the SAS (-0.59) and the lateral acromial angle (-0.41).

Table 23. Correlation matrix for bone morphological properties captured using radiographs.

	Acromial Anterior Slope	Lateral Acromial Angle	Acromial Tilt	Acromion Index	Glenoid Inclination	Minimum Subacromial Space Width
Acromial Anterior Slope		0.13	-0.01	-0.09	0.07	0.12
Lateral Acromial Angle	0.13		-0.16	-0.41	-0.27	0.16
Acromial Tilt	-0.01	-0.16		-0.02	0.20	0.17
Acromion Index	-0.09	-0.41	-0.02		0.18	-0.59
Glenoid Inclination	0.07	-0.27	0.20	0.18		0.01
Minimum Subacromial Space Width	0.12	0.16	0.17	-0.59	0.01	

5.4.1.1 *Measurement Reliability*

Measurement reliability for each of the described characteristics was determined to be adequate based on the combined outcomes of Bland-Altman plots, paired t-tests and intraclass correlation coefficients. Bland-Altman plots generally showed good agreement for both intra-rater and inter-rater measurements, despite the presence of outliers in occasional measurements.

This agreement was supported by paired t-tests that showed no statistically significant (p>0.05) differences present within or between rater measurements. Additionally, intraclass correlation coefficients indicated excellent agreement with coefficients ranging from 0.951 to 0.995 for intra-rater and 0.897 to 0.991 for inter-rater measurements. For ultrasound measurements excellent agreement was similarly identified with intraclass correlation coefficients between 0.868 and 0.983, with no statistically significant (p>0.05) differences present between measurements and a single outlier across all characteristics. Bland-Altman plots for inter- and intra- rater reliability are presented in **Appendix 3**.

5.5   Discussion

The wide distribution of bone and tissue morphological characteristics supported the hypothesis that while most participants had bone morphological characteristics classified as healthy, each of these characteristics were highly variable amongst this population, suggesting their subsequent variable predisposition to SAIS risk. For the acromial anterior slope, lateral acromial angle and acromial tilt, most participants had bone shapes classified as healthy (Table 19). Alternatively, for the acromion index and glenoid inclination, just over half of participants had measurements associated with higher risk of SAIS and/or rotator cuff pathology (Balke et al. 2013, Hughes et al. 2003, Konrad et al. 2006). For both radiograph and ultrasonic measurements of the SAS, all but one participant (on radiograph) was classified as healthy (Table 20).

Calculation of the occupation ratios confirmed a wide range of risk posed to participants based on their bone and tissue morphology (Table 22). Beyond increased risk for individuals, with some demonstrating ratios >80%, the average occupation ratios were also informative. An inverse relationship between the SAS and humeral elevation exists, with SAS less than 4mm at elevated arm postures (Chapter 4 Results; Bey et al. 2007, Graichen et al. 1999a). Given the wide

distribution of values in a neutral arm posture (Table 22), with a mean ratio >50%, even the

"average" participant is at risk for SAIS with arm elevation, and the ends of the distribution will

almost certainly have tissue compression. In a study by Graichen et al. (1999a), the smallest SAS

across the range of elevation was measured at 120°, however, they reported that the SAS vector

passed through the supraspinatus tendon in 100% of participants at 60° of elevation and 50% of

participants at 90° of elevation while at greater elevation angles (such as 120°), the vector passed

lateral to the tendon. More recent research suggests that during scapular plane elevation, the

vector passes lateral to the tendon at angles above 72°, however this upper limit was shown to be

highly variable (Giphart et al. 2012). Thus, this mid-range of elevation likely poses the highest

risk for tendinous injury. This can be visualized by evaluating the overlap between the

distribution of subacromial tissue thicknesses and the SAS at a neutral arm posture (measured in

this research) (Figure 24 & Figure 25) and elevated arm postures (measured in Chapter 4)

(Figure 25). The substantial overlap between the tissue thickness and SAS at 60° and 90°

indicates nearly universal risk for tissue compression with arm elevation.
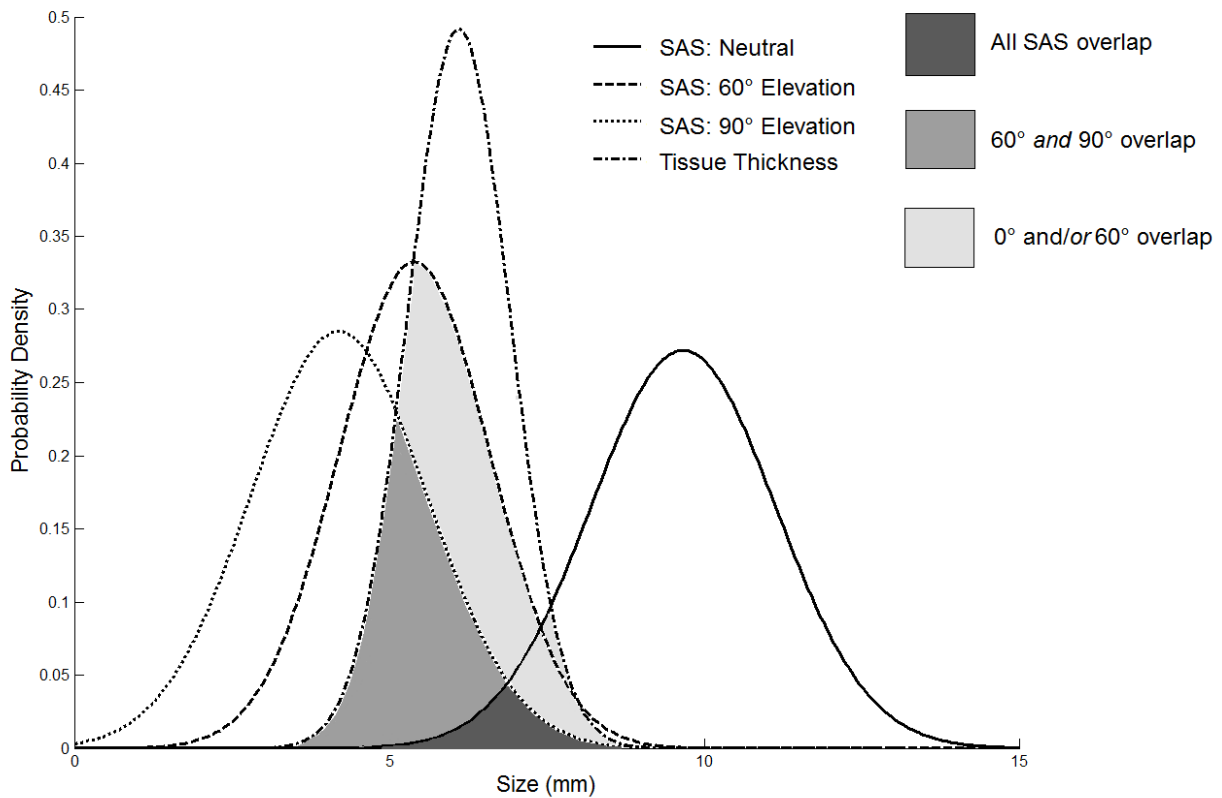
Figure 25. Normal distribution curves for the subacromial tissue thickness (measured in this research), the minimum subacromial space width (SAS) at neutral (measured radiographically in this research), and the SAS at both 60° and 90° of elevation (measured in Chapter 4). Shading indicates areas of overlap between the SAS (at neutral and/or in elevated postures) and the interposed tissues where tissue compression occurs.

As anticipated, a higher occupation ratio was calculated for the radiographic image, given the imaging restrictions of ultrasound. Average ratios of 65.3%, 54.1% and 54.8% were calculated using radiographic and ultrasonic (anterior, mid-lateral) space measurements, respectively (Table 22). The measurement of the SAS on anterior-posterior radiographs seldom occurred at the lateral-most point of the acromion where ultrasound measures are captured.

Additionally, the undersurface of the acromion may be outside the ultrasound imaging area resulting in the subsequent underestimation of the true occupation ratio (Michener et al. 2013). The occupation ratio calculated using exclusively ultrasound with the anterior transducer measurement was nearly identical to that reported by Michener et al. (2013). Despite the previous use of the anterior measurement of the subacromial space, the mid-lateral location elicited a slightly closer magnitude to the radiographic measurement, likely due to higher visibility and thus more robust identification of the inferior acromion on the mid-lateral measurement.

5.5.1 *Morphological covariance*

In evaluating the interdependence of bone morphological characteristics and the minimum (radiographic) subacromial space width several characteristics showed poor to fair correlations, while few showed moderate correlations (Table 23). Both the coefficient magnitudes and directionalities closely agreed with recent research (Balke et al. 2013). The relatively strong relationship between the acromion index and SAS (-0.59) can be explained, as a larger lateral extension of the acromion, which would increase the acromion index, would influence the path of the deltoid muscle around the humeral head and create a higher superior shear force, thereby reducing the subacromial space (Nyffeler et al. 2006). The acromion index had a moderate negative relationship with the lateral acromial angle, likely due to the common glenoid axis between measurements (Balke et al. 2013, Nyffeler et al. 2006). With a reduced lateral acromial angle (downward sloping acromion), the distance between the glenoid axis and the most lateral acromial point is increased, subsequently increasing the acromion index. All other correlations were < 0.30.

144

5.5.2 *Implications of bone and tissue morphological variability*

Despite solely including a young, healthy population, considerable variation in bone and tissue morphological properties suggests that intrinsic genetic variation contributes to eventual SAIS development. Association of specific morphological characteristics, in particular the acromial anterior slope angle, with age-related degeneration or rather genetics has been subject to debate. The distribution of acromial types in the lifespan displays an increased proportion of type III (hooked) acromions and fewer type I (flat) acromions, indicating that acromial morphology is related to age-related degeneration (Wang and Shapiro 1997). Instead of a genetic variant, the hook has been attributed to the development of a bone spur or enthesophyte extending from the anterior-inferior aspect of the acromion as a result of repeated contact with the humeral head (Nicholson et al. 1996, Shah et al. 2001, Wang and Shapiro 1997). Shah et al. (2001) has presented histologic evidence supporting age-related degeneration of the acromion, showing that type II and III acromial types showed degeneration in the collagen, fibrocartilage or bone of the anterior-inferior acromion, while type I types did not. Despite these reports, there is also conflicting data indicating limited to no relationship between acromial type and age, with type III acromions existing across the entire age range (Balke et al. 2013, Banas et al. 1995, Nicholson et al. 1996, Vahakari et al. 2010). While age-related changes to shoulder morphology are certainly possible, the presence of predisposing bone morphology in this research supports the role of genetics in the risk of SAIS and/or rotator cuff pathology.

5.5.3 *Limitations*

Limitations related to image capture and measurement should be considered when interpreting these results. The relationship between the radiographic beam angle and the positioning of the participant can influence post hoc measurements (Fehringer et al. 2008, Stehle

145

et al. 2007). For both radiographic views (anterior-posterior and trans-scapular), the beam was oriented perpendicular to the imaging plate. The caudal tilt angle of the beam has varied between studies (5 to 20°) and has been shown to largely influence the measured angles, particularly the acromial anterior slope (Stehle et al. 2007). Thus, capturing images with no caudal tilt may have resulted in an underestimation of the acromial anterior slope angle, which may have subsequently lead to more participants falsely classified as "healthy". Further, while all measurements had excellent inter- and intra- rater reliability, there were outliers for some measures that may be consequent to the radiograph quality.

Lastly, while all injury classification ranges were based on available data, the glenoid inclination classification may slightly diverge from those in the literature due to the variation in measurement technique. The measurement method in this research was one established recently by Maurer et al. (2012) that was shown to reliably measure inclination on radiographs. Thus, the injury classification of approximately 90° by Hughes et al. (2003) was modified to 95° to include the difference in measurement technique.

5.6   Conclusions

Large variation in bone and tissue morphology around the subacromial space existed among a population of young, healthy males. This large variation extended into unhealthy classifications of bone shapes, suggesting that members of the population may be predisposed to SAIS risk and/or rotator cuff pathology due to their intrinsic genetic morphology. These results also suggest that the risk itself is also highly variable, as evidenced by occupation ratios with a 99% confidence interval ranging from a modest 21.6% to 108.9%. This supports altered rehabilitation and treatment strategies and the prospective utility of morphological evaluations that may enable proactive injury reduction strategies.

Chapter 6

Development of a Probabilistic Model for the Prediction of Subacromial Geometry

Overview

Glenohumeral and scapulothoracic kinematic relationships, as well as morphological characteristics of the scapula and humerus affect the dimensions of the subacromial space. Each of these measures vary considerably within the population, which can lead to misleading estimations of subacromial impingement risk (SAIS). Additionally, the relative influence of each parameter on subacromial space variability is unclear. This research used a probabilistic modelling approach to predict the size of the subacromial space and estimate the SAIS risk using empirically measured distributions of fatigue-induced kinematics and morphological parameters. Through use of the Advanced Mean Value (AMV) probabilistic method, relative sensitivity factors were calculated to establish which parameters contributed more to the variability in SAIS risk. As expected, the predicted minimum subacromial space width (SAS) had considerable variability as evidenced by 1-99% confidence intervals differing by an average of 8mm. While the SAS was not influenced by muscle fatigue, within each fatigue state the space reduced with arm elevation to magnitudes between 4.5-5mm, which were comparable to those measured in vivo. This reduction in space with elevation, coupled with the measured interposed tissue thickness, resulted in an estimated 65-75% of the population at risk for tissue compression at elevation angles of 90 and 120°. Calculated importance factors showed morphological parameters, notably glenoid inclination, to be particularly important in modulating the size of the SAS over the range of elevation, while kinematic parameters depended on elevation angle and fatigue state. This reinforced avoiding overhead work postures if possible, as they certainly pose

147

additional risk for rotator cuff tendon compression. Further, as glenoid inclination is difficult to diagnose and treat, and relates to superior humeral head translation, rotator cuff strengthening programs are recommended to maintain glenohumeral stability, particularly in populations exposed to overhead postures and/or fatiguing exertions.

6.1   Introduction

Incorporating variability into predictive models, particularly in biomechanics research, is crucial for capturing physiological realism. Each variable or parameter that contributes to the overall output has an associated level of uncertainty and thus relying on population mean values to represent each variable fails to capture this variability, subsequently resulting in possibly misleading outcomes (Langenderfer et al. 2006, Laz and Browne 2010). Probabilistic approaches can be used to evaluate the influence of model parameter uncertainty on the predicted output by representing each parameter as a probability distribution. Often, minor perturbations in inputs and/or model parameters can have a remarkable influence on the predicted outputs (Easley et al. 2007, Langenderfer et al. 2006, 2008, 2009, Pal et al 2007). However, despite demonstrating critical utility for characterizing biological tissue variation, the overall use of probabilistic modelling in biomechanics is still limited.

The risk of developing subacromial impingement syndrome (SAIS), and subsequent tissue damage, has been attributed to several bone and tissue morphological characteristics in addition to kinematic alterations that may result from fatiguing overhead and/or repetitive tasks. The considerable interpersonal variability that exists for each of these characteristics (Chapters 4 and 5) coupled with the clinical relevance of small changes in magnitude (~1mm) demonstrates the essential need to apply probabilistic methods in the evaluation of SAIS risk that exists in the population. Our research group has previously tried to evaluate this variability in risk by using a

deterministic modelling approach, which evaluated the influence of humeral head translation and scapular reorientation on the size of the subacromial space, while considering both 'average' and 'worst-case' scenarios for reducing the subacromial space (Chopp and Dickerson 2012). Even in a relatively homogeneous sample (gender, age, health status), there was significant variability in each kinematic parameter, which subsequently led to a highly variable prediction of the minimum subacromial space width (SAS).

The many parameters contributing to subacromial space reduction, and their collective interpersonal variability, reinforced the necessity to apply probabilistic methods to evaluate the distribution of subacromial space geometry resulting from parameter variation. Additionally, employing the Advanced Mean Value (AMV) probabilistic approach enabled the calculation and comparison of importance factors that describe which of the several factors were more contributory towards the output variability. Determining the distribution of subacromial geometry and the primary mechanisms (morphological, kinematic) contributing to the reduction in this space, both in controlled and fatigue-related scenarios, is critical in the prevention of SAIS, as each mechanism may be addressed by different targeted rehabilitative and prevention strategies as well as ergonomic interventions.

Research Objectives:

1. Develop a probabilistic model to predict the distribution of minimum subacromial space width (SAS) of a young, healthy male population, based on varying empirically measured morphological characteristics and fatigue-related glenohumeral and scapulothoracic kinematics.

   ➢ Estimate the probability of SAIS risk by comparing the predicted SAS to the distribution of subacromial tissue thicknesses.

149

2. Determine which parameters (kinematic, morphological) contributed more to subacromial space reduction.

Research Hypotheses:

It was hypothesized that superior humeral head translation would be a more important contributor to subacromial space reduction than three-dimensional scapular orientation following fatigue due to reported fatigue-initiated glenohumeral and scapulothoracic kinematics (Chapter 4 Results; Chen et al. 1999, Chopp et al. 2010, 2011, Cote et al. 2009, Ebaugh et al. 2006, McQuade et al. 1998, Teyhen et al. 2008). This would highlight the importance of rotator cuff strengthening in a population exposed to overhead and/or repetitive tasks that fatigue these muscles. It was also hypothesized that morphological parameters that have shown strong associations with rotator cuff damage and/or SAIS, such as acromial morphology and glenoid inclination (Balke et al. 2013, Hughes et al. 2003, Toivonen et al. 1995), would be as important as the kinematic factors for subacromial space reduction, as demonstrated by model predicted relative sensitivity factors. Further, it was anticipated that the risk, both kinematic and morphological, would vary across the studied population, with certain members at considerably greater risk than others. Confirmation of these hypotheses would reinforce the overall research hypothesis that the SAS size, and subsequent SAIS risk, is highly variable in the population. Specifically, that certain members of the population have innate geometry that predisposes them to SAIS risk which is further exacerbated by fatigue-related kinematic factors, such as humeral head translation, while others demonstrate healthy morphological classifications and kinematic fatigue responses, thus having low risk of SAIS development.

6.2   Model Parameters and Simulations

Nine parameters (four kinematic, five morphological) were treated as continuous random variables in the probabilistic model. Kinematic parameters were obtained from the experimental research described in Chapter 4, and the morphological parameters were obtained from the experimental research described in Chapter 5.

Model Parameters

Kinematic (Chapter 4)

- Superior-inferior translation (mm)
- Upward-downward rotation (°)
- Posterior-anterior tilt (°)
- Retraction-protraction (°)

Morphological (Chapter 5)

- Glenoid inclination (°)
- Lateral acromial angle (°)
- Acromial anterior slope (acromial type) (°)
- Acromial tilt (°)
- Acromion index

The effect of model parameter variability on the minimum subacromial space width (mm) (SAS) was predicted for ten different experimental conditions:

- Humeral Elevation Angle (0°, 30°, 60°, 90°, 120°)
- Fatigue State Session (pre-fatigue, post-fatigue)

It is important to note that only the kinematic parameters varied as a function of these conditions; thus for the acromion and glenoid morphological characteristics, identical distributions were used for each condition (all arm elevation angles and for each fatigue state).

6.3 Model Construction

6.3.1 *Deterministic Subacromial Geometry Model*

The <u>Probabilistic Subacromial Geometry Model</u> first required the development of a <u>Deterministic Subacromial Geometry Model</u> that described and manipulated the geometric relationships and bone morphology (Figure 26). This model was sub-divided into the *Deterministic Morphological Model* and the *Deterministic Kinematic Model*. The *Deterministic Morphological Model* preceded the kinematic model, in that it permitted altering the specific geometry of the humerus and scapula corresponding to the measured morphological parameters, prior to altering the kinematic relationship between the bones. This model is described in Section 6.3.1.1. Following morphological manipulation, the *Deterministic Kinematic Model* established the relationship between the humerus, the scapula and the torso, which permitted modifying glenohumeral superior-inferior translation and scapulothoracic rotations associated with specific humerothoracic positions. This model is summarized in Chopp and Dickerson (2012) and is described briefly in Section 6.3.1.2. The overall output of the <u>Deterministic Subacromial Geometry Model</u> was the calculated minimum subacromial space width (SAS) between the inferior-most point on the acromion and superior-most point on the humeral head.
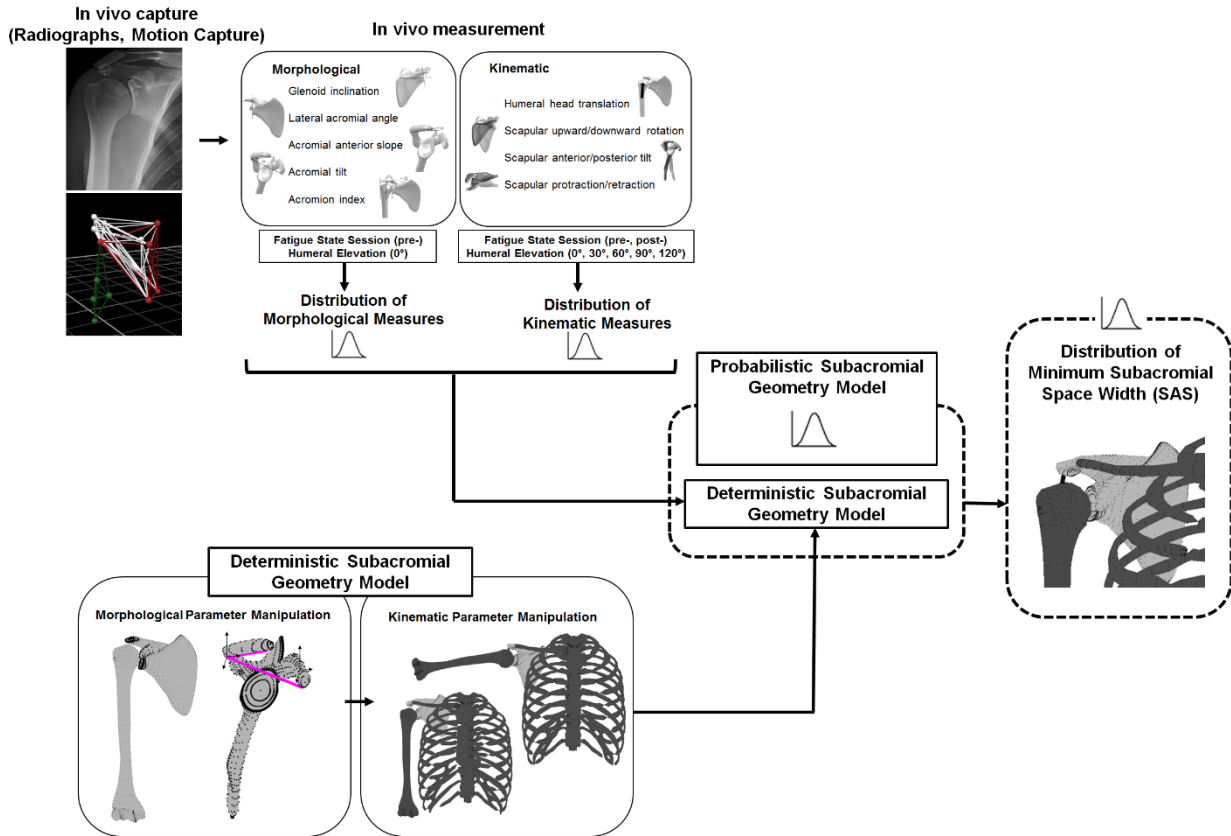
Figure 26. Overview of Subacromial Geometry Model. Morphological and Kinematic Parameters are measured in vivo from which population distributions for each measurement are obtained. The model is manipulated such that the bone shapes correspond to the measured distributions. The morphologically manipulated model is used as input into the kinematic model. The model is then manipulated such that the relationships between the bones correspond to the measured distributions, for each of the ten conditions (fatigue state, elevation angle). The predicted output is a distribution of minimum subacromial space width for each condition.

6.3.1.1 *Deterministic Morphological Model*

The bone segments used in the construction of this model were obtained from the CT images of the Visible Human Male dataset of The Visible Human Project (U.S. National Library of Medicine, Ackerman 1988). The geometric input for this model, specifically the three-

153

dimensional point clouds (coordinate data) of each of the upper extremity bones (humerus, scapula, clavicle, and torso [ribs, spine]) in a common coordinate system, were obtained from the upper extremity model presented in Dickerson et al. (2007). The humerus was constructed from 3807 points[7], the scapula from 3601 points, the clavicle from 1207 points, the ribs from 7659 points and the spine from 19739 points. Each point was defined as a three-dimensional vector in the common 'global' or 'scan'[8] system. Prior to commencing morphological manipulation, the points (three-dimensional coordinates) associated with three sub-segments on the scapula were identified: (1) acromion process, (2) coracoid process, and (3) glenoid cavity.

Five morphological manipulations were performed: (1) Glenoid Inclination, (2) Lateral Acromial Angle, (3) Acromial Anterior Slope, (4) Acromial Tilt, and (5) Acromion Index. Parameters were manipulated in the described order to account for certain landmark/axis dependencies. Each of the first four morphological manipulations followed the same three general steps: (1) determine the global/scan angle, (2) alter the bone geometry so that the angle corresponded to the measured angle specified, and (3) verify that the new angle was correct. Alternatively, the Acromion Index involved a different manipulation protocol. While the first four parameters were 'rotational', the Acromion Index was 'translational'. The morphological manipulation procedure for the first four parameters is described, followed by a description of the Acromion Index manipulation procedure.

---

[7] The term 'point' represents a three-dimensional vertex (x,y,z) on one of the upper extremity bones (humerus, scapula, clavicle, ribs, spine)

[8] For the purpose of model description, the "Scan" coordinate system, represents the "Global" coordinate system

A: Glenoid Inclination, Lateral Acromial Angle, Acromial Anterior Slope, Acromial Tilt

Part I: Determine the 'Scan (Global)' Angle

1. *Local Glenoid System Identification*

The local glenoid system was defined using points located on the superior, inferior, medial and lateral-most borders of the glenoid cavity. The $+X$-axis was directed approximately anteriorly, the $+Y$-axis was directed approximately superiorly, and the $+Z$-axis was directed approximately laterally (as described in Section 2.2.1). Though this system has not been previously defined in the literature, these directions correspond to ISB recommended orientations (Wu et al. 2005), consistent with all other local coordinate systems created in this model.

For all five morphological parameters, as in vivo measurements were obtained from anterior-posterior and trans-scapular radiographs in two-dimensions, the local glenoid system was used as the global reference axis where: the *Glenoid Y-Z plane* represented an anterior-posterior radiograph and the *Glenoid X-Y plane* represented a trans-scapular radiograph. Thus, all parameters were projected onto the local glenoid system, with corresponding angles calculated in two dimensions (consistent with in vivo measurements). This concept is fundamental to the understanding of all morphological manipulations described.

2. *Rotation Matrices from Global ('Scan') system to glenoid local coordinate system*

A rotation matrix between the global system (defined as an identity matrix) and the local glenoid system was created [Eq. 6-1]. Note: for each of the measurements, the original (unaltered) glenoid coordinate system was used to develop the rotation matrix, as the intended goal was to make the local glenoid system synonymous with the radiographic image.

$$R_{GLEN}^{GCS} = \begin{bmatrix} i_{GLEN} \cdot i_{GCS} & j_{GLEN} \cdot i_{GCS} & k_{GLEN} \cdot i_{GCS} \\ i_{GLEN} \cdot j_{GCS} & j_{GLEN} \cdot j_{GCS} & k_{GLEN} \cdot j_{GCS} \\ i_{GLEN} \cdot k_{GCS} & j_{GLEN} \cdot k_{GCS} & k_{GLEN} \cdot k_{GCS} \end{bmatrix} \qquad \text{[Eq.6-1]}$$

Where,

R_{GLEN}^{GCS} is the rotation matrix to rotate points from the global-to-glenoid coordinate system

i, j, k are the unit vectors of the x, y and z axes, respectively

3. *Identification of Anatomical Landmarks required for Angle Definition*

The points corresponding to the anatomical landmarks used to measure the specific angle were identified. Note: specific measurement procedures for each of the parameters have been previously described (Chapter 5).

4. *Rotation/Translation of Points into the Local Glenoid System*

Each of the points identified in *Step 3* were then rotated into the local glenoid system about the glenoid system origin (center of the glenoid cavity) [Eq. 6-2].

$$\vec{P}_{GLEN,p,i} = R_{GLEN}^{GCS} * (\vec{P}_{GCS,p,i} - CG_{GCS}) \qquad \text{[Eq.6-2]}$$

Where,

$\vec{P}_{GLEN,p,i}$ and $\vec{P}_{GCS,p,i}$ are the points/anatomical landmarks ($i = 1,2,...,n$) that create the specific angle for each parameter ($p = glenoid\ inclination, acromial\ anterior\ slope, ...$) in the local glenoid and global (scan) coordinate systems, respectively

R_{GLEN}^{GCS} is the rotation matrix to rotate the points from the global-to-glenoid coordinate system [Eq. 6-1]

CG_{GCS} is the origin of the local glenoid system (center of the glenoid cavity) in the global coordinate system

5. *'Scan' (Global) Angle Calculation*

The 'scan angle' or 'global angle', which corresponded to the parameter angle before being rotated, was calculated [Eq. 6-3]. This angle, however, may have changed if its angle was dependent on previous parameters (i.e. the glenoid inclination and lateral acromial angle parameters both use a common glenoid *y*-axis in its angle manipulation, thus modifying the glenoid inclination would subsequently alter the lateral acromial 'scan' angle).

For the angle calculation, only two coordinates were used to more accurately reflect the two-dimensional in vivo measurement protocol. The Glenoid Inclination, Lateral Acromial Angle, and Acromion Index parameters were obtained from an anterior-posterior radiograph (Y-Z glenoid plane) and thus only *y* and *z* coordinates were used. The Acromial Anterior Slope and Acromial Tilt parameters were obtained from a trans-scapular radiograph (X-Y glenoid plane) and thus only *x* and *y* coordinates were used.

$$\theta_{SCAN,p} = cos^{-1}(\frac{\vec{V_1} \cdot \vec{V_2}}{\|\vec{V_1}\| * \|\vec{V_2}\|})$$ [Eq. 6-3]

Where,

$\theta_{SCAN,p}$ is the scan angle of the parameter (p)

$\vec{V_1}$ and $\vec{V_2}$ are the two vectors that create the specific angle for each parameter (p), calculated using the specific points described in *Step 4* (Chapter 5).

Part II: Change the Angle to the 'Measured' angle

6. Local Coordinate System Construction for Parameter-specific Coordinate Systems

Each parameter was rotated about parameter-specific coordinate systems, consistent with measurement descriptions described in Chapter 5. For example, in the case of the Acromial Anterior Slope, a local coordinate system about the distal acromion was developed.

7. Rotation Matrices from Global ('Scan') system to LCS

Rotation matrices to rotate points from the global 'scan' system to the parameter-specific LCS were constructed [Eq.6-4].

$$R_{LCS,p}^{GCS} = \begin{bmatrix} i_p \cdot i_{GCS} & j_p \cdot i_{GCS} & k_p \cdot i_{GCS} \\ i_p \cdot j_{GCS} & j_p \cdot j_{GCS} & k_p \cdot j_{GCS} \\ i_p \cdot k_{GCS} & j_p \cdot k_{GCS} & k_p \cdot k_{GCS} \end{bmatrix}$$ [Eq.6-4]

Where,

$R_{LCS,p}^{GCS}$ is the rotation matrix to rotate points from the global coordinate system to the parameter-specific local coordinate system

i, j, k are the unit vectors of the x, y, and z axes, of the parameter-specific (p) local coordinate system (LCS) and global (GCS) coordinate systems

8. *Definition of Measured/Manipulation Angle*

To accommodate probabilistic interfacing, the manipulation angle was defined such that altering a single value for each parameter would rotate the required points so that the resulting angle corresponded to that measured in vivo. This was achieved by first subtracting the initial Scan Angle from the measured angle [Eq. 6-5].

$$\beta_p = \theta_{MEASURED,P} - \theta_{SCAN,p} \qquad [Eq.6-5]$$

Where,

β_p is the manipulation angle for each parameter (p)

$\theta_{MEASURED,P}$ and $\theta_{SCAN,p}$ are the measured and scan angles, respectively, expressed in radians

9. *Direction Cosine Matrix Construction*

The manipulation angle was defined about one of the local axes of the parameter-specific coordinate systems described in *Step 6*. For example, in the case of the Acromial Anterior Slope (captured from a trans-scapular radiograph; X-Y glenoid plane), the points would be rotated about the *z*-axis (approximate lateral axis) of the local distal acromion (parameter-specific) coordinate system [Eq. 6-6].

$$R^{\theta_{SCAN,p}}_{\theta_{MEASURED,p}} = \begin{bmatrix} cos\beta_p & -sin\beta_p & 0 \\ sin\beta_p & cos\beta_p & 0 \\ 0 & 0 & 1 \end{bmatrix} \qquad [Eq.6-6]$$

Where,

$R^{\theta_{SCAN,p}}_{\theta_{MEASURED,p}}$ is the rotation matrix to rotate points from the original scan angle to the measured in vivo angle about the local *z*-axis.

10. Rotation of Points to Correct Orientation

The rotation was then applied to each of the points specific to the particular parameter definition (distal acromion, coracoid and/or lateral glenoid cavity) [Eq. 6-7]. The rotation point was specific to each parameter and was selected to most accurately represent the in vivo measurement description. For example, for the Acromial Anterior Slope, the rotation point was the mid-substance of the acromial junction (Figure 27).

$$\vec{V}_{LCS,p,i} = R_{LCS,p}^{GCS} * (\vec{V}_{GCS,p,i} - P_{GCS,p})$$ [Eq. 6-7]
$$\vec{V}_{LCS,p,i,\beta} = R_{\theta_{MEASURED},p}^{\theta_{SCAN},p} * (\vec{V}_{LCS,p,i})$$
$$\vec{V}_{GCS,p,i,\beta} = ([R_{LCS,p}^{GCS}]' * \vec{V}_{LCS,p,i,\beta}) + P_{GCS,p}$$

Where,

$\vec{V}_{GCS,p,i}$ and $\vec{V}_{LCS,p,i}$ are all of the points specific to the parameter definition (i) of the particular parameter (p) in the global and their local coordinate system, respectively

$\vec{V}_{GCS,p,i,\beta}$ and $\vec{V}_{LCS,p,i,\beta}$ are all of the points specific to the parameter definition (i) of the particular parameter (p) in the global and their local coordinate system, respectively, following the angle manipulation

$R_{LCS,p}^{GCS}$ is the rotation matrix to rotate points from the global coordinate system to the parameter-specific local coordinate systems for each particular parameter (p).

$P_{GCS,p}$ is the rotation point for the angle manipulation of a particular parameter (p) in the global coordinate system

Figure 27. Manipulation of the Acromial Anterior Slope (Acromial Type); *Left*: 7.1° ($\mu - 1\sigma$), *Right:* 28.9° ($\mu + 1\sigma$).

Part III: Verify that New Angle is correct

The final step was to ensure that the new angle following the morphological manipulation was equal to the angle specified (in vivo measurement angle). This was achieved by repeating *Steps 4-5* described in *Part I*, using the new rotated points in the angle calculation. Morphological manipulations were rigorously tested to ensure this verification prior to commencing probabilistic simulation.

B: Acromion Index

The Acromion Index is a parameter describing the lateral extension of the acromion process relative to that of the humeral head and thus morphological manipulation involved both a translation of existing points and the addition of new points, depending on the measured ratio. While certain assumptions were required for the manipulation of each morphological parameter,

two important assumptions for the Acromion Index are necessary for the understanding of the morphological manipulation. First, changing the Acromion Index (ratio of [lateral acromion–glenoid axis] to [lateral humerus–glenoid axis]) could result from the bone extension of either the acromion process or humeral head. For the purpose of this research, it was assumed that any modification to the ratio was a result of equal alteration of the acromion and humeral head. Second, as described, the common reference axis for both measurement components (acromion, humerus) was the glenoid axis, as measured in vivo. To maintain physiologically feasible bone morphology, the scan glenoid axis (prior to altering glenoid inclination) was used as the common reference axis. Initial testing using the rotated glenoid axis, resulted in creating bone dimensions that were physiologically impossible.

The manipulation procedure for the Acromion Index is summarized as follows:

1. *Identification of Lateral-most Points on the Acromion Process and Humeral Head*

The lateral-most vertices on the acromion process and humeral head were first identified. These points were obtained by determining the points with the largest z-coordinate magnitude after the vertices were rotated into the local glenoid system, in which $+z$ was directed laterally.

2. *Rotation/Translation of Points into the Local Glenoid System*

Each of the points identified in *Step 1* were then rotated into the local glenoid system about the glenoid system origin [Eq. 6-2]. Only the y and z coordinates were used in further steps as in vivo measurements were obtained from an anterior-posterior radiograph.

3. '*Scan' (Global) Index Calculation*

The scan (global) Acromion Index was calculated by determining the length of two vectors perpendicular to the glenoid axis passing through: (1) the lateral-most acromion point

and (2) the lateral-most humeral point. The ratio of these two vectors defined the Acromion

Index [Eq. 6-8].

$$AI_{SCAN} = \frac{GAA}{GAH}$$
[Eq.6-8]
$$GAA = \frac{\|(P_{GS}-P_{GI})\times(P_A-P_{GI})\|}{\|(P_{GS}-P_{GI})\|}$$
$$GAH = \frac{\|(P_{GS}-P_{GI})\times(P_H-P_{GI})\|}{\|(P_{GS}-P_{GI})\|}$$

Where,

GAA and GAH are the perpendicular vectors between the glenoid axis and the lateral-most acromion point and humeral head point, respectively

P_{GS} and P_{GI} are the superior-most and inferior-most points of the glenoid cavity, respectively, and $(P_{GS} - P_{GI})$ defines the glenoid axis

P_A and P_H are the lateral-most points on the acromion and humeral head, respectively

4. Definition of Measured/Manipulation Index

The Acromion Index measured in vivo was then defined and used to calculate the

required translation for both acromion and humerus points [Eq.6-9].

$$dGAA = \frac{(AI_{MEASURED}*GAH)-GAA}{2}$$
[Eq.6-9]
$$dGAH = \frac{\frac{GAA}{AI_{MEASURED}}-GAH}{2}$$

Where,

$dGAA$ and $dGAH$ are translation terms for the acromion points and humeral head points, respectively

$AI_{MEASURED}$ is the Acromion Index measured in vivo

GAA and GAH are the terms described in [Eq.6-8]

5. Specification of Translation Conditions and Application of Translation

All of the points on the lateral acromion and lateral humerus were identified using a

similar procedure to that described in *Step 1*. Each of these points was then rotated into the local

glenoid system where a translation about the local *z*-axis was applied [Eq.6-10] (Figure 28).

Note: if $AI_{MEASURED} > AI_{SCAN}$, then there was more acromial extension which would

subsequently result in lateral translation of the lateral acromion points (+z) and medial translation of the lateral humeral points (-z). If $AI_{MEASURED} < AI_{SCAN}$, the opposite would occur.

$$\vec{V}_{X,GLEN,i} = R_{GLEN}^{GCS} * (\vec{V}_{X,GCS,i} - CG_{GCS}) \qquad \text{[Eq. 6-10]}$$
$$\vec{V}_{X,GLEN,i,t} = \vec{V}_{X,GLEN,i} + [0\ 0\ d]$$
$$\vec{V}_{X,GCS,i,t} = ([R_{GLEN}^{GCS}]' * \vec{V}_{X,GLEN,i,t}) + CG_{GCS}$$

Where,

$\vec{V}_{X,GCS,i}$ and $\vec{V}_{X,GLEN,i}$ are all of the points (i) on the lateral acromion or humerus (X) in the global and glenoid coordinate systems, respectively

$\vec{V}_{X,GCS,i,t}$ and $\vec{V}_{X,GLEN,i,t}$ are all of the points (i) on the lateral acromion or humerus (X) in the global and glenoid coordinate systems, respectively, following translation

R_{GLEN}^{GCS} is the rotation matrix to rotate points from the global-to-glenoid coordinate system

CG_{GCS} is the origin of the local glenoid system (center of the glenoid cavity) in the global coordinate system

d is the translation term for X (either $dGAP$ or $dGAH$)

Figure 28. Manipulation of the Acromion Index; *Left*: 0.54 ($\mu - 1\sigma$), *Right:* 0.70 ($\mu + 1\sigma$).

6. Verification of New Index

Similar to other morphological parameters, *Steps 1-3* were repeated using the new translated points to ensure that the new Acromion Index was equal to the Index specified (in vivo measurement angle).

7. Addition of New Acromion/Humeral Head Vertices

As the Acromion Index parameter required translational manipulation rather than rotational (as was the case with other parameters), an increase or decrease in Acromion Index from the original Scan Index resulted in a stretch to the acromion and humerus, respectively. This stretch presented as an area with no vertices. As it was possible that the location of the minimum distance (SAS) calculated following kinematic manipulation could exist in this area, a conditional statement was added to the model to create additional points (3D vertices) for each bone segment where the area was stretched and a gap existed. There were 12 points created for the acromion and 36 points created for the humeral head. These vertices were created at 25, 50 and 75% of the distance between the points on either side of the stretched surface.

The 'new' scapula and humerus were used as input into the kinematic model, where humerothoracic, scapulothoracic and glenohumeral rotations and translations were defined and applied to the morphologically varied bones.

6.3.1.2 Deterministic Kinematic Model

The kinematic model involved nine sequential steps, described as follows:

1. Anatomical Landmark Identification and Local Coordinate System Construction

Anatomical landmarks required to construct local coordinate systems (LCS) of the scapula, humerus and torso, as per ISB recommendations, were manually identified from the three-dimensional (3D) coordinate data (Wu et al. 2005) [Eq.6-11]. A local glenoid coordinate system (as described in the morphological model) was additionally constructed.

164

$$z_{SCAP} = \frac{(AA-TS)}{\|(AA-TS)\|}$$

$$temp = \frac{(AA-AI)}{\|(AA-AI)\|}$$

$$x_{SCAP} = \frac{(temp-z_{SCAP})}{\|(temp-z_{SCAP})\|}$$

$$y_{SCAP} = z_{SCAP} \times x_{SCAP}$$

[Eq.6-11]

Where,

$[x_{SCAP}, y_{SCAP}, z_{SCAP}]$ is the local coordinate system of the scapula, defined as per ISB recommendations

AA, TS, IA are the anatomical landmarks used in the LCS definition (Angulus Acromialis, Trignoum Spinae Scapulae, Angulus Inferior)

2. *Rotation Matrices from Global ('Scan') system to LCS*

Rotation matrices to rotate points from the global/scan system to the humerus, scapula and torso LCS were constructed, in addition to a rotation matrix between the glenoid and scapula LCS.

3. *Definition of the Measured Humeral Head Translation Parameter*

The humeral head translation (HHT) parameter was implemented into the model as a translation along the *y*-axis of the glenoid system (to accurately represent the in vivo measurement protocol). This parameter was defined in the local glenoid system ($t_{GLEN} = [0\ HHT\ 0]$) and converted from millimeters to 'scan units' using a scaling factor of 2.7920. This scaling factor was calculated from a conversion factor reported in Garner and Pandy (1999), which presented the 3D coordinates of specific anatomical landmarks and the corresponding distances between landmarks in millimeters, using the same Visible Human Male dataset. The acromioclavicular and sternoclavicular landmarks were used to calculate the scaling factor as they exist on the same segment, thus differences in inter-segmental relationships between this model and that presented by Garner and Pandy (1999) would not affect the scaling factor.

4. *Definition of the Measured Scapulothoracic Parameters and Humerothoracic Position*

        The scapulothoracic parameters (scapula rotation, tilt and protraction/retraction), in addition to the humerothoracic position (elevation, plane of elevation, axial rotation) were implemented into the model using the experimentally measured Euler Angles. As the joint angles were being used to set the bone positions, a reverse process to that described in Chapter 4 was used. Specifically, joint angles (in radians) were used to define direction cosine matrices around X, Y or Z axes, depending on their particular rotation axis. The ISB recommended rotation sequences were then used to create a rotation matrix from the local torso to scapula system [Eq. 6-12] and to humerus system [Eq. 6-13], from which their inverses were obtained [Eq. 6-14]. Note: a *neutral* humerothoracic position was defined as 0° of elevation, 34.3° plane of elevation and 35.7° of external rotation. Plane of elevation and internal/external rotation positions were consistent across conditions evaluated and represented the average positions of those experimentally measured. A *neutral* scapulothoracic position was 0.3° of downward rotation, 19.3° of anterior tilt and 31.8° of protraction which represent the average positions of those experimentally measured in the pre-fatigue state at 0° of elevation. These resting scapulothoracic angles are comparable to those previously reported (Ludewig et al. 2009).

$$R_{T\_S} = R_Z(\alpha)R_X(\beta)R_Y(\gamma) \hspace{3cm} [\text{Eq.6-12}]$$

$$R_{T\_S} = \begin{bmatrix} cos\gamma cos\alpha - sin\gamma sin\beta sin\alpha & -cos\beta sin\alpha & sin\gamma cos\alpha + cos\gamma sin\beta sin\alpha \\ cos\gamma sin\alpha + sin\gamma cos\alpha sin\beta & cos\beta cos\alpha & sin\gamma sin\alpha - cos\gamma cos\alpha sin\beta \\ -sin\gamma cos\beta & sin\beta & cos\gamma cos\beta \end{bmatrix}$$

Where,

    α is scapula anterior/posterior tilt

    β is scapula upward/downward rotation

    γ is scapula protraction/retraction

$$R_{T\_H} = R_{Y'}(\gamma_2)R_X(\beta)R_Y(\gamma) \qquad\qquad\text{[Eq.6-13]}$$

$$R_{T\_H} = \begin{bmatrix} cos\gamma cos\gamma_2 - sin\gamma cos\beta sin\gamma_2 & sin\beta sin\gamma_2 & sin\gamma cos\gamma_2 + cos\gamma cos\beta sin\gamma_2 \\ sin\gamma sin\beta & cos\beta & -cos\gamma sin\beta \\ -cos\gamma sin\gamma_2 - sin\gamma cos\beta cos\gamma_2 & sin\beta cos\gamma_2 & cos\gamma cos\beta cos\gamma_2 - sin\gamma sin\gamma_2 \end{bmatrix}$$

Where,

γ is plane of humeral elevation

β is humeral elevation

γ_2 is humeral internal/external rotation

$$R_{S\_T} = \left[R_{T\_S}\right]'$$
$$R_{H\_T} = \left[R_{T\_H}\right]' \qquad\qquad\text{[Eq.6-14]}$$

Where,

R_{S_T} is the rotation matrix from the local scapula system to the local torso system

R_{H_T} is the rotation matrix from the local humerus system to the local torso system

5. *Definition of the Scapula and Humerus Centers of Rotation*

The centers of rotation of the scapula (acromioclavicular joint) and humerus

(glenohumeral joint center) were rotated into the local torso system. The rotation of the

glenohumeral joint center into the torso system, first involved three-dimensionally aligning it

with the center of the glenoid cavity following which a lateral offset of 9.5 units (26.5mm) along

the glenoid lateral axis (*z*-axis) was applied (Chopp and Dickerson 2012) [Eq. 6-15]. Note: a

neutral posture was defined as having no superior-inferior humeral head translation, thus the

glenohumeral joint center was three-dimensionally aligned with the center of the glenoid cavity

with the lateral offset applied.

$$GH_{TOR} = (R_{TOR}^{SCAP} * (R_{SCAP}^{GLEN} * GH_{GLEN})) + (R_{TOR}^{SCAP} * CG_{SCAP}) + AC_{TOR} \qquad \text{[Eq.6-15]}$$

Where,

GH_{TOR} is the glenohumeral joint center in the local torso system

GH_{GLEN} is the glenohumeral joint center in the local glenoid system incorporating a lateral offset from three-dimensional alignment with CG ($[0\ 0\ \varphi]$) ($\varphi = 9.5\ (26.5mm)$)

CG_{SCAP} is the center of the glenoid cavity, defined as the midpoint between superior and inferior borders of the glenoid cavity, in the local scapula system

R_{TOR}^{SCAP} and R_{SCAP}^{GLEN} are rotation matrices to rotate points from the scapula-to-torso and glenoid-to-scapula coordinate systems

AC_{TOR} is the acromioclavicular joint in the torso system

6. *Rotate points from scan system to local torso system*

The collective points defining each of the segments (humerus, scapula, clavicle, and torso [ribs, spine]) were rotated into the common local torso coordinate system. This sequence of rotation incorporated the measured humerothoracic and scapulothoracic joint angles, in addition to the lateral humeral offset. An example of these rotations and translations, for the humerus segment is demonstrated in [Eq. 6-16].

$$\vec{V}_{HUM,i} = R_{HUM}^{GCS} * (\vec{V}_{GCS,i} - GH_{GCS}) \qquad \text{[Eq. 6-16]}$$
$$\vec{V}_{TOR,i} = (R_{TOR}^{HUM} * \vec{V}_{HUM,i}) + GH_{TOR}$$

Where,

$\vec{V}_{GCS,i}$, $\vec{V}_{HUM,i}$ and $\vec{V}_{TOR,i}$ are all of the points of the humeral head (i) in the global, humerus and torso coordinate systems, respectively.

R_{HUM}^{GCS} and R_{TOR}^{HUM} are rotation matrices to rotate points from the global-to-humerus and from humerus-to-torso coordinate systems, respectively

GH_{GCS} and GH_{TOR} is the glenohumeral joint center in global and torso coordinate systems, respectively

7. *Apply humeral head translation*

The humeral head translation, t_{GLEN} (defined in *Step 3*), was then applied to the new humerus points [Eq. 6-18]. Since the humerus was in the local torso system, t_{GLEN} also needed to

be defined in the torso system (t_{TOR}). This was achieved by a rotation from the local glenoid

system to scapula system and scapula system to torso system [Eq. 6-17].

$$t_{TOR} = R_{TOR}^{SCAP} * (R_{SCAP}^{GLEN} * t_{GLEN})$$ [Eq. 6-17]
$$\vec{Vt}_{TOR,i} = \vec{V}_{TOR,i} + t_{TOR}$$ [Eq. 6-18]

Where,

t_{GLEN} and t_{TOR} are the translation terms in the glenoid and torso systems, respectively

R_{SCAP}^{GLEN} and R_{TOR}^{SCAP} are rotation matrices to rotate points from glenoid-to-scapula and from scapula-to-torso coordinate systems, respectively

$\vec{Vt}_{TOR,i}$ is all of the points of the humeral head (i) in the torso coordinate system with the humeral head translation applied

8. *Determine the minimum distance between each of the points on the humeral head and on the acromion process*

    Each of the points on the humeral head and acromion process were identified and the

distance between these coordinates calculated [Eq. 6-19], from which a minimum distance was

identified (SAS) (Figure 29).

$$Dist_{S,H} = \left\| \vec{V}_{TOR,S} - \vec{Vt}_{TOR,H} \right\|$$ [Eq. 6-19]

Where,

$Dist_{S,H}$ is the distance between each of the points (S) on the acromion ($\vec{V}_{TOR,S}$) and each of the points (H) on the (translated) humeral head $\vec{Vt}_{TOR,H}$ (Note: all points are in the common local torso system)

9. *Scaling factor applied to obtain minimum distance in millimeters*

    The minimum distance obtained from *Step 8* when then converted to millimeters using

the scaling factor described in *Step 3*.
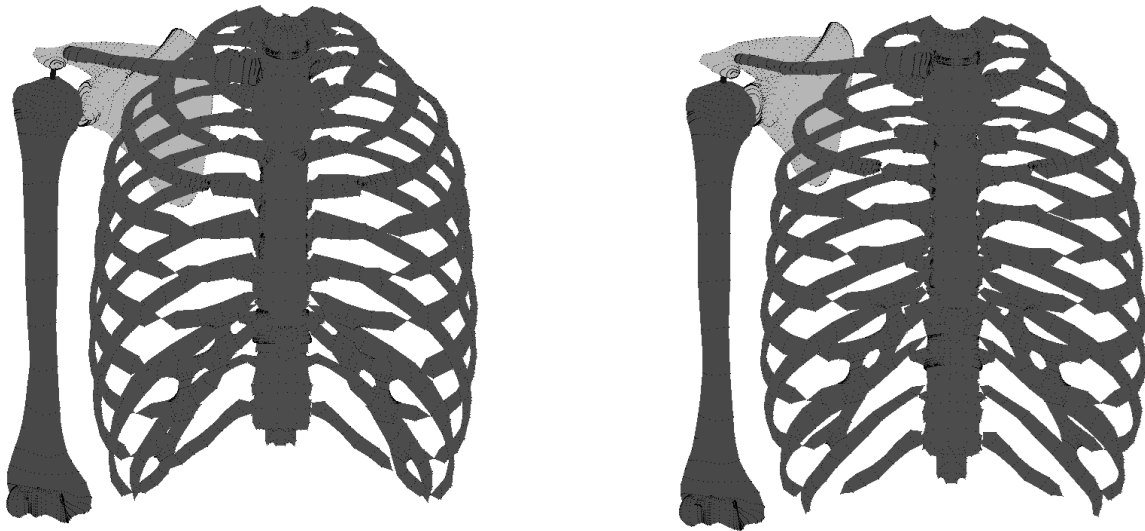
Figure 29. Kinematic Manipulation; *Left*: SAS increasing kinematics – Inferior Translation, Upward Rotation, Posterior Tilt, Retraction, *Right:* SAS decreasing kinematics – Superior Translation, Downward Rotation, Anterior Tilt, Protraction. Orientation magnitudes are: $\mu + 1\sigma$ with subsequent minimum SAS widths of 10.4mm and 8.5mm, respectively.

In addition to the steps described, two constraints were applied within the deterministic model: (1) glenohumeral constraint, and (2) acromiohumeral constraint. The glenohumeral constraint ensured that a minimum medial-lateral glenohumeral distance was maintained to prevent humeral head collision with the glenoid cavity. Following the superior-inferior translation of the humerus (*Step 7*), the distance between the glenohumeral joint center and the most lateral point on the glenoid cavity was calculated. If this distance was less than that calculated in a neutral[9] posture, the humerus was translated a corresponding distance laterally along the glenoid axis (+Z-axis). The acromiohumeral constraint was applied due to polarity limitations associated with calculating the vector norm. Solely calculating the norm of the

---

[9] Recall: a neutral posture is one in which the scapulothoracic angles were α = 19.3°, β = -0.3°, γ = -31.8° and humerothoracic angles were γ = -34.3°, β = 0°, γ2 = 35.7°, with t_{GLEN} = 0mm.

difference between acromion points and humeral head points (as described in *Step 8*) would not

be able to identify whether the humeral head collided with the acromion process. Thus, a

constraint was applied such that if any point on the acromion had a distance from the

glenohumeral joint center that was less than the radius of the humeral head, a collision was

assumed and the minimum distance was zero.

6.3.2 *Probabilistic Subacromial Geometry Model*

The deterministic subacromial geometry model was created such that the characterization

of each of the nine parameters was defined by modifying a single value for each parameter. The

appropriate distribution for each model parameter, determined from empirical data, was applied

within probabilistic analysis software. This software interfaced with the deterministic

subacromial geometry model created in Matlab® to predict a distribution of minimum

subacromial space width (SAS) for each of the ten experimental conditions. A description of the

model input and the construction of the probabilistic model are detailed in the following sections.

6.3.2.1 Model Input

The probabilistic subacromial geometry model required input distributions for each of the

nine model parameters. Collecting empirical data (Chapters 4 and 5) permitted using statistical

tests to evaluate the appropriate distribution for each parameter for each of the measured

conditions (fatigue state sessions, humeral elevation angles). Kolmogorov-Smirnov (K-S)

goodness-of-fit tests ($\alpha = 0.01$) were used to evaluate the error between the proposed theoretical

distribution and the measured data. Each of the characteristics (*i*) measured were normally

distributed with *dmax$_i$* values ranging from 0.06 to 0.17 (*dmax$_i$* < *d* [0.21]). Thus, model input

included the means and standard deviations for each parameter, across conditions (Table 24).

Table 24. Morphological and Kinematic Parameter Input; Morphological Input: Mean (μ) and Standard Deviation (σ) for each of the measured parameters. Kinematic Input: Mean (μ) and Standard Deviation (σ) for each of the measured parameters for each condition (five humeral elevation angles (β) and two fatigue state sessions (Pre/Post)). Note: positive kinematic orientations: superior humeral head translation, scapular upward rotation, scapular anterior tilt, scapular retraction. All morphological parameters were identical across all conditions.

Morphological Parameter Input		
	μ	σ
Glenoid Inclination (°)	95.0	5.9
Lateral Acromial Angle (°)	79.9	9.3
Acromial Anterior Slope (°)	18.0	10.9
Acromial Tilt (°)	31.5	4.7
Acromion Index	0.62	0.08

Kinematic Parameter Input				
	Humeral Head Position (mm)			
	μ		σ	
β (°)	**Pre**	**Post**	**Pre**	**Post**
0	-0.4	-0.6	1.3	1.6
30	0.7	0.5	1.1	1.4
60	1.4	1.4	1.2	1.0
90	2.1	1.8	0.8	0.9
120	2.5	2.4	0.9	1.0

	Scapular Rotation (°)				Scapular Tilt (°)				Scapular Protraction/Retraction			
	μ		σ		μ		σ		μ		σ	
β (°)	**Pre**	**Post**	**Pre**	**Post**	**Pre**	**Post**	**Pre**	**Post**	**Pre**	**Post**	**Pre**	**Post**
0	-0.3	0.4	5.5	6.3	19.3	20.3	7.3	8.3	-31.8	-34.8	6.7	8.3
30	2.6	4.9	7.1	8.0	20.1	19.7	7.4	9.1	-31.3	-32.9	6.3	7.7
60	11.0	12.3	8.3	7.5	20.0	20.8	9.5	9.7	-32.1	-33.0	7.1	7.0
90	18.1	21.7	11.9	9.1	20.1	20.6	11.0	10.9	-33.5	-34.9	8.4	7.9
120	28.6	34.1	13.4	13.8	17.5	18.3	13.9	14.5	-39.0	-36.7	9.8	11.0

Each of the variables, both morphological and kinematic, presented with extensive variability which subsequently produced wide 99% confidence intervals for the measured

population. To ensure physiological realism, in both the input and predicted output, *truncated normal distributions* were used to represent all of the measured values. This distribution assumed a normal distribution about the mean and standard deviation, while constricting the upper and lower limits to a specified value. For this research, limits of ±1 standard deviation were imposed. These limits produced a conservative estimate of the variability of SAIS risk in the population as members of the measured population would likely present with magnitudes outside of the truncated normal distribution, while not necessarily reaching the limits of the entire 1-99% normal distribution.

6.3.2.2 *Probabilistic Simulation and Validation*

Several probabilistic simulations were conducted to evaluate the sensitivity and validity of the modelled output. The probabilistic model was created using NESSUS probabilistic analysis software (SwRI, San Antonio, Texas). This software interfaced with Matlab® such that the statistical information and selected distribution(s) were applied by mapping each of the parameters defined within the deterministic model. This subsequently predicted a distribution of SAS. Six simulations were performed for the entire set or a subset of the ten conditions, which evaluated: different simulation methods, alternate model parameter distributions, parameter covariance assumptions, and additional iterations. The simulations were divided into those addressing predicted output sensitivity and input sensitivity (Table 25).

173

Table 25. Description of probabilistic simulations conducted to evaluate model input and output sensitivity

Output Validation Tests	
Simulation	**Description**
Advanced Mean Value Truncated Normal	Reliability/Optimization-based approach
Monte Carlo 2500 Truncated Normal	Gold-standard approach
Monte Carlo 3000 Truncated Normal	Gold-standard approach with additional iterations
Input Validation Tests	
Simulation	**Description**
Advanced Mean Value Normal	Normal distribution (based on goodness-of-fit to empirical data)
Advanced Mean Value Lognormal	Alternate distribution
Advanced Mean Value Normal Covariance	Normal distribution with correlation matrix applied (calculated from empirical data)

Advanced Mean Value (AMV) is a probabilistic approach that uses a combination of reliability and optimization-based approaches to predict the output at specified discrete probability levels. Monte Carlo iteratively calculates several deterministic solutions to construct an entire cumulative distribution function for the predicted output. AMV is computationally efficient and accurately converges to the Monte Carlo solution (Easley et al. 2007, Langenderfer et al. 2008, 2009). Additionally, as the method requires a transformation of each variable into a non-dimensionalized standard normal solution space, it permits calculation of relative sensitivity (importance) factors which are used to describe the relative importance of each parameter to the predicted output. The validity of the AMV solution was evaluated by comparing the predicted output to the output obtained from 2500 iterations of Monte Carlo simulations. As well, a subset of five conditions were randomly selected in which an additional 500 iterations were performed (3000 iterations total). This was to ensure that 2500 iterations were adequate to converge on the correct solution.

NESSUS probabilistic analysis software permits applying multiple distributions and modelling parameters as independent or co-varying variables. However, while the predicted

output from the conservative truncated normal distributions was the primary output of this research, truncated lognormal distributions and multivariate truncated normal distributions are not currently supported by the software. Thus, to evaluate the influence of the assumed distribution and model parameter covariance, an additional AMV simulation was performed with parameters assuming normal (not truncated) distributions. For the lognormal simulation, each of the parameters with a positive mean value were modelled with a lognormal distribution, while those with negative values (i.e. scapular protraction/retraction in all conditions, and humeral head translation and scapular rotation at neutral) were modelled with a normal distribution. As well, additional simulations were performed by calculating the correlation between each of the parameters (morphological and kinematic) from the measured data for each individual condition and applying a correlation matrix within the software.

6.3.2.3 Predicted Output

The probabilistic subacromial geometry model together with the integrated deterministic model predicted a distribution of the minimum subacromial space width (SAS). As described, Monte Carlo simulations produced continuous cumulative distribution functions, while AMV predicted the output at eleven incremental probability levels along the 1-99% confidence interval. Three probability levels (1%, 50%, 99%) representing the median and tail regions of the curve were selected for comparative purposes between each of the described simulations. Additionally, a comparison between the distributions of model predicted and radiographically measured SAS (Chapter 4) was performed.

As AMV simulations required a transformation of each parameter from its original coordinate system to standard normal space, relative sensitivity factors of each of these non-dimensionalized parameters could be calculated. These sensitivity factors (α) represent the

175

direction cosines of the unit vector (β) at the most probable point, which is coincident with the point of maximal density on the joint probability distribution function in the transformed coordinate system. Since the direction cosines satisfy [Eq.6-20], the relative contribution of each parameter to the predicted SAS width was calculated for each of the ten conditions.

$$\sum_{i=1:9} \alpha_i^2 = 1 \qquad \text{[Eq.6-20]}$$

Where,

α_i is the direction cosine of each of the nine parameters (i)

6.3.3 *Probabilistic Impingement Risk Prediction Model*

A probabilistic impingement risk model was created using the predicted output from the probabilistic subacromial geometry model and the measured tissue thicknesses (Chapter 5). As previously described, the probabilistic subacromial geometry model predicted the distribution of the minimum subacromial space width (SAS) resulting from morphological and kinematic variability. The impingement risk model calculated the probability that the experimentally measured subacromial tissue thicknesses (Chapter 5) would exceed the SAS predicted from the subacromial geometry model, thereby generating an estimate of the SAIS risk. This model was similarly created in NESSUS, whereby a limit state function [Eq.6-21] consisting of the two normally distributed parameters (SAS, subacromial tissue thickness) was used to calculate the probability of 'failure'[10] (tissue thickness > available space) for each of the ten conditions.

---

[10] The probability of failure (probability of tissue compression) is very similar to the traditional $R - S$ problem described in Example 2-1 of section 2.7.2.2 of the Literature Review

$$p_x = SAS_x - T$$
[Eq. 6-21]

Where,

SAS_x is the predicted minimum subacromial space width obtained from the probabilistic subacromial geometry model for each of the ten conditions (x)

T is the combined subacromial tissue thicknesses obtained experimentally

The model calculated the probability of tissue compression; that is $p_x < 0$ or $SAS_x < T$

6.4   Results

The model predicted minimum subacromial space width (SAS) was not influenced by fatigue, but reduced considerably with arm elevation within each fatigue state. Across all conditions, the SAS was highly variable, as evidenced by wide 1-99% confidence intervals. Morphological parameters were particularly important in modulating the size of the SAS over the range of elevation, while kinematic parameters depended on elevation angle and fatigue state. Validation simulations demonstrated that the predicted output was generally robust for the mid-portion of the cumulative distribution function (CDF), while showing some discrepancies at the lower (1%) and upper (99%) limits of the curve.

6.4.1 *Advanced Mean Value versus Monte Carlo Probabilistic Methods*

The Advanced Mean Value (AMV) probabilistic method overall showed excellent agreement for the mid-region of the cumulative distribution function (CDF), with discrepancies towards the tail regions of the curve, with mean differences of 1.1mm and 1.6mm between methods at the 1 and 99% levels, respectively. AMV generally overestimated the SAS at the 1% level and underestimated the SAS at the 99% level, though these discrepancies were not present for all conditions (Figure 30). The largest overestimation by AMV (synonymous with an underestimation of the SAIS risk) was 1.9mm which occurred at 90° of elevation in both pre- and post-fatigue states at the 1% probability level. The largest underestimation by AMV

177

(3.2mm) also occurred at 90° of elevation but at the 99% probability level, with AMV predicting a SAS of 6.5mm, while Monte Carlo a SAS of 9.7mm. Despite these large discrepancies at the tail regions, the mean difference between methods within the 10-90% confidence interval ranged from 0.1mm to 0.6mm. Additionally, for all conditions (fatigue state, elevation angle), there were probability levels with differences ≤ 0.3mm.

Note: Due to the inaccuracies at the lower (1%) and upper (99%) confidence limits, subsequently reported SAS output (and interpretation) will reflect those captured from Monte Carlo analysis unless otherwise stated.
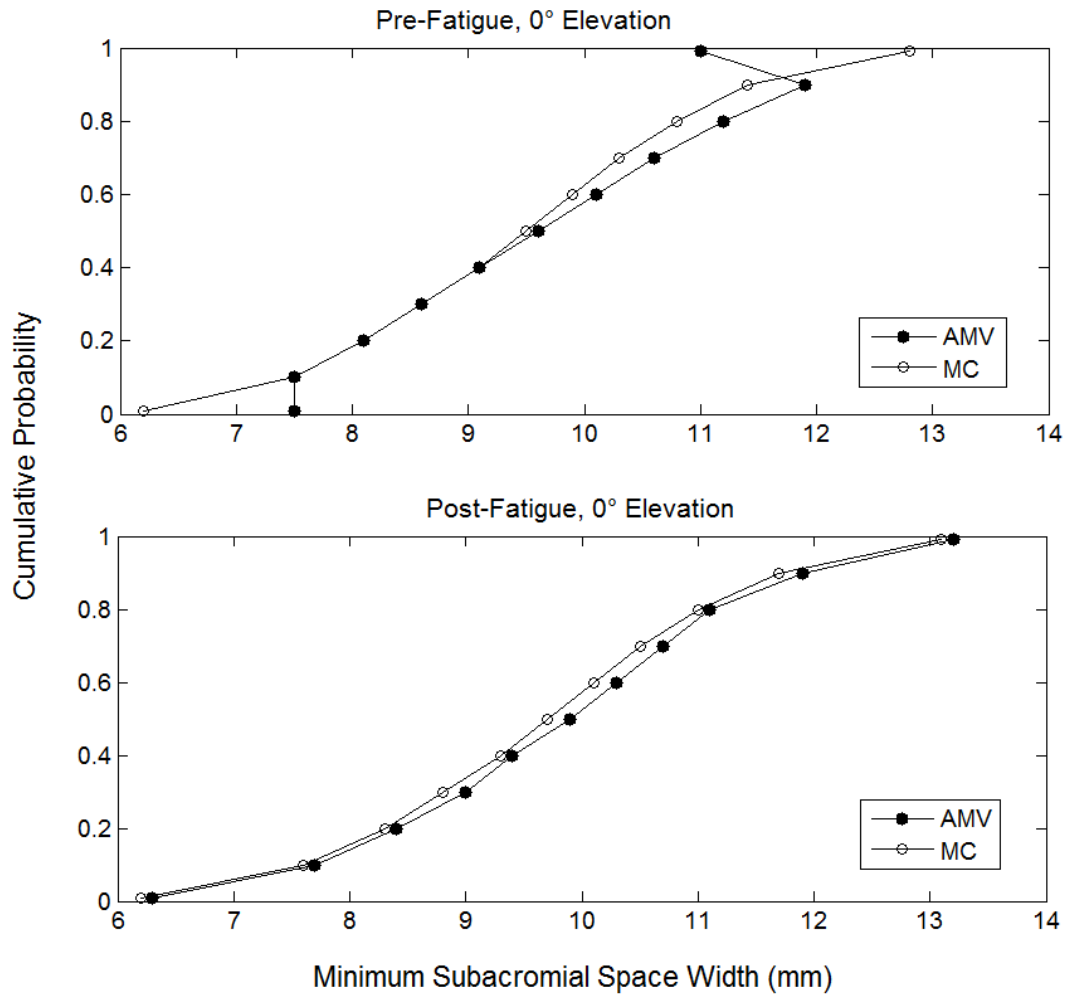
Figure 30. 1-99% Cumulative distribution function (CDF) of model predicted minimum subacromial space width (SAS) for two conditions (Pre-Fatigue, 0° Elevation (top); Post-Fatigue, 0° Elevation (bottom)). Filled markers represent the SAS predicted using the Advanced Mean Value (AMV) probabilistic method and unfilled markers represent the SAS predicted using the Monte Carlo probabilistic method. The Post-Fatigue solution displays a relatively monotonic system with excellent agreement between probability methods, while the Pre-Fatigue solution despite showing excellent agreement in the mid-portion of the curve, behaved non-monotonically at the tail regions of the curve.

6.4.2 *Muscle Fatigue and Elevation Effects on SAS*

Fatigue state had a negligible effect on the SAS. The average difference between sessions across all elevation angles was 0.1 [range, 0 to 0.2] mm, 0.1 [range, 0.1 to 0.2] mm and 0.2 [range, 0.1 to 0.3] mm at the 1%, 50% and 99% probability levels, respectively (Table 26). In fact, the SAS increased these small magnitudes following fatigue. However, the SAS was largely influenced by elevation angle, reducing a mean of 5.5mm at the 50% probability level with arm elevation from 0 to 120° of elevation within each fatigue state (Table 26). The largest reduction in SAS occurred between 30° and 60° of elevation with a mean reduction of 3.4mm at the 50% probability level. Additionally, at each elevation angle and within each fatigue state, the SAS was highly variable, as demonstrated by wide 1-99% confidence intervals (Table 26). The mean difference between 1% and 99% probability levels across all conditions (fatigue state, elevation angle) was 8.0 [range, 6.6 to 8.9] mm, with SAS magnitudes as high as 13.1mm at the 99% probability level at 0° of elevation and as low as 0.5mm at the 1% probability level at 120° of elevation.

Table 26. Minimum subacromial space width (mm) (SAS) for each condition (fatigue state, elevation angle) for 1%, 50% and 99% probability levels, calculated using Monte Carlo analysis.

Fatigue State	Elevation Angle (°)	Minimum Subacromial Space Width (mm)		
		p = 0.01 (1%)	p = 0.50 (50%)	p = 0.99 (99%)
Pre	0	6.2	9.5	12.8
	30	5.9	9.3	12.6
	60	1.9	5.9	10.6
	90	0.7	4.6	9.5
	120	0.5	4.1	9.2
Post	0	6.2	9.7	13.1
	30	6.0	9.4	12.9
	60	2.0	6.1	10.7
	90	0.9	4.7	9.7
	120	0.5	4.2	9.4

6.4.3 *Importance Factors*

Overall, morphological parameters (particularly glenoid inclination) demonstrated consistently high relative importance across the range of elevation and between fatigue states, while kinematic parameters varied in importance as a function of condition. Despite showing modest differences in α-levels across the extracted probability levels between the 1-99% confidence interval, the relative importance of each parameter remained mostly consistent. Due to the non-monotonicity at the tail regions of the distribution (reported in the preceding section), the α-levels documented represent the mean levels between the 10-90% confidence interval. Glenoid inclination had the highest relative importance of all parameters in both fatigue states from 0 to 60° of elevation (α = 0.63 [range, 0.59 to 0.71]) with lower but still high importance at higher elevation angles (α = 0.49 [range, 0.33 to 0.68]) (Table 27, Figure 31). The lateral acromial angle, acromial anterior slope and acromial tilt parameters all demonstrated consistent

moderate α-levels, with means of α = 0.19, 0.22 and 0.28, respectively (Table 27). The acromion

index had high importance at 90 and 120° of elevation (α = 0.52 [range, 0.36 to 0.64]) while low

or no relative importance at lower elevation angles.

The importance factors of kinematic parameters varied by fatigue state and elevation

angle. Humeral head translation demonstrated more importance during initial elevation (0 to

30°), with a mean α = 0.40 [range, 0.32 to 0.60] compared to a mean α = 0.06 (range, 0.0 to 0.20)

at elevation angles exceeding 30° (Table 27). Additionally, at elevation angles between 0 and

60°, its relative importance increased from pre- to post-fatigue states, with a maximum increase

of α = 0.24 at 0° of elevation (Figure 31). Alternatively, scapular tilt and protraction/retraction

increased in importance with elevation angles exceeding 30° (Table 27), with higher relative

importance in the pre-fatigue state. This was particularly evident at 120° of elevation which

showed α = 0.62 and 0.33 in the pre-fatigue state for tilt and protraction/retraction, respectively.

Scapular rotation only demonstrated α > 0.3 in the post-fatigue state at 0 and 30° of elevation and

in both pre- and post- fatigue states at 60° of elevation, however all α-levels were ≤ 0.40 (Table

27).

Table 27. Importance Factors (α-levels) across all conditions (fatigue state, elevation angle).

Dash (−) indicates an α-level of 0.

Model Parameter	Pre 0	Post 0	Pre 30	Post 30	Pre 60	Post 60	Pre 90	Post 90	Pre 120	Post 120
Glenoid Inclination	0.69	0.60	0.59	0.61	0.59	0.71	0.45	0.68	0.33	0.49
Lateral Acromial Angle	0.36	−	0.31	−	0.21	0.19	0.16	0.18	0.17	0.34
Acromial Anterior Slope	0.36	0.31	0.31	0.32	0.21	0.19	0.16	0.18	0.00	0.17
Acromial Tilt	0.36	0.31	0.59	0.32	0.21	0.19	0.16	0.18	0.33	0.17
Acromion Index	−	−	−	0.32	0.40	0.19	0.59	0.36	0.48	0.64
Humeral Head Translation	0.36	0.60	0.32	0.33	−	0.20	−	−	0.17	−
Scapular Rotation	−	0.31	−	0.32	0.40	0.37	−	−	−	0.17
Scapular Tilt	−	−	−	0.32	0.40	0.37	0.59	0.53	0.62	0.34
Scapular Protraction/Retraction	−	−	−	−	0.20	0.19	0.16	0.18	0.33	0.17
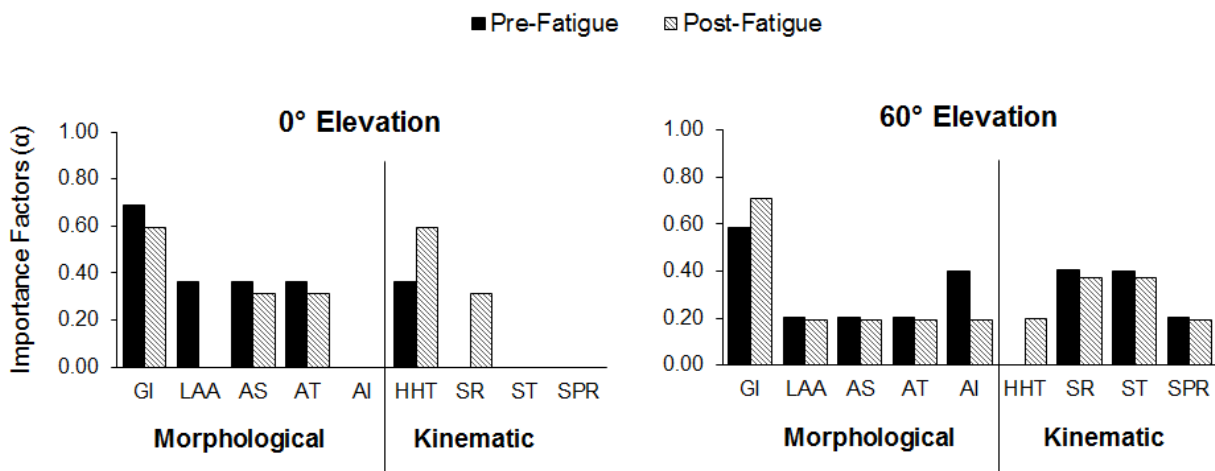
Figure 31. Importance Factors (α-levels) for four conditions (Pre/Post Fatigue State, 0° and 60° Elevation Angle). Morphological Model Parameters: GI = glenoid inclination, LAA = lateral acromial angle, AS = acromial anterior slope, AT = acromial tilt, AI = acromion index; Kinematic Model Parameters: HHT = humeral head translation, SR = scapular rotation, ST = scapular tilt, SPR = scapular protraction/retraction.

$6.4.4$ *Additional Validation and Simulation Considerations*

The additional simulations conducted to evaluate the sensitivity of the output to certain model input and output criteria showed that the simulations were generally robust for the mid-portion of the cumulative distribution function (CDF), while showing some discrepancies at the tails. The influence of model parameter distribution selection, parameter independence and the number of Monte Carlo iterations are discussed as follows.

6.4.4.1 Truncated Normal versus Normal

The differences between the entire normal and truncated normal solutions increased towards the tail regions of the CDF. At the 50% probability level the predicted output from both parameter distributions (entire, truncated) was identical across all conditions, while at the 1% and 99% probability levels there were differences of 2.1 [range, 0.7 to 3.8] mm and 1.8 [range, 0.2 to 3.8] mm, respectively. The importance factors (α-levels) were not affected by truncating the parameter distributions (mean difference = 0.01 [range, 0 to 0.02]).

6.4.4.2 AMV Normal versus Lognormal

Modelling parameters as lognormally distributed variables, rather than normally distributed variables resulted in modest mean differences across conditions and probability levels (0.38mm). However, discrepancies between 2.0 – 2.9mm were present at higher elevation angles (90°, 120°) for both fatigue states at the upper confidence limit.

6.4.4.3 AMV Normal versus Normal Covariance

Model predicted SAS was not highly sensitive to model parameter correlation. Mean differences between simulations with parameters modelled as independent and co-varying normally distributed variables were 0.34 [range, 0 to 1.5] mm, with the largest discrepancies occurring during initial elevation at the upper confidence limit. For each condition, the mean difference between the 10-90% confidence interval was 0.25mm with all differences ≤ 1mm.

6.4.4.4 Monte Carlo 2500 versus Monte Carlo 3000

Monte Carlo analysis with 2500 iterations was sufficient to converge on the correct solution. For the subset of five conditions, across all probability levels, differences between solutions from simulations with 2500 and 3000 iterations were ≤ 0.1mm with a mean difference of 0.024mm.

6.4.5 *SAS: Modelled versus Measured*

The absolute magnitudes and the trend of SAS as predicted by the model and measured in vivo were similar both between fatigue states and across elevation angles. The model predicted SAS generally showed the highest agreement with measured values at 0 and 120° of elevation in both fatigue states (mean = 0.3mm), and lowest agreement at 30° of elevation (1.8mm) (Table 28). While the model underpredicted the SAS at 0° of elevation, it overpredicted the SAS at all other elevation angles in both fatigue states. The variability was generally higher for the measured SAS at low elevation angles, particularly in the post-fatigue state (as evidenced by wider confidence intervals). Differences between confidence intervals (upper limit SAS – lower limit SAS) were less than 1mm for remaining conditions, with the exception of 60° in the post-fatigue state where the modelled SAS was more variable than the measured SAS (Table 28).

Table 28. Comparison of the model predicted and radiographically measured (Chapter 4) minimum subacromial space width (Mean [1-99% confidence interval]) for each condition (fatigue state, elevation angle).

Elevation Angle (°)	Pre-Fatigue (mm) (Mean [1-99% CI])		Post-Fatigue (mm) (Mean [1-99% CI])	
	Modelled	**Measured**	**Modelled**	**Measured**
0	9.5 [6.2 – 12.8]	9.6 [4.1 – 15.2]	9.7 [6.2 – 13.1]	10.0 [3.1 – 16.9]
30	9.3 [5.9 – 12.6]	7.6 [3.4 – 11.8]	9.4 [6.0 – 12.9]	7.6 [2.3 – 12.9]
60	6.3 [1.9 – 10.6]	5.4 [1.3 – 9.5]	6.3 [2.0 – 10.7]	5.9 [2.6 – 9.2]
90	5.1 [0.7 – 9.5]	4.2 [-0.4 – 8.9]	5.3 [0.9 – 9.7]	4.1 [-0.3 – 8.6]
120	4.8 [0.5 – 9.2]	4.6 [-0.1 – 9.3]	4.9 [0.5 – 9.4]	4.4 [0.2 – 8.5]

6.4.6 *Probabilistic Impingement Risk*

The probability that subacromial tissue thickness would exceed the SAS (probability of impinging the tissues) was not influenced by fatigue (maximum difference = 3.5%), but was highly influenced by elevation angle (Table 29). At low elevation angles the probability of impingement was <5%, while at higher elevation angles the probability was as high as 73.6%. Across all conditions, the SAS had considerably higher relative importance compared to tissue thickness in predicting the variability in tissue impingement, as demonstrated by α-levels ranging between [0.87 – 0.92] for SAS and [0.39 – 0.50] for tissue thickness.

Table 29. Probability that the distribution of measured tissue thickness exceeded the predicted minimum subacromial space width for each condition (fatigue state, elevation angle).

Elevation Angle (°)	Probability of SAIS Risk	
	Pre-Fatigue	**Post-Fatigue**
0	1.7%	1.7%
30	2.4%	2.6%
60	46.1%	46.1%
90	68.6%	65.1%
120	73.6%	72.0%

6.5 Discussion

The predicted minimum subacromial space width (SAS) across the measured conditions (fatigue state, elevation angle) generally supported the research hypotheses. Both kinematic and morphological parameters were important in predicting SAS variability. However, kinematic parameters were strongly influenced by elevation angle and fatigue state while morphological parameters showed more consistency across conditions. Additionally, the relatively high importance of glenoid inclination further implicated superior humeral head translation as a risk factor for shoulder pathologies, including SAIS. Finally, across all conditions the predicted SAS demonstrated considerable variability which subsequently suggested a wide distribution of SAIS risk amongst the population.

6.5.1 *Model Predicted SAS: Influence of Muscle Fatigue and Arm Elevation*

The model predicted SAS was generally consistent both with values reported in the literature from a healthy population and those measured experimentally in the current research (subsequently modelled population). With the arm in neutral (0°), in both fatigue states, the predicted SAS was primarily in the documented healthy classification range (Cotton and Rideout

1964, Golding 1962, Weiner and MacNab 1970), with the lower confidence limit within the grey area (approximately 5-7mm; Table 19) between unhealthy and healthy ranges. As the arm was elevated from 30 to 120°, the predicted magnitudes were comparable to those reported (Graichen et al. 1999a, Hinterwimmer et al. 2003). Modelled results overestimated those reported by 2.3mm at 30°, however differed by <1mm at angles of 60, 90 and 120°. Additionally, despite the considerable variability in the predicted output (mean = 8.0mm between 1-99% confidence intervals) the variability was less than that previously reported at elevation angles exceeding 60° (Graichen et al. 1999a, Hinterwimmer et al. 2003). When compared to the experimentally measured SAS magnitudes (Chapter 4), from a population subsequently used to predict the modelled SAS, excellent agreement was demonstrated at the 0 and 120° elevation angles. However, the model moderately overestimated the measured values approximately 1mm at 60 and 90°, and largely overestimated the measured values (mean = 1.8mm) at 30° (Table 28). Aside from the absolute magnitudes, the trend of SAS changes with elevation differed between modelled and measured outputs at the 120° elevation angle. While the mean measured values suggested a reduction of the subacromial space from neutral to 90° followed by a slight increase in space, the model predicted values demonstrated a continuous reduction in space with elevation up to 120°. This trend of continuous reduction was consistent with previous literature (Graichen et al. 1999a, Hinterwimmer et al. 2003). While Graichen et al. (1999a) did report a slight increase in SAS at elevation angles exceeding 120° (specifically 150°), the smallest measured SAS magnitude in their research was observed at the 120° elevation angle.

Through comparisons between the model predicted SAS and those both reported in the literature and measured in the current research (Chapter 4), two overall trends evolved. First, the model consistently overestimated the SAS at the mean and 1% probability levels. The

overestimation at the lower confidence limit was likely due to the decision to model parameters with truncated input distributions, rather than the entire distribution range. While this prediction implied an underestimation of SAIS for those at the lower end of the distribution, truncation was performed to ensure physiological realism for each of the kinematic and morphological parameters. The large variability of each parameter resulted in a 1-99% confidence interval with limits that would likely be physiologically unachievable, such as scapulothoracic collisions. A second trend that existed within each fatigue response was that the largest reduction in SAS occurred between the 30 and 60° elevation angles. This trend can likely be attributed to the humeral portion of the minimum distance (SAS) vector. Between 30 and 60° of elevation was likely the range when the inferior border of the subacromial space transitioned from the superior surface of the humeral head to the greater tuberosity of the humerus. This bony protrusion (and tendon insertion point) is largely responsible for the reduction in subacromial space that occurs with humeral elevation (Graichen et al. 1999b). Thus, while a more gradual transition between 30 to 60° was anticipated, a reduction in the SAS due to the encroachment of the tuberosity was expected.

6.5.2 *Model Parameter Importance: Clinical Implications*

While the model predicted SAS identified new and reinforced existing kinematic trends resulting from fatigue and humeral elevation, the primary innovative contribution of the probabilistic subacromial geometry model is the identification of the relative importance of each parameter to modulating the size of the subacromial space. Overall, morphological parameters, notably glenoid inclination, were the largest and most consistent contributors to SAS variability. While kinematic fatigue responses were not markedly different from the pre-fatigue state, the relative importance of individual kinematic parameters varied by fatigue and humeral elevation

angle. Humeral head translation was an important modifier during initial phases of elevation (particularly in the post-fatigue state), whereas the influence of scapular positioning became more prominent as the arm was elevated. It was anticipated that humeral head translation would have high relative importance across all post-fatigue elevation angles, however its prominence primarily during early elevation is mechanically logical. Throughout the range of elevation, while also generating humeral movement, the rotator cuff muscles are essential in maintaining glenohumeral stability. The supraspinatus acts as a humeral head compressor, while the infraspinatus, subscapularis and teres minor muscles impose both compressive and inferior shear forces (Yanagawa et al. 2008). The deltoid (as well as the pectorals) impose large superior shear forces that promote superior humeral head translation, however, this shearing potential is greatest at low elevation angles (Poppen and Walker 1978). As the arm is elevated, the moment arms of the deltoid fascicles progressively increase, but their angles to the glenoid face similarly increase, subsequently reducing shearing potential. Thus, the high relative importance of humeral head translation at low elevation angles, particularly following fatigue of the muscles that resist this superior translation, is explainable. Its continued dominance at elevated arm angles (as it continued to reduce the SAS) was surpassed by the compensatory scapular movement (rotation, tilt, protraction/retraction) that was concurrently increasing the SAS. Thus, the kinematic importance factors suggest that subacromial space reducing mechanisms are highly prominent during initial elevation, even more so in the presence of upper extremity muscle fatigue, and subacromial space increasing mechanisms are highly prominent during later elevation to alleviate the risk of SAIS.

While kinematic mechanisms showed high relative importance in modulating the size of the subacromial space, morphological factors, in particular glenoid inclination, demonstrated the

highest importance across almost all simulated conditions. While targeted interventions for morphological characteristics which predispose an individual to SAIS are more challenging, glenoid inclination has unique implications directly related to both glenohumeral kinematics and the development of pathologies including SAIS. Both experimental and modelling research has demonstrated that increased glenoid inclination directly relates to superior humeral head translation (Flieg et al. 2008, Wong et al. 2003). Considering the previously described mechanical relationship between the deltoid-rotator cuff force couple and superior translation of the humerus, a more superiorly inclined glenoid would increase the net shearing potential of the deltoid, therefore requiring less total deltoid force to translate the humerus superiorly (Hughes et al. 2003). This was shown experimentally in research by Wong et al. (2003) who reported that the force required to translate the humeral head superiorly decreased between 14.2 to 37.5% as glenoid inclination increased 5° to 15°. Similarly, probabilistic analysis has established the relationship between glenoid inclination and superior humeral translation (Flieg et al. 2008). The probability of superior translation was directly related to glenoid inclination, increasing from approximately 20% to 80% as the glenoid orientation increased from -5° to 20°. Thus, unlike other morphological characteristics that inflict rotator cuff damage likely through intrinsic impingement, glenoid inclination imposes risk by facilitating extrinsic impingement with humeral head translation as the intermediary. As previously discussed, superior humeral head translation can lead not only to SAIS, but additional pathologies including glenohumeral instability, osteoarthritis and musculotendinous abnormalities. Given that glenoid inclination is not conservatively treatable and cannot be identified without imaging techniques, these results support promoting rehabilitation strategies that target glenohumeral stability maintenance and rotator cuff strengthening to prevent superior humeral head translation.

191

6.5.3 *Estimation of SAIS Risk across the Population*

Apart from the prediction of the minimum subacromial space width (SAS) and those characteristics that are predominantly contributing to its reduction, the measurement of subacromial tissues thicknesses on the same population enabled the estimation of SAIS risk as a function of different fatigue and arm elevation conditions. This probabilistic impingement model predicted that the probability of subacromial tissue thicknesses exceeding the predicted SAS (estimation of SAIS risk) increased with arm elevation, while being unaffected by muscle fatigue (Table 29). Notably, the probability of impingement increased from 1-3% at neutral and initial elevation to 46-69% at mid-range elevation, to 74% at 120° of elevation. However, interpretation of this SAIS risk requires consideration of both the location of the SAS vector as well as the location of clinically documented rotator cuff tears. Research evaluating both the SAS and the supraspinatus tendon over the range of abduction reported that at angles between 30 to 90° the SAS vector passed through the tendon, while at 120° the vector passed lateral to the tendon (Graichen et al. 1999a, 1999b). Recent research suggests that this vector passes lateral at angles >72° in scapular plane elevation, however this angle was shown to be highly variable (Giphart et al. 2012). Additionally, while supraspinatus tendon tears most often occur at its insertion point at the greater tuberosity (also known as the tendon footprint), tears may alternatively occur in the mid-substance of the tendon. Research that loaded cadaveric tendons until failure demonstrated that, while the primary site of the tendon tear was its insertion point, 21% of tendons failed at the mid-substance (Itoi et al. 1995). Considering these relationships and the outcomes of this research, it appears that the critical arm posture for SAIS risk is between 60-90° of elevation (possibly even <90°), however impingement at lower and higher elevation angles should not be discounted. At lower elevation angles between 30-60°, the SAS vector may not pass through the

192

tendon footprint if the greater tuberosity has not rotated beneath the acromion process, however tears to the tendon mid-substance may occur if morphological variation results in tissue thickness that exceeds the available space. At higher elevation angles exceeding 90°, the model predicted the highest risk of SAIS (>70%). While evidence indicates that the SAS vector passes laterally to the tendon at elevation angles as low as 72° (Giphart et al. 2012, Graichen et al. 1999a, 1999b), it is important to consider that the subacromial bursa may still be at risk of compression at these elevated postures (Kibler et al. 2013). Additionally, this critical range was demonstrated to be highly variable, likely due to the variability in humeral head morphology. Thus, reporting the absolute minimum subacromial space width aids both in establishing relative risk (considering occupation ratios, etc.) and comparisons; however SAIS risk assessment should focus more specifically on how the relationship between the minimum distance and the location of the interposed tissues changes with humeral elevation and the potential contributors to variation in that relationship. It is likely that internal impingement is a more prominent contributor to pain in these elevated arm postures, however SAIS should not be entirely discounted particularly at angles close to 90°. Thus, while the current results indicated that muscle fatigue did not increase the risk of SAIS, the high probability of tissue compression (tissues thickness > SAS) at mid-range arm elevation, implicates repetitive arm elevation in initiating and/or furthering the progression of cumulative rotator cuff tissue damage.

6.5.4 *Probabilistic Simulation Methods: Implications on Predicted Results*

The predicted output from the Advanced Mean Value (AMV) simulations had excellent agreement with Monte Carlo simulations for the mid-portion of the cumulative distribution function (CDF) (≤1mm), although there were discrepancies at the tail regions (1% and 99%). These discrepancies were not consistent across the tested conditions, however those with

discrepancies had clinically meaningful magnitudes; >1mm for 40% of conditions tested at the 1% probability level and 80% of conditions at the 99% level. Divergence at the tail regions is not an uncommon limitation of the AMV method, and can be attributed to the non-monotonic behaviour of the function when transformed to standard normal space (Wu et al. 1990). Errors may also arise from multiple parameter combinations predicting the same p-value or z-value. Due to the clinical implications of small magnitude differences (~1mm), interpretations at the tail regions were performed on the Monte Carlo solution. However, the excellent agreement between solutions for the remainder of the CDF permitted the interpretation of the importance factors.

Several additional probabilistic simulations were conducted to test the sensitivity of the output to various modelling selections and methods. Similar to comparisons with Monte Carlo, predicted output was generally robust for the 10-90% confidence interval with discrepancies at the lower and upper confidence limits. Overall, the verification simulations generated three main suggestions or outcomes. First, the differences in predicted output (predominantly at the upper confidence limit) from using normal and lognormal input distributions, reinforced the utility of mathematically determining the appropriate distribution for each model parameter using empirical data, if at all possible. Second, 2500 iterations of Monte Carlo were adequate for this research, confirming previous suggestions (Langenderfer et al. 2009). Lastly, including model parameter covariance had little influence on the predicted output. Similar to previous research, differences between univariate and multivariate predictions at the lower and upper confidence limits were observed (though generally <1mm), while no differences were present at the median probability level (Hughes and An, 1997). However, it should be noted that even in the univariate solution, all parameters cannot be considered independent as certain parameters include common axes. For example, both morphological and kinematic parameters, specifically glenoid

194

inclination, lateral acromial angle, acromion index and humeral head translation are all influenced by a common glenoid axis.

Thus, while caution should be exercised when interpreting the tail regions of the CDF curve, as they are sensitive to differences in simulation method and input distributions, the excellent convergence throughout the remainder of the curve demonstrates the considerable utility of the AMV simulation method, primarily for the prediction of relative importance factors.

6.5.5 *Model Assumptions*

Several assumptions were required in the construction of the deterministic model. While important decisions were described in the methodology (Section 6.3.1), general assumptions specifically regarding the bone geometry should also be considered. First, it was assumed that bone shape (morphological characteristics) was not influenced by the muscle fatiguing protocol or by humeral elevation. Second, for parameters that involved altering more than one bone segment (acromial tilt, acromion index) it was assumed that each segment equally contributed to its modification. As well, while bone morphological properties of the scapula and humerus were manipulated in the model, the dimensions of the bones were not scaled from the original Visible Human Project dataset. With respect to the Probabilistic Impingement Model, the risk of SAIS was estimated by determining the probability of subacromial tissue thickness exceeding the available subacromial space. This estimation results in impingement being defined as a finite point rather than a continuous process. In a clinical sense, while a point certainly exists where the tissues begin to become compressed, a SAIS-related injury (rotator cuff tendinitis, tendinosis, bursitis, biceps rupture) is most often a cumulative process in which continued compression results in the degradation of the tissues. Therefore, while the model predicted a likelihood of 70% for SAIS at high elevation angles, this is not equivalent to asserting that 70% of the

195

population lifting their arm will develop rotator cuff pathologies. Additionally, truncation of the normal input distributions was performed to promote physiological realism in the model predictions. Due to the considerable variability in both kinematic and morphological parameters, including the entire distribution resulted in output errors, primarily scapulothoracic collisions. These errors can be attributed to the bone scaling limitation in addition to not considering alterations in the clavicular rhythm, particularly with humeral elevation >90° (Fung et al. 2001). Truncating the distribution underestimates the risk (overestimation of the lower confidence limit). This underestimation can be confirmed by plotting individual subject data along the predicted cumulative distribution function, which demonstrated that even subjects in the measured population fell outside of the predicted 1-99% confidence interval (Figure 32). Lastly, while the input distributions were populated by empirically measured data, the influence of fatigue on the predicted (and measured) outputs may have been understated by both the sample size and the selected population. Though the sample size was of adequate statistical power, a larger sample (i.e. exceeding 100) may have demonstrated an altered distribution. Similarly, fatigue responses may be markedly different in other population sub-groups. In the current research, while age and health status were controlled, activity level was not. Thus, including solely an athletic population or alternately a sedentary population may have elicited different fatigue responses.
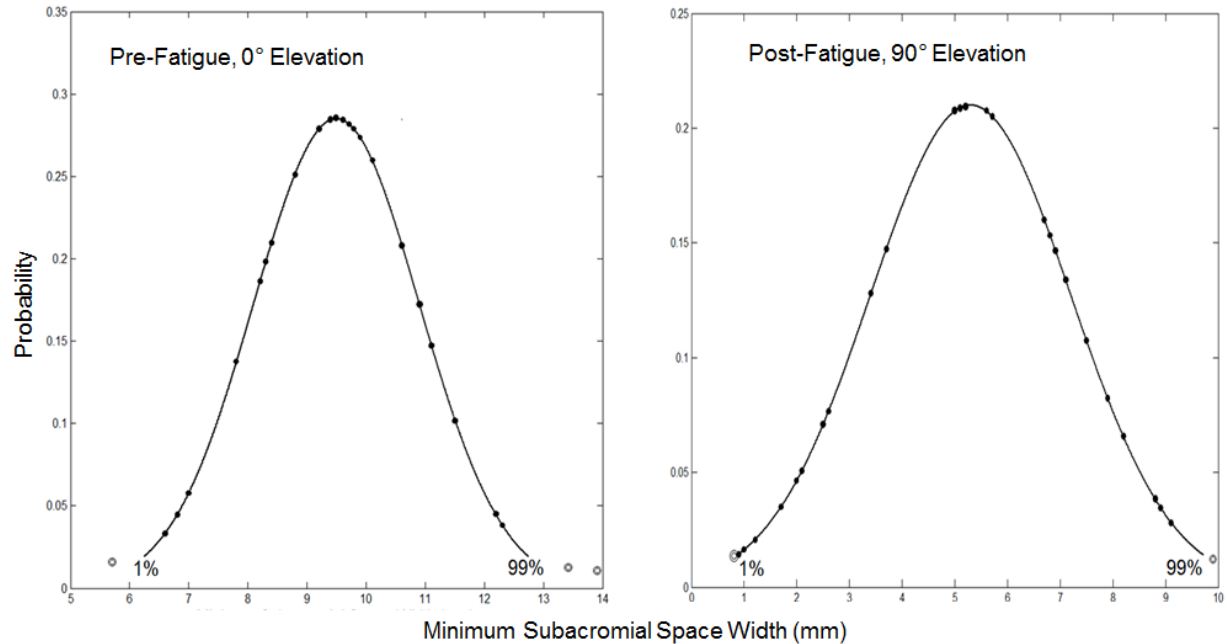
Figure 32. Probability density function (PDF) of model predicted minimum subacromial space width for two conditions (Pre-Fatigue, 0° Elevation (left); Post-Fatigue, 90° Elevation (right)). Markers indicate subject-specific results with filled markers representing those that reside along the 1-99% confidence interval, and unfilled markers representing outliers.

6.6   Conclusion

The model predicted SAS was considerably variable across all measured conditions. While muscle fatigue did not influence the predicted SAS and subsequent probability of SAIS risk, arm elevation angle greatly influenced risk when interposed tissue dimensions were considered. The high probability of tissue compression at critical elevation angles (60-90°) suggested that repetitive arm elevation may be an important contributor to rotator cuff degeneration. Additionally, while superior humeral head translation (SAS reducing) was important during initial elevation and scapular orientation (SAS increasing) at higher elevation, the high relative importance of glenoid inclination across all conditions supports glenohumeral

stability maintenance and rotator cuff strengthening to alleviate the risk of SAIS and additional

shoulder pathologies.

Chapter 7

Overall Research Outcomes and Future Direction

7.1   Summary of Research

The aim of this research was to explore, both experimentally and computationally, how shoulder bone morphology and fatigue-related kinematic relationships influence the size of the subacromial space; enabling an estimation of subacromial impingement (SAIS) risk. In addition, using a probabilistic modelling approach, this researched aimed to establish which parameters (morphological, kinematic) were more contributory to the subacromial space size. Measured and predicted output both supported and refuted certain aspects of the overall research hypothesis. While the kinematic responses to fatigue for the "average" person did not suggest an elevated risk of SAIS, both individual morphological characteristics and kinematic relationships varied widely, subsequently resulting in diffusely distributed subacromial space measurements and predictions. This interpersonal variability was also related to calculated correlation coefficients between parameters that varied greatly by elevation angle and were generally of small magnitudes. This subsequently resulted in negligible differences between univariate and multivariate simulations. In addition, estimating the risk of SAIS by considering variability in subacromial space dimensions in the context of the interposed tissues suggested that a considerable portion of the population is at risk for tissue compression with arm elevation, which can be exacerbated by muscle fatigue. Further, while not as strongly implicated in the development of SAIS as hypothesized, fatigue did initiate altered kinematics; similar alterations have implications for other shoulder pathologies, particularly for persons with certain

199

morphological variants (i.e. increased glenoid inclination). Thus, this research suggested that solely considering the population mean may strongly underestimate the risk of SAIS and subsequent rotator cuff pathology resulting from upper extremity fatiguing tasks. As well, it demonstrated that even the average person is at risk for cumulative shoulder injuries from short-duration fatiguing tasks as well as eventual SAIS development if exposed to repetitive arm elevation (overhead tasks).

7.2   Implications for the Average and Entire Population

The risk of SAIS development from upper extremity muscle fatigue and differing arm elevation angles was estimated from the collective outcomes of each experimental/modelling study which generated specific conclusions for both the **average person** and **population distribution** from this young, healthy male population:

AVERAGE member of this population – risk for SAIS

A)   *A short-duration fatiguing protocol alters glenohumeral and scapulothoracic kinematics, but does not affect the overall size of the subacromial space.*

- ➢ Alterations do not immediately elevate the risk for SAIS – the scapulothoracic relationship adapts to compensate for subacromial space reducing glenohumeral translation (superior humeral head translation) (Chapter 4).
- ➢ Alterations immediately elevate the risk for developing additional pathologies – fatigue causes the humerus to translate superiorly along the glenoid cavity, despite maintaining a consistent subacromial space width (Chapter 4).

200

B)   *The risk for tissue compression (and subsequent SAIS) increases with arm elevation.*

➢ The average occupation ratio (Subacromial tissue width : Minimum subacromial space width) was 65.3% when the arm was at neutral (arm posture in which the space is the largest ~ 9-10mm) (Chapter 5).

➢ The subacromial space reduced to between 4-5mm for elevation angles ≥90°; this resulted in an estimated 65-75% of the population at risk for tissue compression (probabilistic impingement risk prediction model, Chapter 6) and an estimated average occupation ratio exceeding 100% (Chapters 4 & 5) when the arm is elevated.

ENTIRE distribution of this population – risk for SAIS

A)   *A short-duration fatiguing protocol causes highly variable kinematic responses, which subsequently leads to a highly differential risk of SAIS.*

➢ The 1-99% confidence interval for each measured and modelled output indicated considerable variability in SAIS across the population (Chapters 4 – 6) from:

1. Morphological characteristics (bone variants and subacromial tissue thickness)

2. Controlled and fatigue-related kinematic relationships (superior humeral head translation, scapular orientation)

➢ Despite negligible mean fatigue responses, an average of 35 to 57% of participants exhibited fatigue-related changes that would reduce the subacromial space (superior humeral head translation, downward scapular rotation, anterior scapular tilt, scapular protraction), with half of the population demonstrating fatigue-induced reduction in the subacromial space following fatigue at elevation angles ≥60° (Chapter 4).

B)   *The risk for tissue compression (and subsequent SAIS) is highly variable at neutral and mid-range elevation and increases considerably with arm elevation above 60°, with members of the population almost certainly at risk for tissue compression.*

➢ The occupation ratio with the arm at neutral ranged from 21.6 – 108.9%, indicating that even in a neutral posture, members of the population would have tissue compression (Chapter 5).

➢ Subacromial tissue thickness ranged from 3.4 – 8.8mm and the subacromial space size reduced to as low as <1mm with arm elevation, with estimated average occupation ratios exceeding 100%. This magnitude of reduced space (<1mm) was present at the 1% confidence limit despite truncating the input distribution (reducing the input variability) (Chapters 4 – 6).

7.3   Practical Implications of Research

The outcomes of this research have different practical implications for both ergonomic and clinical applications which can inform specific recommendations.

7.3.1 *Applying Variability in Ergonomic Design*

With the consistent overarching conclusion that the risk of SAIS is highly variable even among a young, healthy population, the practicality of designing for the *population* rather than the *mean* needs to be addressed. Probabilistic modelling was extremely useful for conceptualizing the extent to which variability in certain anatomical factors or model parameters affects the predicted output. The study presented in **Chapter 3** highlighted that predicted muscle force capability can differ by up to 50% based on modest changes in model parameter definitions. The study presented in **Chapter 6** confirmed the highly variable risk of SAIS that exists, based on variability in kinematic fatigue responses and morphological characteristics.

These studies showed the potential utility of probabilistic modelling for practical applications, such as job design. However, as the anticipated benefit for designing an inclusive job environment that considers the entire population range (1-99% confidence interval) may not be feasible or warrant the resulting financial cost, recommendations can be made to assist with assessing this trade-off.

1. If the 'average' person (as predicted from a deterministic model) is at risk, it is critical to consider those residing outside of the mean.

   ➢ In this research, the average person was not classified as at risk for SAIS at lower elevation angles and was not at any additional risk following muscle fatigue. However, they were at elevated risk with arm elevation ≥60°. **Thus, overhead work should be avoided to prevent shoulder injuries.**

2. If the average person is not predicted to be at risk, consider the standard deviation (68%) or the inter-quartile range (50%) surrounding the mean.

   ➢ In this research, considering modest variability by truncating the input distributions to ±1 standard deviation resulted in over 46% of the population having tissue compression at elevation angles ≥60° and over 65% of the population having tissue compression ≥90°. However, <5% were at risk when the arm posture was <60°. **This reinforces the importance avoiding overhead work while demonstrating a relatively safe work space at lower arm postures.**

3. If the average person, with modest variability (±1 standard deviation) is not at risk, considering a greater proportion of the population distribution, including the outliers (toward the tail regions of the curve) becomes a job-specific or task-specific problem that

must be weighed against the cost, as well as the implications of the risk and/or potential injury severity (i.e. injuries causing death).

7.3.2 *Prevention Strategies to Maintain Shoulder Health*

The relative sensitivity (importance) factors, calculated from the probabilistic simulations, provided insight into which parameters (morphological, kinematic) were more predictive for the development of SAIS. These importance factors have excellent practical applications as they can assist with the development of more targeted prevention and rehabilitation strategies used to maintain shoulder health. While kinematic importance factors varied by elevation angle and fatigue state, overall, glenoid inclination had the highest relative importance compared to all other morphological and kinematic factors. The identified fatigue-related superior humeral head translation (Chapter 4, alternative humeral head translation measurement) coupled with the demonstrated relationship between glenoid inclination and superior humeral translation reinforced that rotator cuff strengthening is critical in maintaining glenohumeral stability. Targeting these muscles, which are largely responsible for maintaining a neutral glenohumeral position, would assist in preventing excessive movement of the humerus on the glenoid face. This would subsequently: (1) prevent bone degeneration, osteophyte formation and altered contact stresses (which may reduce stability), and (2) reduce the likelihood for SAIS development, particularly for those with morphological predisposition to impingement (inclined glenoid, hooked acromion), as well as for those whose scapulothoracic positioning demonstrates less compensatory adaptions with fatigue and/or arm elevation, for example those with scapular dyskinesis (downward rotation, anterior tilt, protraction).

7.4   Future Direction

The outcomes of this work inspire additional considerations and future directions in this research area. The probabilistic subacromial geometry model developed for this research was used to calculate a single output (SAS) over a narrow subset of postural conditions. In future work, this model can be used and further improved to address several other research questions related to the subacromial space. These may include: (1) evaluating the distribution of SAS over multi-plane evaluation, while also considering different hands loads (integration of **Study 1** and **Study 4**), (2) determining how the location of the minimum distance vector changes over the range of elevation, and whether variability in morphological features significantly influence this location, (3) determining whether the acromio-humeral interval is consistently the limiting factor over the range of multi-plane elevation and rotation. Additionally, this work studied a young, healthy male population to examine the variability that existed in morphology and kinematic relationships prior to age-related degenerative changes. This model can be employed in future work to study different population sub-groups, for example different age groups and those with shoulder pathologies. As well, the evaluation of morphological and fatigue-related kinematic variability in a female population should be considered as the distribution of the SAS and subsequent SAIS risk may be markedly different from males.

Apart from SAIS risk, this research determined that significant fatigue-induced superior glenohumeral translation occurred, despite maintaining a consistent subacromial space size. This prompts the consideration of translation-related shoulder damage, apart from SAIS, which may include studying differences in contact area and contact stresses that exist from varying the glenohumeral position (present in injured sub-groups or induced in cadaveric specimens). Additionally, while the scapula demonstrated adaptation strategies following fatigue to

compensate for the superior humeral head translation, the effect of excessive scapular movement on glenohumeral stability should be considered.

Including three-dimensional imaging techniques, particularly for the measurement of kinematic parameters at elevated postures would assist with validating and/or strengthening both the measured and modelled outputs. Validation of the deterministic subacromial geometry model in addition to developing and refining ultrasound techniques to reliably capture subacromial characteristics are two future goals which would have considerable financial and practical benefits, as it would reduce the necessity to capture three-dimensional images (CT, MRI) to study SAIS risk.

7.5   Overall Conclusions and Contributions

The primary product of this current research is the development of a novel probabilistic orthopaedic model for the evaluation of subacromial geometric variability. This model and the outputs generated regarding SAIS risk provide significant contributions to the shoulder biomechanics literature, in addition to motivating several possible future applications. This model permits rapid, cost-effective study of glenohumeral and scapulothoracic trends, including those related to differing tasks and population sub-groups. Additionally, the application of probabilistic techniques enables a more detailed risk assessment, including assessment of risk distribution as well as the relative contribution of task or anthropometric parameters.

Several outputs and accompanying trends were generated from this work, which yielded three central conclusions:

1. The size of the SAS, interposed tissue thickness and subsequent SAIS risk are all highly variable even amongst the measured young, healthy male population and thus solely considering the 'average' person may highly underestimate the risk.

206

2. The average member of the population will not acutely develop rotator cuff damage (through SAIS) from a short-duration fatiguing protocol. However, both repetitive overhead work and/or upper extremity muscle fatigue may lead to SAIS as well as additional pathologies long-term.

   ➤ Repetitive arm elevation promotes continuous incidences of occupation ratios exceeding 100% (tissue > space), which can cumulatively lead to extrinsic impingement and subsequent rotator cuff disease.

   ➤ Short-term muscle fatigue causes superior decentering of the humeral head (in 84% of the measured population) which can lead to osteophyte formation, glenoid degeneration, GH instability and subsequently intrinsic impingement and rotator cuff disease.

This research therefore supported and explained previously reported injury trends, including the highly researched and documented trend of increasing rotator cuff pathologies with advancing age. These findings imply that cumulative fatigue-initiated kinematics are in part contributing to rotator cuff pathologies, in addition to age-related tissue degeneration.

3. SAIS and rotator cuff damage is not limited to elderly populations and can exist in young populations due to interpersonal variability in both subacromial morphology and kinematic responses to fatigue.

   ➤ Certain morphological variants (notably glenoid inclination) can facilitate altered kinematics (superior humeral head translation) or pose risk for tissue damage independently (i.e. acromial characteristics)

> ➢ Short-duration fatigue responses were highly variable, with a large percentage of the population showing subacromial space reducing orientation changes.

Thus, depending on innate morphology or individual kinematic responses, even younger populations can develop SAIS from fatiguing tasks (work-related, sport-related), or even from activities of daily living (awkward arm postures).

While further work is required to quantify a broader range of tasks for a more comprehensive population group, specific recommendations for the prevention of SAIS and subsequent rotator cuff damage stemmed from this research:

1. Avoid prolonged/repetitive work in overhead postures (≥60° elevation) to prevent subacromial tissue compression.
2. If overhead work is unavoidable, ensure frequent/adequate rest breaks to prevent superior humeral head translation and subsequent degenerative damage and/or instability.

Additionally, although its current use is limited, characterization of population variability is rapidly becoming recognized for its importance amongst the biomechanics community. The outcomes of the probabilistic modelling studies presented in Chapter 3 (for the prediction of rotator cuff muscle force) and Chapter 6 (for the prediction of minimum subacromial space width) strongly highlight and reinforce the utility of incorporating probabilistic methods in biomechanics research.

Letters of Copyright Permission

1. Permission letter from <u>Springer</u> to include content (Chapter 3) published in *Annals of Biomedical Engineering*.

> Chopp-Hurley JN, Langenderfer JE, Dickerson CR. (2014). Probabilistic evaluation of predicted force sensitivity to muscle attachment and glenohumeral stability uncertainty. Annals of Biomedical Engineering, 42(9), 1867-1879.

2. Permission letter from <u>Springer</u> to include a figure (Figure 7) published in *Surgical and Radiologic Anatomy*.

> Graichen H, Bonel H, Stammberger T, Englmeier KH, Reiser M, Eckstein F. (1999a). Subacromial space width changes during abduction and rotation – a 3-D MR imaging study. Surgical and Radiologic Anatomy, 21(1), 59-64.

3. Permission letter from <u>Southwest Research Institute</u> to include figures (Figure 10 & Figure 11) published in *NESSUS Theoretical Manual*.

> NESSUS Theoretical Manual. (Version 7.01, 2001). Southwest Research Institute.

Springer

PERMISSION LETTER

January 26, 2015

Your project

Requestor:	Jaclyn N. Chopp-Hurley
	jaclyn.hurley@uwaterloo.ca
University:	University of Waterloo
Purpose:	Dissertation/Thesis

With reference to your request to reuse material in which Springer Science+Business Media controls the copyright, our permission is granted free of charge under the following conditions:

Springer material
- represents original material which does not carry references to other sources (if material in question refers with a credit to another source, authorization from that source is required as well);
- requires full credit (Springer and the original publisher, book/journal title, chapter/article title, volume, year of publication, page, name(s) of author(s), original copyright notice) to the publication in which the material was originally published by adding: "With kind permission of Springer Science+Business Media";
- may not be altered in any manner. Abbreviations, additions, deletions and/or any other alterations shall be made only with prior written authorization of the author and/or Springer Science+Business Media;
- Springer does not supply original artwork or content.

This permission
- is non-exclusive;
- is valid for one-time use only for the purpose of defending your thesis and with a maximum of 100 extra copies in paper. If the thesis is going to be published, permission needs to be reobtained.
- includes use in an electronic form, provided it is an author-created version of the thesis on his/her own website and his/her university's repository, including UMI (according to the definition on the Sherpa website: http://www.sherpa.ac.uk/romeo/);
- is subject to courtesy information to the co-author or corresponding author;
- is personal to you and may not be sublicensed, assigned, or transferred by you to any other person without Springer's written permission;
- is only valid if no personal rights, trademarks, or competitive products are infringed.

This license is valid only when the conditions noted above are met.

Springer

PERMISSION LETTER

Your project
Requestor: Jaclyn N. Chopp-Hurley
                 jaclyn.hurley@uwaterloo.ca
University: University of Waterloo
Purpose: Dissertation/Thesis

With reference to your request to reuse material in which **Springer Science+Business Media** controls the copyright, our permission is granted free of charge under the following conditions:

Springer material
- represents original material which does not carry references to other sources (if material in question refers with a credit to another source, authorization from that source is required as well);
- requires full credit (Springer and the original publisher, book/journal title, chapter/article title, volume, year of publication, page, name(s) of author(s), original copyright notice) to the publication in which the material was originally published by adding: "With kind permission of Springer Science+Business Media";
- figures, illustrations, and tables may be altered minimally to serve your work. Any other abbreviations, additions, deletions and/or any other alterations shall be made only with prior written authorization of the author and/or Springer Science+Business Media;
- Springer does not supply original artwork or content.

This permission
- is non-exclusive;
- is valid for one-time use only for the purpose of defending your thesis limited to university-use only and with a maximum of 100 extra copies in paper. If the thesis is going to be published, permission needs to be reobtained.
- includes use in an electronic form, provided it is an author-created version of the thesis on his/her own website and his/her university's repository, including UMI (according to the definition on the Sherpa website: http://www.sherpa.ac.uk/romeo/);
- is subject to courtesy information to the author (address is given in the publication);
- is personal to you and may not be sublicensed, assigned, or transferred by you to any other person without Springer's written permission;
- is only valid if no personal rights, trademarks, or competitive products are infringed.

This license is valid only when the conditions noted above are met.
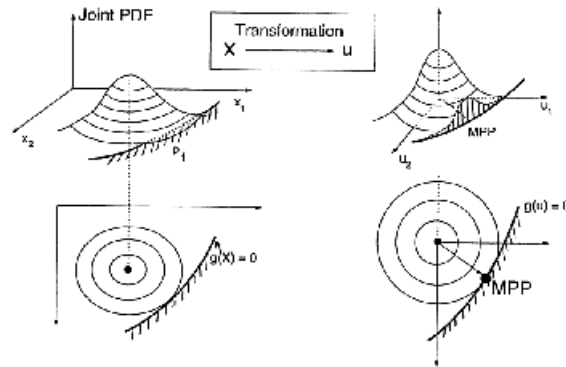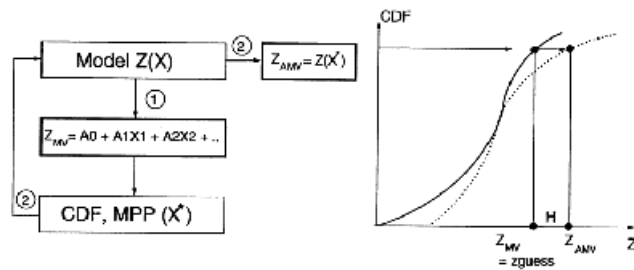
Figure 2.1

$$Z_{AMV} = Z_{MV} + H(Z_{MV})$$

Figure 9.1

212

References

Ackerman MJ (1988). The visible human project. Proceedings of the IEEE, 86(3), 504-11.

Anetzberger H, Schulz C, Pfahler M, Refior HJ, Muller-Gerbl M. (2002). Subchondral mineralization patterns of the glenoid after tear of the supraspinatus. Clinical Orthopaedics and Related Research, (404), 263-8.

Anglin C, Wyss UP, Nyffeler RW, Gerber C. (2001). Loosening performance of cemented glenoid prosthesis design pairs. Clinical Biomechanics, 16(2), 144-50.

Aoki M, Ishii S, Usui M. (1986). The slope of the acromion and rotator cuff impingement. Orthopaedic Transactions, 10, 228.

Balke M, Schmidt C, Dedy N, Banerjee M, Bouillon B, Liem D. (2013). Correlation of acromial morphology with impingement syndrome and rotator cuff tears. Acta Orthopaedica, 84(2), 178-83.

Banas MP, Miller RJ, Totterman S. (1995). Relationship between the lateral acromion angle and rotator cuff disease. Journal of Shoulder and Elbow Surgery, 4(6), 454-61.

Bernard, B. (1997). Musculoskeletal Disorders and Workplace Factors. DHHS (NIOSH) Publication No. 97-141. US Department of Health and Human Services, NIOSH, Cincinnati, OH.

Bey MJ, Brock SK, Beierwaltes WN, Zauel R, Kolowich PA, Lock TR. (2007). In vivo measurement of subacromial space width during shoulder elevation: Technique and preliminary results in patients following unilateral rotator cuff repair. Clinical Biomechanics, 22, 767-73.

Bey MJ, Kline SK, Zauel R, Lock TR, Kolowich PA. (2008). Measuring dynamic in-vivo glenohumeral joint kinematics: Technique and preliminary results. Journal of Biomechanics, 41(3), 711-4.

Bezer M, Yildirim Y, Akgun U, Erol E, Guven O. (2005). Superior excursion of the humeral head: A diagnostic tool in rotator cuff tear surgery. Journal of Shoulder Elbow Surgery, 14(4), 375-9.

Bigliani LU. (1986). The morphology of the acromion and its relationship to rotator cuff tears. Orthop Trans, 10, 228.

Bishop JL, Kline SK, Aalderink KJ, Zauel R, Bey MJ. (2009). Glenoid inclination: In vivo measures in rotator cuff tear patients and associations with superior glenohumeral joint translation. Journal of Shoulder and Elbow Surgery, 18(2), 231-6.

Bjelle A. (1989). Epidemiology of shoulder problems. Bailliere's Clinical Rheumatology, 3(3), 437-51.

Blajer W, Czaplicki A, Dzlewiecki K, Mazur Z. (2010). Influence of selected modeling and computational issues on muscle force estimates. Multibody System Dynamics, 24(4), 473-492.

Bland JM, Altman DG. (2010). Statistical methods for assessing agreement between two methods of clinical measurement. International Journal of Nursing Studies, 47(8), 931-6.

Boone DC, Azen SP. (1979). Normal ranges of motion of joints in male subject. Journal of Bone and Joint Surgery, 61, 756-759.

Borg GA. (1982). Psychophysical bases of perceived exertion. Medicine & Science in Sports & Exercise, 14, 371-81.

Borstad JD, Szucs K, Navalgund A. (2009). Scapula kinematic alterations following a modified push-up plus task. Human Movement Science, 28(6), 738-51.

Brand RA, Pedersen DR, Friederich JA. (1986). The sensitivity of muscle force predictions to changes in physiological cross-sectional area. Journal of Biomechanics, 19(8), 589-96.

Braman JP, Zhao KD, Lawrence RL, Harrison AK, Ludewig PM. (2014). Shoulder impingement revisited: evolution of diagnostic understanding in orthopedic surgery and physical therapy. Medical and Biological Engineering and Computing, 52(3), 211-9.

Brookham RL, Middlebrook EE, Grewal TJ, Dickerson CR. (2011). The utility of an empirically derived co-activation ratio for muscle force prediction through optimization. Journal of Biomechanics, 44(8), 1582-7.

Brookham RL, Dickerson CR. (2013). Empirical quantification of internal and external rotation muscular co-activation ratios in healthy shoulders. Medical & Biological Engineering & Computing, 52(3), 257-64.

Chen SK, Simonian PT, Wickiewicz TL, Otis JC, Warren RF. (1999). Radiographic evaluation of glenohumeral kinematics: A muscle fatigue model. Journal of Shoulder Elbow Surgery, 8(1), 49-52.

Choi S-K, Grandhi RV, Canfield RA. (2007). Reliability-based structural design. London, UK: Springer-Verlag London Limited.

Cholewinski JJ, Damian JK, Wojciechowski P, Cielinski LS, Zoladz MP. (2008). Ultrasound measurement of rotator cuff thickness and acromio-humeral distance in the diagnosis of subacromial impingement syndrome of the shoulder. Knee Surgery, Sports Traumatology, Arthroscopy, 16(4), 408-14.

Chopp JN, O'Neill JM, Hurley K, Dickerson CR. (2010). Superior humeral head migration occurs after a protocol designed to fatigue the rotator cuff: A radiographic analysis. Journal of Shoulder Elbow Surgery, 19(8), 1137-44.

Chopp JN, Fischer SL, Dickerson CR. (2011). The specificity of fatiguing protocols affects scapular orientation: Implications for subacromial impingement. Clinical Biomechanics, 26(1), 40-5.

Chopp JN, Dickerson CR. (2012). Resolving the contributions of fatigue-induced humeral migration and scapular reorientation on the subacromial space: An orthopaedic geometric simulation analysis. Human Movement Science, 31(2), 448-60.

Clauser CW, McConville JT, Young JW. (1969). Weight, volume and center of mass of segments of the human body. AMRL-TR-69-70, Aerospace Medical Research Laboratories, Dayton, OH.

Cohen J. (1992). Statistical Power Analysis. Current Directions in Psychological Science, 1(3), 98-101.

Cote MP, Gomlinski G, Tracy H, Mazzocca AD. (2009). Radiographic analysis of commonly prescribed scapular exercises. Journal of Shoulder Elbow Surgery, 18(2), 311-6.

Cotton RE, Rideout DF. (1964). Tears of the humeral rotator cuff. Journal of Bone Joint Surgery, 46, 314-28.

Cram JR, Kasman GS. (1998). Introduction to surface electromyography. Gaithersburg, MD: Aspen Publishers.

Crowninshield RD, Brand RA. (1981). A physiologically based criterion of muscle force prediction in locomotion. Journal of Biomechanics, 14(11), 793-801.

Curtis AS, Burbank KM, Tierney JJ, Scheller AD, Curran AR. (2006). The insertional footprint of the rotator cuff: An anatomic study. Arthorscopy: The Journal of Arthoscopic and Related Surgery, 22(6), 603-9.

de Witte PB, Nagels J, van Arkel ERA, Visser CPJ, Nelissen RGHH, de Groot JH. (2011). Study protocol subacromial impingement syndrome: The identification of pathophysiologic mechanisms (SISTIM). BMC Musculoskeletal Disorders, 12(282), 1-12.

de Witte PB, de Groot JH, van Zwet EW, Ludewig PM, Nagels J, Nelissen RGHH, Braman JP. (2014). Communication breakdown: clinicians disagree on subacromial impingement. Medical and Biological Engineering and Computing, 52(3), 221-31.

Delp SL, Maloney W. (1993). Effects of hip center location on the moment-generating capacity of the muscles. Journal of Biomechanics, 26(4/5), 485-99.

Deutsch A, Altchek DW, Schwartz E, Otis JC, Warren RF. (1996). Radiologic measurement of superior displacement of the humeral head in the impingement syndrome. Journal of Shoulder Elbow Surgery, 5(3), 186-93.

Devore JL. (2008). Probability and statistics for engineering and the sciences. Pacific Grove, CA: Duxbury Press.

Dickerson CR. (2005). A biomechanical analysis of shoulder loading and effort during load transfer tasks. PhD Dissertation – University of Michigan, Ann Arbor, MI.

Dickerson CR, Chaffin DB, Hughes RE. (2007). A mathematical musculoskeletal shoulder model for proactive ergonomic analysis. Computer Methods in Biomechanics and Biomedical Engineering, 10(6), 389-400.

Dickerson CR, Hughes RE, Chaffin DB. (2008). Experimental evaluation of a computational shoulder musculoskeletal model. Clinical Biomechanics, 23(7), 886-894.

Dickerson CR, Brookham RL, Chopp JN. (2011). The working shoulder: Assessing demands, identifying risks, and promoting healthy occupational performance. Physical Therapy Reviews, 16(5), 310-20.

Dimitrova NA, Dimitrov GV. (2003). Interpretation of EMG changes with fatigue: Facts, pitfalls, and fallacies. Journal of Electromyography and Kinesiology, 13(1), 13-36.

Drake JDM, Callaghan JP. (2006). Elimination of electrocardiograph contamination from electromyogram signals: An evaluation of currently used removal techniques. Journal of Electromyography and Kinesiology, 16(2), 175-87.

Dul J. (1988). A biomechanical model to quantify shoulder load at the work place. Clinical Biomechanics, 3(3), 124-8.

Dul J, Townsend MA, Shiavi R, Johnson GE. (1984). Muscular synergism – I. On criteria for load sharing between synergistic muscles. Journal of Biomechanics, 17(9), 663-673.

Easley SK, Pal S, Tomaszewski PR, Petrella AJ, Rullkoetter PJ, Laz PJ. (2007). Finite element-based probabilistic analysis tool for orthopaedic applications. Computer Methods and Programs in Biomedicine, 85(1), 32-40.

Ebaugh DD, McClure PW, Karduna AR. (2005). Three-dimensional scapulothoracic motion during active and passive arm elevation. Clinical Biomechanics, 20(7), 700-9.

Ebaugh DD, McClure PW, Karduna AR. (2006). Effects of shoulder muscle fatigue caused by repetitive overhead activities on scapulothoracic and glenohumeral kinematics. Journal of Electromyography and Kinesiology, 16(3), 224-35.

Edelson JG. (1995). The 'hooked' acromion revisited. Journal of Bone and Joint Surgery, 77B(2), 284-7.

Endo K, Ikata T, Katoh S, Takeda Y. (2001). Radiographic assessment of scapular rotational tilt in chronic shoulder impingement syndrome. Journal of Orthopaedic Science, 6, 3-10.

Faul F, Erdfelder E, Lang A-G, Buchner A. (2007). G*Power 3: A flexible statistical power analysis program for the social, behavioural, and biomedical sciences. Behavioural Research Methods, 39(2), 175-91.

Fehringer EV, Rosipal CE, Rhodes DA, Lauder AJ, Puumala SE, Feschuk CA, Mormino MA, Hartigan DE. (2008). The radiographic acromiohumeral interval is affected by arm and radiographic beam position. Skeletal Radiology, 37(6), 535-9.

Flatow EL, Soslowsky LJ, Ticker JB, Pawluk RJ, Hepler M, Ark J, Mow VC, Bigliani LU. (1994). Excursion of the rotator cuff under the acromion. American Journal of Sports Medicine, 22(6), 779-88.

Flieg NG, Gatti, CJ, Case Doro L, Langenderfer JE, Carpenter JE, Hughes RE. (2008). A stochastic analysis of glenoid inclination angle and superior migration of the humeral head. Clinical Biomechanics, 23(5), 554-61.

Freedman L, Munro RR. (1966). Abduction of the arm in the scapular plane: Scapular and glenohumeral movements: A roentgenographic study. Journal of Bone and Joint Surgery, 48(8), 1503-10.

Frost P, Andersen JH. (1999). Shoulder impingement syndrome in relation to shoulder intensive work. Occupational and Environmental Medicine, 56(7), 494-8.

Frost P, Bonde JPE, Mikkelsen S, Andersen JH, Fallentin N, Kaegaard A, Thomsen JF. (2002). Risk of shoulder tendinitis in relation to shoulder loads in monotonous repetitive work. American Journal of Industrial Medicine, 41(1), 11-8.

Fung M, Kato S, Barrance PJ, Elias JJ, McFarland EG, Nobuhara K, Chao EY. (2001). Scapular and clavicular kinematics during humeral elevation: A study with cadavers.

Garner BA, Pandy MG. (1999). A kinematic model of the upper limn based on the visible human project (VHP) image dataset. Computer Methods in Biomechanics and Biomedical Engineering, 2, 107-24.

Gatti CJ, Dickerson CR, Chadwick EK, Mell AG, Hughes RE. (2007). Comparison of model-predicted and measured moment arms for the rotator cuff muscles. Clinical Biomechanics, 22(6), 639-644.

Geiringer SR. (1999). Anatomic localization for needle electromyography. Philadelphia, PA: Hanley & Belfus, Inc.

Gill TJ, McIrvin E, Kocher MS, Homa K, Mair SD, Hawkins RJ. (2002). The relative importance of acromial morphology and age with respect to rotator cuff pathology. Journal of Shoulder and Elbow Surgery, 11(4), 327-30.

Giphart JE, van der Meijden OAJ, Millett PJ. (2012). The effects of arm elevation on the 3-dimensional acromiohumeral distance: a biplane fluoroscopy study with normative data. Journal of Shoulder and Elbow Surgery, 21(11), 1593-1600.

Girometti R, De Candia A, Sbuelz M, Toso F, Zuiana C, Bazzocchi M. (2006). Supraspinatus tendon US morphology in basketball players: Correlation with main pathologic models of

secondary impingement syndrome in young overhead athletes. Preliminary report. Radiologia Medica, 111(1), 42-52.

Golding FC. (1962). The shoulder – the forgotten joint. British Journal of Radiology, 35, 149-58.

Graichen H, Bonel H, Stammberger T, Englmeier KH, Reiser M, Eckstein F. (1999a). Subacromial space width changes during abduction and rotation – a 3-D MR imaging study. Surgical and Radiologic Anatomy, 21(1), 59-64.

Graichen H, Bonel H, Stammberger T, Haubner M, Rohrer H, Englmeier KH, Reiser M, Eckstein F. (1999b). Three-dimensional analysis of the width of the subacromial space in healthy subjects and patients with impingement syndrome. American Journal of Roentgenology, 172(4), 1081-6.

Graichen H, Stammberger T, Bonel H, Karl-Hans E, Reiser M, Eckstein F. (2000). Glenohumeral translation during active and passive elevation of the shoulder — a 3D open-MRI study. Journal of Biomechanics, 33(5), 609-13.

Graichen H, Hinterwimmer S, von Eisenhart-R, Vogl T, Englmeier K-H, Eckstein F. (2005). Effect of abducting and adducting muscle activity on glenohumeral translation, scapular kinematics and subacromial space width in vivo. Journal of Biomechanics, 38(4), 755-60.

Grewal T-J. (2011). Quantifying the shoulder rhythm and comparing non-invasive methods of scapular tracking for overhead and axially rotated humeral postures. MSc Thesis – University of Waterloo, Waterloo, ON.

Grieve JR, Dickerson CR. (2008). Overhead work: Identification of evidence-based exposure guidelines. Occupational Ergonomics, 8(1), 53-66.

Gruber G, Bernhardt GA, Clar H, Zacherl M, Glehr M, Wurnig C. (2010). Measurement of the acromiohumeral interval on standardized anteroposterior radiographs: A prospective study of observer variability. Journal of Shoulder and Elbow Surgery, 19(1), 10-3.

Haldar A, Mahadevan S. (2000). Probability, reliability, and statistical methods in engineering design. New York, NY: John Wiley & Sons, Inc.

Hinterwimmer S, von Eisenhart-Rothe R, Siebert M, Putz R, Eckstein F, Vogl T, Graichen H. (2003). Influence of adducting and abducting muscle forces on the subacromial space width. Medicine and Sciences in Sports and Exercise, 35(12), 2055-9.

Herberts P, Kadefors R. (1976). A study of painful shoulder in welders. Acta Orthopaedica Scandinavica, 47(4), 381-7.

Herberts P, Kadefors R, Broman H. (1980). Arm positioning in manual tasks: An electromyographic study of localized muscle fatigue. Ergonomics, 23(7), 655-65.

Herberts P, Kadefors R, Andersson G, Petersen I. (1981). Shoulder pain in industry: An epidemiological study on welders. Acta Orthopaedica Scandinavica, 52(2), 299-306.

Herzog W. (1992). Sensitivity of muscle force estimations to changes in muscle input parameters using nonlinear optimization approaches. Journal of Biomechanical Engineering, 114(2), 267-268.

Hogfors C, Sigholm G, Herberts P. (1987). Biomechanical model of the human shoulder – I. Elements. Journal of Biomechanics, 20(2), 157-66.

Hogfors C, Peterson B, Sigholm G, Herberts P. (1991). Biomechanical model of the human shoulder joint – II. The shoulder rhythm. Journal of Biomechanics, 24(8), 699-709.

Hogfors C, Karlsson D, Peterson B. (1995). Structure and internal consistency of a shoulder model. Journal of Biomechanics, 28(7), 767-77.

Hughes RE, An K-N. (1997). Monte Carlo simulation of a planar shoulder model. Medical & Biological Engineering & Computing, 35(5), 544-8.

Hughes RE, Bryant CR, Hall JM, Wening J, Huston LJ, Kuhn JE, Carpenter JE, Blasier RB. (2003). Glenoid inclination is associated with full-thickness rotator cuff tears. Clinical Orthopaedics and Related Research, 407, 86-91.

Inman VT, Saunders JBD, Abbott LC. (1944). Observations on the function of the shoulder joint. Journal of Bone and Joint Surgery, 25, 1-30.

Itoi E, Berglund J, Grabowski JJ, Schultz FM, Growney ES, Morrey BF, An K-N. (1995). Tensile properties of the supraspinatus tendon. Journal of Orthopaedic Research, 13(4), 578-84.

Jobe CM, Coen MJ, Screnar P. (2000). Evaluation of impingement syndromes in the overhead-throwing athlete. Journal of Athletic Training, 35(3), 293-9.

Joensen J, Couppe C, Bjordal JM. (2009). Increased palpation tenderness and muscle strength deficit in the prediction of tendon hypertrophy in symptomatic unilateral shoulder tendinopathy: An ultrasonographic study. Physiotherapy, 95(2), 83-93.

Karlsson D, Peterson B. (1992). Towards a model for force predictions in the human shoulder. Journal of Biomechanics, 25(2), 189-99.

Keener JD, Wei AS, Kim HM, Steger-May K, Yamaguchi K. (2009). Proximal humeral migrations in shoulders with symptomatic and asymptomatic rotator cuff tears. Journal of Bone and Joint Surgery, 91, 1405-13.

Kelkar R, Wang VM, Flatow EL, Newton PM, Ateshian GA, Bigliani LU, Pawluk RJ, Mow VC. (2001). Glenohumeral mechanics: A study of articular geometry, contact, and kinematics. Journal of Shoulder and Elbow Surgery, 10(1), 73-84.

Kessel L, Watson M. (1977). The painful arc syndrome. Journal of Bone and Joint Surgery, 59-B(2), 166-72.

Kibler WB, Ludewig PM, McClure PW, Michener LA, Bak K, Sciascia AD. (2013). Clinical implications of scapular dyskinesis in shoulder injury: the 2013 consensus statement from the 'scapular summit'. British Journal of Sports Medicine, 47(14), 877-85.

King AI, Viano DC, Mizeres N, States JD. (1995). Humanitarian benefits of cadaver research on injury prevention. The Journal of Trauma: Injury, Infection, and Critical Care, 38(4), 564-9.

Kitay GS, Iannotti JP, Williams GR, Haygood T, Kneeland BJ, Berlin J. (1995). Roentgenographic assessment of acromial morphologic condition in rotator cuff impingement syndrome. Journal of Shoulder and Elbow Surgery, 4(6), 441-8.

Konrad GG, Markmiller M, Jolly JT, Ruter AE, Sudkamp NP, McMahon PJ, Debski RE. (2006). Decreasing glenoid inclination improves function in shoulders with simulated massive rotator cuff tears. Clinical Biomechanics, 21(9), 942-9.

Kuechle DK, Newman SR, Itoi E, Morrey BF, An K-N. (1997). Shoulder muscle moment arms during horizontal flexion and elevation. Journal of Shoulder and Elbow Surgery, 6(5), 429-39.

Kuechle DK, Newman SR, Itoi E, Niebur GL, Morrey BF, An KN. (2000). An. The relevance of moment arm of the shoulder muscles with respect to axial rotation of the glenohumeral joint in four positions. Clinical Biomechanics, 15(5), 332-329.

Langenderfer JE, Carpenter JE, Johnson ME, An K-N, Hughes RE. (2006). A probabilistic model of glenohumeral external rotation strength for healthy normal and rotator cuff tear cases. Annals of Biomedical Engineering, 34(3), 465-76.

Langenderfer JE, Laz PJ, Petrella AJ, Rullkoetter PJ. (2008). An efficient probabilistic methodology for incorporating uncertainty in body segment parameters and anatomical landmarks in joint loadings estimated from inverse dynamics. Journal of Biomechanical Engineering, 130(1), 014502.

Langenderfer JE, Rullkoetter PJ, Mell AG, Laz PJ. (2009). A multi-subject evaluation of uncertainty in anatomical landmark location on shoulder kinematic description. Computer Methods in Biomechanics and Biomedical Engineering, 12(2), 211-6.

Laudner KG, Myers JB, Pasquale MR, Bradley JP, Lephart SM. (2006). Scapular Dysfunction in Throwers with Pathologic Internal Impingement. Journal of Orthopaedic and Sports Physical Therapy, 36(7), 485-94.

Laz PJ, Browne M. (2010). A review of probabilistic analysis in orthopaedic biomechanics. Proceedings of the Institution of Mechanical Engineers, Part H: Journal of Engineering in medicine, 224(H8), 927-43.

Leclerc A, Chastang J-F, Niedhammer I, Landre M-F, Roquelaure Y, Study Group on Repetitive Work. (2004). Incidence of shoulder pain in repetitive work. Occupational and Environmental Medicine, 61(1), 39-44.

Lehtinen JT, Belt, EA, Lyback, CO, Kauppi MJ, Kaarela K, Kautiainen HJ, Lehto MUK. (2000). Subacromial space in the rheumatoid shoulder: A radiographic 15-year follow-up study. Journal of Shoulder and Elbow Surgery, 9(3), 183-7.

Leong H-T, Tsui S, Ying M, Leung VY-F, Fu SN. (2012). Ultrasound measurements on acromio-humeral distance and supraspinatus tendon thickness: Test-retest reliability and correlations with shoulder rotational strengths. Journal of Science and Medicine in Sport, 15(4), 284-291.

Lewandowski A. (1982). Issues in model validation. International Institute for Applied Systems Analysis. RR(82-37), 1-11.

Lin J-J, Hanten WP, Olson SL, Roddey TS, Soto-quijano DA, Lim HK, Sherwood AM. (2005). Functional activity characteristics of individuals with shoulder dysfunctions. Journal of Electromyography and Kinesiology, 15(6), 576-86.

Lippitt S, Matsen F. (1993). Mechanisms of glenohumeral joint stability. Clinical Orthopaedics and Related Research, 291, 20-8.

Ludewig PM, Cook TM, Nawoczenski DA. (1996). Three-dimensional scapular orientation and muscle activity at selected positions of humeral elevation. Journal of Orthopaedic & Sports Physical Therapy, 24(2), 57-65.

Ludewig PM, Cook TM. (2000). Alterations in shoulder kinematics and associated muscle activity in people with symptoms of shoulder impingement. Physical Therapy, 80(3), 276-91.

Ludewig PM, Cook TM. (2002). Translations of the humerus in persons with shoulder impingement symptoms. Journal of Orthopaedic & Sports Physical Therapy, 32(6), 248-59.

Ludewig PM, Reynolds JF. (2009). The association of scapular kinematics and glenohumeral joint pathologies. Journal of Orthopaedic & Sports Physical Therapy, 39(2), 90-104.

Ludewig PM, Phadke V, Braman JP, Hassett DR, Cieminski CJ, LaPrade RF. (2009). Motion of the shoulder complex during multiplanar humeral elevation. Journal of Bone and Joint Surgery, 91-A(2), 378-89.

Lukasiewicz AC, McClure P, Michener L, Pratt N, Sennett B. (1999). Comparison of 3-dimensional scapular position and orientation between subjects with and without shoulder impingement. Journal of Orthopaedic & Sports Physical Therapy, 29(10), 574-86.

MacGillivray JD, Fealy S, Potter HG, O'Brien SJ. (1998). Multiplanar analysis of acromion morphology. The American Journal of Sports Medicine, 26(6), 836-40.

Makela M, Heliovaara M, Sainio P, Knekt P, Impivaara O, Aromaa A. (1999). Shoulder joint impairment among Finns aged 30 years or over: Prevalence, risk factors and co-morbidity. Rheumatology, 38(7), 656-62.

Makhsous M. (1999). Improvements, validation and adaptation of a shoulder model. PhD Dissertation – Chalmers University of Technology, Goteborg, Sweden.

Massey FJ. (1951). The Kolmogorov-Smirnov test for goodness of fit. Journal of the American Statistical Association, 46(253), 68-78.

Mathiassen SE, Moller T, Forsman M. (2003). Variability in mechanical exposure within and between individuals performing a highly constrained industrial work task. Ergonomics, 46(8), 800-24.

Matsuki K, Matsuki KO, Yamaguchi S, Ochiai N, Sasho T, Sugaya H, Toyone T et al. (2012). Dynamic in vivo glenohumeral kinematics during scapular plane abduction in healthy shoulder. Journal of Orthopaedic & Sports Physical Therapy, 42(2), 96-104.

Maurer A, Fucentese SF, Pfirrmann CWA, Wirth SH, Djahangiri A, Jost B, Gerber C. (2012). Assessment of glenoid inclination on routine clinical radiographs and computed tomography examinations of the shoulder. Journal of Shoulder and Elbow Surgery, 21(8), 1096-1103.

Mavris DN, Bandte O. (1997). Comparison of two probabilistic techniques for the assessment of economic uncertainty. 19th annual conference of the International Society of Parametric Analysts in New Orleans.

McClure PW, Michener LA, Sennett BJ, Karduna AR. (2001). Direct 3-dimensional measurement of scapular kinematics during functional movements: An in vivo study in healthy volunteers. Journal of Shoulder and Elbow Surgery, 10, 269-77.

McClure PW, Michener LA, Karduna AR. (2006). Shoulder function and 3-dimensional scapular kinematics in people with and without shoulder impingement syndrome. Physical Therapy, 86(8), 1075-90.

McQuade KJ, Dawson J, Smidt GL. (1998). Scapulothoracic muscle fatigue associated with alterations in scapulohumeral rhythm kinematics during maximum resistive shoulder elevation. Journal of Orthopaedic & Sports Physical Therapy, 28(2), 74-80.

Michener LA, McClure PW, Karduna AR. (2003). Anatomical and biomechanical mechanisms of subacromial impingement syndrome. Clinical Biomechanics, 18, 369-79.

Michener LA, Subasi Yesilyaprak SS, Seitz AL, Timmons MK, Walsworth MK. (2013). Supraspinatus tendon and subacromial space parameters measured on ultrasonographic imaging in subacromial impingement syndrome. Knee surgery, sports traumatology, arthroscopy, DOI: 10.1007/s00167-013-2542-8.

Milgrom C, Schaffler M, Gilbert S, van Holsbeeck M. (1995). Rotator-cuff changes in asymptomatic adults. Journal of Bone and Joint Surgery, 77B(2), 296-8.

Miranda H, Viikari-Juntura E, Heistaro S, Heliovaara M, Riihimaki H. (2005). A population study on differences in the determinants of a specific shoulder disorder versus nonspecific shoulder pain without clinical findings. American Journal of Epidemiology, 161(9), 847-55.

Murray WM, Buchanan TS, Delp SL. (2002). Scaling of peak moment arms of elbow muscles with upper extremity bone dimensions. Journal of Biomechanics, 35(1), 19-26.

Neer CS. (1972). Anterior acromioplasty for the chronic impingement syndrome in the shoulder. Journal of Bone and Joint Surgery, 54A(1), 41-50.

Neer CS. (1983). Impingement Lesions. Clinical Orthopaedics and Related Research, (173), 70-7.

Nemeth G, Kronberg M, Brostrom LA. (1990). Electromyogram (EMG) recordings from the subscapularis muscle – description of a technique. Journal of Orthopaedic Research, 8(1), 151-3.

NESSUS Theoretical Manual. (Version 7.01, 2001). Southwest Research Institute.

Nicholson GP, Goodman DA, Flatow EL, Bigliani LU. (1996). The acromion: Morphological condition and age-related changes. A study of 420 scapulas. Journal of Shoulder and Elbow Surgery, 5(1), 1-11.

Nussbaum MA, Zhang X. (2000). Heuristics for locating upper extremity joint centres from a reduced set of surface markers. Human Movement Science, 19(5), 797-816.

Nussbaum MA, Chaffin DB, Rechtien, CJ. (1995). Muscle lines-of-action affect predicted forces in optimization-based spine muscle modelling. Journal of Biomechanics, 28(4), 401-409.

Nyffeler RW, Werner CML, Sukthankar A, Schmid MR, Gerber C. (2006). Association of a large lateral extension of the acromion with rotator cuff tears. Journal of Bone and Joint Surgery, 88A(4), 800-5.

Oberg T, Sandsjo L, Kadefors, (1990). R. Electromyogram mean power frequency in non-fatigued trapezius muscle. European Journal of Applied Physiology and Occupational Physiology, 61(5-6), 362-9.

Olofsson P. (2005). Probability, statistics and stochastic processes. Hoboken, NJ: Wiley-Interscience.

O'Neill, JMD. (2008). Musculoskeletal ultrasound: Anatomy and technique. New York, NY: Springer. DOI: 10.1007/978-0-387-76610-2.

Pal S, Langenderfer JE, Stowe JQ, Laz PJ, Petrella AJ, Rullkoetter PJ. (2007). Probabilistic modeling of knee muscle moment arms: Effects of methods, origin-insertion, and kinematic variability. Annals of Biomedical Engineering, 35(9), 1632-42.

Paletta GA, Warner JJP, Warren RF, Deutsch A, Altchek DW. (1997). Shoulder kinematics with two-plane x-ray evaluation in patients with anterior instability or rotator cuff tearing. Journal of Shoulder and Elbow Surgery, 6(6), 516-27.

Park HB, Yokota A, Gill HS, El Rassi G, McFarland EG. (2005). Diagnostic accuracy of clinical tests for the different degrees of subacromial impingement syndrome. Journal of Bone and Joint Surgery Am, 87(7), 1446-55.

Petersson CJ, Redlund-Johnell I. (1984). The subacromial space in normal shoulder radiographs. Acta Orthopaedica Scandinavica, 55(1), 57-8.

Phadke V, Camargo PR, Ludewig PM. (2009). Scapular and rotator cuff muscle activity during arm elevation: A review of normal function and alterations with shoulder impingement. Revista Brasileira de Fisioterapia, 13(1), 1-9.

Pope DP, Croft PR, Pritchard CM, Silman AJ. (1997). Prevalence of shoulder pain in the community: The influence of case definition. Annals of the Rheumatic Diseases, 56(5), 308-12.

Poppen NK, Walker PS. (1976). Normal and abnormal motion of the shoulder. Journal of Bone and Joint Surgery, 58A(2), 195-201.

Poppen NK, Walker PS. (1978). Forces at the glenohumeral joint in abduction. Clinical Orthopaedics and Related Research, (135), 165-70.

Punnett L, Fine LJ, Keyserling WR, Herrin GD, Chaffin DB. (2000). Shoulder disorders and postural stress in automobile assembly work. Scandinavian Journal of Work, Environment and Health, 26(4), 283-91.

Raikova RT, Prilutsky BI. (2001). Sensitivity of predicted muscle forces to parameters of the optimization-based human leg model revealed by analytical and numerical analyses. Journal of Biomechanics, 34(10), 1243-55.

Rao SS. (1992). Reliability-based design. Toronto, ON: McGraw-Hill.

Reinbolt JA, Haftka RT, Chmielewski TL, Fregly BJ. (2007). Are patient-specific joint and inertial parameters necessary for accurate inverse dynamics analyses of gait? IEEE Transactions on Biomedical Engineering, 54(5), 782-93.

Rockwood CA, Matsen FA, Wirth MA, Lippitt SB. (2009). The Shoulder – Volumes 1-2. Fourth Edition. Philadelphia, PA: Saunders, an imprint of Elsevier Inc.

Royer PJ, Kane EJ, Parks KE, Morrow JC, Moravec RR, Christie DS, Teyhen DS. (2009). Fluoroscopic assessment of rotator cuff fatigue on glenohumeral arthrokinematics in shoulder impingement syndrome. Journal of Shoulder and Elbow Surgery, 18(6), 968-75.

Sakakibara H, Miyao M, Kondo T-A, Yamada S. (1995). Overhead work and shoulder-neck pain in orchard farmers harvesting pears and apples. Ergonomics, 38(4), 700-6.

Seitz AL, McClure PW, Finucane S, Boardman ND, Michener LA. (2011). Mechanisms of rotator cuff tendinopathy: Intrinsic, extrinsic or both? Clinical Biomechanics, 26(1), 1-12.

Seitz AML, Michener LA. (2011). Ultrasonographic measures of subacromial space in patients with rotator cuff disease: A systematic review. Journal of Clinical Ultrasound, 39(3), 146-54.

Shah NN, Bayliss NC, Malcolm A. (2001). Shape of the acromion: congenital or acquired – a macroscopic, radiographic, and microscopic study of acromion. Journal of Shoulder and Elbow Surgery, 10(4), 309-16.

Sher JS, Uribe JW, Posada A, Murphy BJ, Zlatkin MB. (1995). Abnormal findings on magnetic resonance images of asymptomatic shoulders. Journal of Bone and Joint Surgery, 77-A(1), 10-5.

Solem-Bertoft E, Thuomas K-A, Westerberg C-E. (1993). The influence of scapular retraction and protraction on the width of the subacromial space: An MRI study. Clinical Orthopaedics and Related Research, (296), 99-103.

Stehle J, Moore SM, Alaseirlis DA, Debski RE, McMahon PJ. (2007). Acromial morphology: effects of suboptimal radiographs. Journal of Shoulder and Elbow Surgery, 16(2), 135-42.

Su KPE, Johnson MP, Gracely EJ, Karduna AR. (2004). Scapular rotation in swimmers with and without impingement syndrome: Practice effects. Medicine and Science in Sports and Exercise, 36(7), 1117-1123.

Suzuki H, Swanik KA, Huxel KC, Kelly JD, Swanik CB. (2006). Alterations in upper extremity motion after scapular-muscle fatigue. Journal of Sport Rehabilitation, 15(1), 71-88.

Svendsen SW, Gelineck J, Mathiassen SE, Bonde JP, Frich LH, Stengaard-Pedersen K, Egund N. (2004). Work above shoulder level and degenerative alterations of the rotator cuff tendons: A magnetic resonance imaging study. Arthritis and Rheumatism, 50(10), 3314-22.

Terrier A, Reist A, Vogel A, Farron A. (2007). Effect of supraspinatus deficiency on humerus translation and glenohumeral contact force during abduction. Clinical Biomechanics, 22(6), 645-51.

Tetreault P, Krueger A, Zurakowski D, Gerber C. (2004). Glenoid version and rotator cuff tears. Journal of Orthopaedic Research, 22(1), 202-7.

Teyhen DS, Miller JM, Middag TR, Kane EJ. (2008). Rotator cuff fatigue and glenohumeral kinematics in participants without shoulder dysfunction. Journal of Athletic Training, 43(4), 352-8.

Teyhen DS, Christ TR, Ballas ER, Hoppes CW, Walters JD, Christie DS, Dreitzler G, Kane EJ. (2010). Digital fluoroscopic video assessment of glenohumeral migration: Static vs. dynamic conditions. Journal of Biomechanics, 43(7), 1380-5.

Thompson MD, Landin D, Page PA. (2011). Dynamic acromiohumeral interval changes in baseball players during scaption exercises. Journal of Shoulder and Elbow Surgery, 20(2), 251-8.

Toivonen DA, Tuite MJ, Orwin JF. (1995). Acromial structure and tears of the rotator cuff. Journal of Shoulder and Elbow Surgery, 4(5), 376-83.

Torrens C, Lopez J-M, Puente I, Caceres E. (2007). The influence of the acromial coverage index in rotator cuff tears. Journal of Shoulder and Elbow Surgery, 16(3), 347-51.

Tsai N, McClure PW, Karduna AR. (2003). Effects of muscle fatigue on 3-dimensional scapular kinematics. Archives of Physical Medicine and Rehabilitation, 84(7), 1000-5.

Tsai Y-H, Huang T-J. Hsu W-H, Huang K-C, Li Y-Y, Peng K-T, Hsu R W-W. (2007). Detection of subacromial bursa thickening by sonography in shoulder impingement syndrome. Chang Gung Medical Journal, 30(2), 135-140.

Tuite MJ, Toivonen DA, Orwin JF, Wright DH. (1995). Acromial angle on radiographs of the shoulder: Correlation with the impingement syndrome and rotator cuff tears. American Journal of Roentgenology, 165(3), 609-13.

U.S. National Library of Medicine. The Visible Human Project®. http://www.nlm.nih.gov/research/visible/visible_human.html

Vahakari M, Leppilahti J, Hyvonen P, Ristiniemi J, Paivansalo M, Jalovaara P. (2010). Acromial shape in asymptomatic subjects: A study of 305 shoulders in different age groups. Acta Radiologica, 51(2), 202-6.

van Andel C, van Hutten K, Eversdijk M, Veeger D, Harlaar J. (2009). Recording scapular motion using an acromion marker cluster, 29(1), 123-8.

van der Helm FCT. (1994). A finite element musculoskeletal model of the shoulder mechanism. Journal of Biomechanics, 27(5), 551-569.

van der Windt, DAWM, Koes BW, de Jong BADE, Bouter LM. (1995). Shoulder disorders in general practice: Incidence, patient characteristics, and management. Annals of Rheumatic Diseases, 54, 959-64.

van der Windt DAWM, Koes BW, Boeke AJ, Deville W, de Jong BADE, Bouter LM. (1996). Shoulder disorder in general practice: Prognostic indicators of outcome. British Journal of General Practice, 46(410), 519-23.

van Holsbeeck M, Strouse PJ. (1993). Sonography of the shoulder: Evaluation of the subacromial-subdeltoid bursa. American Journal of Roentgenology, 160(3), 561-4.

van Rijn, Huisstede BMA, Koes BW, Burdorf A. (2010). Associations between work-related factors and specific disorders of the shoulder – systematic review of literature. Scandinavian Journal of Work, Environment and Health, 36(3), 189-201.

von Eisenhart-Rothe R, Muller-Gerbl, Wiedemann E, Englmeier K-H, Graichen H. (2008). Functional malcentering of the humeral head and asymmetric long-term stress on the glenoid: Potential reasons for glenoid loosening in total shoulder arthroplasty. Journal of Shoulder and Elbow Surgery, 17(5), 695-702.

Wallny T, Wagner UA, Prange S, Schmitt O, Reich H. (1999). Evaluation of chronic tears of the rotator cuff by ultrasound. Journal of Bone and Joint Surgery, 81B(4), 675-8.

Wang JC, Shapiro MS. (1997). Changes in acromial morphology with age. Journal of Shoulder and Elbow Surgery, 6(1), 55-9.

Wang H-K, Lin J-J, Pan S-L, Wang T-G. (2005). Sonographic evaluations in elite college baseball athletes. Scandinavian Journal of Medicine and Science in Sports, 15(1), 29-35.

Weiner DS, MacNab I. (1970). Superior migration of the humeral head. Journal of Bone and Joint Surgery, 52B(3), 524-7.

Wells R, Van Eerd D, Hagg G. (2004). Mechanical exposure concepts using force as the agent. Scandinavian Journal of Work, Environment and Health, 30(3), 179-90.

Wiker SF, Chaffin DB, Langolf GD. (1989). Shoulder posture and localized muscle fatigue and discomfort. Ergonomics, 32(2), 211-37.

Woltring HJ. (1991). Representation and calculation of 3-D joint movement. Human Movement Science, 10(5), 603-16.

Wong AS, Gallo L, Kuhn JE, Carpenter JE, Hughes RE. (2003). The effect of glenoid inclination on superior humeral head migration. Journal of Shoulder and Elbow Surgery, 12(4), 360-4.

Workplace Safety and Insurance Board of Ontario (WSIB). By the Numbers: 2013 WSIB Statistical Report.

Wu Y-T, Millwater HR, Cruse TA. (1990). Advanced probabilistic structural analysis method for implicit performance functions. AIAA Journal, 28(9), 1663-9.

Wu G, van der Helm FCT, Veeger HEJ, Makhsous M, Van Roy P, Anglin C, et al. (2005). ISB recommendation on definitions of joint coordinate systems of various joints for the reporting of human joint motion—Part II: Shoulder, elbow, wrist and hand. Journal of Biomechanics, 38(5), 981–992.

Yamaguchi K, Sher JS, Andersen WK, Garretson R, Uribe JW, Hechtman K, Neviaser RJ. (2000). Glenohumeral motion in patients with rotator cuff tears: A comparison of asymptomatic and symptomatic shoulders. Journal of Shoulder and Elbow Surgery, 9(1), 6-11.

Yanagawa T, Goodwin CJ, Shelburne KB. (2008). Contributions of the individual muscles of the shoulder to glenohumeral joint stability during abduction. Journal of Biomechanical Engineering, 130(2), 021024-1-9.

Zatsiorsky V, Seluyanov V. (1993). Estimation of the mass and inertia characteristics of the human body by means of the best predictive regression equations. Biomechanics IX-B, Human Kinetics.

Zuckerman JD, Kummer FJ, Cuomo F, Simon J, Rosenblum S, Katz N. (1992). The influence of coracoacromial arch anatomy on rotator cuff tears. Journal of Shoulder and Elbow Surgery, 1(1), 4-14.

Appendix 1

The specific steps of a Monte Carlo simulation are described as follows given a simple

example that was created using the explanations by Choi et al. (2007), Haldar and Mahadevan

(2000) and Rao (1992).

STEP 1: Define the function and the statistical parameters for each of the random variables.
$$J = 3C - H + 2$$
Where,

      C is a *uniformly* distributed random variable with endpoints [5, 10]
      H is a *normally* distributed random variable with a mean, $\mu_H = 20$ and standard
      deviation, $\sigma_H = 5$

STEP 2: Generate uniformly distributed random numbers, μ_C, between 0 and 1.
For this example only 5 numbers will be generated (using Excel), however generally many
thousands of iterations are performed.

μ_C
0.320264
0.026759
0.019510
0.694102
0.553795

STEP 3: Transform the uniformly distributed random variables, $0 \leq \mu_C \leq 1$, to the appropriate
characteristics for each random variable.
(**Step 3A**) C: uniformly distributed with endpoints [5,10]
      $\mu_C = \frac{x_C - a}{b - a}$ therefore $x_C = a + (b - a)\mu_C$

Where,

      a is the lower limit of the distribution
      b is the upper limit of the distribution
      μ_C is the random number generated with a uniform distribution (no additional
      transformation required)
      x_C is the value for C with the appropriate characteristics

μ_C	x_C
0.320264	6.601319
0.026759	5.133794
0.019510	5.097551
0.694102	8.470512
0.553795	7.768977

(**Step 3-B**) H: normally distributed with mean, $\mu_H = 20$ and standard deviation, $\sigma_H = 5$

The uniformly distributed random numbers need to be transformed to a normal distribution using the inverse of the CDF for a standard normal variable.

$$\mu = F_H(x_H) = \phi(s_i) = \frac{x_H - \mu_H}{\sigma_H} \qquad \text{therefore} \qquad x_H = \mu_H + \sigma_H \phi^{-1}(\mu_C)$$

μ_C	μ (normal)	x_H
0.320264	-0.47	17.65
0.026759	-1.93	10.35
0.019510	-2.06	9.70
0.694102	0.51	22.55
0.553795	0.13	20.65

Note: the values of $\phi^{-1}(\mu_C)$ can be obtained from widely available tables.
This process can be applied to any of the distributions discussed.

***STEP 4*:** Substitute each value for each of the random variables into the function presented in Step 1 to obtain 5 'realizations' of the function.

$x_C (= C)$	$x_H (= H)$	$J = 3C - H + 2$
6.601319	17.65	-2.447
5.133794	10.35	1.918
5.097551	9.70	2.495
8.470512	22.55	-3.609
7.768977	20.65	-3.112

STEP 5: If we were to assume this was a reliability problem where $J < 0 =$ failure and $J > 0 =$ safe, then we can calculate the probability of failure.

$$p_f = \frac{N_f}{N}$$

Where,
   p_f is the probability of failure
   N_f is the number of iterations that $J < 0$
   N is the total number of iterations

$$p_f = \frac{N_f}{N} = \frac{3}{5} = 60\% \text{ probability of failure}$$

***STEP 6*:** Given Step 5, we can also calculate the error associated with the simulation.

$$\varepsilon\% = \sqrt{\frac{(1-p_f)}{N \times p_f}} \times 200\%$$

$$\varepsilon\% = \sqrt{\frac{(1-0.60)}{5 \times 0.60}} \times 200\% = 73.0\% \text{ error}$$

This high level of error is due to the limited number of iterations. If the desired error level was 10%, given this probability of failure we would need to run 267 simulations.

$$10\% = \sqrt{\frac{(1-0.60)}{N \times 0.60}} \times 200\% \qquad N = 267$$

Appendix 2

The following example is based on <u>Example 2-1</u> in Section 2.7.2.2 (Haldar and Mahadevan 2000); it evaluates the limit state function $g(x) = R - S$ for the Hasofer-Lind Advanced First-Order Method. The steps and corresponding equations are reiterated for clarity.

STEP 1: Define the limit state equation.

$$g(x) = R - S = 0$$

STEP 2: Provide an initial assumption for $x_i{}^*$, (i=1,2,...,n). Note: In most cases, the mean value (μ) of each random variable is used. Then, calculate the coordinates of each variable in the standard normal space $(x_i'^*)$.

$\mu_R = 120$ Mean R

$\mu_S = 50$ Mean S

$\sigma_R = 18$ Standard deviation R

$\sigma_S = 12$ Standard deviation S

Coordinates of variables in standard normal space:

$$x_i'^* = \frac{x_i{}^* - \mu_{X_i}}{\sigma_{X_i}}$$

$$R' = \frac{R - \mu_R}{\sigma_R} = \frac{120 - 120}{18} = 0 \qquad\qquad S' = \frac{S - \mu_S}{\sigma_S} = \frac{50 - 50}{12} = 0$$

Note: Since in this example both R and S are normal random variables, the equivalent mean and standard deviation are the same as the original mean and standard deviation.

Note: If R was a *lognormal* random variable, the following equations would be used to calculate its equivalent mean and standard deviation:

$$\zeta_R = \sqrt{ln\left(1 + \frac{\sigma_R}{\mu_R}\right)^2} = \sqrt{ln\left(1 + \frac{18}{120}\right)^2} = 0.149$$

$$\lambda_R = ln\,\mu_R - \frac{1}{2}\zeta_R{}^2 = ln(120) - \frac{1}{2}(0.149)^2 = 4.776$$

$$\mu_R^N = \mu_R(1 - ln\,\mu_R + \lambda_R) = 120(1 - ln(120) + 4.776) = 118.665$$

$$\sigma_R^N = \zeta_R\mu_R = (0.149)(120) = 17.9$$

Where μ_R^N and σ_R^N are the equivalent normal mean and standard deviation of the lognormal variable R.

Therefore, the coordinate of R in standard normal space:

$$R' = \frac{R - \mu_R^N}{\sigma_R^N} = \frac{120 - 118.665}{17.9} = 0.075$$

STEP 3: Evaluate the partial derivatives of R' and S' and then calculate α_i.

Partial Derivatives:

$$\frac{\partial g}{\partial R'} = \frac{\partial g}{\partial R}\sigma_R = (1)(18) = 18$$

$$\frac{\partial g}{\partial S'} = \frac{\partial g}{\partial S}\sigma_S = (-1)(12) = -12$$

α_i:

$$\alpha_R = \frac{\left(\frac{\partial g}{\partial R'}\right)^*}{\sqrt{\left(\frac{\partial g}{\partial R'}\right)^2 + \left(\frac{\partial g}{\partial S'}\right)^2}} = \frac{(18)}{\sqrt{(18)^2 + (-12)^2}} = 0.832$$

$$\alpha_S = \frac{\left(\frac{\partial g}{\partial S'}\right)^*}{\sqrt{\left(\frac{\partial g}{\partial R'}\right)^2 + \left(\frac{\partial g}{\partial S'}\right)^2}} = \frac{(-12)}{\sqrt{(18)^2 + (-12)^2}} = -0.555$$

STEP 4: Obtain the new value for the MPPs R' and S' in terms of β

$$\beta = -\frac{R'\left(\frac{\partial g}{\partial R'}\right) + S'\left(\frac{\partial g}{\partial S'}\right)}{\sqrt{\left(\frac{\partial g}{\partial R'}\right)^2 + \left(\frac{\partial g}{\partial S'}\right)^2}} = \frac{(0)(18) + (0)(-12)}{\sqrt{(18)^2 + (-12)^2}} = 0$$

$$R' = -\alpha_R\beta = -(0.832)(0) = 0$$

$$S' = -\alpha_S\beta = -(-0.555)(0) = 0$$

STEP 5: Algebraically substitute the new R' and S' into the reduced limit state equation and solve for β.

Recall: $g(x) = R - S = 0$

Recall: $R' = \frac{R - \mu_R}{\sigma_R}$ *and* $S' = \frac{S - \mu_S}{\sigma_S}$

$$g(x') = \sigma_R R' - \sigma_S S' + \mu_R - \mu_S = 0$$

Recall: $R' = -\alpha_R\beta$ *and* $S' = -\alpha_S\beta$

$$g(x') = (\sigma_R)(-\alpha_R\beta) - (\sigma_S)(-\alpha_S\beta) + \mu_R - \mu_S = 0$$

$$\beta = \frac{\mu_S - \mu_R}{\alpha_S\sigma_S - \alpha_R\sigma_R} = \frac{50 - 120}{(-0.555)(12) - (0.832)(18)} = 3.24$$

STEP 6*:* Using the new β obtained in Step 5, re-calculate R' and S'

$R' = -\alpha_R \beta = -(0.832)(3.24) = $ -2.69

$S' = -\alpha_S \beta = -(-0.555)(3.24) = 1.79$

STEP 7*:* Repeat STEPS 3-8 until the value of β converges to within a specified tolerance (0.001 is often used as a tolerance level).

Note: because both R and S are normal random variables the value of β in the second iteration will be identical. Therefore, to solve for the coordinates in the original system:

$$R = \mu_R - \alpha_R \sigma_R \beta = 120 - (0.832)(18)(3.24) = 71.47$$
$$S = \mu_S - \alpha_S \sigma_S \beta = 50 - (-0.555)(12)(3.24) = 71.57$$
$$g(x) = R - S = 71.4776 - 71.5784 = -0.1$$

Thus, *R=71.47* and *S=71.57* are the failure points.

The probability of failure can be determined as: $p_f = 1 - \phi(\beta) = 1 - \phi(3.24) = 0.0006$
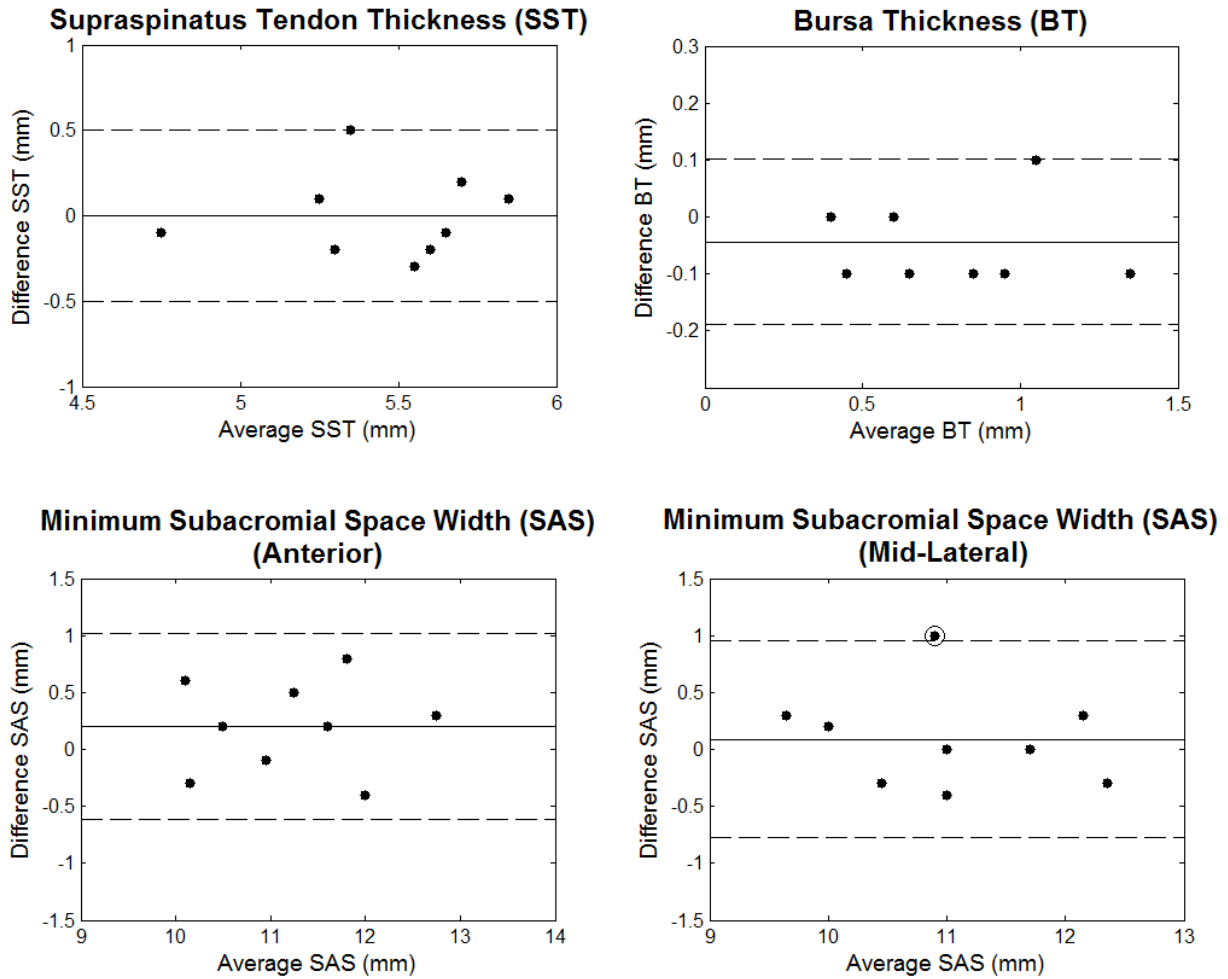
Appendix 3
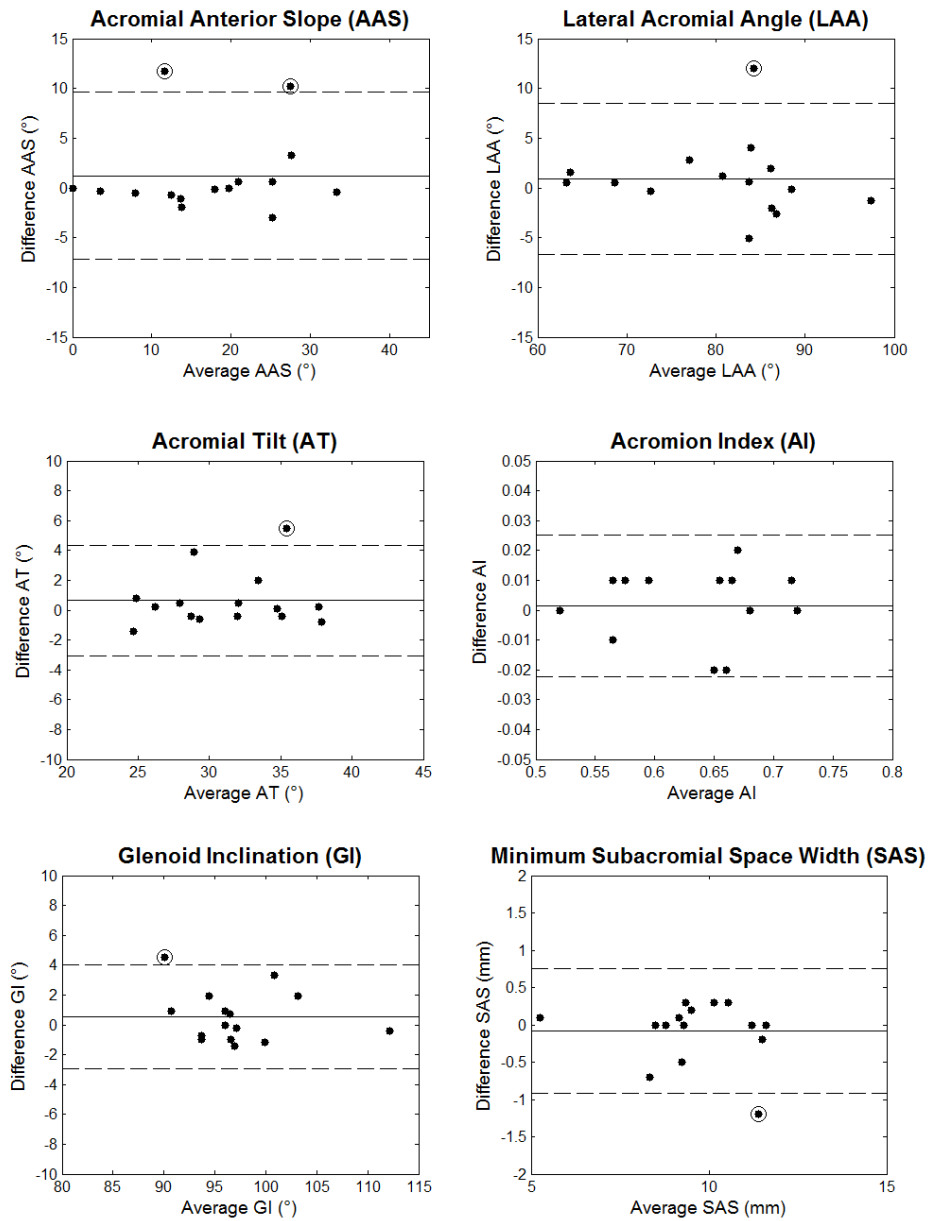
Figure A3-1. Intra-rater reliability Bland-Altman plots for each bone morphological property captured using radiographs. The mean measurement (*x-axis*) plotted against the difference between measurements, *d,* (*y-axis*). Solid line indicates the mean of measured differences, $\bar{d}$ and dashed lines indicate the approximate 95% confidence limits ($\bar{d} \pm 2*$standard deviation). Encircled points represent outliers.
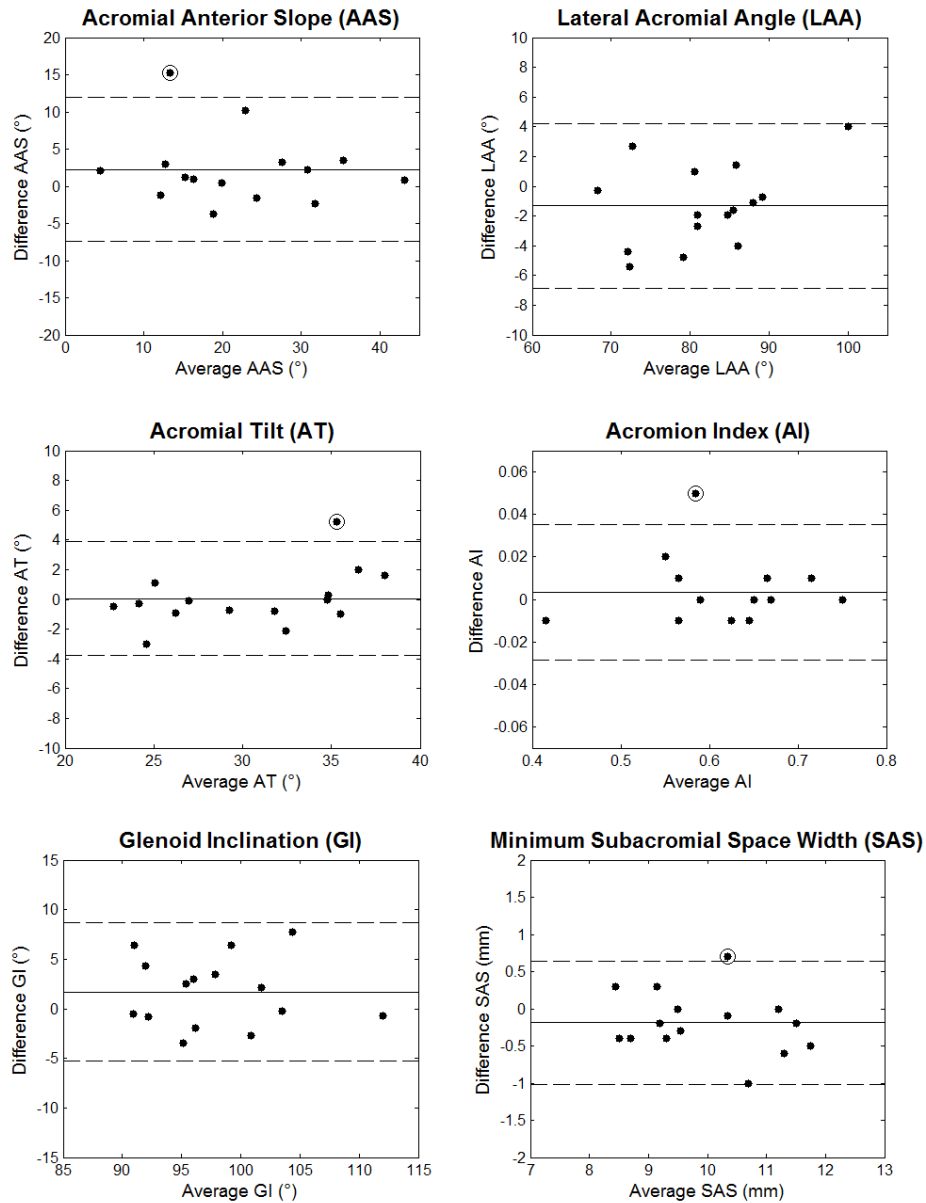
Figure A3-2. Inter-rater reliability Bland-Altman plots for each bone morphological property captured using radiographs. The mean measurement (*x-axis*) plotted against the difference between measurements, *d, (y-axis)*. Solid line indicates the mean of measured differences, $\bar{d}$ and dashed lines indicate the approximate 95% confidence limits ($\bar{d} \pm 2*$standard deviation). Encircled points represent outliers.

Figure A3-3. Intra-rater reliability Bland-Altman plots for each morphological property captured using ultrasound. The mean measurement (*x-axis*) plotted against the difference between measurements, *d,* (*y-axis*). Solid line indicates the mean of measured differences, $\bar{d}$ and dashed lines indicate the approximate 95% confidence limits ($\bar{d} \pm 2*$standard deviation). Encircled points represent outliers.
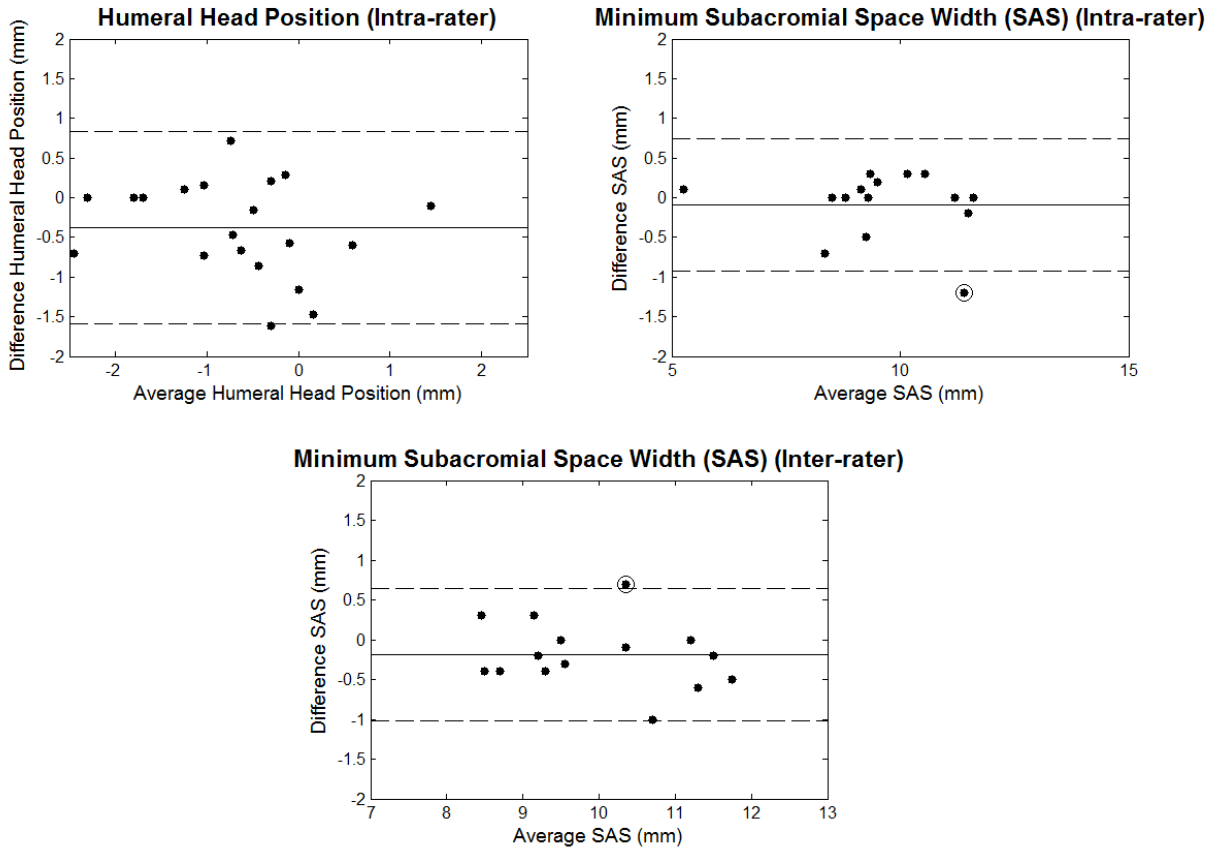
Figure A3-4. Bland-Altman plots for humeral head position (intra-rater) and minimum subacromial space width (intra- and inter-rater). The mean measurement (*x-axis*) plotted against the difference between measurements, *d*, (*y-axis*). Solid line indicates the mean of measured differences, $\bar{d}$ and dashed lines indicate the approximate 95% confidence limits ($\bar{d} \pm 2*$standard deviation). Encircled points represent outliers.